UNIVERSITY OF BIRMINGHAM

DIVERSITY AND MIMO FOR BODY-CENTRIC WIRELESS COMMUNICATION CHANNELS

By

IMDAD KHAN

A Thesis submitted to the College of

Engineering and Physical Sciences, University

of Birmingham, for the degree of

DOCTOR OF PHILOSOPHY

School of Electronics, Electrical, & Computer Engineering,

University of Birmingham, Edgbaston,

Birmingham, B15 2TT,

UK.

September 2009

ABSTRACT

Due to its increasing applications in personal communications systems, body-centric wireless communications has become a major field of interest for researchers. Fading and interference are the two concerns that affect the reliability and quality of service of wireless links. Diversity has been used to overcome these two problems. This thesis looks into the use of receive diversity for on-body channels. Space, pattern, and polarization diversity performance is analyzed and quantified by actual measurements in real environments. Significant diversity gains of up to 10 dB are achieved for most of the on-body channels. The on-body diversity channels have also been characterized by performing the statistical and spectral analyses. The fast fading envelope best fits the Rician distribution, with moderate K-factor values, and the slow fading envelope best fits the Log-normal distribution. Diversity has been found effective in the BAN-BAN interference rejection and significant rejection gain values are achieved. A new algorithm for BAN-BAN interference rejection has been proposed and compared with the conventional adaptive algorithms. The use of multiple antennas at both the transmitter and receiver end, i.e., MIMO has been investigated for on-body applications. It has been noticed that MIMO provides significant capacity increase for these channels despite the line-of-sight.

DEDICATION

This thesis is dedicated to

My Parents

My Wife

And

My lovely Daughter

ACKNOWLEDGEMENTS

First and the foremost, I would like to thank Almighty Allah for bestowing His blessings upon me and giving me the strength to carry out and complete this work.

I am extremely grateful to my supervisor Professor Peter S. Hall for all of the support, resources, and invaluable guidance that he provided in completing this work and in pursuing my PhD degree. Apart from his valuable academic advice and guidelines, he has been extremely kind, friendly, and helpful as a human being.

I would also like to express my deep gratitude to my good friend and colleague, Dr. Yuriy I. Nechayev, who has been very supportive and generous in sharing his knowledge. I am very grateful to Mr. Alan Yates for providing all the technical support in using the equipment and making the antennas. Special thanks to my other brilliant colleagues and very nice friends, Lida Akhoonzadeh-Asl, Zen H Hu (Sampson), Qing Bai (Simon), Elham Ebrahimi, Dr. Khalida Ghanem, Dr. Farid Ghanem, Anda Guraliuc, Dr. Andrea Serra, and Kamarudin M Ramlee, for all the help they have provided and all the exceptionally good time that we have spent together.

And last, but not the least, I am very grateful to COMSATS Institute of Information Technology, Pakistan and the Higher Education Commission (HEC), government of Pakistan, for providing me the opportunity and full funding to pursue my PhD degree.

TABLE OF CONTENTS

LIST OF FIGURES

LIST OF TABLES

LIST OF PUBLICATIONS

Journal publications

[1] **I. Khan,** Y. I. Nechayev, K. Ghanem, P.S. Hall, "BAN-BAN Interference Rejection with Multiple Antennas at the Receiver", *IEEE Transactions on Antennas and Propagation, 2009, in press.*

[2] **I. Khan**, Y. I. Nechayev, P.S. Hall, "On-body Diversity Channel Characterization", *IEEE Transactions on Antennas and Propagation, 2009, in press.*

[3] **I. Khan**, P.S. Hall, "Experimental Evaluation of MIMO Capacity and Correlation for Body-Centric Wireless Channels", *IEEE Transactions on Antennas and Propagation, 2009, in press.*

[4] A.A. Serra, A. R. Guraliuc, P. Nepa, G. Manara, **I. Khan**, P. S. Hall, "Dual-Polarization and Dual-Pattern Planar Antenna for Diversity in Body-Centric Communications", *IET Microwaves, Antennas & Propagation Journal, 2009, in press*.

[5] **I. Khan**, Y. I. Nechayev, P.S. Hall, "Second-order Statistics of Measured On-body Diversity Channels", *Microwave and Optical Technology Letters, Vol. 51, No. 10, October 2009*.

[6] **I Khan**, P.S. Hall, A.A Serra, A.R. Guraliuc, P. Nepa, "Diversity Performance Analysis for On-body Communication Channels at 2.45 GHz", *IEEE Transactions on Antennas and Propagation, Vol. 57, No. 4, April 2009.*

[7] **I. Khan**, P.S. Hall, "Multiple Antenna Reception at 5.8 and 10 GHz for Body-Centric Wireless Communication Channels", *IEEE Transactions on Antennas and Propagation, Vol. 57. No. 1, January 2009.*

[8] A.A. Serra, A. Guraliuc, P. Nepa, G. Manara, **I. Khan**, P.S. Hall, "Diversity Gain Measurements for Body-centric Communication Systems", *International Journal on Microwave and Optical Technology (IJMOT), Vol. 3, No. 3,pages 283-289, ISSN: 1553-0396, July 2008.*

[9] Akhoondzadeh-Asl L., **Khan I**., Hall P. S., "Polarization Diversity Performance for On-Body Communication Applications", *submitted to IET Microwave, Antennas, and Propagation Journal,, in September, 2009.*

[10] K. Ghanem, **I. Khan**, P. Hall, "On-body MIMO Channel Modelling and Capacity Evaluation for Body Area Networks", *submitted to IEEE Transactions on Antennas and Propagation, in April 2009.*

Conference Publications

[1] P. S. Hall, **Khan I**, Nechayev Y. I. Akhoondzadeh-Asl L, "On-Body Channel Modelling: Diversity, Multiple Input Multiple Output (MIMO) and Interference Reduction", *2nd IET seminar on Antennas and Propagation for Body-Centric Wireless Communications, 20 April 2009, The IET, Savoy Place, London, UK.*

[2] **I Khan**, Y I Nechayev, Peter S Hall, "Inter-Body Interference Cancellation in Body-Area Networks", *IEEE APS-URSI 2009, IEEE International Sym. on Antennas and Propagation, Charleston, SC, USA, 1-5 June 2009.*

[3] Akhoondzadeh-Asl L., **Khan I**., Nechayev Y I, Hall P. S., "Investigation of Polarization on the Body", *in proceeding of 3rd European Conference on Antennas and Propagation (EuCAP), Berlin, Germany, 23-27March 2009.*

[4] **I Khan,** Peter S. Hall, A. R. Guraliuc, P. Nepa, "Reciprocity and Repeatability of Diversity Measurements for On-body Communication Channels at 2.45 GHz", *IEEE APS-URSI 2008, IEEE International Symp on Antennas and Propagation, San Diego, California, USA, July 5-12, 2008*.

[5] A.A. Serra, **I. Khan**, P. Nepa, G. Manara and P.S. Hall, "Dual-polarization and Dual-pattern Planar Antenna for Diversity in Body-centric Communications", *IEEE APS-URSI 2008, IEEE International Symposium on Antennas and Propagation, San Diego, California, USA, July 5-12, 2008*.

[6] A.A. Serra, A. Guraliuc, P. Nepa, G. Manara, **I. Khan**, P.S. Hall, "Diversity Gain Measurements for Body-centric Communication Systems", *ISMOT2007, 11th International Symposium on Microwave and Optical Technology, Monte Porzio Catone, Italy, 17-21 Dec 2007.*

[7] **I Khan**, L Yu, Y I. Nechayev, P S. Hall, "Space and Pattern Diversity for On-body Communication Channels in an Indoor Environment at 2.45 GHz", *2nd European Conference on Antennas and Propagation (EuCAP), Edinburgh, UK, pp. 1-6, 11-16 Nov 2007.*

[8] **I Khan**, M R. Kamarudin, L Yu, Y I. Nechayev, P S. Hall, "Comparison of Space and Pattern Diversity for On-body Channels*", 5th European Workshop on Conformal Antennas, Bristol, UK, pp. 47-50, 10- 11 September 2007.*

Chapter 1

Introduction

1.1 Introduction to the PhD Project

With the increasing use and advancement of mobile technology, personal communication systems are getting more and more challenging. New trends in communications are evolving and with the advent of wearable computers [1], a new range of body-worn devices has emerged which leads to a new area of research called the body-centric wireless communications. Body-Centric communications uses the human body as a supporting environment for communication between two or more devices on the body [2]. An overview of body-centric communications and body-area networks (BAN) is given in Chapter 2. Much work has been done to investigate on-body channels at the ISM bands such as 2.45 GHz. At this frequency, propagation involves two main forms. Firstly, propagation takes place over the surface of the body by creeping waves [2]. Such propagation may be significantly affected by the motion of the body. Second is the multipath propagation due to multiple propagation paths around the body and due to reflections from the surrounding environment and the body parts. Propagation through the body is negligible at this and higher frequencies.

In mobile communications, the base station antennas are fixed and the mobile unit moves around in the scattering propagation environment. As opposed to mobile, in

the on-body channels, both the transmitter and receiver move and change their position in the scattering environment and with respect to each other. Fading will occur due to the large relative movement of the body parts, polarization mismatch, and scattering due to the body. The body itself causes fading due to the shadowing of links and due to reflections from the body parts. There is yet another source of fading in the on-body propagation channels, which is the multiple signal paths on the body, such as the two possible paths from front to back around the body from both sides. The surrounding environment is responsible for the fading as well. Fading due to the floor or ground, which is present in most cases, and fading due to local environment such as furniture, walls of room, cabin of car etc. are good examples of this. Apart from the fading, another very important concern for the devices mounted on the body is the transmitted power, which is to be kept as low as possible. 0 dBm is still believed to be high transmitted power for the body area networks. It is desirable to reduce the power level to increase the battery life and reduce the Specific Absorption Rate (SAR) value. In a scenario where, apart from the desired transmitted signal, the receiving device receives significant level of unwanted signal from other transmitters transmitting in the surrounding BANs and operating in the same band of frequency, the output signal to interference plus noise ratio (SINR) can be severely reduced. Rejection of the interference from a nearby BAN becomes more significant when the BANs are operating very close to each other and the level of the desired and interference signals are almost the same.

Apart from the above mentioned issues, the ever increasing use of wireless devices in personal healthcare, entertainment, security and personal identification, fashion, and

personalized communications etc. drives research to establish more reliable and efficient link between the devices mounted on the body. The current standards for wireless communications like Bluetooth [3], Zigbee [4], and BodyLAN [5] etc. are already operating but there is still a lot of scope for improvement. The high data rate and reliable transmission between the body-worn wireless devices and sensors, such as in military applications, sports and entertainment, and patient monitoring systems, demand the use of multiple antennas for the on-body and off-body channels.

To address these issues, it is, therefore, important that the fading must be overcome as much as possible and the output signal to noise ratio (SNR) be increased without increasing the transmit power. Antenna diversity is a well known technique to overcome fading and provide a power efficient link in mobile communications, in which two or more signals from various uncorrelated diversity branches are combined in different ways to achieve the diversity combined signal. Diversity can also be exploited to cancel the co-channel interference. The use of multiple-input multiple-output (MIMO) techniques can provide a significant increase in the channel capacity for high data rate applications. This area for on-body communications has received less attention, as much of the work on body-centric communication focuses on the antenna design [6], channel characterization [7 and 8], and the effect of human body presence on the link performance. Some preliminary measurements are reported with two monopole antennas at the receiver end for on-body channels in [9 and 10]. Cotton and Scanlon [11 and 12] have presented first and second order statistics and some diversity results for channels with wearable receiving antennas and transmitter at a fixed position in the room thus characterizing off-body channels,

and some on-body channels as well. The work in this thesis focuses on the use of multiple antennas at the receiver end to combat fading and reject the BAN-BAN interference, and at both the transmitter and receiver sides to increase the throughput of the system for on-body channels. Statistical analysis of the on-body channels with multiple antennas is also performed. Second-order statistics and spectral analysis is done and the body Doppler shift is investigated.

1.2 Objectives of the Project

The main objectives of this research were as follows:

1. To investigate the usefulness of multiple antennas at the receiver side for the on-body channels and quantify the maximum achievable improvement in the output SNR due to the use of diversity techniques.
2. To study the effectiveness of diversity reception in rejection of interference from nearby BANs and determine the improvement in the output SINR for various on-body channels.
3. To study the performance of some basic diversity antenna structures and work out the best antenna choice for on-body diversity channels.
4. To characterize the on-body diversity channels and determine a statistical distribution for the short-term and long-term fading envelopes.
5. To use multiple antennas at both the transmitter and receiver side i.e. MIMO and quantify the capacity increase for various on-body channels.

1.3 Layout of the Thesis

The thesis is composed of 10 chapters. An overview of each chapter is given below.

Chapter 2 provides a brief introduction to body-centric wireless communication channels. The categorization of body-centric communications is discussed and the on-body channels are briefly described along with antenna design and channel characterization issues.

Some theoretical background of diversity and MIMO systems is given in Chapter 3. The different types of diversity and the diversity combining methods are presented. The diversity gain and its dependence on branch signal correlation is briefly discussed. The capacity increase due to the use of MIMO is also given.

Chapter 4 presents a detailed description of the measurement equipment and the environments. Mounting antennas on the body, to constitute various on-body channels, is discussed and the details of the measurement setup are given. The movements performed during the measurements are also described.

Chapter 5 describes the use of space diversity for on-body channels at three frequencies using monopole antennas. The detailed description of the antennas is given and the processing performed on the data, in order to obtain the desired results, is described. The diversity gains and correlation coefficients for various on-body channels at the three frequencies are given and discussed. The repeatability and uplink-downlink diversity performance is also presented.

Chapter 6 of the thesis looks into the use of polarization and pattern diversity for on-body channels with two types of realistic and low-profile diversity antennas at two frequencies of operation and a polarization diversity antenna. The design parameters of the antennas are given and the same results, like diversity gain, correlation coefficients, and mean received powers, are presented. A comparison of space, pattern, and polarization diversity for on-body channels is also done along with the repeatability and uplink-down-link diversity.

Chapter 7 provides the on-body channel characterization at the three frequencies. A best-fit statistical distribution is determined for the branch and combined signals and the statistical analysis is done. The second-order statistics such as LCR and AFD are determined and the spectral analysis is presented.

The use of diversity reception for BAN-BAN interference rejection is discussed in Chapter 8. Two conventional interference rejection combining techniques are applied and the SINR improvement is presented. A new interference rejection combining technique is proposed for the on-body channels and is compared with the conventional techniques.

Chapter 9 discusses the use of MIMO for on-body channels. The MIMO system model for on-body channels and the improvement in channel capacity with MIMO, MISO, and SIMO over SISO is discussed and compared for three on-body channels. The spatial correlation matrices are given for each channel and the effect of Rician K-factor on the channel capacity is presented.

Chapter 10 summarizes some important conclusions derived from this study and also gives some possible future extension of the work.

REFERENCES

[1] C. Baber, J. Knight, D. Haniff, and L. Cooper, "Ergonomics of Wearable Computers", *Mobile Networks and Applications, 4, 1999, pp. 15-21*.

[2] P S Hall, Y Hao, editors of "Antennas and Propagation for Body-Centric Wireless Communications", *Artech House, London, 2006*.

[3] http://www.ieee802.org/15/pub/TG1.html

[4] *http://www.zigbee.org/*

[5] Carvey, P.P., "Technology for the Wireless Interconnection of Wearable Personal Electronic Accessories", *IX VLSI Signal Processing Workshop, Oct. 30 – Nov 1, 1996, pp. 13-22.*

[6] M.R Kamarudin, Y.I.Nechayev, P.S.Hall, "Performance of Antennas in the On-body Environment", *IEEE Antennas and Propagation Society International Symposium, 2005, 3-8 July 2005 Page(s):475-478 vol. 3A*.

[7] Y I Nechayev, P S Hall, C C Constantinou, Y Hao, A Alomainy, R Dubrovka, and C Parini, "Antennas and Propagation for On-Body Communication Systems", *11th Int. Symposium on Antenna Tech and Applied Electromagnetics – ANTEM, France, 2005.*

[8] Y. I. Nechayev and P. S. Hall, "Multipath Fading of On-body Propagation Channels," *IEEE International AP-S Symposium - USNC/URSI National Radio Science Meeting, San Diego, CA, 2008*.

[9] A.A. Serra, P. Nepa, G. Manara, P.S. Hall, "On the Performance Analysis of Diversity Techniques in Body-Centric Communication Systems," *IET Seminar on Antenna and Propagation for Body-Centric Wireless Communications*, *London, UK, April 24, 2007, pp. 63-66.*

[10] A.A. Serra, P. Nepa, G. Manara, and P.S. Hall, "Diversity Measurements for On-Body Communication Systems," *IEEE Antenna and Wireless Propagation Letters, vol. 6 (1), pp. 361 – 363, 2007.*

[11] S L. Cotton, W G. Scanlon, "Characterization and Modeling of the Indoor Radio Channel at 868 MHz for a Mobile Body-worn Wireless Personal Area Network", *IEEE Antennas and Wireless Propagation Letters, Vol. 6, 2007*.

[12] S. L. Cotton, W. G. Scanlon, "Channel Characterization for Single- and Multiple-Antenna Wearable Systems Used for Indoor Body-to-Body Communications", *IEEE Transactions on Antennas and Propagation, Vol. 57, No. 4, April, 2009.*

Chapter 2

Overview of Body-Centric Wireless Communications

2.1 Introduction

Wireless Personal Communication Systems (PCS) are getting more and more exciting and challenging and have driven the attention of many researchers in the recent years. New trends in PCS are evolving and with the advent of wearable computers [1], a new range of body-worn devices has emerged which can be worn on the body or carried in the pocket by the users. Fig. 2.1 shows a wearable computer setup with wired connections developed at the University of Birmingham [1]. These body-worn devices lead to a relatively new and interesting area, known as the Body-Centric Communications Systems (BCS) [2]. In body-centric communications, a number of nodes are placed on the body, or in its close proximity, communicating with each other or with other nodes placed away from the body such as base stations, central data storage devices, central processing units etc. An important aspect of the body-worn devices is the inter-connectivity. Wired connection is not a feasible choice as it can create great inconvenience and obstruction in motion of the body parts. Other choices, like special fabrics, can be used but it may not be desirable to wear purpose-built fabrics at all times, as it may be in conflict with personal preferences of a user. Some other methods are also proposed, e.g. body current mechanism and near field communication. Body current method uses the emission of

electric field on the surface of the body to use it as a transmission path [3, 4, 5]. Near-Field communication uses magnetic field induction for very short-range communication [6 and 7]. Both these techniques have their limitations and are not suitable for high data rate applications like video streaming and multimedia. The best available choice is then the wireless connectivity with antennas.

Fig.2.1: Wearable computer with wired connections developed at the UoB, *source:* [2]

The wireless BCS uses human body as a supporting environment for communication between two or more devices on the body [2]. Various standards for wireless connections have been developed, like WiFi [8], WLAN [9], UWB [10], Bluetooth [11], BodyLAN [12] and Zigbee [13]. Bluetooth has become popular recently with mobile phone applications but one major drawback is its consumption of large amount of battery power. Wireless BCS also has certain issues like the antenna design and performance, channel characterization, the effect of human body presence

and movement, and the transmitted power etc. The wearable devices are required to be small and light-weighted, with a high data rate support. The power consumption of these devices should be small. Thus, use of high frequencies and high efficient links is required [2]. The knowledge of electromagnetic properties of the human body is essential for effective design and understanding of the channels. A detailed study of electromagnetic properties and modeling of human body is given in chapter 2 of [2] and further details are given in Section 2.3.

The body-centric communications can be classified in three ways given below. The classification, given in [2], is based on the channel used for the propagation of the signals.

- **Off body:** This is the communication between devices on body with other devices away from the body. Good examples of this type of communication are the mobile to base station uplink and the downlink communication, wearable RFID tags, and body-worn sensors to and from the data acquisition system or server, as shown in Fig. 2.2 for a medical support network with wireless sensors placed on the body. The antennas should have radiation patterns directed away from the body, providing all-round coverage. The antennas must be screened from the body to avoid the effect of human body tissues on the antenna efficiency [2]. The off-body link has been extensively studied for mobile cellular systems and medical sensor networks. A variety of wearable antennas have been designed and proposed for this type of communication.

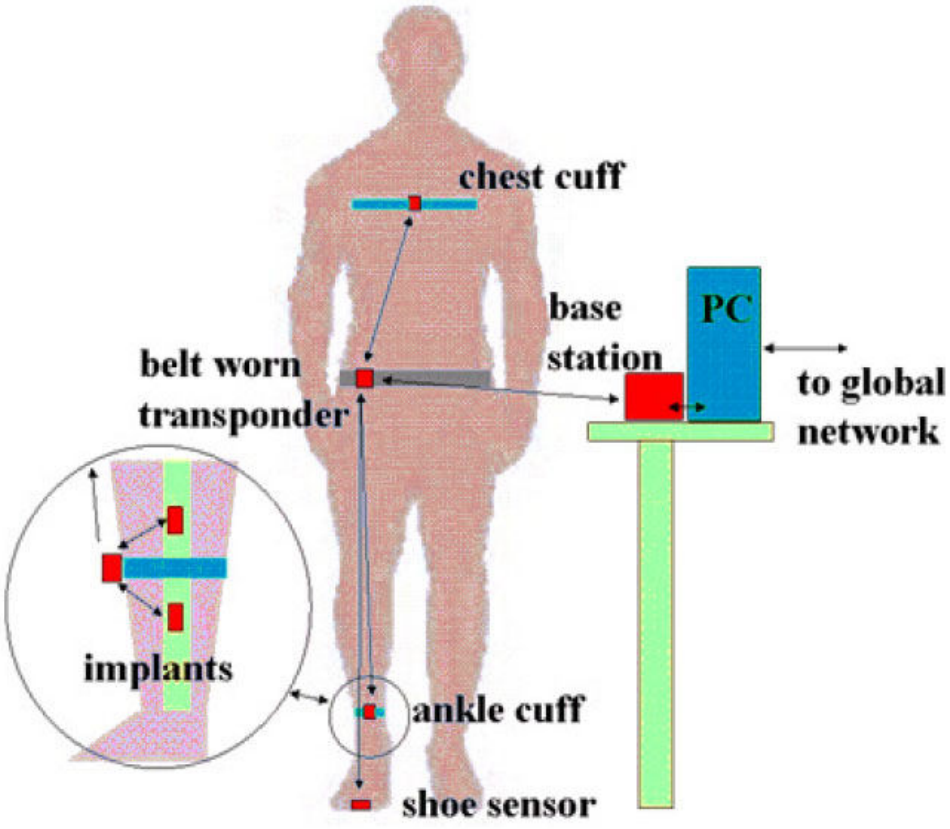

Fig.2.2: Medical support network with wearable devices [2]

- **On-body:** This is the communication between two or more devices, which are mounted on the same human body. The examples are, the wearable computer shown in Fig. 2.1 (if connected through wireless links rather than wired connection), sensors placed on various locations of the body (communicating with each other and to a central device mounted on the body), and the communication between a mobile phone placed in the pocket and the Bluetooth headset or a Bluetooth wrist watch (shown in Fig. 2.3) [14]. The watch communicates with the mobile phone for incoming call alerts, displays the number, and has accept/reject call functionality. Another

interesting gadget is the Nike shoe with built-in ipod volume controller [15], shown in Fig. 2.4, which controls the volume of the ipod according to the speed of running. The antennas for on-body applications should ideally have radiation patterns along the surface of the body.

Fig.2.3: The Bluetooth wrist watch by Sony Ericsson [14]

- **In-body:** This refers to the communication between two or more devices through the human body. A significant amount of the channel part is inside the human body. Major application area for this kind of communication is medical diagnostics and patient monitoring, where implantable medical devices, communicating with the outside world, are put inside the human body. These include heart pacemakers, cochlea implants, glaucoma sensor, retinal implants, and drug release devices etc. The emergence of technologies, like sub-micron electronics, nanotechnology, and Micro-Electromechanical Systems (MEMS), promises an immeasurable impact on the development of implantable devices to improve the standard and quality of medical sensor networks and patient lifestyle [2].

Fig.2.4: The Nike Musical shoe kit [15]

Body Area Network (BAN) is a wireless network that has nodes situated on or near the human body. The concept of BAN was first used for medical diagnostics in which various sensors, like temperature sensor, ECG, blood pressure monitoring kit, blood sugar device etc., are put on the body of a patient and they interact with a base unit on or off the body. The term BAN is now a days used in a broader spectrum to include all types of body-centric communications. Similarly, the term on-body communication has been used by some of the researchers to mean any communication that involves antennas mounted on the body whether on-body or off-body communication. This work, however, sticks to the definition cited above, and on-body communication means communication of the devices mounted on the body among themselves only, and not off-body. Efforts have been made to develop standards for the BAN and an IEEE task group, IEEE 802.15.6 (IEEE 802.15.BAN), has been established for this purpose in November 2007. This task group is the sixth

task group of the IEEE 802.15 working group. The IEEE 802.15 is an IEEE standard for Wireless Personal Area Networks (WPAN) [16] and has, so far, 7 task groups and 1 interest group for Terahertz called IGTHz. The task group 802.15.6 or 802.15.BAN and task group 802.15.7 are still in the process of developing new standards for BAN and Visible Light Communication (VLC), respectively. IEEE 802.15.1, first published in June 2002, is a standard for WPAN based on Bluetooth, whereas, 802.15.2 provides recommendations for the coexistence of the WPANs and Wireless Local Area Networks (WLAN). The details of other task groups of IEEE 802.15 are given on its website [16].

2.2 Human body modeling and Phantoms

To fully understand the propagation mechanism in and on the body, it is important to know the dielectric properties of the human body tissues and their dependence upon the frequency. The penetration depth of the lower frequencies is more compared to the higher frequencies. The penetration depth and conductivity for muscle and fat tissues are shown in Fig. 2.5 for a certain frequency range and the electromagnetic properties of human body tissues at 2.45 GHz are listed in Table 2.1 [2]. The table shows that each body tissue has different properties at this frequency. The penetration depth for muscle and the bone tissues is not much compared to the lower frequencies and thus the propagation will be confined to the surface of the body at this and higher frequencies.

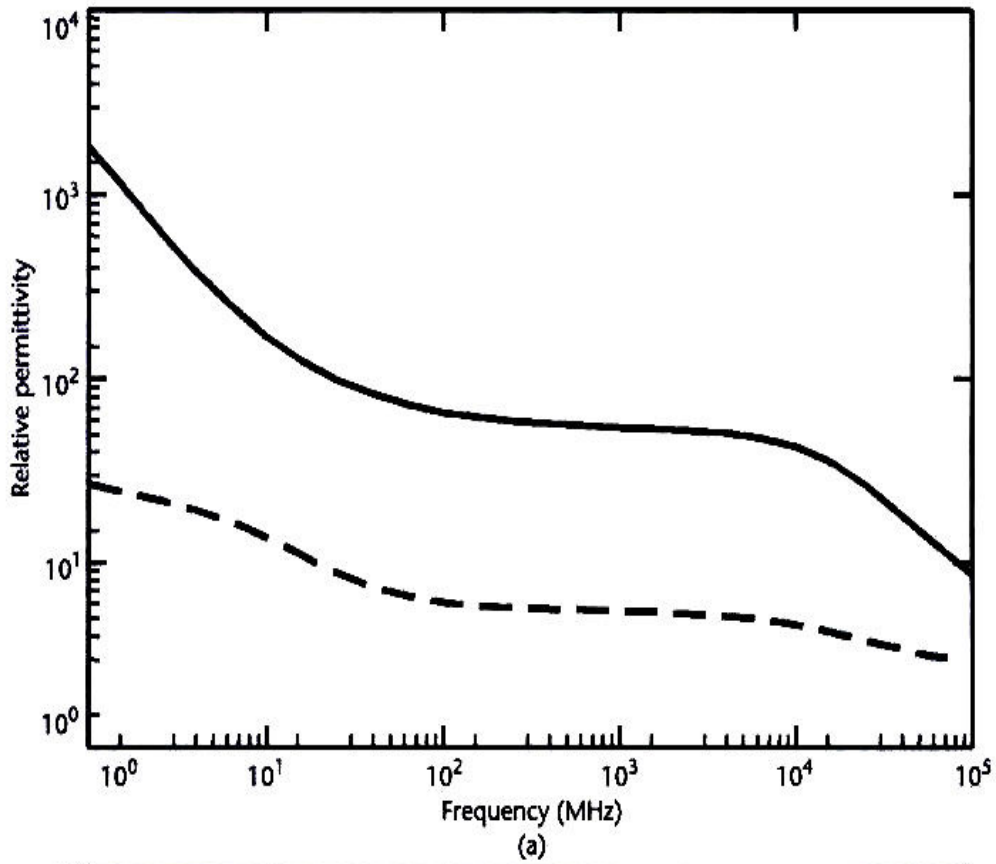

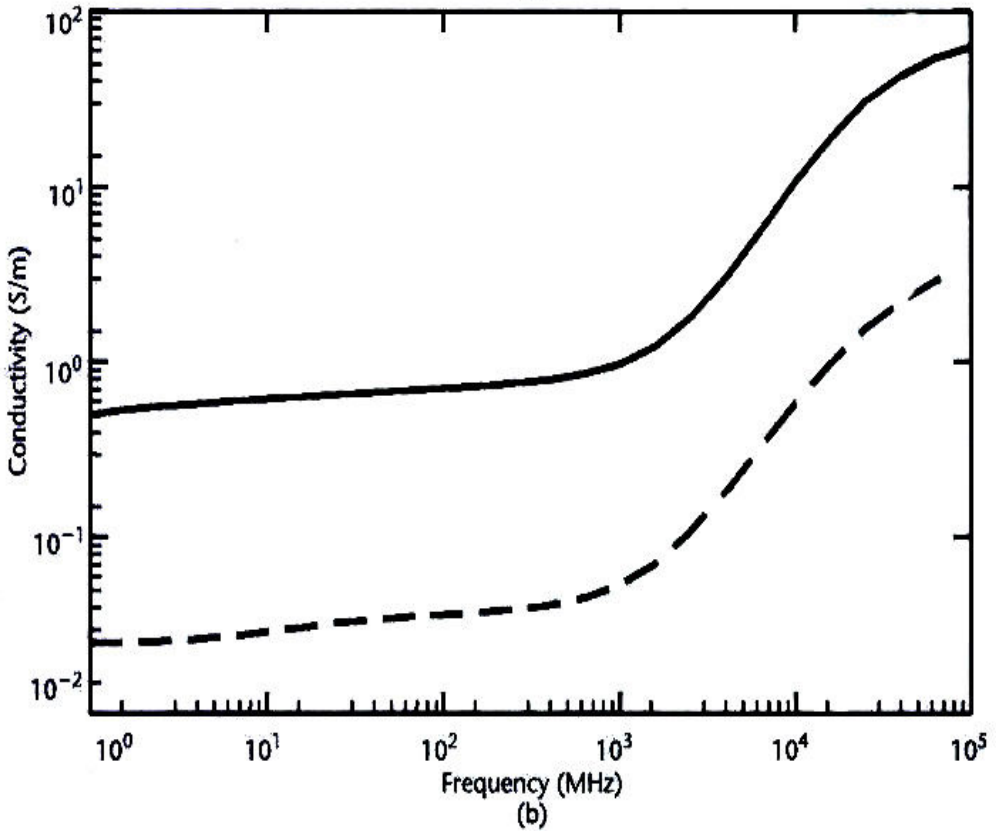

PTO for full caption

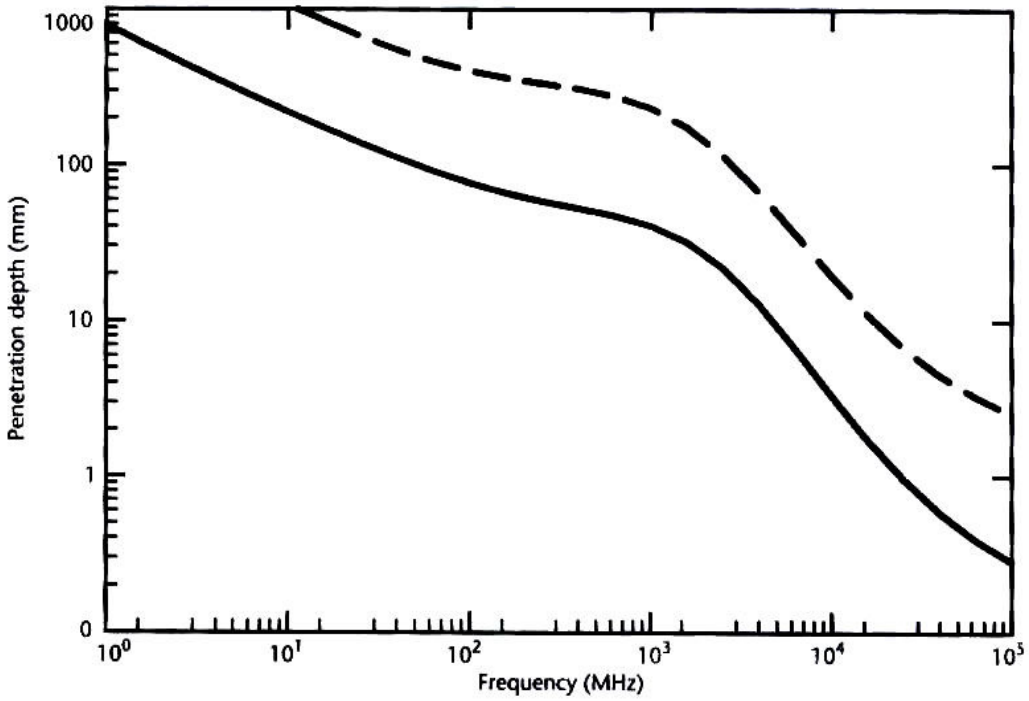

(c)

Fig.2.5: Variation of electromagnetic properties of Muscle (solid) and Fat (dotted) tissues with frequency (a) Relative Permittivity (b) Conductivity and (c) Penetration depth [2]

By knowing the electromagnetic properties of the human body tissues, it is possible to model the human body either physically, using solid or liquid materials with similar properties as the tissues, or numerically by using numerical electromagnetic computation [2]. This physical or numerical model used to represent the human body is called phantom. Thus, phantoms can be used to simulate a human body for measurements and testing of body-worn antennas. Phantoms provide a controlled and stable propagation environment but are only approximation of the human body. The accuracy of this approximation depends upon the complexity of the phantom. Complex and non-homogenous phantoms give better approximation but are very computation intensive in case of numerical simulations and very difficult to build in case of physical phantoms.

TABLE 2.1: ELECTROMAGNETIC PROPERTIES OF HUMAN BODY TISSUES AT 2.45 GHZ [2]

Tissue name	Conductivity (S/m)	Relative permittivity	Loss tangent	Penetration depth (m)
Aorta	1.467	42.47	0.24837	0.023761
Bladder	0.69816	17.975	0.27927	0.032545
Blood	2.5878	58.181	0.31981	0.015842
Bone Cancellous	0.82286	18.491	0.31996	0.028087
Bone Cortical	0.40411	11.352	0.25597	0.044616
Brain Grey Matter	1.843	48.83	0.27137	0.02031
Breast Fat	0.14067	5.137	0.1969	0.085942
Cartilage	1.7949	38.663	0.3338	0.018638
Cerebro Spinal Fluid	3.5041	66.168	0.38078	0.012537
Cornea	2.3325	51.533	0.32544	0.016548
Eye Sclera	2.0702	52.558	0.28321	0.018773
Fat	0.10672	5.2749	0.14547	0.11455
Gall Bladder Bile	2.8447	68.305	0.29945	0.015592
Heart	2.2968	54.711	0.30185	0.017286
Kidney	2.4694	52.63	0.33736	0.015811
Liver	1.7198	42.952	0.2879	0.020434
Lung Inflated	0.81828	20.444	0.28779	0.02963
Muscle	1.773	52.668	0.24205	0.021886
Skin Dry	1.4876	37.952	0.28184	0.022198
Skin Wet	23.984	20.369	0.84665	0.0010736
Small Intestine	3.2132	54.324	0.42529	0.012438
Stomach	2.2546	62.078	0.26114	0.018707
Testis	2.2084	57.472	0.27628	0.018394
Tongue	1.8396	52.558	0.25167	0.021083

2.2.1 Physical Phantoms

Physical phantoms can be classified as solid (dry), semi-solid (gel), and liquid phantoms. Homogenous dry phantoms, like the ones shown in Fig. 2.6, are made up of dielectric material having dielectric properties similar to a single human tissue, like bone, and are useful in simulating the propagation in and around the human body [2]. It is possible to make non-homogenous phantoms with several different layers

representing different tissues. The common materials used to make phantoms include ceramic and graphite powder mixtures, silicon rubber mixed with carbon fiber, and conductive plastic with carbon black [2]. The solid or dry phantoms have an advantage that they keep their shape for a long period of time and have stable characteristics. These can be built from a single organ phantom to whole body phantoms, depending upon the application.

Semi-solid or gel phantoms are easy to modify in shape but are not as long lasting as the solid phantoms because they have high water content, which is lost over time. These are useful to simulate organs with high water content like muscle and brain etc [2]. Fig. 2.7 shows an example of semi-solid phantom [2].

One of the earliest methods of simulating a human body tissue was to use some liquid, filled in a container, having the same dielectric properties as the tissue [2]. These types of phantoms are called liquid phantoms. Usually, the liquid is filled in a shell made of fibreglass having low permittivity and conductivity. The shell can be shaped to represent a human body organ e.g. hand, head etc., or the whole body torso. For simpler applications, a basic shape, like a rectangular box, can be used. To insert the measurement probe for measurement of field distribution inside the tissue (represented by the liquid phantom), the shell must have a hole [2]. Liquid phantoms are homogenous phantoms and thus the representation of the human body is not as good as other types of phantoms, but it is an easy and convenient way to simulate the body. The range of frequencies for which the liquid has the desired dielectric properties may be limited [2].

Fig.2.6: Solid human body phantoms placed at EECE department, University of Birmingham

Fig.2.7: An example of semi-solid gel phantom [2]

2.2.2 Numerical Phantoms

Sometimes, it is desirable to use computational simulations, instead of real-time measurements with human body or physical phantoms. Thus a numerical phantom is required to model the human body. Numerical phantoms can be categorized as theoretical phantoms or voxel phantoms [2]. Theoretical phantoms are very simple shaped homogenous numerical phantoms, like spheres or cylinders, which can approximate the human body up to a reasonable accuracy. For more precise modelling, more complex and realistic numerical phantoms are required. These phantoms are composed of several voxels, as shown in Fig. 2.8, and are called voxel phantoms [2]. Fig. 2.9 shows some examples of voxel phantoms e.g. NORMAN (normalized man) [2], HUGO [17], and Japanese male and female phantoms [2].

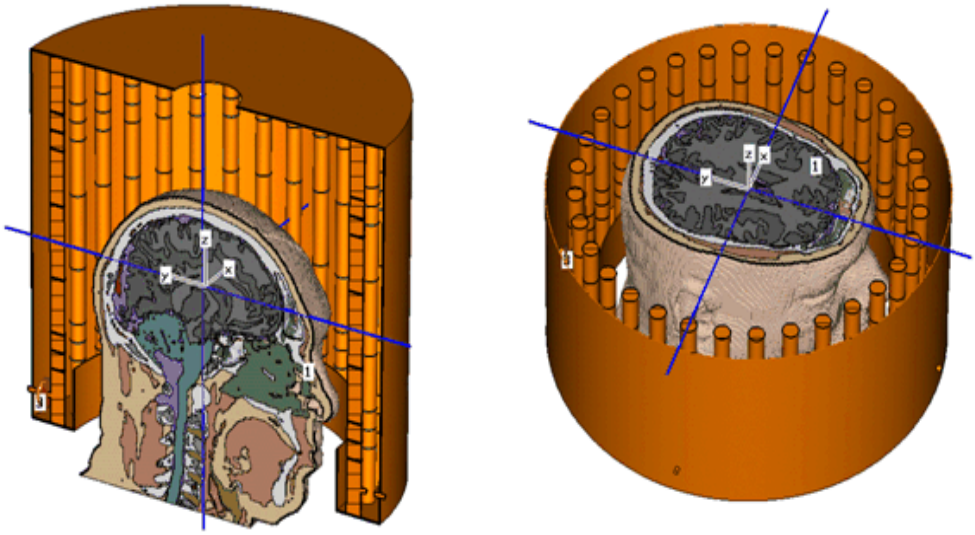

Fig.2.8: Cross-section of the head of voxel phantom used in CST Microwave Studio [17]

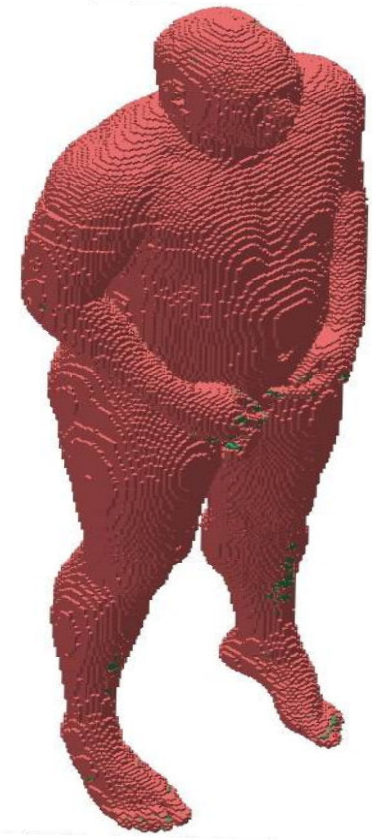

(a) NORMAN [2]

(b) HUGO [17]

(c) Japanese Male [2]

(d) Japanese Female [2]

Fig.2.9: Examples of numerical whole body human voxel models

2.3 Antennas for On-Body Channels

One of the concerns of body-centric communications is the health hazard associated with electromagnetic radiation very close to the human body and, as a result, the absorption of energy by the human tissues. The amount of energy absorbed is usually measured in Specific Absorption Rate (SAR), which is the maximum allowable power absorbed per unit mass of the body tissue. This level is 2.0 W/kg [18, 19]. Careful consideration is required to design the wearable antennas and other circuits, as there are limitations on the maximum power to which the human body can be exposed. It is, for this reason, very important to keep the transmitted power as low as possible for body-worn devices and use antennas with very low or no back radiation.

For BAN applications, the proper antenna design is a critical stage. The antennas are required to be compact, light weighted, low profile, and should have a suitable feeding structure for proper integration in small-sized body-worn devices. It is worth noting that some of the antenna performance parameters, like gain, radiation pattern, efficiency, matching etc., change significantly compared to the free space operation when the antenna operates on or in close proximity of a lossy medium, such as human body tissue. The antennas can detune when mounted on the body. The amount of detuning depends upon the type of antenna and the type of tissue. The use of ground plane to screen the antenna from the body may be helpful in avoiding this problem in some cases, but with antennas having no or small ground plane, the design should be aimed for a high bandwidth of the antenna to minimize the effect of detuning. The radiation pattern of the antenna is another important parameter to be considered. For off-body communication, the pattern must be directed away from the

body. For on-body applications, the radiation pattern should be such that the maximum beam direction is along the surface of the body. This means that the antenna should be able to launch waves, which can travel along the body surface. These waves propagate along the surface of the body as creeping waves [2]. In general, the antennas with omni-directional radiation pattern in the plane tangential to the surface of the body are considered suitable for on-body applications. The radiation pattern of the antenna is changed compared to the free space radiation pattern when the antenna is placed on the body. In some cases, the gain of the antenna on the body is significantly reduced compared to the free space gain. Hence, the antenna design requires careful consideration.

Various antennas, like rectangular patch, monopole, PIFA, and circularly polarized patch antennas, are characterized and their parameters, like radiation patterns, return loss, and efficiencies, are compared through a series of simulations in [4 and 20]. The same sort of comparison is done with similar and some other antennas through real time measurements in [21]. It has been concluded that some antennas are better than the others in some aspects, but worse in other aspects. For example, monopole antennas are the best in terms of path gain but have a major disadvantage in shape. Patch antennas and other planar antennas are low-profile and light-weighted and provide more stable performance in terms of mismatch, but the link performance is not satisfactory. Some wearable antennas are fabricated in the clothing, called textile or fabric antennas. Along with the above-mentioned design issues, the textile antennas must be flexible and ideally planar. The antenna must be capable to resist against the changes due to bending and crumpling, as well as against the changing

operating environment e.g. dampness. Wearable and textile antennas have been a hot area of research in recent years and a variety of wearable antennas have been proposed.

2.4 On-Body Propagation Channel Characterization

Unlike the mobile communications system, where the link between the mobile unit and the base station is affected mainly by scattering due to objects in the propagation environment and interference between the multipath components, the on-body channels are influenced by the movement of the body around the antennas and the antenna position on the body as well. There are various issues that need to be addressed for on-body channels to achieve optimum performance. These include the choice of best antenna, the best location of antennas on the body, the choice of suitable frequency, the effect of body movements, and the effect of scattering due to the environment and the body. The best location for the antenna on the human body is a challenging task as the dielectric properties of different human body tissues are different and also the shape and size of the body varies from person to person. To address this and all the other issues related to the propagation channels, the on-body channel characterization has been done by many researchers through real measurements and simulations. The on-body channel characterization for narrowband signal at 2.45 GHz is done in [22]. With transmitter mounted on belt, fourteen channels are characterized, and path losses for each channel are given. Path gain for various paths and postures is discussed in [23].

In [24-26] some antennas are characterized and compared for on-body channels by measuring the channel performance in terms of pathloss for various on-body channels and body postures. Cotton and Scanlon has characterized and presented channel statistics for on-body and off-body channels at 846 MHz and 2.45 GHz in an indoor environment [27 and 28] whereas in [29] body-worn receiver channel characterization and modeling is presented at 5.2 GHz. They observed that two thirds of the investigated paths were Nakagami distributed, with the other one third Rician distributed. A channel model, for wireless BANs at 400 MHz, 900 MHz, and 2.4 GHz with numerical simulations for propagation around the body, is presented by Ryckaert *et al*. [30]. On-body channel characterization is still a hot topic of research within the area and needs more fine tuning before any standardization can be done.

2.5 Application Areas

There is a significant breadth of potential to the work on body-centric communication. By way of example, the remit of IEEE 802.15 Task Group 6 (BAN) [16] is quoted as "*developing a communication standard optimized for low power devices and operation on, in or around the human body (but not limited to humans) to serve a variety of applications including medical, consumer electronics / personal entertainment and other*". There is also a large, but little reported, interest from the defence community, with emphasis on equipping the future soldier with personal wireless connected on-body equipment. The medical sensor network area seems to be perhaps the biggest potential market with many new products coming on to the market, some of which, in current and future generations, use on-body channels. Medical implants, patient monitoring and diagnostic systems, and personal health

care are already taking advantage of the technology. Entertainment and personalized multimedia, security, police, sports training, fire fighters, personal identification, fashion, and personalized communications are few more application areas where body-centric communication can fit itself. Some examples of the application areas have already been presented in section 2.1. The wearable computer, shown in Fig. 2.1, is a very good example of on-body communication if the components are connected wirelessly. BAN has become a part of the 4th generation communication systems research and development and will be an integral part of the future personalized communication systems.

REFERENCES

[1] C. Baber, J. Knight, D. Haniff and L. Cooper, "Ergonomics of Wearable Computers", *Mobile Networks and Applications, 4, 1999, pp15-21.*

[2] P S Hall, Y Hao, editors of "Antennas and Propagation for Body-Centric Wireless Communications", *Artech House, London, 2006.*

[3] Ubiquitous Communication through Natural Human Actions, *http://www.redtacton.com/en.*

[4] A Alomainy, "Antennas and Radio Propagation for Body-centric Wireless Networks", *PhD Thesis, Queens Mary Uni, London, May 2007.*

[5] H J Yoo, S J Song, N Cho, H J Kim, "Low-Energy On-body Communication for BSN", *Body Sensor Networks, 26-28 March 2007, Aachen, Germany.*

[6] http://www.nfc-forum.org

[7] TG Zimmerman, "Personal Area Networks: Near-field Intra-body Communication", *IBM System Journal, Vol 35, No. 3-4, pp. 609-617, 1994.*

[8] http://www.wi-fi.org

[9] *http://ieee802.org/11*

[10] *http://www.uwbforum.org/*

[11] *http://www.ieee802.org/15/pub/TG1.html*

[12] Carvey, P.P., "Technology for the Wireless Interconnection of Wearable Personal Electronic Accessories", *IX VLSI Signal Processing Workshop, Oct. 30 – Nov 1, 1996, pp. 13-22.*

[13] *http://www.zigbee.org/*

[14] http://www.sonyericsson.com/bluetoothwatch/default.asp?lc=en&cc=au

[15] http://www.apple.com/uk/ipod/nike/

[16] http://ieee802.org/15/index.html

[17] http://www.cst.com/Content/Products/MWS/ImpExp.aspx

[18] ICNIRP, "Guidelines For Limiting Exposure To Time-Varying Electric, Magnetic, And Electromagnetic Fields (Up To 300 GHz)", *Health Physics, Vol. 74, No. 4, Pp. 494-522, 1998.*

[19] IEEE, "IEEE Recommended Practice For Determining The Peak Spatial-Average Specific Absorption Rate (SAR) In The Human Head From Wireless Communications Devices: Measurement Techniques", *IEEE Std. 1528-2003, 2003.*

[20] T Salim, "Antennas for On-Body Communication Systems", *PhD thesis, University of Birmingham, September 2006.*

[21] K M Ramlee, "Design and Performance of Antennas for On-Body Communication Channels and Antenna Diversity", *PhD thesis, University of Birmingham, September 2007.*

[22] Y. I. Nechayev, P. S. Hall, C. C. Constantinou, Y. Hao, A. Alomainy, R. Dubrovka, C. G. Parini, "On-Body Path Gain Variations with Changing Posture and Antenna Position", *the 2005 IEEE AP-S International Symposium on Antennas and Propagation and USNC/URSI National Radio Science Meeting, Washington DC, USA on July 3-8, 2005.*

[23] Hall, P.S, Ricci, M., Hee, T.M., "Characterization of On-body Communication Channels". *Microwave and Millimetre Wave Technology, 2002. Proceedings. ICMMT 2002. 2002 3rd. Int Conference on, 17-19 Aug. 2002 Pages: 770 – 772.*

[24] Nechayev Y I, Hall P S, Constantinou C C, Hao Y, Alomainy A, Dubrovka R and Parini C, "Antennas and Propagation for On-Body Communication Systems", *11th Int Symposium on Antenna Tech and Applied Electromagnetics – ANTEM, France, 2005.*

[25] M.R Kamarudin, Y.I.Nechayev, P.S.Hall, "Performance of Antennas in the On-body Environment", *IEEE Antennas and Propagation Society International Symposium, 2005, 3-8 July 2005 Page(s):475-478 vol. 3A*.

[26] Alomainy, A., Hao, Y., Parini, C.G., Hall, P.S., "Comparison between Two Different Antennas for UWB On-body Propagation Measurements", *Antennas and Wireless Propagation Letters Volume 4, 2005, pp. 31-34.*

[27] W G. Scanlon and S L. Cotton, "Understanding On-Body Fading Channels At 2.45 GHz Using Measurements Based On User State And Environment", *Loughborough Antennas & Propagation Conference, 17-18 March 2008, Loughborough, UK.*

[28] S L. Cotton, W G. Scanlon, "Characterization and Modelling of the Indoor Radio Channel at 868 MHz for a Mobile Body-worn Wireless Personal Area Network", *IEEE Antennas and Wireless Prop Letters, Vol. 6, 2007*.

[29] K. I. Ziri-Castro, W. G. Scanlon, N. E. Evans, "Indoor Radio Channel Characterization and Modelling for a 5.2-GHz Body-worn Receiver", *IEEE Antennas and Wireless Propagation Letters, Vol. 3, 2004.*

[30] J. Ryckaert, P D Doncker, R Meys, A de Le Hoye, and S Donny, "Channel Model for Wireless Communication Around Human Body", *IEEE Electronics Letter, Vol. 40, No. 9, pp. 543-544, April 2004.*

Chapter 3

Overview of Diversity and MIMO Systems

3.1 Channel Fading

Fading is the time variation of signal power at the receiver due to changes in the transmission path. Fading can be categorized as short-term fading and long-term fading [1]. Long-term fading, often called shadowing, is caused by the change in path length due to the motion of transmitter and/or receiver relative to each other or due to an obstruction or shadowing in the propagation path.

On the other hand, short-term fading is mainly caused by the superposition of multiple copies of the received signal, which are different in magnitude, phase, or time. This happens due to a very common phenomenon in wireless communications called multipath propagation, i.e., signal from the transmitter to the receiver travel via more than one path, each having different time delay and attenuation factor. The reasons for multipath propagation are scattering of the signal from buildings, trees or other obstructions. At the receiver end, multiple copies of the signal are received, arriving from different directions and at different time intervals, i.e., the signal is spread in the time domain. This spread is called the delay spread. These time-delayed copies of the signal have a relative phase difference. The multiple copies of the signal, with random phase shift, superimpose to produce an enhanced or reduced energy signal on the receiver. If signals are in phase, they will intensify the resultant

signal; otherwise, the resultant signal is weakened due to phase difference. This causes rapid fluctuation in the signal amplitude along the propagation path, as shown in Fig 3.1. The short-term fading caused by the multipath propagation is also called multipath fading.

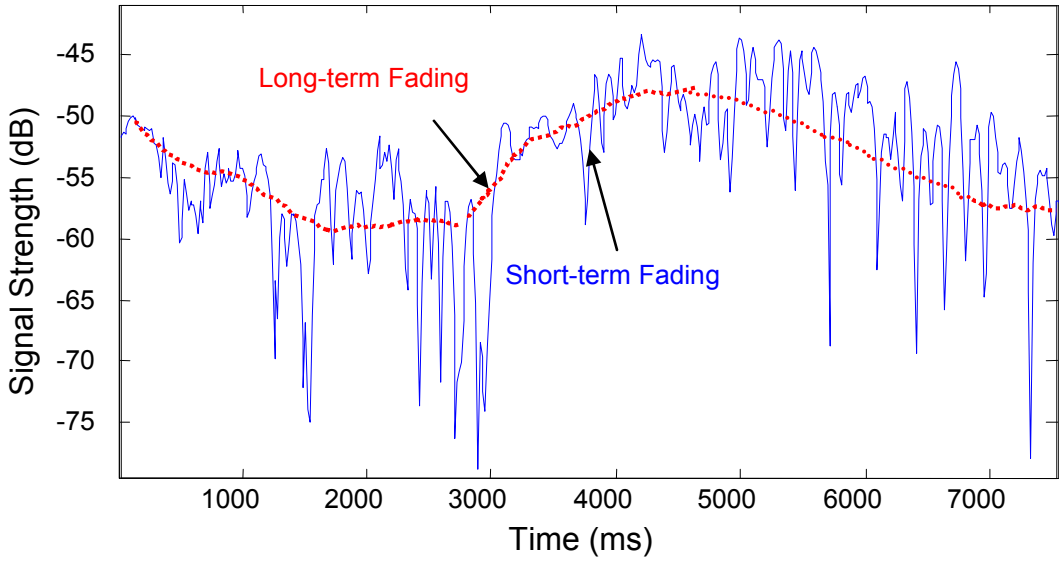

Fig. 3.1: An example of a received signal envelope with both the short-term and long-term fading (dotted line follows the long-term variation)

When all the spectral components of a transmitted signal are affected the same way by the channel, the fading is referred to as flat fading, whereas if different spectral components come across different amplitude and phase variation, the fading is not the same for all the spectral components, and is called frequency selective fading [1]. If a signal is composed of various frequency components (having a certain bandwidth as in the case of real modulated carriers transmitted from the transmitter), the relative phase shift is different for different frequency components of the signal and as a result, the signal becomes distorted. If the frequency components are close enough, the electrical path for the different frequency components is almost the same

and the amplitude and phase of the frequency components fade in a similar way. The bandwidth or frequency separation over which the spectral components are affected almost the same way is called coherence bandwidth of the channel [1]. If the bandwidth of the signal is less than the coherence bandwidth of the channel, the effect of frequency selective fading is negligible. Frequency selective fading is not discussed in this thesis, as all the measurements were done in a small laboratory environment or anechoic chamber with very small delay spread and hence large coherence bandwidth. Also, the transmitted and received signals were narrowband. This work thus applies either to narrowband systems or small delay spread channels. The term "fading" means flat fading throughout the contents unless otherwise stated.

In a situation where the transmitter and/or receiver move relative to each other, the frequency of the received signal is increased or decreased due to the rate of change of phase with motion. This change in frequency is called Doppler shift, which produces a frequency spread in the spectrum of the signal called Doppler spread. The maximum Doppler shift, f_m, can be calculated as [1]:

$$f_m = \frac{v}{\lambda} \quad \text{(Hz)} \tag{3.1}$$

where v is the velocity of relative motion in m/s and λ is the free space wavelength of the transmitted signal in metres. The reciprocal of the maximum Doppler spread is proportional to the coherence time, which is the time separation in which two time components of the signal undergo independent attenuation. It is defined as [1, 2]:

$$t_c \geq \sqrt{\frac{9}{16\ \pi f_m{}^2}} \quad \text{(s)} \qquad (3.2)$$

Fading can be classified as “fast” or “slow” based on the variation of the signal or the symbol duration. If the signal varies faster than the coherence time of the channel or the symbol duration is smaller than the coherence time, the effect of fading is negligible over the symbol duration and the fading is called slow fading [1]. On the other hand, if the signal variation is slower than the coherence time of the channel or the symbol duration is larger than the coherence time, the distortion due to Doppler spread is considerable and the fading is called fast fading [1].

Due to the rapid variation of the signal and deep fades, multipath fading effectively reduces the signal to noise ratio (SNR) of the system and the bit-error-rate (BER) is increased. This degrades the quality of service. Besides the multipath fading, the transmitted signal on its way to the receiver comes across various impairments that affect the quality of reception. These may include degradation of signal strength with distance, addition of noise in the channel, noise produced by the transmitter/receiver circuits, and interference etc. These impairments put a limit on the increasing demand for data rate, quality of service, and reliability.

3.2 Diversity overview

To improve the performance and overcome fading, diversity has been used as a very powerful tool. By using more than one communication channel, the fading in wireless channel can be minimized, hence, reliable and efficient transmission can be

achieved. The principle behind diversity is the use of two or more uncorrelated branches with independent fading statistics. If two or more channels are separated sufficiently in time, frequency, space, radiation pattern, and / or polarization, the fading on the individual channels is independent due to the different channel conditions [3]. It is highly improbable that all the branch signals will be at the same fade level at a certain instant. Therefore, if the branch signals are combined properly, the deep fades can be minimized thus yielding an overall improvement in SNR. In principle, diversity works at its best if fading at the branches is uncorrelated and the branch signals have the same average power level [4].

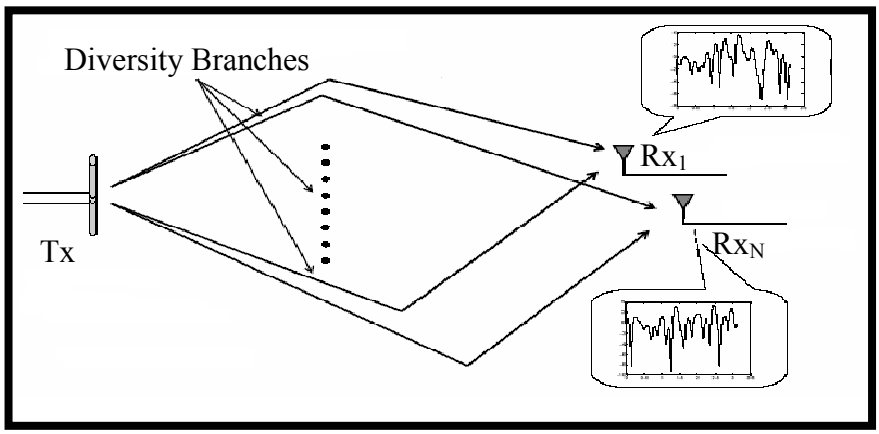

Fig. 3.2: Diversity Reception

Diversity can be implemented in many ways. The various diversity types are discussed later in this chapter. Antenna diversity generally refers to the implementation of diversity system in which two or more antennas are used to achieve the diversity branches. Antenna diversity can be achieved in various ways, as depicted in Fig. 3.3. A system with single antenna at the receiver and transmitter is

termed as Single-Input Single-Output (SISO) system. In receive diversity, also termed as Single-Input Multiple-Output (SIMO), one transmit antenna and multiple receiving antennas are used. Transmit diversity or Multiple-Input Single-Output (MISO) on the other hand, refers to multiple antennas at the transmitter side and a single antenna at the receiver side. In Multiple-Input Multiple-Output (MIMO), both the transmitter and receiver are equipped with more than one antenna.

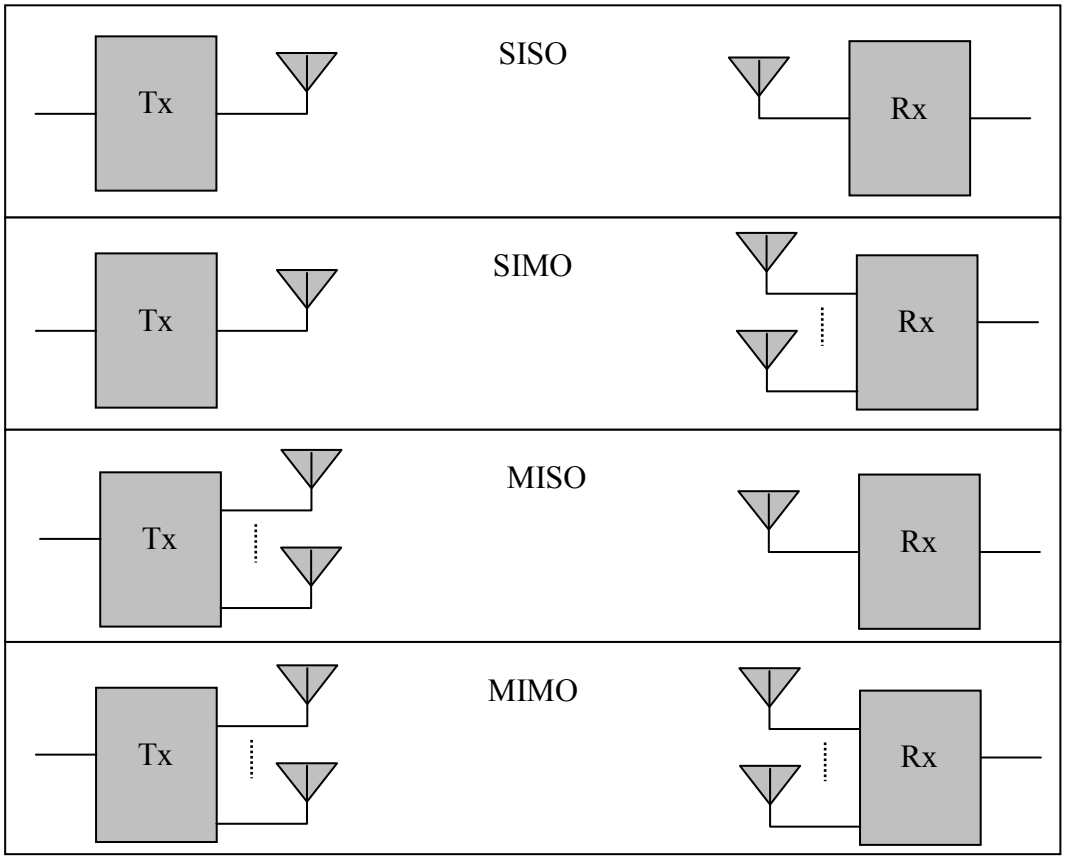

Fig. 3.3: Communication system classification based on number of antennas

With diversity reception or SIMO, the cost and complexity of the receiver is increased if they are equipped with multiple antennas. In the case of MISO, this cost and complexity is added up at the transmitter, and the receiver has a single antenna.

But in terms of channel capacity improvement, SIMO outperforms MISO [5]. In mobile cellular communications system, the base station is generally equipped with multiple antennas and the mobile handsets have single antennas because implementing diversity at the handset receiver can significantly increase the cost and size of the handsets, which is undesirable. Contrary to the mobile cellular system, where one base station transmits to a large number of receivers, on-body channel communication generally takes place between a single transmitter-receiver pair. So, the cost of implementing diversity either at the transmitter or at the receiver is the same. There may be some applications where a single transmitter communicates with multiple devices mounted on the body. Even then, the number of receivers are only few. Hence, diversity reception (SIMO) is a much better choice for on-body channels compared to its counterpart; transmit diversity (MISO), due to better performance. The term diversity would mean antenna receive diversity, hereafter, unless otherwise stated.

Much work has been done on the use of diversity at the mobile hand-held devices and the base station. The performance benefits of diversity for portable wireless systems have been reported in [6]. Reference [7] shows an experimental investigation of various diversity configurations and a diversity gain of up to 10 dB at 1% probability has been reported in for non-line of sight (NLOS) scenario. Reference [8] gives an experimental study of three-branch diversity system with various antennas. The correlation coefficients and the effect of mutual coupling are also discussed there. Colburn *et. al.* [9] has presented diversity performance with experimental data using PIFA, monopole and other antenna combinations for mobile

hand-held terminals in Rayleigh and Rician fading environments. The effect of human body, especially head and the hand, on the performance of diversity antenna at the mobile handset is discussed in [10] by presenting the change in diversity gain and envelope correlation with angle of inclination of the antenna and its distance from the head. Very limited amount of work has been done so far to investigate and quantify the diversity performance for body-centric wireless communication channels and specifically for on-body channels. [11] and [12] report some preliminary diversity measurements for on-body channels and [13] reports the use of diversity for Bluetooth devices. Cotton and Scanlon [14] have reported some diversity measurements with wearable antennas.

3.3 Diversity Combining Schemes

In an *N*-branch diversity receiver, the signals from the *N* diversity branches are combined to achieve a signal with improved signal to noise ratio. The diversity combining can be done in four common ways [3] namely, Switched Combining (SWC), Selection Combining (SC), Equal Gain Combining (EGC), and Maximal Ratio Combining (MRC). A brief description of each scheme is given below. The combining can be done before or after the detection stage, thus referred to as pre-detection or post-detection combining, respectively [3]. An RF combiner circuit may be used at the RF stage to avoid using a separate receiver for each diversity branch thus minimizing the cost and size of the diversity receiver [8]. Conversely, a separate receiver circuit is needed for each branch.

In most of the communication systems, linear combiners are used, where signals from various branches are weighted individually and then added [3 and 4]. Assume an *N*-branch diversity receiver, i.e., having *N* receiving antennas. The simplified block diagram of the diversity combiner is shown in Fig. 3.4. In general, the combined signal, *y(t),* achieved from superposition of *N* branches is [3]:

$$y(t) = \sum_{i=1}^{N} a_i r_i(t) \tag{3.3}$$

where $r_i(t)$ is the received signal at the i^{th} antenna, $y(t)$ is the diversity combined signal at the output of the combiner, and a_i is the scaling factor or the weight of the i^{th} branch signal.

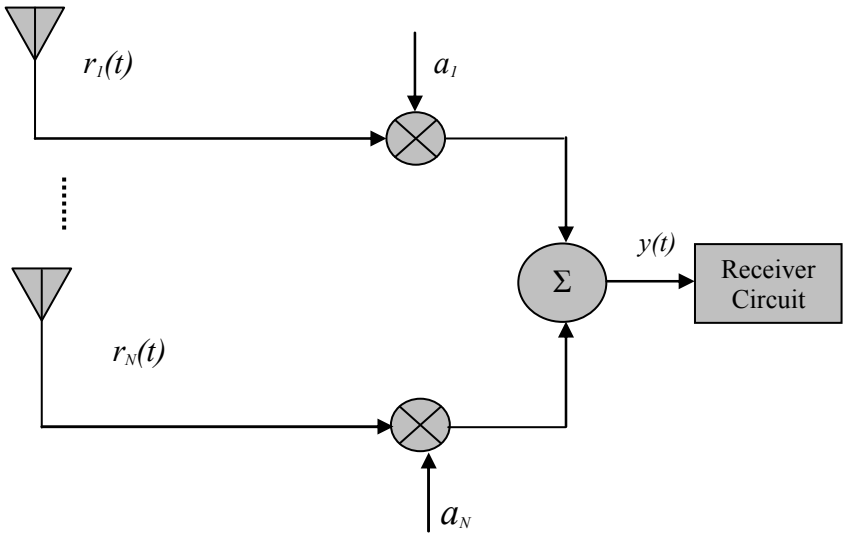

Fig. 3.4: Simplified block diagram of a diversity combiner at RF stage

In switched combining, the branch with SNR higher than a pre-defined threshold value is selected as an output of the combiner and connected to the rest of the receiver circuit. This branch signal is used until its SNR goes below the threshold. In practical systems, it is difficult to measure the SNR so the branch with highest signal power plus noise power is selected [3]. Thus, in eq. (3.3), only one value of the weight a_i among the N values is 1 and the rest are 0. All the branches are then scanned in a specific order until the branch with signal plus noise value higher than the threshold is sensed. This process is then repeated. In the context of eq. (3.3), the weight a_i is defined as:

$$a_i = \begin{cases} 1, & SNR_i \geq T \\ 0, & SNR_i < T \end{cases} \tag{3.4}$$

where SNR_i is the SNR of the i^{th} branch and T is the pre-defined threshold value.

Selection combining implements the same concept of switching but in a more sophisticated way. Rather than switch-and-stay-connected to a branch, all the branch signals are scanned instantaneously and the branch with the highest SNR is selected. The selection decision is taken instantaneously rather than based on a threshold value. If at any particular time instant, branch j has the highest SNR, the weight a_i in this case can then be defined as [15]:

$$a_i = \begin{cases} 1, & i = j \\ 0, & i \neq j \end{cases} \tag{3.5}$$

The MRC and EGC use the combined effect of all the signals. In these two techniques, the signals are weighted and then added. Before combining, the branch signals must be cophased. Cophasing of the branch signals in a two-branch diversity receiver can be done by adjusting the phase of one branch signal according to the relative phase difference between the two branch signals, as shown in Fig. 3.5 [3]. Other methods of cophasing are also given in [3].

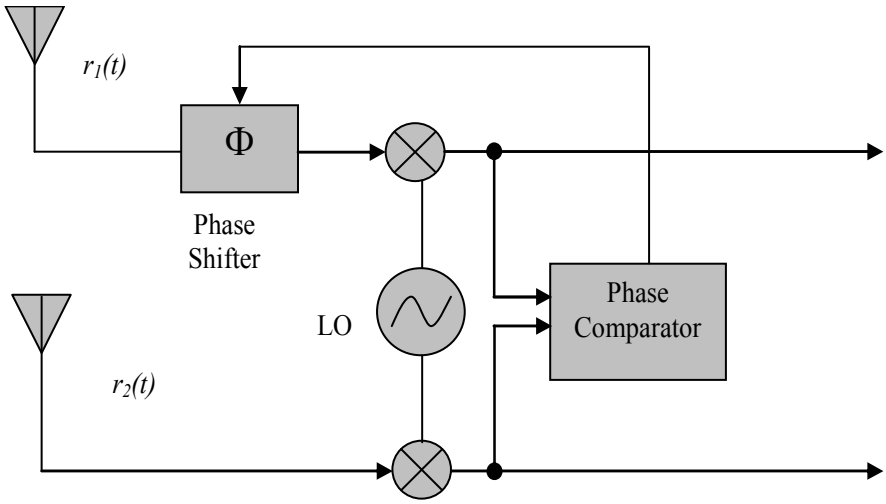

Fig. 3.5: Cophasing circuit for a two-branch diversity receiver [3]

EGC is simple in a sense that the weight for all the branches is set to 1, i.e., all the branch signals are simply added together. Assuming that the cophasing has been done, the weight for EGC is, a_i =1 in eq. (3.3).

In MRC, first proposed by Kahn and termed as ratio squarer [16], branch signals are weighted proportional to their signal voltage to noise power ratio such that the output is the sum of their SNR. The weight a_i in eq. (3.3) is thus directly proportional to the

RMS value of the branch signal and inversely proportional to the average noise power at the i^{th} branch [4, 15], i.e.

$$a_i = \frac{r_{i(RMS)}}{< n_i^2 >} \tag{3.6}$$

where $r_i(RMS) = \sqrt{< r_i^2 >}$ is the RMS value of the signal and $<n_i^2>$ is the average noise power at the i^{th} branch.

The simplified expressions to obtain the diversity-combined signal with SC, EGC and MRC for an N-branch diversity combiner are given in [17] as:

$$SC(t) = \max(r_1(t), r_2(t), \ldots\ldots r_N(t)) \tag{3.7}$$

$$EGC(t) = \frac{(r_1(t) + r_2(t) + \ldots\ldots r_N(t))}{\sqrt{N}} \tag{3.8}$$

$$MRC(t) = \sqrt{(r_1^2(t) + r_2^2(t) + \ldots\ldots r_N^2(t)} \tag{3.9}$$

where $r_i(t)$ is the received signal envelope at the i^{th} branch. More details and the probability distribution functions of the diversity combining techniques are given in [3, 15]. The derivation of equations (3.8 and 3.9) can be found in Appendix B.

Amongst all the combining schemes, selection combining and switched combining are the simplest and cheapest methods. They do not rely on the phase information of the received signals and are thus easy to implement. The performance is though not as good as the EGC and MRC schemes. MRC is the optimum combining technique in terms of the diversity improvement [4] but is complicated and expensive.

3.4 Correlation of the branch signals

The performance of a diversity receiver greatly depends upon the correlation between the received signals at the diversity branches. Low correlation is desirable as it assures that the branch signals fade differently. A correlation coefficient of 0.7 is considered suitable for most of the mobile communication scenarios [4]. Correlation coefficient can be used in three different forms, the power correlation coefficient, ρ_p, the envelope correlation coefficient, ρ_e, and the complex signal correlation coefficient, ρ_s. The complex signal correlation coefficient is useful in system design as it contains both the phase and amplitude correlation, whereas the power correlation coefficient gives a good insight of the correlated power in the diversity branches. For a two-branch diversity system, the correlation coefficients can be computed as [17]:

$$\rho_s = \frac{\sum_{k=1}^{N} V_1(k) V_2^*(k)}{\sqrt{\sum_{k=1}^{N} V_1(k) V_1^*(k)} \sqrt{\sum_{k=1}^{N} V_2(k) V_2^*(k)}} \tag{3.10}$$

$$\rho_p = \frac{\sum_{k=1}^{N} S_1(k) S_2(k)}{\sqrt{\sum_{k=1}^{N} S_1(k) S_1(k)} \sqrt{\sum_{k=1}^{N} S_2(k) S_2(k)}} \tag{3.11}$$

$$\rho_e = \frac{\sum_{k=1}^{N} (r_1(k) - \overline{r_1})(r_2(k) - \overline{r_2})}{\sqrt{\sum_{k=1}^{N} (r_1(k) - \overline{r_1})^2} \sqrt{\sum_{k=1}^{N} (r_2(k) - \overline{r_2})^2}} \tag{3.12}$$

where S_1 and S_2 represent the zero-meaned received power signals, V_1 and V_2 represent the zero-meaned complex voltage signals, and r_1 and r_2 are the received short-term fading signal envelopes. $\overline{r_i}$ is the mean value of the signal envelope at the i^{th} branch and * represents the complex conjugate. In Rayleigh fading environment, $|\rho_s|^2 = \rho_e$ and $\rho_e \approx \rho_p$ [4], but this assumption may not be valid for on-body channels with fading distribution other than Rayleigh. This has been verified by looking at the correlation coefficients of the measured on-body channels given in the forthcoming chapters.

3.5 Diversity Gain

Diversity gain (DG) is a figure of merit to measure the improvement due to the use of diversity. It is an improvement in the signal strength, or SNR, or bit error rate (BER), over a single antenna with no diversity, at a certain level of outage probability [4, 9, 18]. It is a common practice to calculate the diversity gain as a difference in signal levels (or SNR) of the diversity combined signal and the strongest branch signal (taken as a reference) among all the diversity branches at

some outage probability, as depicted in eqs. (3.13) and (3.14). Probability level of 10% and 1% are commonly used. Fig. 3.6 shows the Cumulative Distribution Function (CDF) of two branch signals and a diversity combined signal with diversity gain calculated at 1% probability.

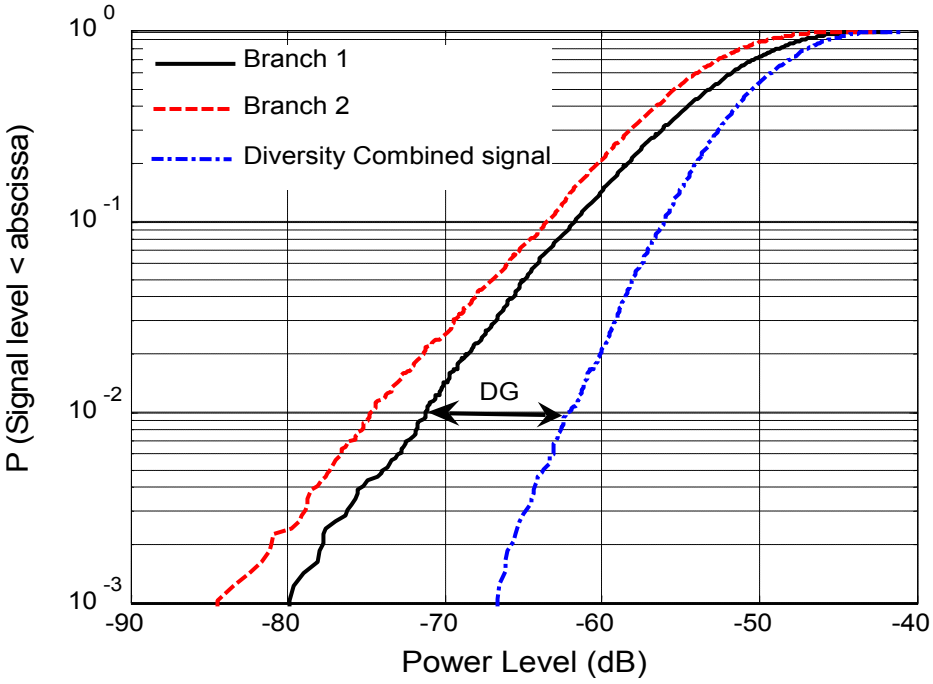

Fig. 3.6: Diversity gain calculation

$$DG = \frac{P_{div}}{P_{ref}} \tag{3.13}$$

$$DG = P_{dBdiv} - P_{dBref} \quad \text{(dB)} \tag{3.14}$$

where P_{div} is the power level of the diversity combined signal and P_{ref} is the power level of the reference signal (which is strongest among the branch signals) at a

certain probability level. P_{dBdiv} and P_{dBref} are the same values expressed in dB. These expressions can also be presented in terms of SNR or BER. Diversity gain greatly depends upon the correlation among the branch signals. It is, perhaps a common thought that the more the branches are uncorrelated, the higher is the diversity gain. But the power imbalance among the received branch signals is another factor affecting the diversity gain. If the power difference among the branch signals is more, the diversity combiner will favour the strongest signal for most of the time and hence, no or very small diversity gain will be achieved. If the power imbalance is very high, the performance of EGC becomes worse than that of SC because the branch with very low power level introduces additional noise and very less improvement to the desired signal is achieved, which results in overall decrease in the output SNR [17]. The variation in diversity gain with correlation and power imbalance has been depicted in [7, 17, and 18]. Turkmani *et. al.* has established an empirical relationship between the DG, correlation coefficient and power imbalance in [17]. The maximum achievable diversity gain at 1% probability for a two branch diversity system is, 10 dB using selection combining and 11.5 dB using MRC, with zero power imbalance and no correlation among the branches in a Rayleigh independent and identically distributed (IID) channel [3].

3.6 Types of Diversity

Diversity can be achieved in various ways, e.g. time diversity, frequency diversity, space (spatial) diversity, polarization diversity, and pattern (angle) diversity [3]. A brief description of the diversity types is given below.

3.6.1 Time Diversity

In this scheme of diversity, the amplitude samples of the signal are transmitted in different time slots. If the separation between the time slots is sufficient, the sequential amplitude samples of the fading signal will be uncorrelated [3]. The time separation should be at least the reciprocal of the fading bandwidth [3].

3.6.2 Frequency Diversity

As explained in section 3.1, if the spacing between two frequency components of a signal is greater than the coherence bandwidth, the two components experience uncorrelated fading. Keeping in view this fact, if different frequencies are used for the diversity branches, another type of diversity, called frequency diversity, can be achieved. The spacing between frequencies must be greater than the coherence bandwidth [3]. Frequency diversity utilizes much more bandwidth than the other diversity schemes and a separate transmitter-receiver pair is required for each branch.

3.6.3 Space Diversity

This diversity scheme uses multiple antennas on transmit and/or receive side to get diversity branches distributed in space. Two or more identical antennas are separated by certain spacing between them to achieve a space diversity antenna. This technique does not consume extra spectrum [3, 4] and the basic issue is the spacing of the antennas, which determines the amount of mutual coupling between the adjacent branch antennas and the correlation among the branch signals. The spacing between the antennas should be such that the mutual coupling and correlation is minimized

and the received signals on the antenna are faded independently. A spacing of λ/2 is sufficient for most of the applications [3, 4].

The correlation between two branch signals varies with the spacing between the antennas in a space diversity receiver. Clarke [19] has derived the relationship between the correlation and the antenna spacing.

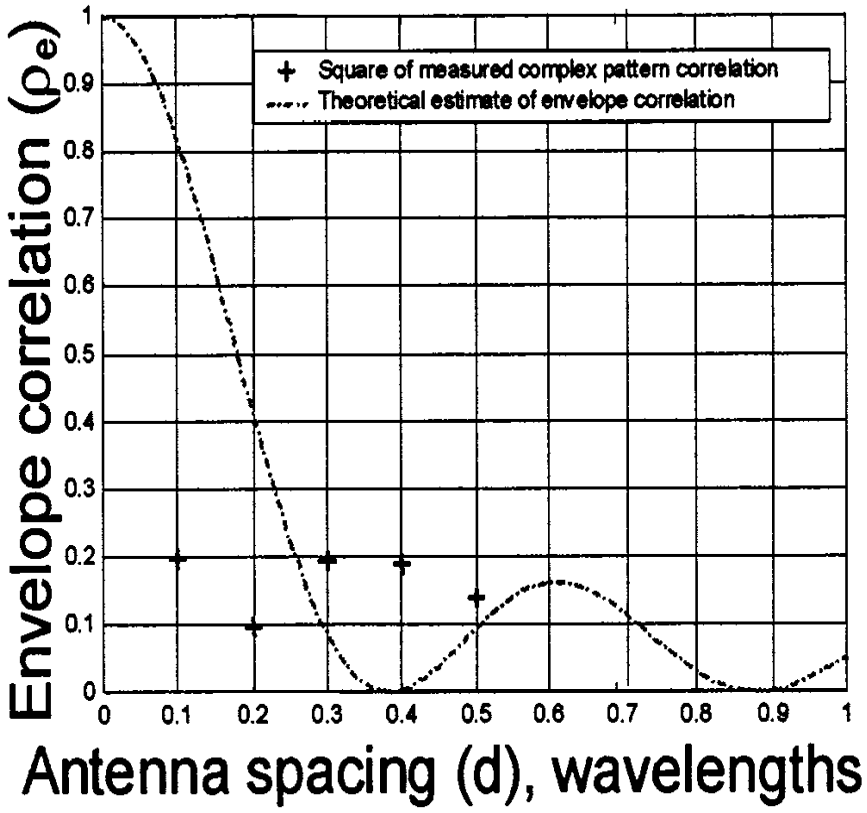

Fig. 3.7: Correlation coefficient variation with antenna spacing [9]

For two omni-directional antennas spaced apart by distance, *d*, the envelope correlation coefficient varies with antenna spacing as [7, 19]:

$$\rho_e = J_o^2 \left(\frac{2\pi d}{\lambda} \right) \tag{3.15}$$

where J_o is the zero-order Bessel function of the first kind, and λ is the wavelength. The basic assumption for this expression is that the angle of arrival in azimuth is uniform and no angle of arrival in elevation. However, if the antennas are too close to each other, the patterns of the antennas are distorted due to mutual coupling and the correlation decreases [7]. Fig. 3.7 shows the relationship of correlation coefficient and the antenna spacing for the theoretical case and a measured case [7].

3.6.4 Pattern Diversity

If directional antennas are used either at transmitter or at receiver, another kind of diversity scheme can result, called radiation pattern diversity or angle diversity. The diversity branches are produced by directing the radiation pattern in different angles. The most desirable situation is where the overlap between the adjacent radiation patterns is minimal and the combination gives an omni-directional pattern. The signals radiated in different directions undergo different fading and hence are uncorrelated. In most cases, an array with appropriate beam switching is used at either transmitter, or receiver, or both. Pattern diversity is more effective in situation when the angle of arrival has more spread and variation [6].

3.6.5 Polarization diversity

This diversity scheme exploits the fact that if two signals are transmitted or received with orthogonal polarization, the fading in the signals is uncorrelated [3, 4]. Thus,

two antennas with different polarization or a single dual-polarized antenna can be used to constitute a two-branch diversity system. It has an advantage over space diversity that it does not always require two antennas separated by some distance, as a single dual-polarized antenna can be used to implement it and thus offers size and cost reduction compared to the space diversity receiver [17]. In case of a single polarization transmitted, the difference between the co-polar and the cross-polar components received at the receiver is supposed to be very high if the environment does not provide significant depolarization. This difference, often called the cross-polarization discrimination (XPD), is required to be lower for polarization diversity to work effectively; otherwise, the power imbalance between the two diversity branches will be large, resulting in low diversity gain. Full benefits of polarization diversity can be achieved in a scenario where the scattering environment causes significant amount of depolarization of the transmitted signal and hence the XPD at the receiver is low. Alternately, the antennas can be inclined such that the level of both received polarizations is comparable. Turkmani *et. al.* [17] has investigated the impact of angle of inclination of the antennas on the correlation and diversity gain for polarization diversity and a comparison of space and polarization diversity is also given.

3.6.6 Comparison of Space, Pattern, and Polarization diversity

A good comparison of space, pattern, and polarization diversity is presented in [7]. It has been reported that polarization diversity can give up to 12 dB diversity gain in a certain scenario, whereas, space and pattern diversities perform better in other situations. Space diversity is more useful than other types of diversities in open

terrain or situations where the incoming angles of arrival are uniform. In a situation where there is not much depolarization of the transmitted wave due to the environment, or in LOS scenario, the XPD may be large for polarization diversity antennas and space or pattern diversity outperform the polarization diversity. Space and polarization diversity techniques are compared in [7, 9, 17] and it has been concluded that polarization diversity can perform equally well compared to space diversity in an NLOS scenario, where the terminals are oriented randomly. Polarization diversity antennas have another advantage over the space diversity antennas, which is the small size. As discussed above, polarization diversity antenna can be designed as a single antenna with dual polarization, whereas, space diversity requires more than one antenna separated by some space. The significance of polarization diversity for indoor scenario has been shown in [20, 21]. It has been shown in [21] that in Rician fading environment, despite relatively high correlation compared to the Rayleigh fading environment, the diversity gains with polarization diversity are reasonable. Pattern diversity performs similar to the space diversity in rich cluttered indoor environment. A comparison of space and pattern diversity is presented in [22, 23]. Mattjaiijssen *et. al*. [23] has shown that pattern diversity has a slight edge over the space diversity antennas due to approximately equal performance but more compact size. In most of the cases, the polarization diversity and pattern diversity cannot be distinguished separately. Two antennas with different radiation patterns usually have different polarization characteristics as well. Similarly, it is very difficult to design a polarization diversity antenna with different polarizations but identical patterns in the two branches. For this reason, pattern diversity and polarization diversity are usually mentioned as a combination.

3.7 Diversity Antenna Design

There are various issues related to the design of antennas for use in diversity systems. Some of these are general issues such as size, mutual coupling, radiation pattern, and radiation efficiency etc., whereas, some are specific to the on-body channels, like specific absorption rate (SAR), detuning due to placement on the body, compactness and structure, etc. Some of the issues are related to a specific type of diversity, like spacing between the antennas and similar radiation patterns for space diversity systems, XPD for polarization diversity, and radiation pattern shape and the overlap between the patterns of the branches for pattern diversity systems.

The diversity antenna must be as compact as possible due to the trend of miniaturization of modern communication devices. For body-worn devices, it is desired to be low-profile as well, along with the small size. One of the limiting factors on the overall size of the diversity antenna is the spacing between the antennas. This is not an issue for polarization diversity but an important aspect of the space diversity and up to some extent, the pattern diversity. If the spacing between the antennas for diversity branches is reduced, the mutual coupling between the antenna elements is increased. In principle, high mutual coupling can increase the correlation between the branch signals and can decrease the capacity gain and the diversity performance. High mutual coupling can significantly distort the radiation pattern of the antenna elements and can reduce the radiation efficiency of the elements. However, it has been reported in the literature that for very closely spaced antennas, mutual coupling can actually cause de-correlation of the branch signals and thus increase the capacity [7, 24-25]. In general, the antenna should be designed such

that it is compact, have low mutual coupling and low correlation between the elements, and has high radiation efficiency.

Among the other antenna design issues, the two main issues related specifically to space diversity are the antenna spacing and the radiation patterns. For pure space diversity application, the radiation patterns of all the elements should be approximately the same. A spacing of half wavelength or more is usually considered suitable for most of the applications. Similarly, the design issues specifically associated with the pattern diversity antennas is the shape of the radiation patterns and the overlap between the patterns of the elements. Ideally, there should be no overlap between the radiation patterns of the elements and the radiation patterns should be such that the power imbalance in the diversity branches is minimized. For polarization diversity, the XPD should be kept as low as possible to minimize the power imbalance.

For on-body applications, the antennas must be designed to give minimum SAR. The calculation of SAR values is beyond the scope of this thesis; however, effort has been made to minimize SAR by suitable ground plane of the antennas to reduce back radiation. Low-profile antennas are desirable because of the small and thin size of the body-worn devices. The antennas can detune in some cases when mounted on the body. Thus, care should be taken for narrowband antennas to keep the reflection coefficient of the antenna low enough at the desired frequency when mounted on the body. It has been proved in [26] that the wave propagates along the surface of the body as creeping wave and is attenuated much more rapidly compared to the free

space attenuation. Also, the wave polarized parallel to the surface of the body attenuates more than the perpendicularly polarized wave. Therefore, the polarization should be kept in mind while designing antennas for on-body applications. A variety of diversity antenna designs are available for space, pattern, polarization diversity applications for the mobile communication devices [27, 28, 29] and address the issues discussed above one way or the other depending upon the application and type of diversity.

3.8 Diversity for Interference Rejection

Co-channel interference is a concern for mobile communication systems, especially at the edge of cells with two nearby cells using the same frequency band. It becomes even more significant for Personal Communication Systems (PCS) and body-centric communications when two body-area networks (BAN) operate in the near vicinity of each other. The mobility of persons, carrying the body-worn devices, can introduce large amount of interference in other BANs or PCS terminals operating in the same frequency band. In mobile cellular network, co-channel interference can be minimized by keeping the transmitted power within a range where it cannot reach the closer cell using the same frequency. Unlike this situation, in PCS or BAN applications, it is very hard to keep a safe distance between the moving terminals to avoid interference. Specifically in BAN, the mobile terminals carrying transmitters and receivers can operate very close to other mobile terminals carrying similar devices. Thus, interference rejection becomes more important in this scenario. Among the many other interference rejection techniques, receive diversity is a way to reject the interference and maximize the output SINR. Just like the diversity

combining to maximize the SNR, the received branch signals can be combined in an optimum way to increase the output SINR and thus reject the interference. This combining technique is usually referred to as Interference Rejection Combining (IRC). Various IRC algorithms have been proposed in the literature [30-32]. The received branch signals are scaled with appropriate weight factors and then combined. The weights are estimated from the received signals' correlation and are updated adaptively through an adaptive feedback loop. In adaptive beamforming, the maximum beam direction is steered along the direction of arrival of the desired signal and the nulls are steered along the direction of interferers. Adaptive beamforming and smart antenna techniques are beyond the scope of this thesis. The final expressions of Weiner-Hopf solution [33, 34] and the optimum combining [31, 32] are used for interference cancellation. Further details of the IRC algorithms used, along with a new algorithm for interference rejection, are given in Chapter 8.

3.9 Multiple-Input Multiple-Output (MIMO) systems

The high data rate demand in current and future wireless communication devices requires high capacity links to be established between the transmitting and receiving devices. The use of multiple antennas at both ends, i.e., the transmitter and receiver, commonly known as Multiple-Input Multiple-Output (MIMO) system, has been known to increase the capacity of the system in a highly scattering environment providing rich multipath. MIMO can provide joint transmit-receive diversity as compared to transmit diversity or receive diversity only. For a system with m transmitting and n receiving antennas, the n x m MIMO system can provide diversity order of nm. This aspect of the MIMO, however, is not addressed in this thesis and is

left for future work. The work on MIMO for on-body channels in this thesis emphasizes on the channel capacity. A MIMO system exploits the multipath to achieve an increase in channel capacity by creating multiple parallel channels. The number of parallel channels is equal to minimum of *n* and *m,* hence providing spatial multiplexing gain of *min(n,m)* over a SISO system [35] with no additional RF power and bandwidth.

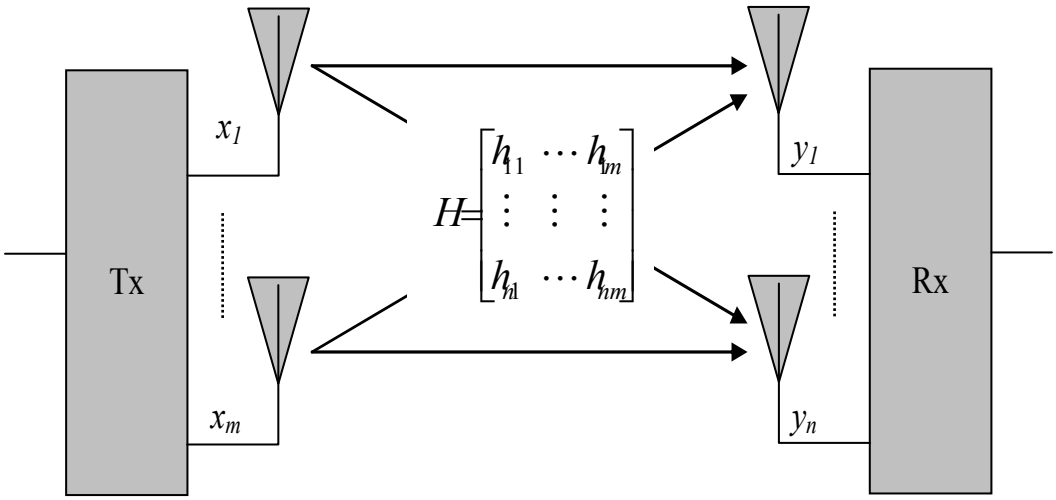

Fig. 3.8: An *n*x*m* MIMO system with *m* Tx and *n* Rx antennas

For a narrowband, single-user MIMO channel with *m* transmit and *n* receive antennas, as shown in Fig. 3.8, the input-output relationship between the Tx and Rx is expressed as [35]:

$$Y = HX + N \tag{3.16}$$

where X is the [m x 1] transmitted vector, Y is the [n x 1] received vector, N is receive additive white Gaussian noise (AWGN) vector, and H is the n x m channel matrix. For a 2x2 MIMO channel, H can be written as [35]:

$$H = \begin{bmatrix} h_{11} & h_{12} \\ h_{21} & h_{22} \end{bmatrix} \tag{3.17}$$

where h_{ij} is the complex random variable representing the channel-fading coefficients or the complex subchannel gains from transmitting antenna j to receiving antenna i, as shown in Fig. 3.8.

If the channel is completely unknown at the transmitter, i.e., channel state information (CSI) is not available at the transmitter, the channel capacity can be expressed by eq. (3.18) given below, assuming transmitted power to be uniformly distributed among the m transmitting antennas [35, 36, 37]:

$$C = \log_2\left(\det\left[I_n + \frac{\xi}{m} H_n H_n^*\right]\right) \quad \text{bps/Hz} \tag{3.18}$$

where I_n is n x n identity matrix and ξ is the average signal-to-noise ratio per receive antenna. Here, H_n is the normalized channel matrix and * represents the complex conjugate transpose. Eq. (3.18) is used for the case when $n<m$. For $n \geq m$, the term $H_n H_n^*$ is replaced by $H_n^* H_n$ and identity matrix I_n is replaced by I_m [38, 39]. The normalization of H matrix is usually done such that the average power per element of

the matrix or average power per subchannel is unity. Further details of the normalization are given in Chapter 9.

MIMO wireless channels have been studied extensively for indoor and outdoor environments. For example in [36 and 40], MIMO capacity and correlation is studied through measurements for Personal Area Networks (PAN) and BAN. The MIMO channel capacity analysis is presented for indoor LOS environment for WLAN applications in [41]. Reference [42] presents similar analysis for Broadband-Fixed Wireless Access (BFWA) and WLAN applications with measurements at 2.4 GHz in an indoor environment. The significance of MIMO for indoor channels at 1800 MHz with indoor and outdoor base stations is discussed in [43] by extensive measurement campaign, whereas, [44] gives a simulation model based analysis for 3GPP-3GPP2 spatial channel model. Foschini and Gans gave a strong theoretic approach and the basic issues related to multiple antennas in [37].

In contrast to the theoretic spectral efficiencies described for MIMO systems in [35, 37], the maximum throughput of a wireless MIMO channel for practical systems is limited by many factors, like the channel statistics, correlation, SNR, the distance between the antennas, and the number of antennas at each side etc. For a fixed number of transmitting and receiving antennas, the two important factors are the average received SNR and the correlation among the subchannels. The higher the received SNR, the higher will be the channel capacity. LOS links usually exhibit high SNR but on the other hand, the spatial correlation among the subchannels is reduced due to low scattering. A common perception is that MIMO is not useful for

LOS links or Rician fading channels due to the strong correlations. It has been shown in [45-48] that at a fixed receive SNR, the MIMO channel capacity decreases with increase in the Rician K-factor. Nevertheless, some studies [36, 40, 41] have shown that despite the LOS link, the capacity increase with MIMO is significant in the Rician fading environment.

REFERENCES

[1] R Prasad, "Universal Wireless Personal Communications", *Artech House, London, 1998.*

[2] B H Fleury, "An Uncertainty Relation for WSS Processes and Its Application to SWWUS Systems", *IEEE Transactions on Communications, Vol. 44, No., 12, December, 1996.*

[3] W. C. Jakes, "Microwave Mobile Communications", *New York Wiley, 197.*

[4] R G. Vaughan, J Bach Andersen, "Antenna Diversity in Mobile Communications", *IEEE transaction On Vehicular Technology, Vol. VT-36. No. 4 Nov 1987.*

[5] J.Gong, J.F.Hayes and M.R.Soleymani, "Comparison of Capacities of the Transmit Antenna Diversity with the Receive Antenna Diversity in the MIMO Scheme*", in Proc. IEEE CCECE, May 4–7, 2003, vol. 1, pp. 179–182.*

[6] P. Irazoqui-Pastor, J. T. Bernhard, “Examining the Performance Benefits of Antenna Diversity Systems in Portable Wireless Environments”, *IEEE Antenna Applications Symposium, Allerton Park, Sep 15-17, 1999.*

[7] C B. Dietrich, Jr., K Dietze, J. R Nealy, and W L. Stutzman, “Spatial, Polarization, and Pattern Diversity for Wireless Handheld Terminals”, *IEEE Transactions on Antennas and Propagation, Vol. 49, No. 9, September 2001.*

[8] M. Karaboikis, C. Soras, G. Tsachtsiris and V. Makios, “Three-branch Antenna Diversity Systems on Wireless Devices Using Various Printed Monopoles", *2003 IEEE International Symposium on Electromagnetic Compatibility*, Istanbul (May 11-16, 2003).

[9] J S. Colburn, Y Rahmat-Samii, M A. Jensen, and G J. Pottie, “Evaluation of Personal Communications Dual-Antenna Handset Diversity Performance”, *IEEE Transactions On Vehicular Technology, Vol. 47, No. 3, August 1998.*

[10] K Ogawa, T Matsuyoshi, and K Monma, “An Analysis of the Performance of a Handset Diversity Antenna Influenced by Head, Hand, and Shoulder Effects at 900 MHz: Part II—Correlation Characteristics”, *IEEE Transactions on Vehicular Technology, Vol. 50, NO. 3, May 2001.*

[11] A.A. Serra, P. Nepa, G. Manara, P.S. Hall, “Experimental Investigation of Diversity Techniques for On-Body Communication Systems”, *IET*

Seminar: Antennas & Propagation for Body- Centric Wireless Communications, April, 2007.

[12] A.A. Serra, P. Nepa, G. Manara, P.S. Hall, "Diversity Measurements of On-body Communication Systems", *IEEE Antennas and Wireless Propagation Letters, Vol. 6, 2007.*

[13] F Bektas, B Vondra, P E. Veith, L Faltin, A P Arpad L. Scholtz, "Bluetooth Communication Employing Antenna Diversity", *Proceedings of the Eighth IEEE International Symposium on Computers and Communication (ISCC'03), 2003.*

[14] S. L. Cotton & W. G. Scanlon, "Indoor Channel Characterization for a Wearable Antenna Array at 868 MHz", *IEEE Wireless Communications & Networking Conf., Las Vegas, April 2006.*

[15] D. G. Brennan, "Linear Diversity Combining Techniques", *Proceedings of the IEEE, Vol. 91, No. 2, February 2003.*

[16] L. R. Kahn, "Ratio Squarer," *Proc. IRE, vol. 42, p. 1704, November 1954*.

[17] M. D. Turkmani, A. A. Arowojolu, P. A. Jefford, and C. J. Kellett "An Experimental Evaluation of the Performance of Two-Branch Space and Polarization Diversity Schemes at 1800 MHz", *IEEE Transactions on Vehicular Technology, Vol. 44, No. 2, May 1995.*

[18] Per-Simon Kildal, K Rosengren, "Electromagnetic Analysis of Effective and Apparent Diversity Gain of Two Parallel Dipoles*", IEEE Antennas and Wireless Propagation Letters, Vol. 2, 2003.*

[19] R. H. Clarke, "A Statistical Theory of Mobile-Radio Reception," *Bell Systems Tech. Journal, pp. 957–1000, July–Aug. 1968.*

[20] L.C. Lukama, D.J. Edwards and A. Wain, "Application of Three-branch Polarization Diversity in the Indoor Environment", *IEE Proc.-Communications, Vol. 150, No. 5, October 2003.*

[21] R M. Narayanan, K Atanassov, V Stoiljkovic, and G R. Kadambi, "Polarization Diversity Measurements and Analysis for Antenna Configurations at 1800 MHz", *IEEE Transactions On Antennas And Propagation, Vol. 52, No. 7, July 2004.*

[22] P L. Perini, and C L. Holloway, "Angle and Space Diversity Comparisons in Different Mobile Radio Environments", *IEEE Transactions on Antennas and Propagation, Vol. 46, No. 6, June 1998.*

[23] P Mattheijssen, M H. A. J. Herben, G Dolmans, and L Leyten, "Antenna-Pattern Diversity vs. Space Diversity for Use at Handhelds", *IEEE Transactions on Vehicular Technology, Vol. 53, No. 4, July 2004.*

[24] T. Svantesson and A. Ranheim, "Mutual Coupling Effects on the Capacity of Multi-Element Antenna Systems," *in Proc. IEEE Int. Conf. Acoustics, Speech, and Signal Processing (ICASSP)'01, vol. 4, Salt Lake, UT, May 2001, pp. 2485–2488.*

[25] R. G. Vaughan and N. L. Scott, "Terminated In-Line Monopoles for Vehicular Diversity," *in Proc. Int. Union of Radio Science (USRI) Triennial Symp. Electromagnetic Theory, Sydney, Australia, Aug. 1992, pp.111–113.*

[26] P S Hall, Y Hao, editors of, "Antennas and Propagation for Body-Centric Wireless Communications", *Artech House, London, 2006*.

[27] A.Khaleghi, J.C.Bolomey, A.Azoulay, "A Pattern Diversity Antenna with Parasitic Switching Elements for Wireless LAN Communications", *IEEE 2nd International Symposium on Wireless Comm Systems, 5-7 Sep, 2005.*

[28] A Forenza, and R W. Heath, Jr, "Benefit of Pattern Diversity via Two-Element Array of Circular Patch Antennas in Indoor Clustered MIMO Channels", *IEEE Transactions On Comms, Vol. 54, No. 5, May 2006.*

[29] R Vaughan, "Switched Parasitic Elements for Antenna Diversity", *IEEE Transactions on Antennas and Propagation, Vol. 47, No. 2, February 1999.*

[30] J Karlsson and J Heinegard, "Interference Rejection Combining for GSM", *in Proc. of 5th IEEE Int. Conf. on Universal Personal Comm., 1996.*

[31] D Bladsjo, A Furuskar, S Javerbring, E Larsson, "Interference Cancellation using Antenna Diversity for EDGE-Enhanced Data Rates in GSM and TDMA/136", *in Proc. of the 50th IEEE Vehicular Tech Conf., Fall 1999.*

[32] J H Winters, "Optimum combining in Digital Mobile Radio with Co-channel Interference", *IEEE Journal on selected areas in communications, Vol. SAC-2, No. 4, July, 1984.*

[33] R.T. Compton, “Adaptive Antennas, Concepts and Performance”, *Prentice-Hall Inc., New Jersey, 1988*.

[34] M Melvasalo, P Jänis, V Koivunen, “MMSE Equalizer and Chip Level Inter-Antenna Interference Canceller for HSDPA MIMO Systems”, *63rd IEEE Vehicular Technology Conference, VTC Spring 2006, vol. 4, pp. 20082012, Melbourne, Australia, 2006.*

[35] E Biglier, R Calderbank, A Constantnides, A Goldsmith, A Paulraj, H. V Poor, “ MIMO Wireless Communications”, *Cambridge Uni. Press, New York, 2007.*

[36] D Neirynck, C. Williams, A Nix, M. Beach, “Exploiting Multiple-Input Multiple-Output in the Personal Sphere”, *IET Microwaves, Antennas and Propagations, Vol. 1, No. 6, Dec. 2007.*

[37] GJ Foschini, MJ Gans, “On limits of Wireless communications in Fading Environment When Using Multiple Antennas”, *Wireless personal communications 6: pp 311-335, March 1998.*

[38] I Hen, “MIMO Architecture for Wireless Communication”, *Intel Technology Journal, Vol. 10, Issue 2, May 2006.*

[39] B Vucetic, J Yuan, “Space Time Coding”, *pp. 7-9, John Wiley & Sons, 2003.*

[40] D Neirynck, C Williams, A Nix, M Beach, "Experimental Capacity Analysis for Virtual Array Antennas in Personal and Body Area Networks", *International workshop on Wireless Adhoc Networks, May 2005*.

[41] K Sakaguchi, HY Chua, K Araki, "MIMO Channel Capacity in an Indoor Line-of-Sight Environment*", IEICE Transactions on Comm. Vol. E88-B, No. 7, July 2005.*

[42] R Jaramillo E, O Fernandez, RP Torres, "Empirical Analysis of 2x2 MIMO Channel in Outdoor-Indoor Scenarios for BFWA Applications", *IEEE Antennas and Propagation Magazine, Vol. 48, No. 6, Dec. 2006.*

[43] L Garcia, N Jalden, B Lindmark, P Zetterberg, L Haro, "Measurements of MIMO Indoor Channels at 1800 MHz with Multiple Indoor and Outdoor Base Stations", *EURASIP Journal on Wireless comms and Networking, Vol. 2007, Article ID 28073*.

[44] S Pan, S Durrani, M E Bialkowski, "MIMO Capacity for Spatial Channel Model Scenario", *2007 Australian Communication Theory Workshop, Australia, 5-7 February, 2007*.

[45] H Ozcelik, M. Herdin, R. Prestros, E Bonek, "How MIMO Capacity is Linked With Single Element Fading Statistics*", International Conference on Electromagnetics in Advanced Applications, Torino, Italy, 8-12 Sep. 2003, pp. 775-778.*

[46] Z Tang, A S Mohan, "Experimental Investigation of Indoor MIMO Ricean Channel Capacity", *IEEE Antennas and Wireless Prop letters, Vol. 4, 2005.*

[47] S K Jayaweera, H Vincent Poor, "MIMO Capacity Results for Rician Fading Channels", *IEEE Global Telecommunications Conference, 2003. GLOBECOM, Volume 4, 1-5 Dec. 2003 Page(s): 1806 – 1810.*

[48] I Sarris, A R. Nix, "Maximum MIMO Capacity in Line-of-Sight", *Fifth International Conference on Information, Communications and Signal Processing, 2005.*

Chapter 4

Measurement Setup and Procedure

4.1 Overview

To investigate and analyze the performance of multiple antennas for body-centric wireless communication channels, various approaches can be adopted. It can either be predicted through detailed simulations with antennas on a full body numerical phantom or can be investigated by real time measurements of the on-body propagation channels with antennas mounted on a human subject. The third approach may be using a statistical channel model, which completely characterizes the on-body propagation channels and the environment. The first approach is very computing intensive and becomes even more so with multiple antennas mounted on a numerical phantom. It seems almost unrealistic if random body movement is introduced in the simulations, and seems much less valuable for static postures with no movements at all, as system design is typically based on statistical channel models. The third approach cannot be adopted due to the absence of a standard statistical channel model for on-body channels. Hence, on-body propagation channel measurements are useful in real environments with naturalistic movements of a real human body to quantify the significance of multiple antenna systems for body-worn devices. To do so in this work, antennas were mounted on a human subject performing various random movements. The measurements were categorized in three areas. First category was diversity measurements, which are utilized in Chapter 5, 6,

and 7. Second category was measurements for interference rejection, which is described in Chapter 8. The third category was the MIMO measurements, which are analyzed in Chapter 9. Measurement specific details like antenna sizes etc. are given in the respective chapters. The interference and MIMO measurements were performed at 2.45 GHz ISM band, whereas, the diversity performance is investigated for three frequencies, which were the two ISM, bands at 2.45 GHz and 5.8 GHz and the 10 GHz. Most of the measurements were carried out in an indoor environment with rich scattering, but some measurements were also done in an anechoic chamber and a big office environment with less scattering. Co-axial cables were used to connect the antennas mounted on the body to the measurement equipment. During the measurements a sequence of randomized activities was done that could represent all the possible types of movements. These movements are described later in this chapter with each category of measurement. The description of how the antennas were mounted on the body is given in Section 4.2. The details of the measurement equipment used are presented in Section 4.3. Section 4.4 describes the measurement setup and the details of the environment for each category of the measurement.

4.2 Mounting Antennas on the Body

Various on-body channels were selected for measurements. The subject was a male with height of 173 cm and weight of 76 kg. For each on-body channel, the transmitting antenna was placed at the waist (belt) position on the left side of the body, about 100 mm away from the body centre line. The receiving antennas were placed at right side of the chest, back in the centre, right side of the head, right wrist, and right ankle positions, thus forming five on-body channels named belt-chest, belt-

back, belt-head, belt-wrist, and belt-ankle, respectively. A pictorial view of positioning the antenna on the body is given for each on-body channel in Fig. 4.1. The belt-chest channel represents the line of sight (LOS) scenario. The belt-back channel is a good representative of the NLOS scenario. Both of these channels are static channels in which the distance between the transmitting and receiving antennas is almost constant apart from few postures. To mimic a dynamic channel, in which the path length varies randomly with movement of the body, the belt-wrist channel was selected. Most often, there are scenarios where there is partial LOS or a transition of LOS and NLOS. The belt-head and belt-ankle channels are good examples of this. Diversity analysis at 2.45 GHz is done for the five on-body channels. For other measurements, only three channels, which show significance in current application areas, were investigated. These were the belt-head, belt-chest, and belt-wrist channels. The distance between the body and the antennas mounted on the body was kept to about 7-10 mm including the clothing. The coaxial cables used during the measurement were firmly strapped to the body to minimize the effect of moving cables over the duration of the channel measurement.

(a) Tx on Waist

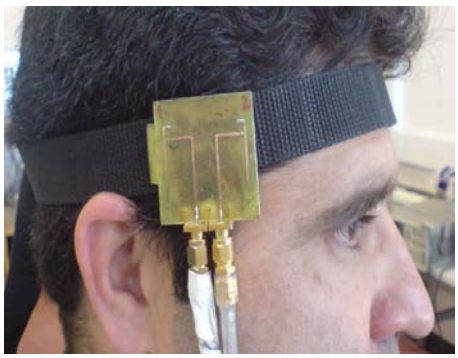

(b) Rx on Head

PTO for full caption

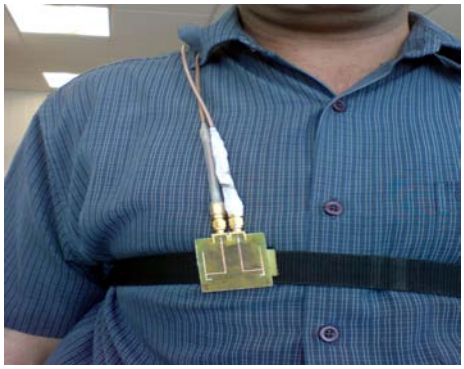

(c) Rx on Chest

(d) Rx on Back

(e) Rx on Wrist

(f) Rx on Ankle

(g) Standing Posture during the measurement

Fig. 4.1: Antennas mounted on the body

4.3 Measurement Equipment

For all the measurements, a two-port vector network analyzer (VNA), HP/Agilent 8719/20/22, was used as receiver to measure the channel gain. The VNA was controlled by computer software written by Dr. Yuriy I. Nechayev of the University of Birmingham. The data measured by the VNA was stored in a computer hard disk by the software in the form of a text file containing the magnitude (in dBm) and phase (in degrees) of the channel transfer gain S_{21}. For 2.45 GHz measurements, a signal generator, HP8640D, was used to generate the desired 2.45 GHz signal. This signal generator works only up to 4 GHz and hence could not be used for 5.8 GHz and 10 GHz measurements. During the measurements, the VNA was always calibrated to exclude the losses that incurred in the cables and thus the measured data reflected the signal measured at the ports of the antenna. The calibration also ensured that a total power of 0 dBm is transmitted by the transmitting antenna. In case of the signal generator being used, the VNA and the signal generator were synchronized by connecting the 10 MHz reference output signal from the signal generator to the reference input of the VNA.

4.4 Measurement Setup

4.4.1 Diversity measurements at 2.45 GHz

Initial diversity measurements at 2.45 GHz were carried out in an indoor environment in a typical laboratory, which was an L-shaped room, shown in Fig. 4.2, containing equipment, tables, chairs, and computers thus providing a rich multipath propagation environment. The size of one arm was 5 m x 2 m and the other arm was

7.5 m x 1.5 m. Some measurements were also done with monopole antennas in a big office environment and in an anechoic chamber in order to investigate the effect of the body movement in the absence of multipath caused by the environment. Due to the presence of metallic floor in the chamber, some multipath components were present. The transmitting antenna was connected to the signal generator generating the desired 2.45 GHz frequency signal. The two receiving antennas were connected to the two ports of the VNA calibrated in tuned dual channel receiver mode. The setup is shown in Fig. 4.3. The VNA was set to a single frequency sweep at 2.45 GHz frequency with a total of 1601 points in one sweep. The sampling time was set to 10 ms thus the time for one sweep was about 16 s. A total of 10 such sweeps were carried out, thus a total of 16010 points were collected for each channel measurement.

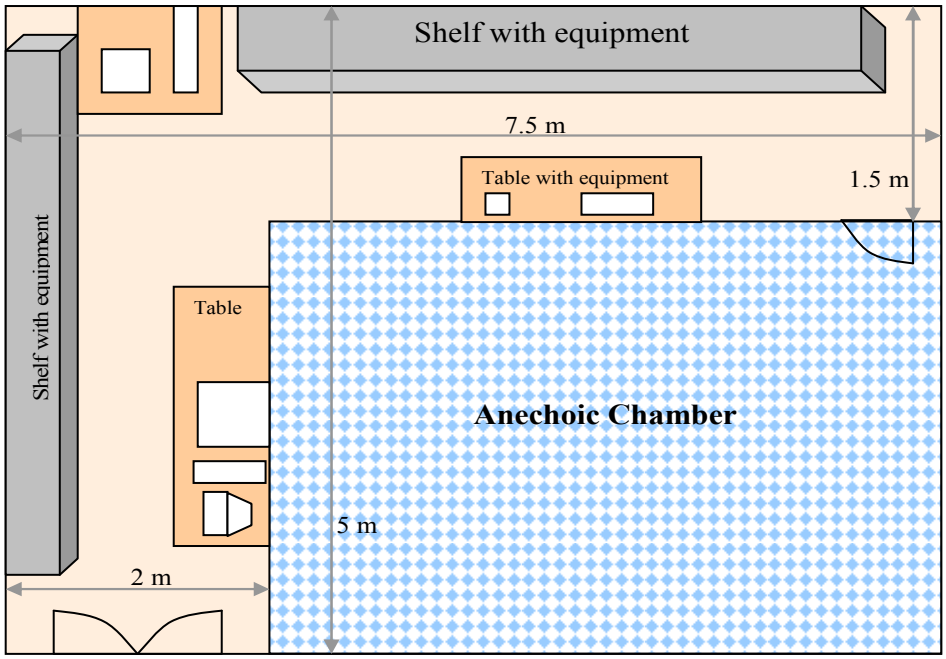

Fig. 4.2: Schematic layout of the laboratory where the diversity measurements were carried out

The sampling time of 10 ms (sampling frequency of 100 Hz) was selected to ensure that all the variations caused by the fast movement of the body were captured, by making the sampling frequency more than twice the maximum body Doppler shift. The maximum Doppler shift was calculated using eq. (3.1) in Chapter 3, assuming relative speed of motion of the antennas up to 3 m/s during the movements. These give shifts of about 8.17 Hz with average speed of motion of 1 m/s and about 24.5 Hz with 3 m/s. The noise floor for the measurement was at -110 dBm. During the measurements, random activities, such as walking, moving hands, eating, bending down etc., were performed and the same activities were repeated for every measurement. The detail of movements performed in each sweep of the measurement is given in Table 4.1.

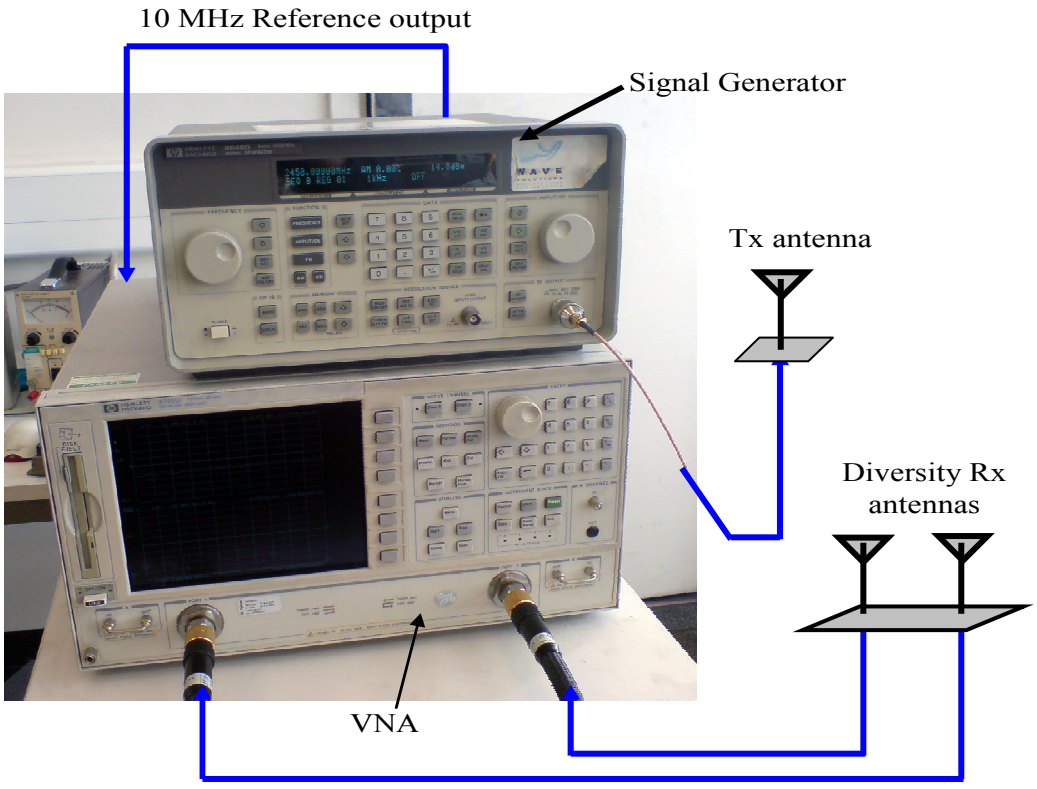

Fig. 4.3: Setup for diversity measurements at 2.45 GHz

TABLE 4.1

MOVEMENTS DONE FOR EACH CHANNEL DURING DIVERSITY MEASUREMENTS

Sweep	Belt-Head	Belt-Wrist	Belt-Ankle	Belt-Back and Belt-Chest
1	Looking right	Walking	Walking	Moving hands
2	Looking left	Hand on chest	Sit stand	Walking
3	Shaking head left-right	Hand on back	Leaning forward and sideways	Leaning forward and sideways
4	Shaking head up-down	Stretching and holding hand in front	Kicking	Typing and writing
5	Eating and drinking	Eating and drinking	Running	Eating and drinking
6	Leaning forward and sideways	Writing and typing	Keeping the foot back in air	Sitting in a chair and lifting things
7	Moving hands randomly near head	Lifting things from floor	Tighten laces	Sit stand
8	Lifting things from floor	Waving bye-bye	Eating and drinking while sitting in a chair	Exercise
9	Walking	Moving hands randomly near head	Lifting things from floor while sitting in a chair	Running
10	Exercise	Clapping	Moving feet while sitting	Random activities

4.4.2 Diversity measurements at 5.8 GHz and 10 GHz

The diversity measurements at 5.8 GHz and 10 GHz were carried out in the same laboratory environment as stated in Section 4.4.1. In this case, only three channels, i.e., belt-head, belt-wrist, and belt-chest, were measured. As stated above, the signal generator could not be used for these frequencies. So, the measurements were performed with the VNA by using one port of VNA as transmitter and the other port as a receiver. The two receiving antennas were connected through an RF switch to

the receiving port and the transmitting antenna was connected to the transmitting port of the VNA, as shown in Fig. 4.4. The response through calibration was done in this case by connecting the transmitter and the receiver ports of the analyzer through the cables used. The switching time between the two antennas was 40 μs. This was much shorter than the coherence time of the measured channels, which was calculated using eq. (3.2) in Chapter 3. To synchronize the switching process with the VNA, the VNA was set to external-trigger-on-point mode. In this mode, the VNA requires an external trigger signal at each sampling point in the sweep to take the measurement. The external trigger signal was supplied through a microcontroller, which was controlling the switch as well. The microcontroller was programmed to send the trigger signal after switching to a position, thus operating on a "switch and sample" approach. More details of the RF switch and the microcontroller circuit are given in Appendix A. The maximum Doppler shift was calculated by the same procedure stated above in Section 4.4.1 and the calculated values were 19.3 Hz and 33.3 Hz with average speed of 1 m/s, and 57.9 Hz and 100 Hz with average speed of 3 m/s for 5.8 GHz and 10 GHz, respectively. The calculated coherence times, using the expression (3.2), with the given maximum Doppler shifts were greater than or equal to 21.9 ms and 7.3 ms with 1 m/s and 3 m/s, respectively, at 5.8 GHz and greater than or equal to 12.7 ms and 4.23 ms with 1m/s and 3 m/s, respectively, at 10 GHz. The sampling time was set to 21.2 ms (47 Hz sampling frequency) for 5.8 GHz measurements and 9.2 ms (108.6 Hz sampling frequency) for 10 GHz measurements. As stated before, these sampling times were selected to ensure that all the variations caused by the fast movement of the body were captured by making the sampling frequency twice the body Doppler shift with average speed of movements of 1 m/s.

However, with faster movements like at 3 m/s, the sampling frequency is close to the maximum Doppler shift, especially at 10 GHz, which may result in under-sampling for faster movements. The sampling times for these frequencies could not be reduced due to limitations of the hardware. Thus, these sampling times were limited to maximum speed of motion of about 1 m/s and efforts were made to keep the body movements within that limit. The VNA was set to take a single frequency sweep and a total of 1601 points were collected in each sweep with alternate samples for each of the two antennas. Thus, 800 points per branch were collected in one sweep. A total of 10 such sweeps were carried out giving 8000 points for each diversity branch per measurement. The noise floor for the measurement was at -90 dBm. The same activities, as given in Table 4.1, were performed and repeated.

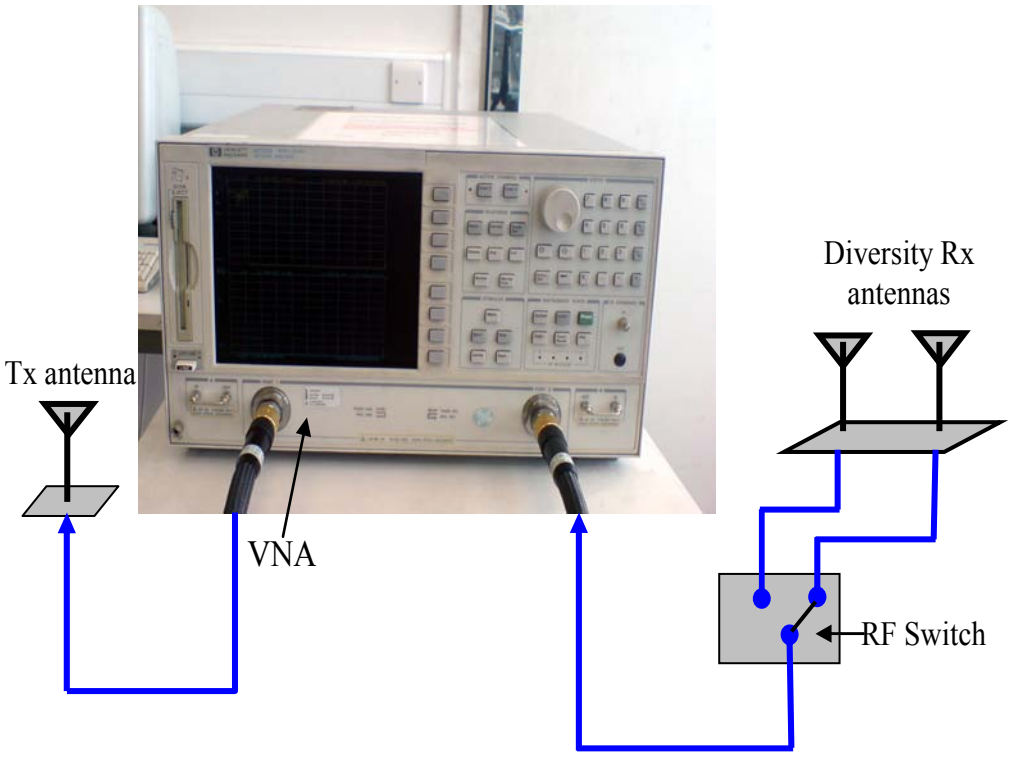

Fig. 4.4: Setup for diversity measurement at 5.8 GHz and 10 GHz

4.4.3 BAN-BAN Interference Rejection measurements

To investigate the BAN-BAN interference rejection, three on-body channels were selected and measured at 2.45 GHz frequency. In each case, the desired signal transmitting antenna was mounted at the belt position and the antenna transmitting the interference signal was mounted at the same position on another person's waist. Measurements were performed in an indoor environment, which was a 7.5 m x 9 m sized laboratory containing equipment, tables, chairs, and computers thus providing a rich multipath propagation environment. Fig. 4.5 shows a pictorial view of the indoor laboratory environment where the measurements were carried out. The two transmitting antennas, i.e. the desired and the interferer, were connected through the RF switch to signal generator operating at 2.45 GHz. The same switch-and-sample approach was used here. The two receiving antennas were connected to the two ports of the VNA calibrated in tuned dual channel receiver mode with a single frequency sweep at 2.45 GHz. The setup is shown in Fig. 4.6. The noise floor for the measurement was at -90 dBm. A total of 1600 points were collected for one sweep of 12 s duration. Thus, each receiving antenna was collecting 1600 samples, with alternate samples from each transmitter, with a sampling time of 15 ms giving 800 samples each for the desired and the interference signals. A total of 6 such sweeps were carried giving 4800 samples each for the desired and interference signals. During the measurement, the two subjects were walking around each other in the room in a random manner.

Fig. 4.5: Pictorial view of the room where the interference and MIMO measurements were carried out

4.4.4 MIMO measurements

The MIMO measurements were performed in the same indoor environment described in Section 4.4.3. The two transmitting antennas, which were the two elements of the transmitting array in this case, were connected through the RF switch to the signal generator operating at 2.45 GHz. The rest of the setup was similar to the setup described in Section 4.4.3 and shown in Fig. 4.6. The number of points and the sampling time were also the same. Hence, in this case, each receiving antenna was collecting 1600 samples with alternate samples from each transmitter with a sampling time of 15 ms, giving 800 instances of one of the four spatial subchannels. Thus, 800 instances of the 2 x 2 MIMO channel matrix with four subchannels were constructed. A total of 6 such sweeps were carried out, with different random movements of the body for each sweep, giving a total of 4800 instances of the channel matrix. The movements performed in this case are given in Table 4.2.

TABLE 4.2

MOVEMENTS DONE FOR EACH CHANNEL DURING MIMO MEASUREMENTS

Sweep	Belt-Head	Belt-Chest	Belt-Wrist
1	Shaking the head left and right	Walking	Walking
2	Shaking the head up-down	Leaning forward and side ways	Eating, drinking, and moving hands
3	Eating, drinking, and moving hands	Eating and typing while sitting	Writing and typing
4	Lifting things from floor	Lifting things while sitting in a chair	Lifting things from floor
5	Walking	Sit stand	Waving bye-bye
6	Exercise	Exercise	Clapping

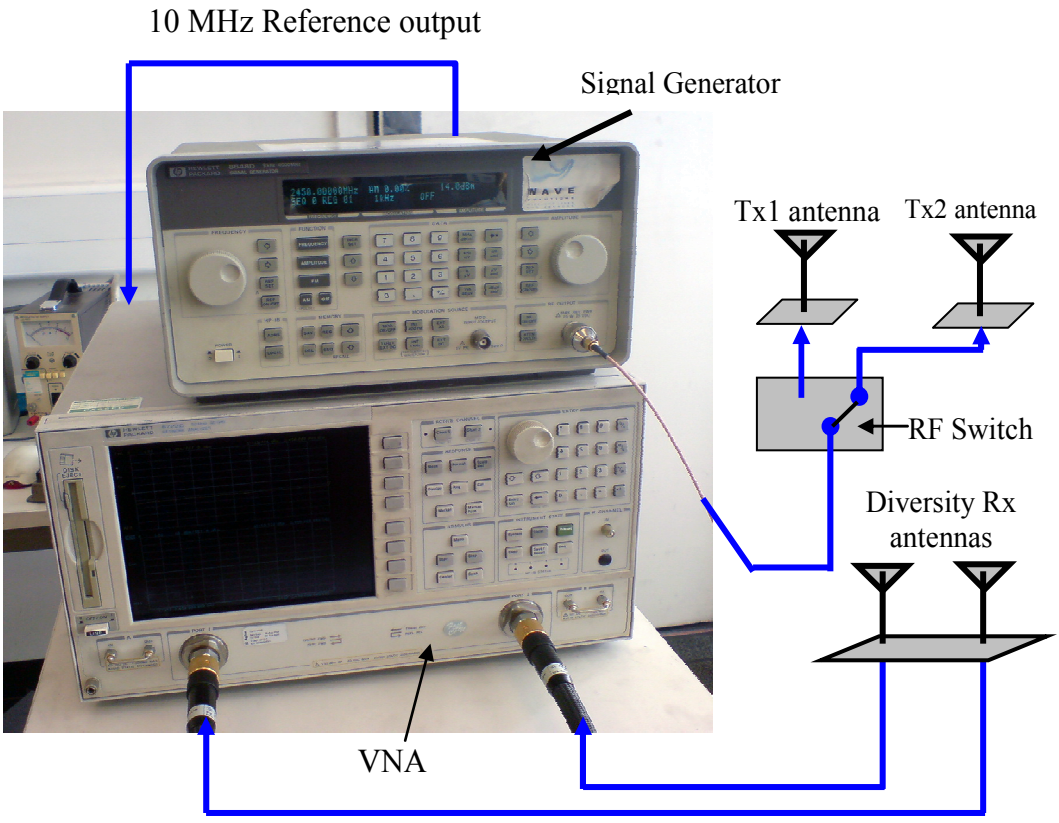

Fig. 4.6: Setup for interference rejection and MIMO measurements (Tx1 is the desired signal transmitter and Tx2 is the interference signal transmitter for interference measurements whereas they are the two elements of the transmitting array for MIMO)

Chapter 5

Space Diversity for On-body Channels

5.1 Introduction

It has been discussed in the previous chapters that like other wireless communication channels, on-body channels are prone to fading. Also, it is desirable to use very low transmit power for the body-worn devices. It is an established fact that diversity can mitigate fading and can provide significant improvement in the output signal to noise ratio (SNR). Hence, it can be useful if low transmit power is used and can provide significant improvement in the output SNR for the on-body channels as well. On-body channels and antennas are characterized in various ways [1, 2, 3] but apart from some preliminary results in [4, 5], no significant work has been done to show the amount of improvement offered by diversity for the on-body communication channels. This work quantifies the achievable limit in the improvement through diversity for various on-body communication channels and focuses on the diversity performance on the basis of experimental data with actual antennas and real environment. Thus, it provides a more realistic view of the antenna diversity performance for on-body channels.

In this chapter, the diversity analysis and performance for on-body communication channels is presented using space diversity monopole antennas at 2.45 and 5.8 GHz ISM bands and also at 10 GHz. The 10 GHz frequency was just an arbitrary choice

close to double the frequency of 5.8 GHz to see the trend at higher frequencies, as the demand for high data rate requires the use of higher frequencies. Measurements were taken with various spacings of space diversity monopole antennas at the three frequencies for various on-body channels with random movements of the body for each channel. The signals received on the two diversity branches were processed, using demeaning, to extract the short-term fading envelope and remove the correlated long-term fading. Diversity gain (DG) and correlation coefficients are calculated and the Cumulative Distribution Function (CDF) is plotted for each case. To verify the reliability of the measurements and repeatability of the diversity performance, the measurements were repeated several times for each channel. If the belt position is considered as a central unit, the transmission from belt to any other position can be considered as the downlink. A comparison of uplink and downlink diversity performance is also presented. The work presented here has already been published in [6-9]. A description of the antennas used in the measurements is presented in Section 5.2. The details of the measurement procedure are summarized in Section 5.3 whereas Section 5.4 gives the details of analysis performed on the measured data. The results at the three frequencies as well as the repeatability and uplink-downlink diversity results are discussed in Section 5.5, and Section 5.6 summarizes the conclusions drawn from the results.

5.2 Space Diversity Monopole Antennas

It has been shown in [3], that monopole antenna gives best performance in terms of path gain for the on-body channels. In order to investigate the diversity performance, monopoles were selected initially. Two thin wire quarter-wavelength monopole

antennas were placed some distance (d) apart on the same ground plane to implement the space diversity, as shown in Fig 5.1. The heights of the monopoles were 30.6 mm, 12.9 mm, and 7.5 mm for 2.45 GHz, 5.8 GHz, and 10 GHz, respectively, which are λ/4 in each case, where λ is the free space wavelength. The wire diameter was 0.4 mm. The spacing between the antennas was varied from 10 mm (0.08 λ) to 80 mm (0.65 λ) with a step of 10 mm for the 2.45 GHz measurements. The size of the ground plane was also increased with the spacing between the antennas. The ground plane width was equal to the antenna spacing and the length was twice the spacing. Two spacings, i.e. λ/2 and λ/4, were used for 5.8 GHz, whereas, only λ/2 spacing was used for 10 GHz. The ground plane size was fixed to 40 mm x 55 mm for 5.8 GHz diversity antennas and 30 mm x 20 mm for 10 GHz diversity antenna. The size of the ground plane was selected to be as small as possible so that the overall antenna can fit in the size of the headset and the handsets used for current Bluetooth devices and at the same time big enough to screen the antennas from the body and hence preventing significant detuning when mounted on the body.

The mutual coupling between the space diversity antennas varied with the spacing between the antennas. The maximum mutual coupling was -4 dB for the spacing of 10 mm at 2.45 GHz. For the rest of the cases, it was below -8 dB. The radiation efficiency of the antennas was reduced only slightly for spacing larger than λ/4 when compared to the isolated antenna in the simulations. The transmitting antenna in each case was a similar thin wire λ/4 monopole with ground plane sizes of 60 mm x 60 mm for 2.45 GHz, 40 mm x 40 mm for 5.8 GHz, and 20 mm x 20 mm for 10 GHz. The measured radiation patterns of the isolated monopole and diversity monopole

antennas in the proximity of other monopole, half-wavelength apart, where the other monopole was terminated by 50 ohms (to simulate the termination of antenna port by a 50 ohms transmission line during the measurements), are shown in Figs. 5.2 – 5.7 for the three frequencies of operation. The plots are directivity plots. There is some distortion in the radiation patterns of the diversity monopole antennas due to the mutual coupling between the two neighbouring antennas. Although, the mutual coupling was low but still its effect can be observed on the radiation patterns. The patterns of the two elements of the diversity antennas are not symmetrical because of termination of neighbouring antenna by 50 ohms and not a matched load.

Very little detuning was observed for small sized antennas by placing the antennas close to the body, but for all the antennas the reflection coefficient at the desired frequency was less than -12 dB.

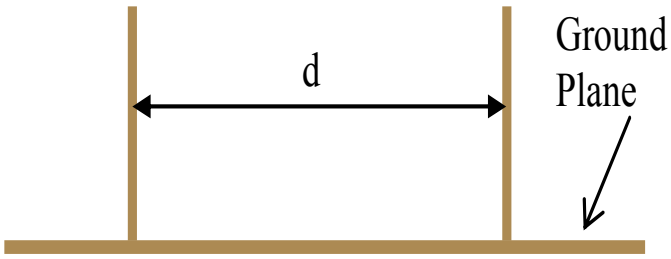

Fig 5.1: Space diversity monopole antenna with variable spacing “d”

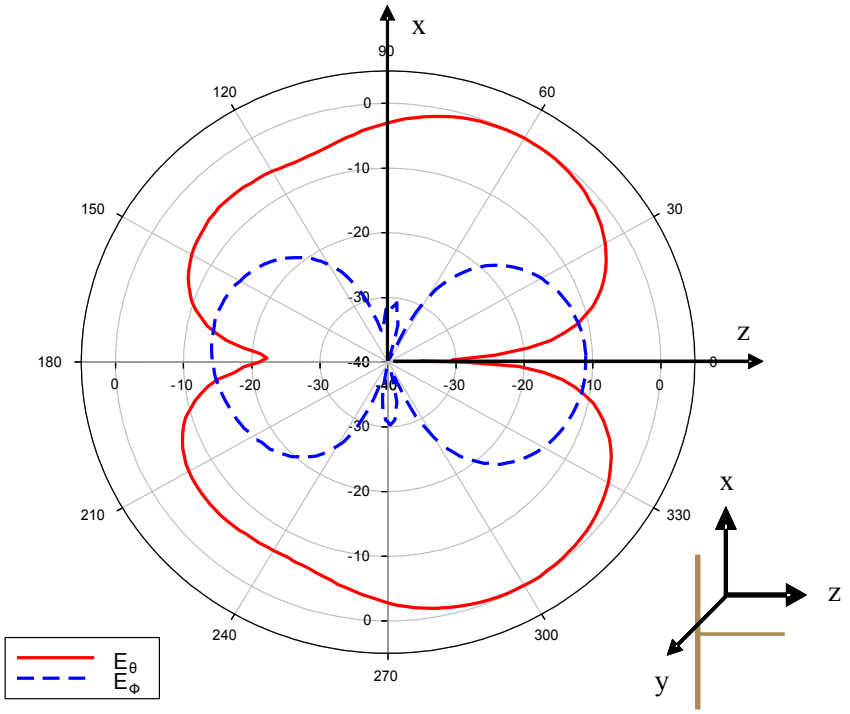

Fig 5.2: Measured radiation patterns of the single monopole antenna at 2.45 GHz

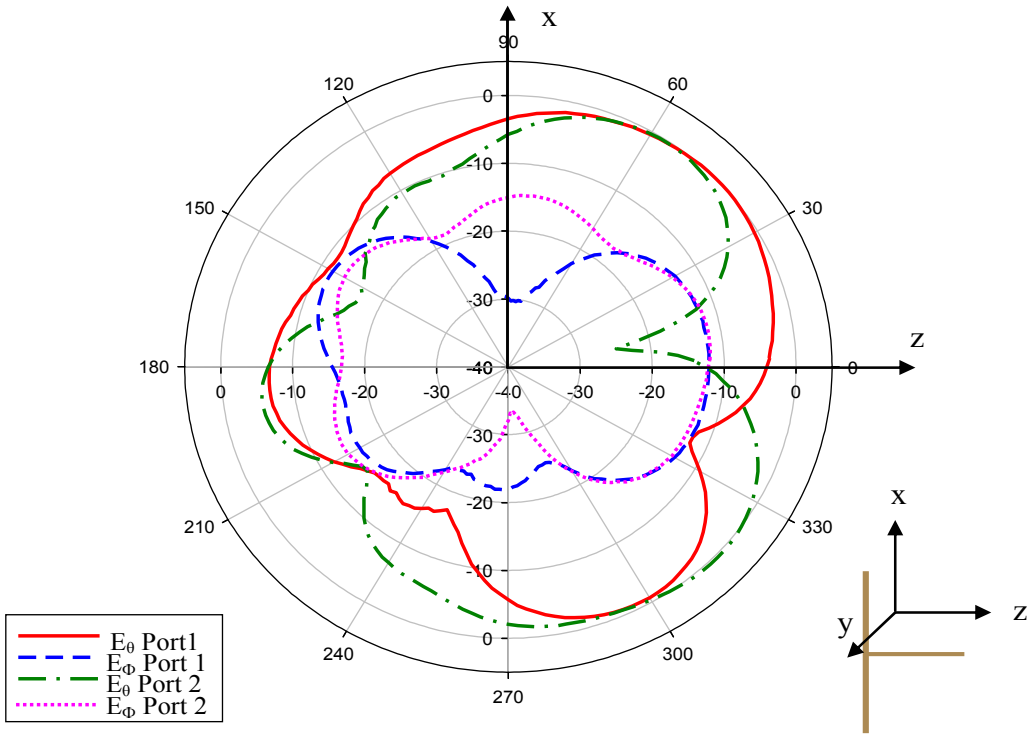

Fig 5.3: Measured radiation patterns of the diversity monopole antennas with d = λ/2 at 2.45 GHz

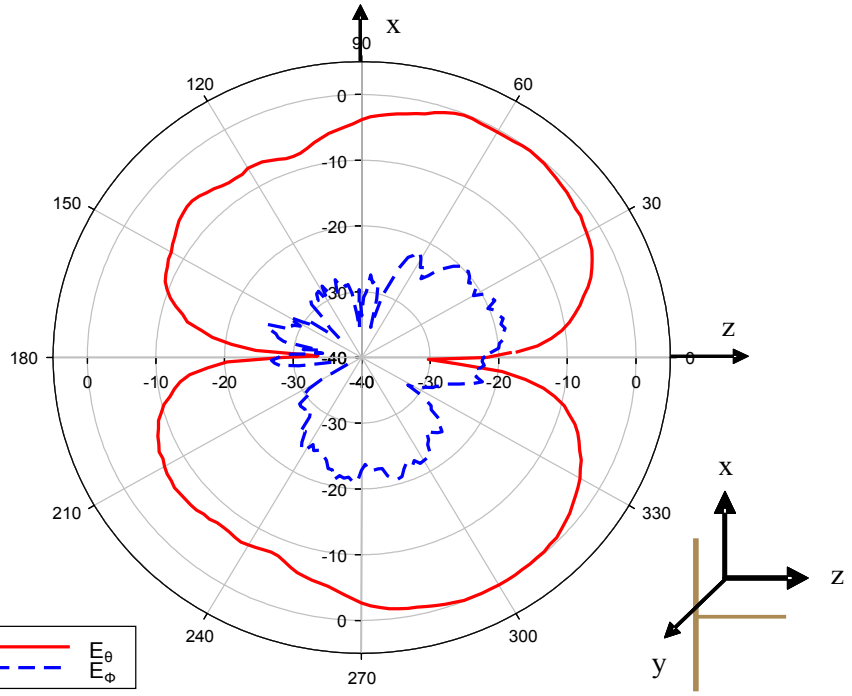

Fig 5.4: Measured radiation patterns of the single monopole antenna at 5.8 GHz

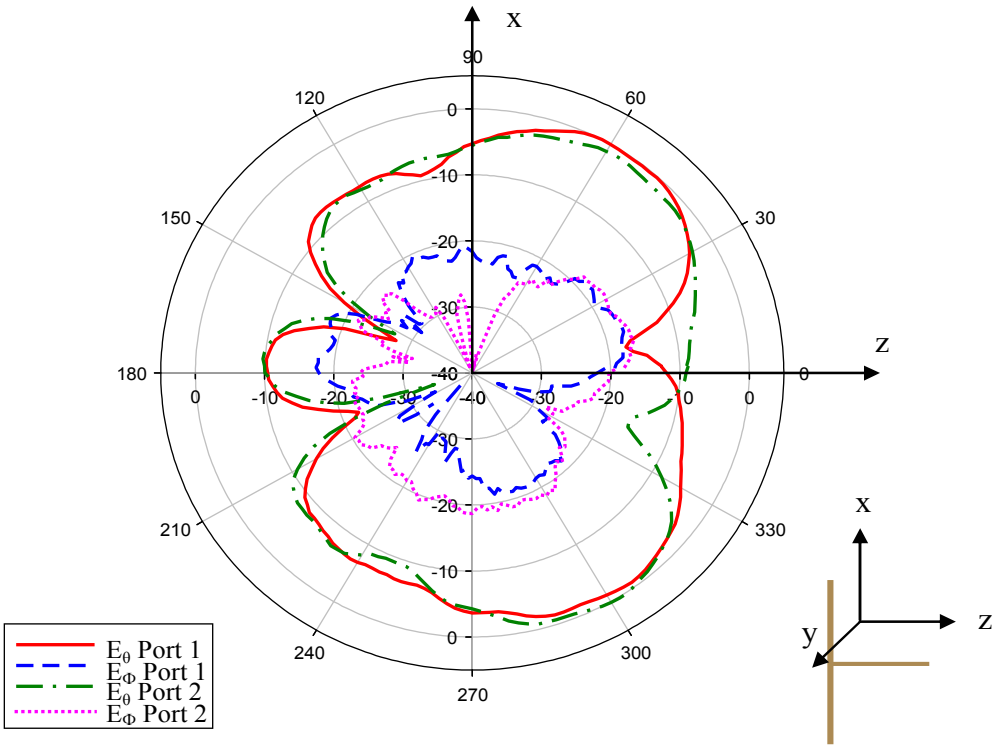

Fig 5.5: Measured radiation patterns of the diversity monopole antennas with d = λ/2 at 5.8 GHz

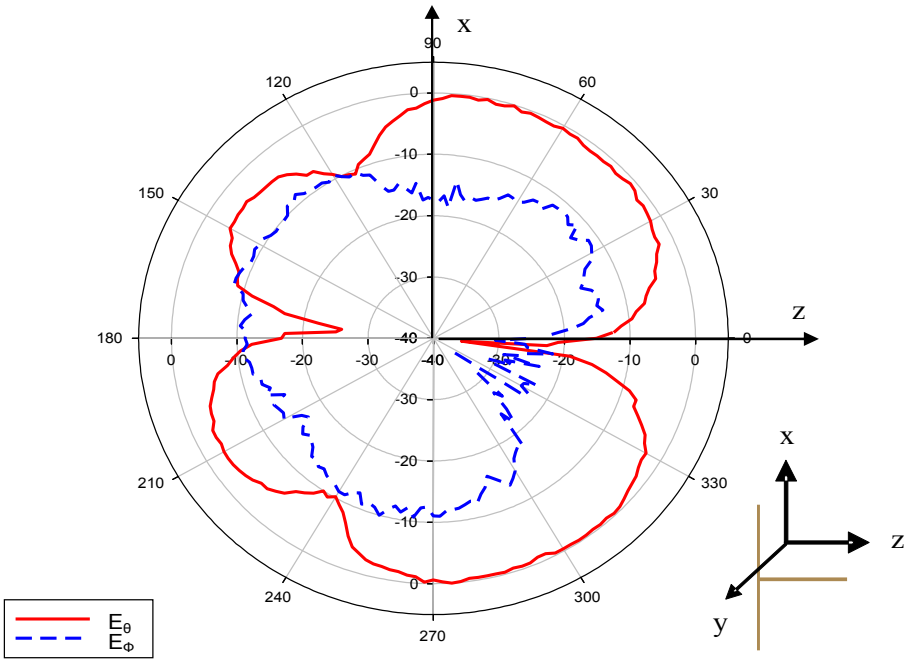

Fig 5.6: Measured radiation pattern for the single monopole at 10 GHz

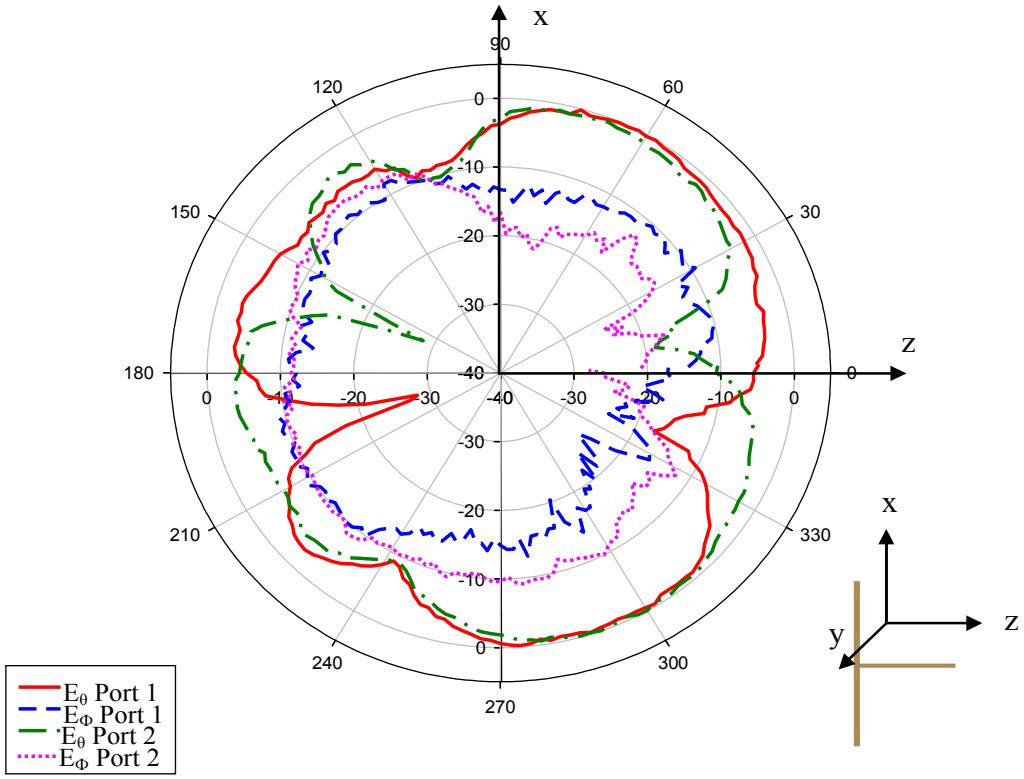

Fig 5.7: Measured radiation pattern for the diversity monopole antennas with d = λ/2 at 10 GHz

5.3 Measurement Procedure

To characterize the diversity performance analysis of space diversity monopole antennas, measurements were conducted in three different environments, i.e., an anechoic chamber, a big office with less scattering, and a rich scattering laboratory environment, by mounting the antennas on a human subject. The 5.8 GHz and 10 GHz measurements were conducted only in the indoor laboratory environment. Five on-body channels, i.e., belt-ankle, belt-chest, belt-back, belt-wrist, and belt-head, were measured at 2.45 GHz, whereas, for the other two frequency measurements only belt-head, belt-chest, and belt-wrist channels were selected. The details of mounting the antennas on the body are given in Section 4.2 and the measurement setup along with description of the environments is presented in Section 4.4. By swapping the Tx antenna and Rx diversity antennas, uplink diversity was measured and compared to the same type and orientation of the downlink diversity.

5.4 Data Analysis

Diversity can mitigate multipath fading but it cannot be useful to minimize the effect of long-term fading or shadowing caused by lack of power density [10, 11]. The long-term fading at the diversity branches is usually correlated, as shown in Fig. 5.8 for one case as an example, and effectively has no part to play in diversity performance. Thus, it is a common practice to remove the long-term variation from the received branch signals by demeaning [11-13]. The long-term fading envelope (shadowing), which represents the local average power of the received signal [14], is

superimposed on multipath components (short-term fading). It is usually assumed that long-term fading is multiplicative factor to the received signal envelope [11-13]:

$$x(t) = r(t)M(t) \tag{5.1}$$

where *x(t)* is the received signal envelope, *r(t)* is the short-term fading envelope, and *M(t)* is the local mean envelope constituting the long-term fading [11, 12] where

$$M(t) = \frac{1}{2w}\int_{t-w}^{t+w} x(\tau)d\tau \tag{5.2}$$

and thus

$$r(t) = \frac{x(t)}{M(t)} \tag{5.3}$$

2w is the local averaging sliding window size. The window was selected such that there were sufficient short-term fading oscillations (approx. 4 to 6) inside the window and yet small enough compared to the time scale of the long-term variation. The window size used for various channels at various frequencies falls within the 5λ to 20λ interval and are given in Table 5.1. This window is usually a sliding window so that at each instant, the received signal envelope is normalized to its local average value, and hence the long-term variation is removed to achieve the short-term fading envelope *r(t)*. After removing the long-term fading, the resultant short-term fading

signal was scaled to its mean value before demeaning in order to preserve the power imbalance between the two branch signals, which is crucial in determining the diversity gain. Fig. 5.9 shows an example of received signal before and after removing the long-term fading.

TABLE 5.1

SIZE OF THE DEMEANING WINDOW FOR VARIOUS CHANNELS WITH MONOPOLE ANTENNAS

Channel	Window size (ms)		
	2.45 GHz	5.8 GHz	10 GHz
Belt-Ankle	1000	-	-
Belt-Chest	1000	636	184
Belt-Back	1000	-	-
Belt-Head	1000	636	184
Belt-Wrist	1000	424	147.2

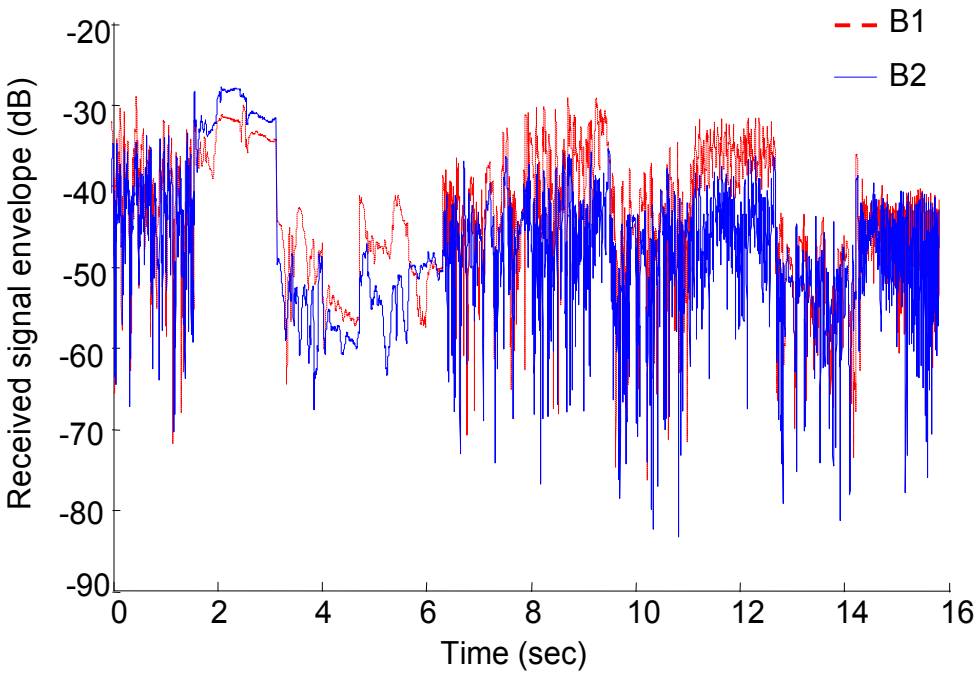

Fig 5.8: Received signal envelopes at the two diversity branch antennas for belt-ankle channel in the laboratory environment at 2.45 GHz

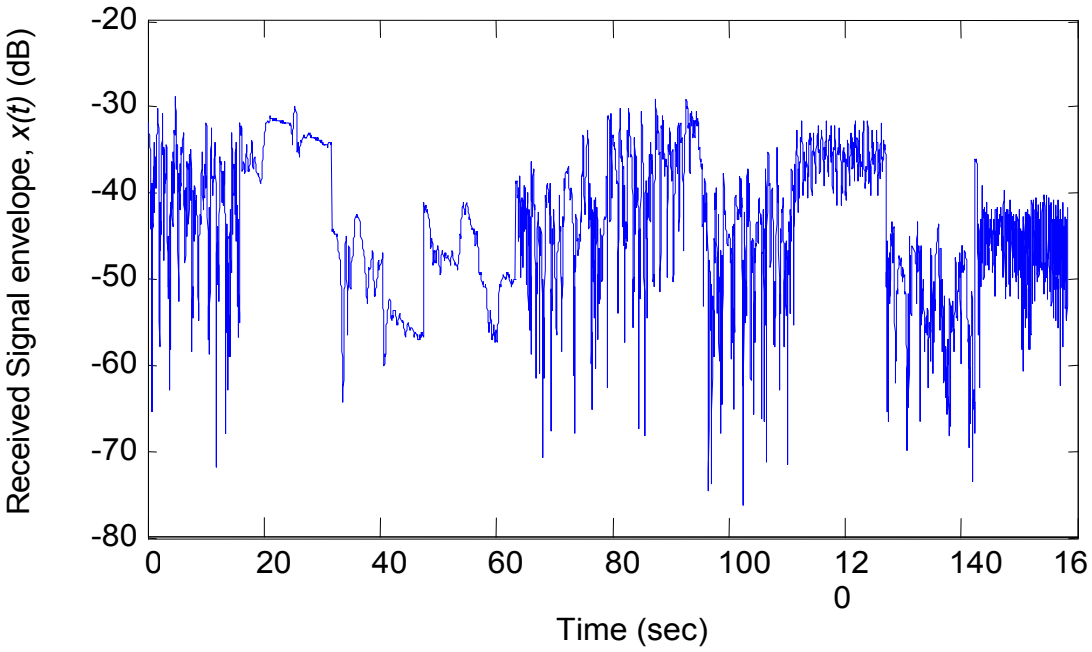

(a)

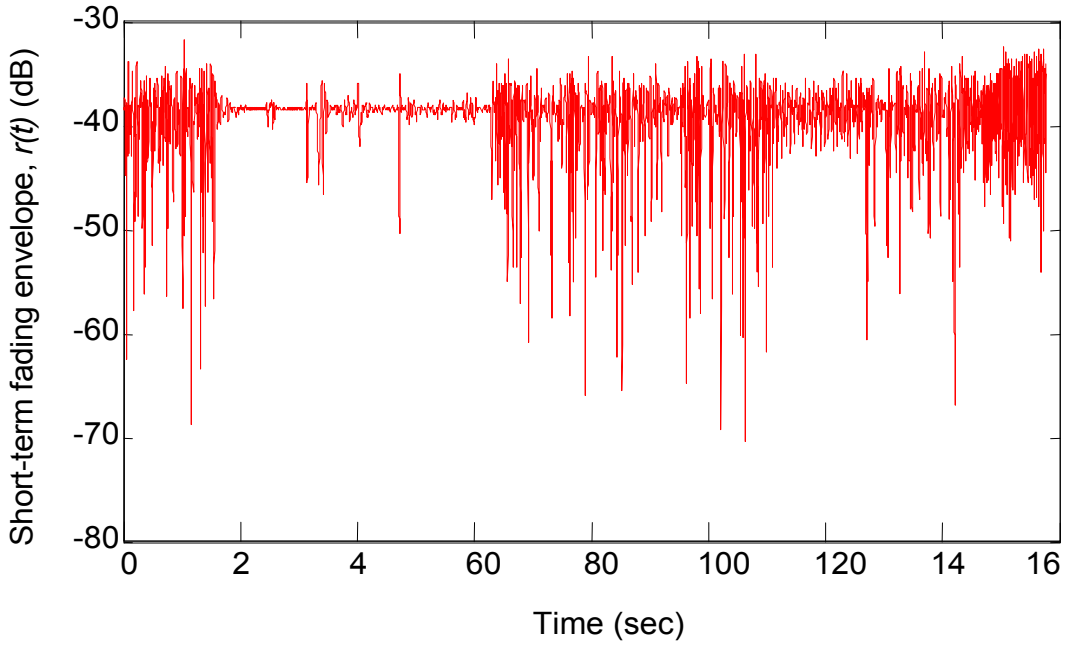

(b)

Fig. 5.9: Received Signal envelopes (a) before demeaning and (b) after demeaning and scaling to its mean value for belt-wrist channel in the laboratory environment at 2.45 GHz

The complex signal correlation coefficient (ρ_s) and the envelope correlation coefficient (ρ_e) between the two branch signals were calculated using eq. (3.10) and eq. (3.12), respectively. The three common schemes for diversity combining, i.e., Selection Combining (SC), Equal Gain Combining (EGC), and Maximal Ratio Combining (MRC), were applied and diversity gains were calculated. The diversity combined signal was achieved by using eqs. (3.7) – (3.9) with the short-term fading envelopes *r(t)* of the received branch signals. If complex signal values of the branch signals without demeaning are used in the equations, there is only a slight increase in the calculated DG value. But this increase is less than 1 dB in most of the cases. This is because the long-term fading envelopes of both the branches are highly correlated, as explained above. Co-phasing of the branch signals is required before EGC and MRC if complex signals are used [15], as explained in Chapter 3. The results are presented for MRC only in some cases, as it is optimal among the three. The experimental Cumulative Distribution Function (CDF) of the two branch signals and the diversity combined signal were plotted. The DG was calculated from these plots as the difference between the diversity combined signal and the strongest branch signal at 1% probability level or 99% reliability.

5.4.1 Effect of demeaning widow size

The length *2w* of the averaging window used for demeaning is considered critical for the indoor mobile channel characterization. For on-body diversity analysis, however, it was observed that the exact choice of the window size does not affect the diversity gains and the correlation between the diversity branches, as shown in Figs 5.10 - 5.12 for some cases. The same behavior was noted for all the cases. It was noted that the

diversity gains and correlation coefficients are insensitive to a certain range of window size and a noticeable change occurs outside this range. This range is different for different channels and is dependent on the speed and kind of movement involved. For this reason, different window sizes were selected for different channels, within the range for each channel. As explained above, the window was selected such that there were sufficient oscillations of the short-term fading inside the window and yet small enough to remove the correlated long-term variation. The selection was done by carefully analyzing each data set and then looking for a proper window size. The recommended window sizes, in each case, are given in Table 5.1.

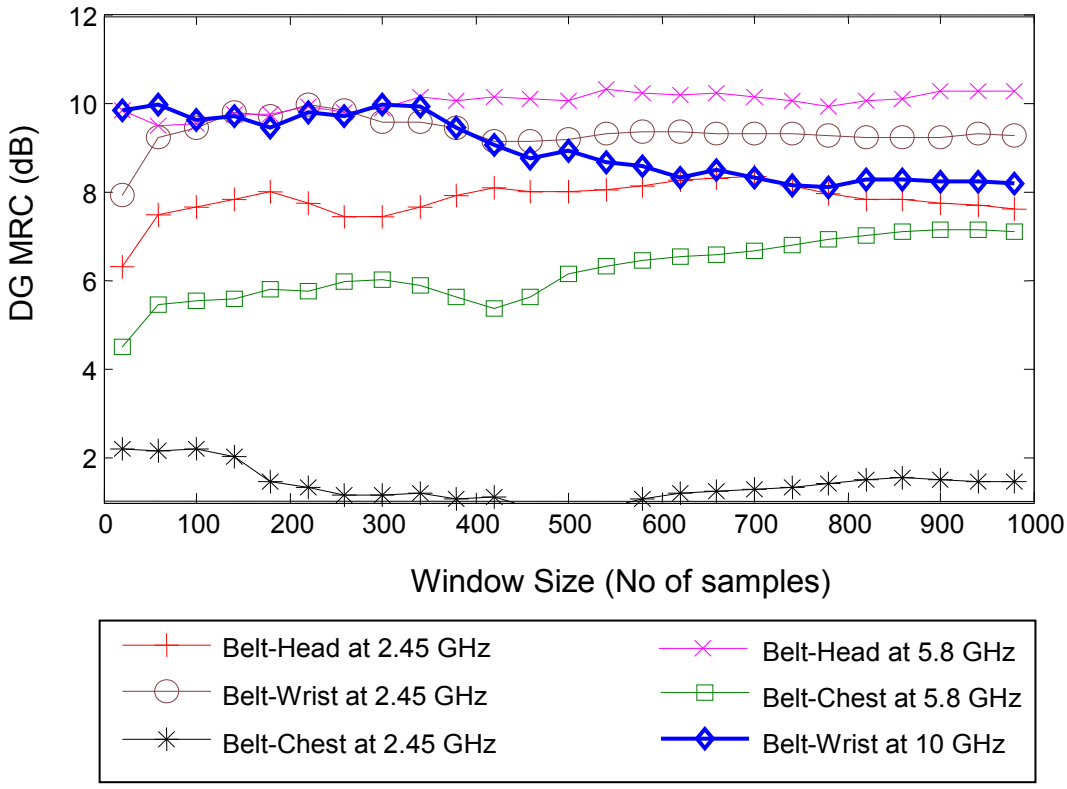

Fig 5.10: DG vs. demeaning window size for various on-body channels in the laboratory environment

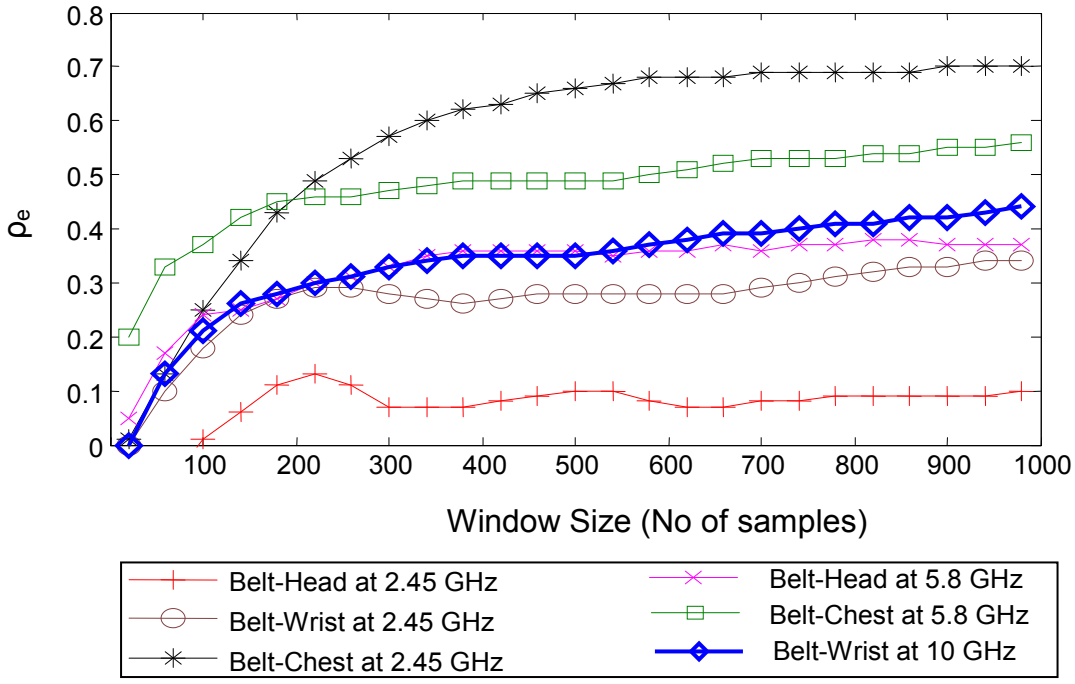

Fig 5.11: Envelope correlation coefficient vs. window size for various on-body channels in the laboratory environment

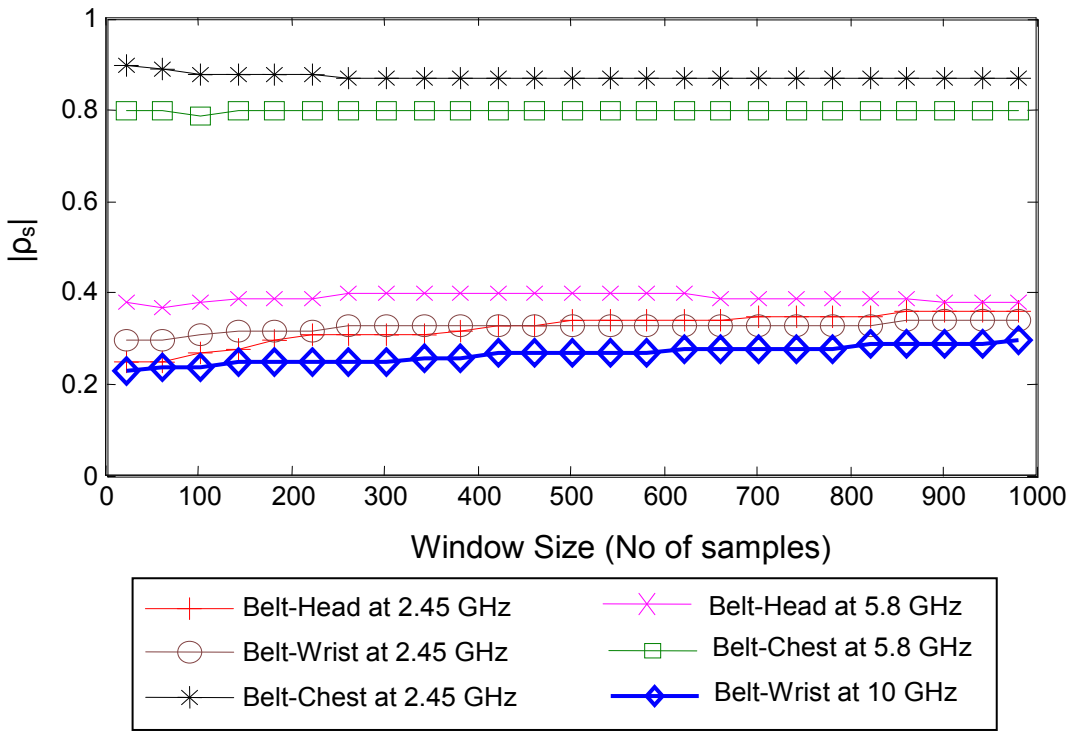

Fig 5.12: Complex correlation coefficient vs. window size for various on-body channels in the laboratory environment

5.5 Results

5.5.1 Results for 2.45 GHz measurements

The CDF plots of the received branch signals and the diversity combined signals are given in Fig. 5.13 for the five on-body channels measured at 2.45 GHz. The plots are shown for the measurement in the indoor laboratory environment only with spacing of λ/2 between the diversity monopoles. Tables 5.2-5.6 list the DG values, complex correlation coefficient (ρ_s), envelope correlation coefficient (ρ_e), the mean received power at each branch, and the power imbalance between the two branches for the five on-body channels.

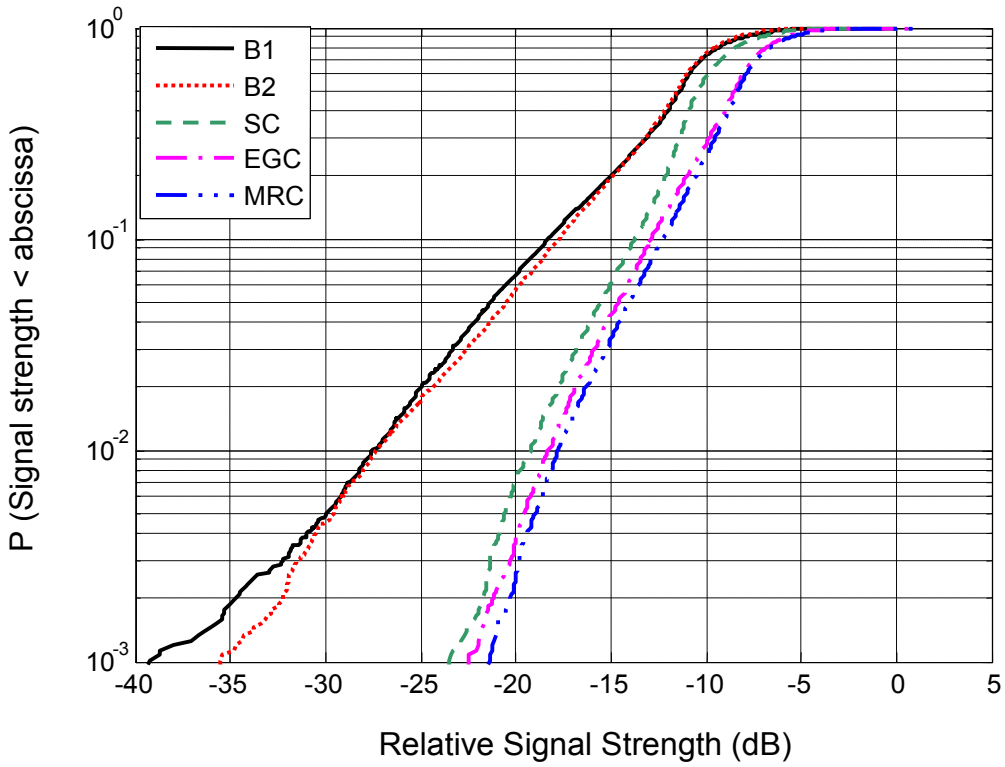

(a) Belt-Ankle

PTO for full caption

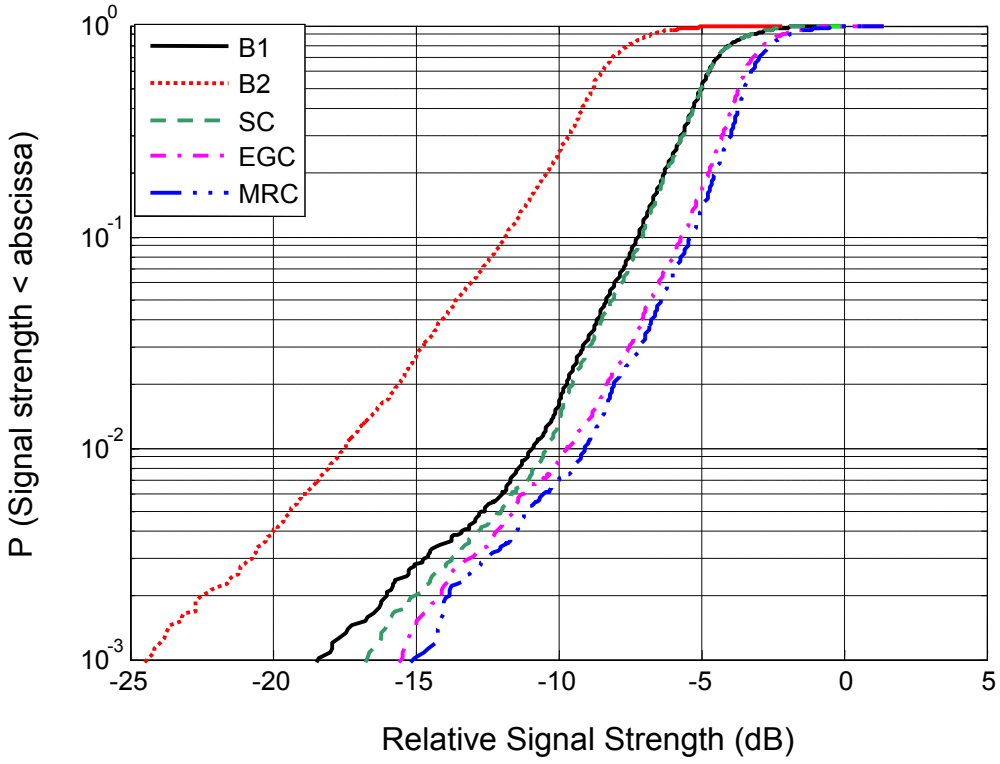

(b) Belt-Chest

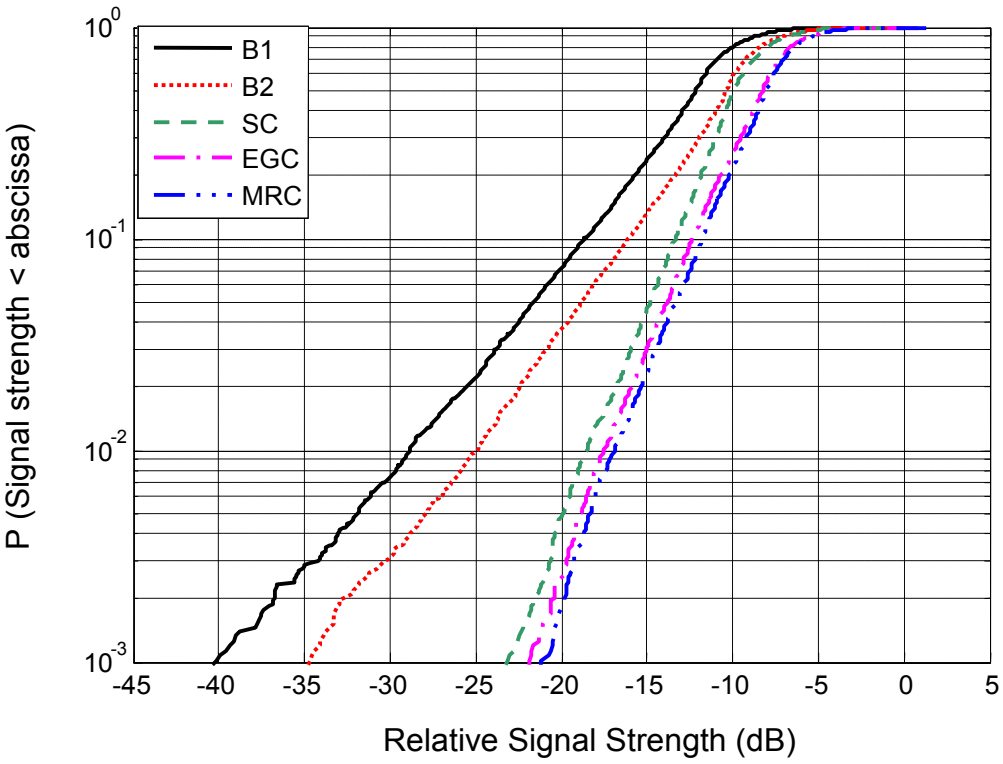

(c) Belt-Back

PTO for full caption

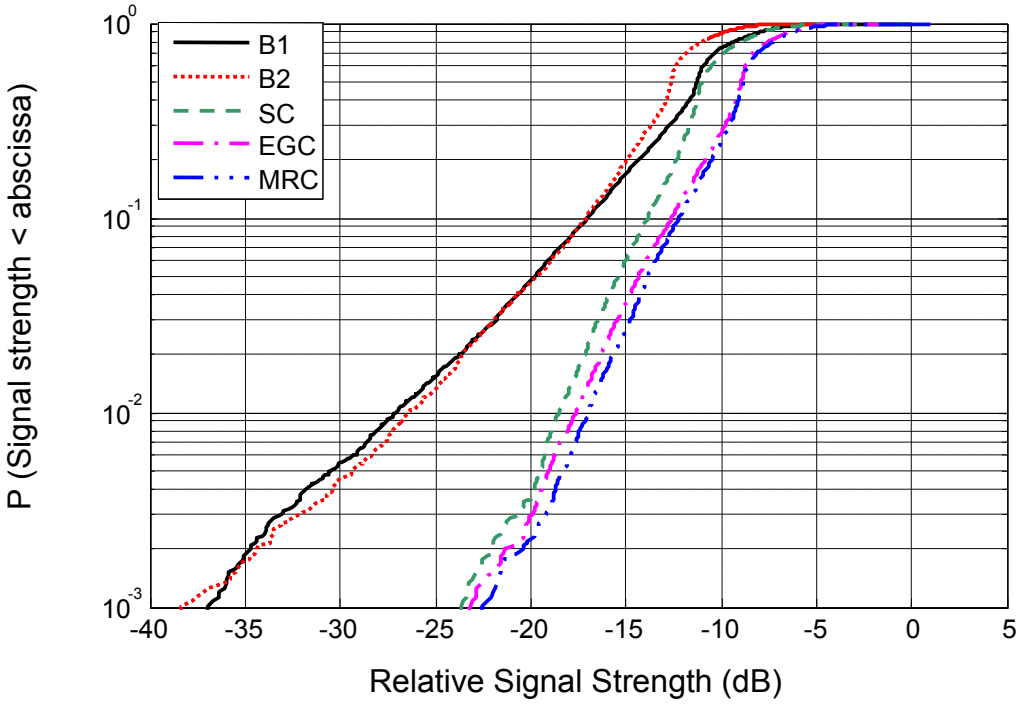

(d) Belt-Wrist

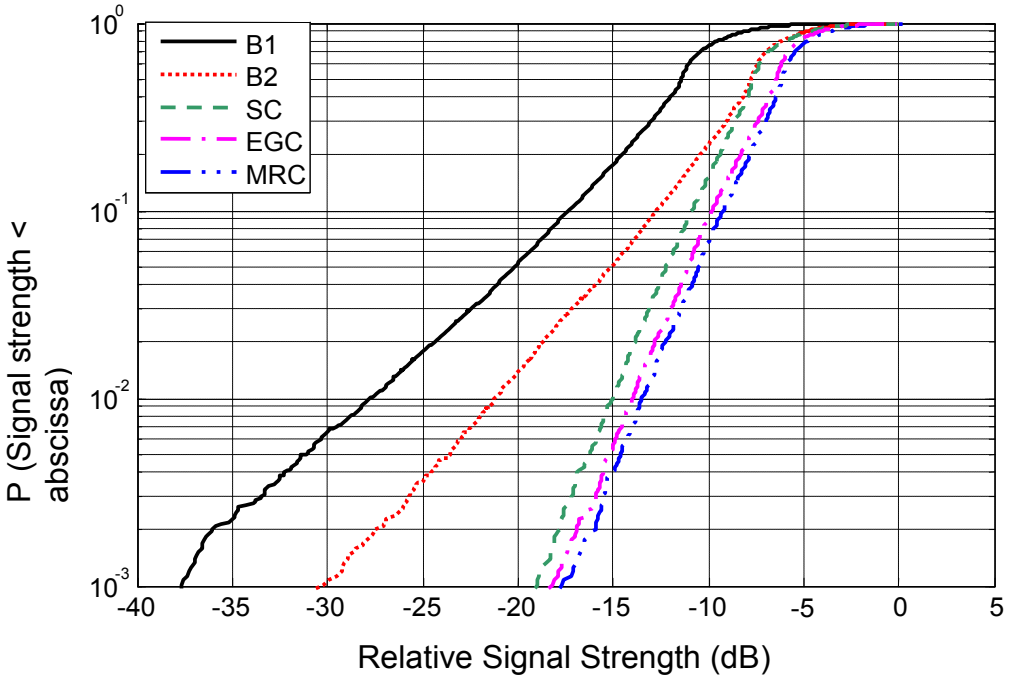

(e) Belt-Head

Fig 5.13: CDF plots for the five on-body channels with monopole spacing of λ/2 in the indoor laboratory environment at 2.45 GHz, signal strength is relative to the maximum value of the reference signal as all the signals were normalized to it

TABLE 5.2

RESULTS FOR BELT-ANKLE CHANNEL WITH MONOPOLES AT 2.45 GHz IN THE THREE ENVIRONMENTS

Anechoic Chamber								
Spacing (multiple of λ)	DG (dB)			ρ_s	ρ_e	Mean Power (dB)		Power difference (dB)
	SC	EGC	MRC			B1	B2	
0.08	7.4	8.2	8.9	0.52 - 0.27i	0.43	-49.3	-51.5	2.17
0.16	4.5	5.1	5.7	0.66 + 0.23i	0.67	-51.9	-50.6	1.28
0.25	6.0	6.8	7.4	0.06 + 0.15i	0.23	-53.3	-47.9	5.38
0.33	6.3	7.1	7.7	0.38 + 0.10i	0.42	-47.4	-44.8	2.57
0.41	6.7	7.5	8.0	0.04 + 0.59i	0.34	-51.2	-48.6	2.56
0.49	6.8	7.6	8.2	0.31 + 0.62i	0.48	-47.6	-46.7	0.91
0.65	6.5	7.7	8.3	-0.03 + 0.30i	0.28	-49.0	-47.2	1.83
Big Office Environment								
Spacing (multiple of λ)	DG (dB)			ρ_s	ρ_e	Mean Power (dB)		Power difference (dB)
	SC	EGC	MRC			B1	B2	
0.25	5.1	5.9	6.6	-0.40 - 0.06i	0.16	-43.9	-50.9	7.02
0.33	6.8	7.7	8.2	-0.30 - 0.39i	0.15	-45.5	-42.5	2.94
0.41	6.1	7.1	7.8	0.01 - 0.71i	0.39	-38.3	-37.2	1.06
0.49	5.8	7.0	7.5	0.09 - 0.66i	0.37	-44.2	-42.2	1.92
0.65	6.6	7.3	8.0	-0.61 - 0.02i	0.31	-41.7	-41.4	0.28
Indoor Laboratory Environment								
Spacing (multiple of λ)	DG (dB)			ρ_s	ρ_e	Mean Power (dB)		Power difference (dB)
	SC	EGC	MRC			B1	B2	
0.08	6.8	7.7	8.3	0.60 + 0.41i	0.45	-49.0	-49.5	0.52
0.16	6.6	7.5	8.1	0.11 - 0.40i	0.35	-45.4	-49.2	3.75
0.25	6.4	7.0	7.7	-0.16 + 0.22i	0.16	-44.7	-48.6	3.81
0.33	7.8	8.5	9.3	0.18 + 0.08i	0.20	-46.2	-49.7	3.52
0.41	7.2	8.1	8.6	-0.09 + 0.33i	0.18	-47.1	-46.7	0.44
0.49	8.1	9.1	9.5	0.03 + 0.25i	0.19	-45.4	-45.5	0.12
0.65	8.9	9.5	10.2	-0.02 - 0.01i	0.15	-45.6	-45.5	0.07

TABLE 5.3

RESULTS FOR BELT-CHEST CHANNEL WITH MONOPOLES AT 2.45 GHz IN THE THREE ENVIRONMENTS

Anechoic Chamber								
Spacing (multiple of λ)	DG (dB)			ρ_s	ρ_e	Mean Power (dB)		Power difference (dB)
	SC	EGC	MRC			B1	B2	
0.08	0.0	0.1	1.1	0.84 + 0.01i	0.25	-31.9	-38.5	6.68
0.16	0.5	2.3	2.6	0.74 - 0.33i	0.55	-32.6	-37.2	4.61
0.25	0.3	1.3	1.8	0.87 + 0.33i	0.30	-33.4	-28.8	4.61
0.33	0.2	1.3	1.7	0.66 + 0.62i	0.34	-32.2	-28.5	3.69
0.41	0.7	1.8	2.2	0.28 + 0.85i	0.35	-30.8	-26.3	4.48
0.49	0.0	0.7	0.9	0.12 + 0.87i	0.31	-32.0	-26.4	5.58
0.65	1.1	2.1	2.6	-0.38 + 0.63i	0.19	-31.8	-28.8	2.99
Big Office Environment								
Spacing (multiple of λ)	DG			ρ_s	ρ_e	Mean Power (dB)		Power difference
	SC	EGC	MRC			B1	B2	
0.25	2.2	3.8	4.1	0.29 - 0.76i	0.32	-32.1	-36.1	3.98
0.33	0.3	0.8	1.6	0.10 - 0.83i	0.19	-35.3	-29.2	6.04
0.41	0.5	1.4	1.9	0.51 - 0.71i	0.41	-31.0	-25.9	5.09
0.49	0.7	1.3	2.1	0.17 - 0.89i	0.43	-32.0	-29.5	2.44
0.65	0.7	2.4	2.6	-0.64 - 0.59i	0.35	-32.1	-29.6	2.49
Indoor Laboratory Environment								
Spacing (multiple of λ)	DG (dB)			ρ_s	ρ_e	Mean Power (dB)		Power difference (dB)
	SC	EGC	MRC			B1	B2	
0.08	2.2	3.7	4.1	0.91 + 0.07i	0.40	-32.3	-34.1	1.73
0.16	0.5	1.1	1.9	-0.24 + 0.82i	0.32	-34.6	-29.8	4.85
0.25	0.8	1.7	2.2	0.02 + 0.84i	0.11	-29.9	-35.8	5.89
0.33	0.0	1.5	1.8	0.44 + 0.74i	0.29	-28.0	-33.3	5.21
0.41	1.3	2.4	2.9	-0.46 + 0.71i	0.14	-29.7	-26.5	3.19
0.49	0.6	1.8	2.1	0.57 + 0.68i	0.25	-27.4	-31.2	3.77
0.65	0.8	2.3	2.8	-0.79 + 0.02i	0.31	-31.3	-28.8	2.57

TABLE 5.4

RESULTS FOR BELT-BACK CHANNEL WITH MONOPOLES AT 2.45 GHz IN THE THREE ENVIRONMENTS

Anechoic Chamber								
Spacing (multiple of λ)	DG (dB)			ρ_s	ρ_e	Mean Power (dB)		Power difference (dB)
	SC	EGC	MRC			B1	B2	
0.08	3.3	4.4	4.9	0.84 - 0.29i	0.88	-60.4	-60.1	0.25
0.16	0.9	2.6	2.8	-0.83 + 0.31i	0.73	-56.1	-54.1	1.98
0.25	5.3	6.1	6.7	0.28 - 0.32i	0.07	-55.9	-59.9	3.97
0.33	1.5	2.4	3.1	0.30 - 0.73i	0.35	-51.7	-56.6	4.91
0.41	3.2	3.9	4.5	0.13 - 0.81i	0.31	-51.9	-56.2	4.31
0.49	2.6	3.8	4.2	-0.24 - 0.70i	0.32	-52.4	-55.8	3.46
0.65	2.9	3.6	4.3	-0.81 - 0.07i	0.37	-51.9	-55.6	3.66
Big Office Environment								
Spacing (multiple of λ)	DG			ρ_s	ρ_e	Mean Power (dB)		Power difference
	SC	EGC	MRC			B1	B2	
0.25	5.9	6.9	7.5	0.25 + 0.46i	0.19	-49.7	-45.5	4.24
0.33	7.9	8.9	9.5	-0.43 + 0.19i	0.14	-48.8	-50.4	1.57
0.41	8.5	9.4	10.1	-0.57 + 0.27i	0.26	-48.8	-48.7	0.10
0.49	5.2	6.2	6.8	-0.34 + 0.69i	0.48	-48.6	-50.6	2.02
0.65	7.0	7.9	8.5	0.34 - 0.08i	0.18	-50.5	-51.4	0.98
Indoor Laboratory Environment								
Spacing (multiple of λ)	DG (dB)			ρ_s	ρ_e	Mean Power (dB)		Power difference (dB)
	SC	EGC	MRC			B1	B2	
0.08	7.6	8.5	9.1	0.04 + 0.69i	0.41	-52.4	-53.0	0.55
0.16	7.1	8.3	8.8	-0.48 + 0.19i	0.22	-54.0	-50.7	3.32
0.25	7.3	7.9	8.7	-0.30 - 0.22i	0.07	-50.5	-48.6	1.91
0.33	6.9	7.5	8.2	-0.53 - 0.29i	0.24	-50.9	-46.5	4.36
0.41	6.2	7.0	7.8	0.48 - 0.23i	0.17	-48.1	-50.9	2.79
0.49	6.4	7.4	8.0	-0.29 - 0.49i	0.22	-50.2	-48.5	1.77
0.65	6.5	7.6	8.2	-0.14 - 0.56i	0.29	-48.6	-50.7	2.12

TABLE 5.5

RESULTS FOR BELT-WRIST CHANNEL WITH MONOPOLES AT 2.45 GHz IN THE THREE ENVIRONMENTS

Anechoic Chamber								
Spacing (multiple of λ)	DG (dB)			ρ_s	ρ_e	Mean Power (dB)		Power difference (dB)
	SC	EGC	MRC			B1	B2	
0.08	4.9	5.9	6.4	0.52 + 0.22i	0.89	-56.5	-56.6	0.07
0.16	4.5	5.6	6.2	-0.06 + 0.29i	0.53	-47.3	-47.2	0.10
0.25	4.9	6.2	6.7	0.34 - 0.10i	0.34	-40.2	-37.9	2.28
0.33	6.0	7.0	7.5	-0.49 - 0.15i	0.65	-40.8	-42.2	1.33
0.41	4.0	5.0	5.4	-0.11 - 0.53i	0.53	-40.0	-35.9	4.14
0.49	6.7	7.4	8.1	-0.12 - 0.55i	0.49	-38.9	-38.6	0.37
0.65	6.8	7.8	8.4	-0.45 - 0.22i	0.41	-38.6	-37.6	1.07
Big Office Environment								
Spacing (multiple of λ)	DG (dB)			ρ_s	ρ_e	Mean Power (dB)		Power difference (dB)
	SC	EGC	MRC			B1	B2	
0.25	7.5	8.5	9.0	-0.26 - 0.17i	0.26	-36.3	-36.9	0.60
0.33	4.8	5.9	6.5	0.27 + 0.11i	0.31	-42.9	-39.8	3.16
0.41	6.5	7.1	7.8	0.10 + 0.39i	0.37	-37.3	-37.5	0.20
0.49	6.5	7.5	8.1	-0.09 + 0.44i	0.25	-36.5	-39.6	3.15
0.65	6.9	7.6	8.3	0.32 - 0.08i	0.29	-40.4	-38.4	1.95
Indoor Laboratory Environment								
Spacing (multiple of λ)	DG (dB)			ρ_s	ρ_e	Mean Power (dB)		Power difference (dB)
	SC	EGC	MRC			B1	B2	
0.08	5.8	6.7	7.3	0.23 + 0.47i	0.59	-43.7	-44.3	0.56
0.16	4.7	5.6	6.2	0.28 + 0.11i	0.44	-43.9	-41.9	2.06
0.25	6.8	7.7	8.2	-0.22 + 0.11i	0.14	-39.0	-40.0	1.00
0.33	5.4	6.6	7.1	-0.25 - 0.13i	0.29	-38.7	-38.9	0.23
0.41	6.5	7.6	8.0	0.34 - 0.28i	0.39	-38.4	-39.1	0.72
0.49	7.8	8.7	9.4	-0.13 - 0.28i	0.18	-39.1	-40.5	1.39
0.65	7.3	8.0	8.7	0.06 - 0.39i	0.21	-40.4	-41.6	1.17

TABLE 5.6

RESULTS FOR BELT-HEAD CHANNEL WITH MONOPOLES AT 2.45 GHz IN THE THREE ENVIRONMENTS

Anechoic Chamber								
Spacing (multiple of λ)	DG (dB)			ρ_s	ρ_e	Mean Power (dB)		Power difference (dB)
	SC	EGC	MRC			B1	B2	
0.08	1.2	2.3	2.6	0.53 + 0.68i	0.88	-50.5	-50.8	0.30
0.16	2.7	3.8	4.3	0.34 + 0.67i	0.80	-47.7	-47.2	0.49
0.25	2.4	4.0	4.4	-0.28 + 0.23i	0.08	-44.5	-51.0	6.48
0.33	1.4	2.2	2.7	0.65 + 0.04i	0.40	-45.0	-50.1	5.07
0.41	4.8	6.0	6.3	0.39 + 0.44i	0.36	-46.3	-48.7	2.45
0.49	2.2	3.9	4.2	0.67 - 0.26i	0.21	-44.4	-48.8	4.43
0.65	4.2	5.1	5.7	0.81 + 0.00i	0.38	-45.7	-49.1	3.42
Big Office Environment								
Spacing (multiple of λ)	DG (dB)			ρ_s	ρ_e	Mean Power (dB)		Power difference (dB)
	SC	EGC	MRC			B1	B2	
0.25	1.8	2.6	3.2	-0.20 - 0.12i	0.09	-50.7	-41.5	9.16
0.33	3.3	4.1	4.7	-0.37 - 0.53i	0.26	-41.3	-46.0	4.70
0.41	6.3	7.3	7.9	-0.12 - 0.36i	0.16	-44.0	-47.1	3.09
0.49	4.4	5.3	5.9	-0.18 - 0.59i	0.25	-42.4	-45.5	3.07
0.65	6.1	7.1	7.6	-0.29 + 0.15i	0.27	-41.0	-40.6	0.41
Indoor Laboratory Environment								
Spacing (multiple of λ)	DG (dB)			ρ_s	ρ_e	Mean Power (dB)		Power difference (dB)
	SC	EGC	MRC			B1	B2	
0.08	5.8	6.6	7.2	0.39 + 0.65i	0.66	-47.5	-46.9	0.62
0.16	7.3	8.0	8.8	0.37 + 0.32i	0.38	-48.0	-48.6	0.59
0.25	4.1	4.9	5.7	0.14 + 0.24i	0.02	-46.6	-41.1	5.56
0.33	8.2	9.1	9.7	0.20 + 0.19i	0.06	-46.2	-44.1	2.11
0.41	6.6	7.5	8.0	0.00 + 0.37i	0.05	-44.5	-47.6	3.10
0.49	6.1	7.2	7.6	-0.13 + 0.23i	0.01	-48.1	-44.5	3.62
0.65	7.4	8.1	8.9	0.01 + 0.24i	0.09	-45.1	-47.3	2.17

By plotting the diversity gains against the antenna spacing, as shown in Fig. 5.14 for the five channels tested in the laboratory environment, it can be seen that DG tends to increase slightly in some case with increase in the antenna spacing. There are a few exceptions, however, in which either the power imbalance is larger or the correlation is high and hence the DG reduces. The same trend was observed for the measurement data in the anechoic chamber and the office environment. Fig. 5.15 and Fig. 5.16 show the relationship of envelope correlation coefficients and the complex correlation coefficients with the antenna spacing. It can be seen from the plots that the first minimum is at about λ/4 for all the cases. For all on-body channels, it was observed that the DG was higher in the lab environment compared to that in the anechoic chamber and big office environment (shown in Fig. 5.17 for one case) due to the presence of rich multipath. The moderate values of DG in the anechoic chamber confirm the presence of multipath due to the movement of body parts and the fact that its contribution in the diversity gain is not the dominant factor.

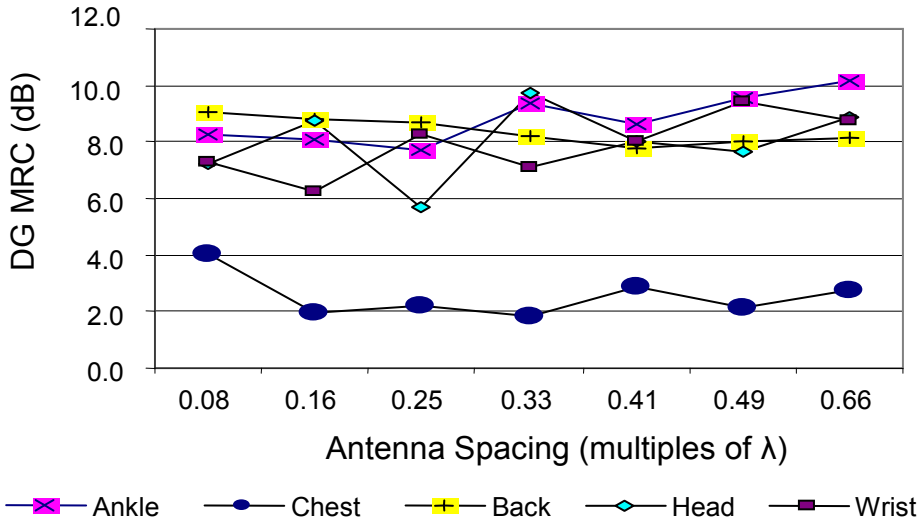

Fig 5.14: DG vs. antenna spacing for the five on-body channels using MRC with monopole antennas in the laboratory environment

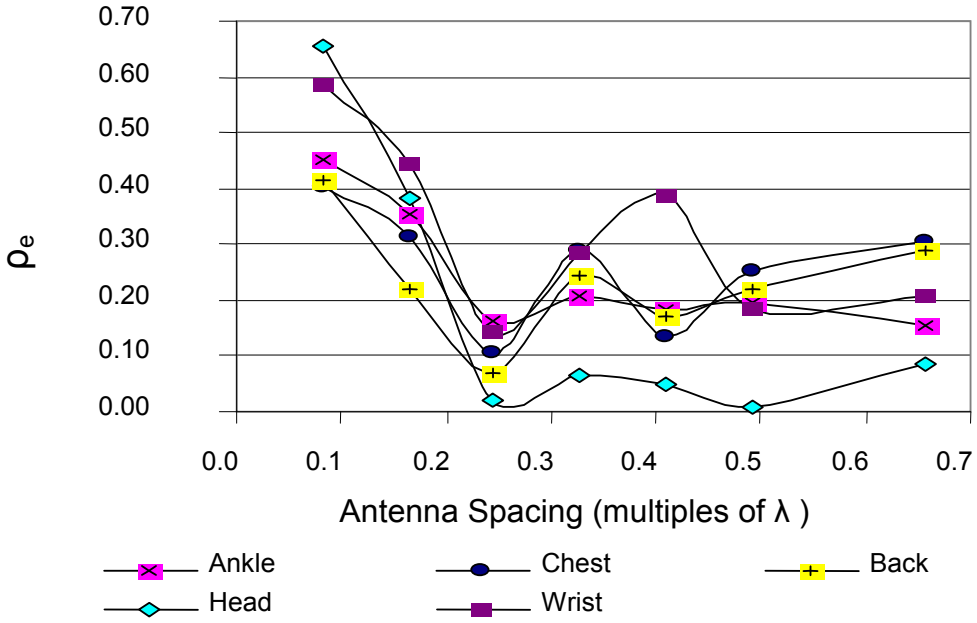

Fig 5.15: Envelope correlation coefficient vs. antenna spacing for the five on-body channels with monopole antennas in the laboratory environment

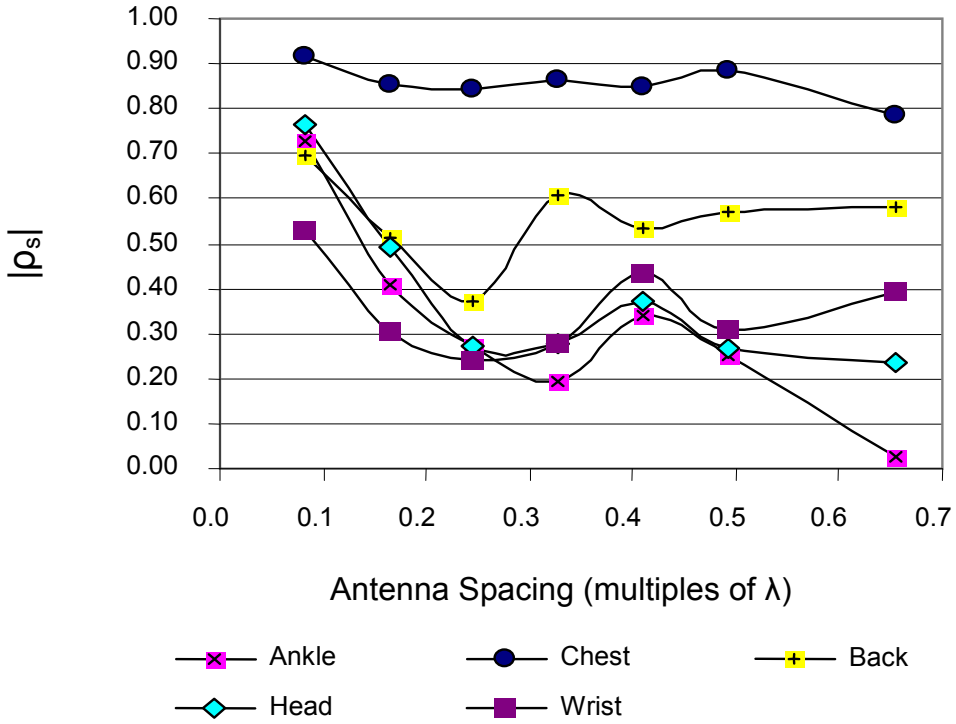

Fig 5.16: Complex correlation coefficient vs. antenna spacing for the five on-body channels with monopole antennas in the laboratory environment

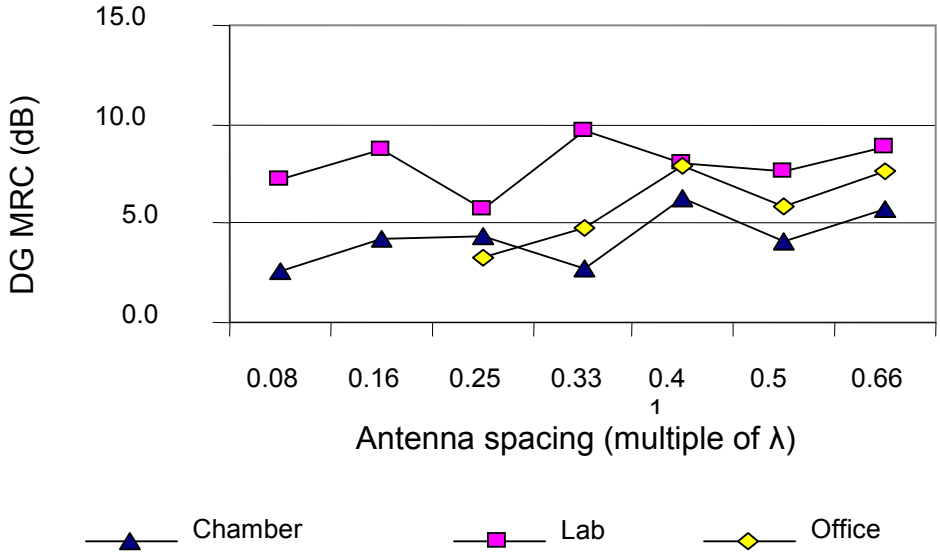

Fig 5.17: Comparison of the diversity gains (MRC) for belt-head channel in the anechoic, big office, and laboratory environments

5.5.2 Results for 5.8 GHz measurements

The CDF plots of the received branch signals and the diversity combined signals are given in Fig. 5.18 for the three on-body channels measured at 5.8 GHz in the indoor laboratory environment with spacing of λ/2 between the diversity monopoles. Table 5.7 lists the DG values, complex correlation coefficient (ρ_s), envelope correlation coefficient (ρ_e), the mean received power at each branch, and the power imbalance between the two branches for the three on-body channels. It can be noticed that the correlation between the diversity branches is lower at λ/2 spacing than the λ/4 spacing but there is an increase in the power imbalance for λ/2 spacing, which reduces the diversity gain slightly. Thus, λ/4 spacing is a good choice due to the small size of the diversity antenna and almost the same diversity performance as higher spacing.

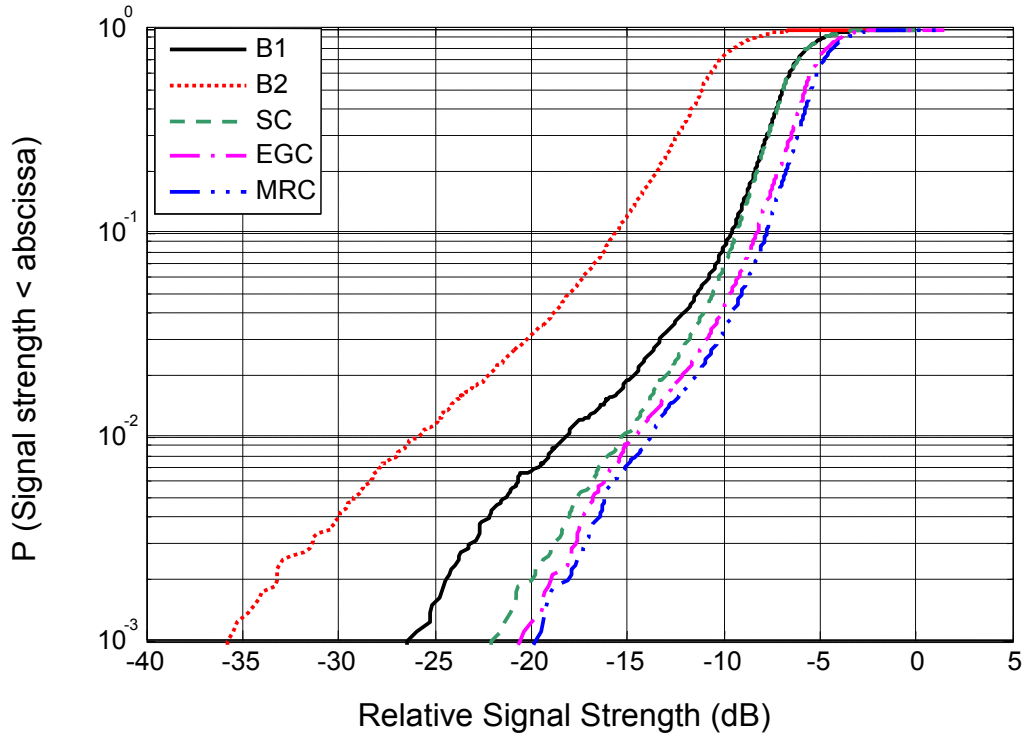

(a) Belt-Chest

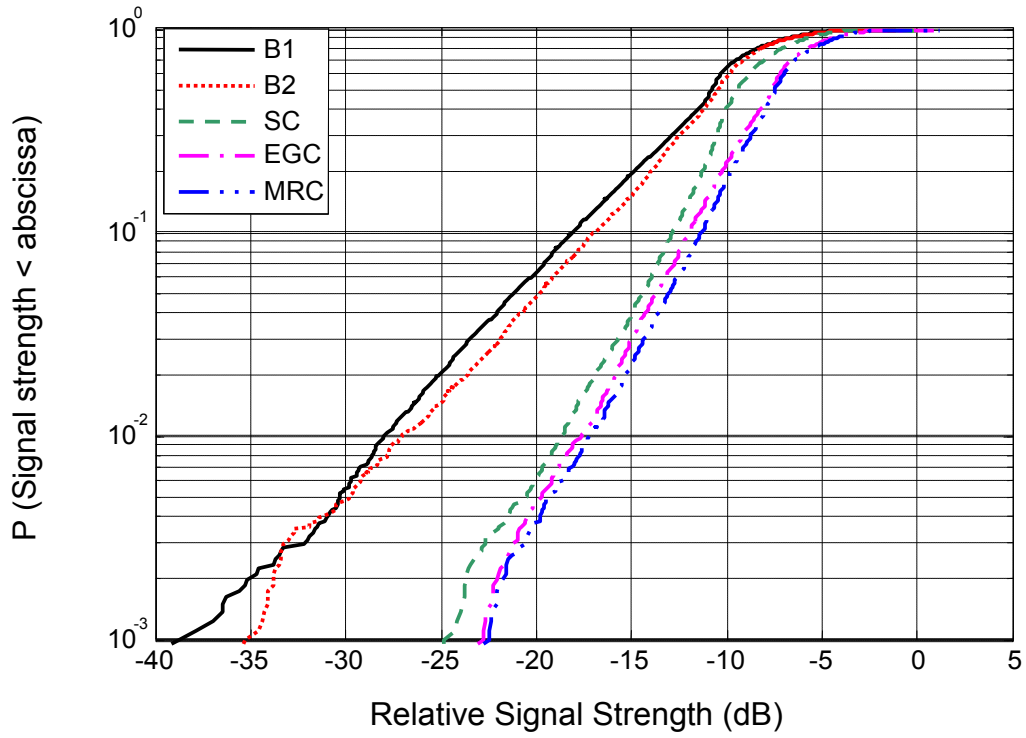

(b) Belt-Head

PTO for full caption

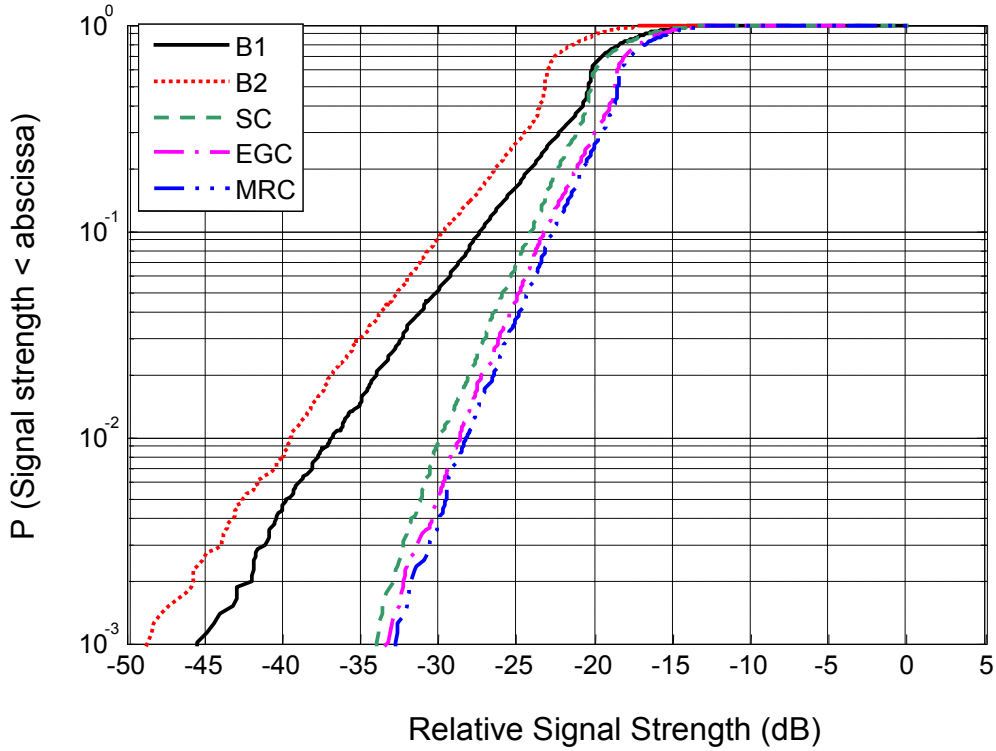

(c) Belt-Wrist

Fig 5.18: CDF plots of the three on-body channels with monopole spacing of λ/2 in the indoor laboratory environment at 5.8 GHz, signal strength is relative to the maximum value of the reference signal as all the signals were normalized to it

TABLE 5.7

RESULTS FOR THE 3 CHANNELS WITH MONOPOLES AT 5.8 GHz

Channel	Spacing	DG (dB)			ρ_s	ρ_e	Mean Power (dB)		Power diff (dB)
		SC	EGC	MRC			B1	B2	
Belt-Chest	λ/4	4.4	5.3	5.7	0.29 + 0.75i	0.44	-44.9	-42.6	2.3
	λ/2	2.9	3.6	4.4	0.61 - 0.42i	0.27	-42.3	-46.5	4.1
Belt-Head	λ/4	8.4	9.2	10.0	0.23 + 0.26i	0.26	-57.8	-58.5	0.6
	λ/2	8.4	9.4	9.8	0.14 + 0.31i	0.16	-56.9	-56.6	0.3
Belt-Wrist	λ/4	7.2	8.1	8.8	-0.21+ 0.06i	0.21	-51.9	-53.7	1.7
	λ/2	7.0	8.0	8.6	-0.36 - 0.08i	0.13	-49.8	-52.8	2.9

5.5.3 Results for 10 GHz measurements

The CDF plots of the received branch signals and the diversity combined signals are given in Fig. 5.19 for the three on-body channels measured at 10 GHz in the indoor laboratory environment with spacing of λ/2 between the diversity monopoles. Table 5.8 lists the DG values, complex correlation coefficient (ρ_s), envelope correlation coefficient (ρ_e), the mean received power at each branch, and the power imbalance between the two branches for the three on-body channels.

It is clear from the table that the correlation among the received branch signal envelopes is very low. The fading at this frequency is more severe and fast compared to the fading at the other two frequencies. The body movements in this case introduce significant de-correlation between the two branch signals even in the belt-chest case and hence high DG values are achieved. The signal is more attenuated compared to the attenuation at the other two frequencies, which can be verified by the low mean power values.

TABLE 5.8

RESULTS FOR THE 3 CHANNELS USING MONOPOLES WITH SPACING OF λ/2 at 10 GHz

Channel	DG (dB)			ρ_s	ρ_e	Mean Power (dB)		Power diff (dB)
	SC	EGC	MRC			B1	B2	
Belt-Chest	3.8	4.9	5.5	0.63 + 0.44i	0.14	-49.2	-50.33	2.31
Belt-Head	8.3	9.4	9.9	0.4 - 0.21i	0.03	-60.6	-60.50	0.17
Belt-Wrist	7.9	9.0	9.6	0.1 + 0.1i	-0.10	-56.2	-55.40	1.57

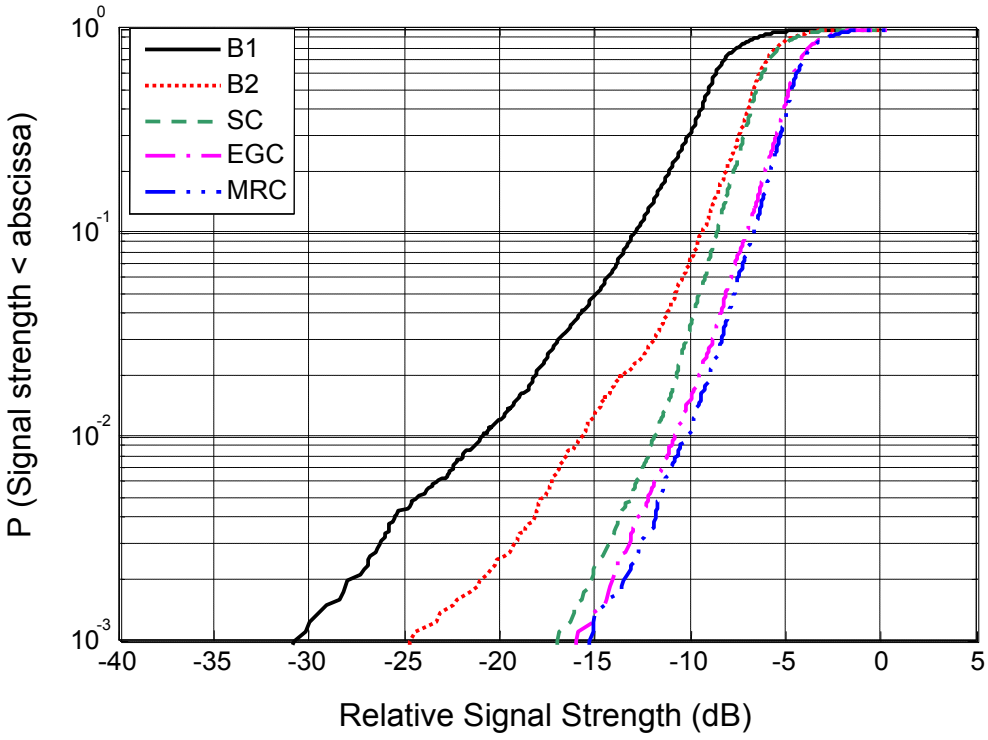

(a) Belt-Chest

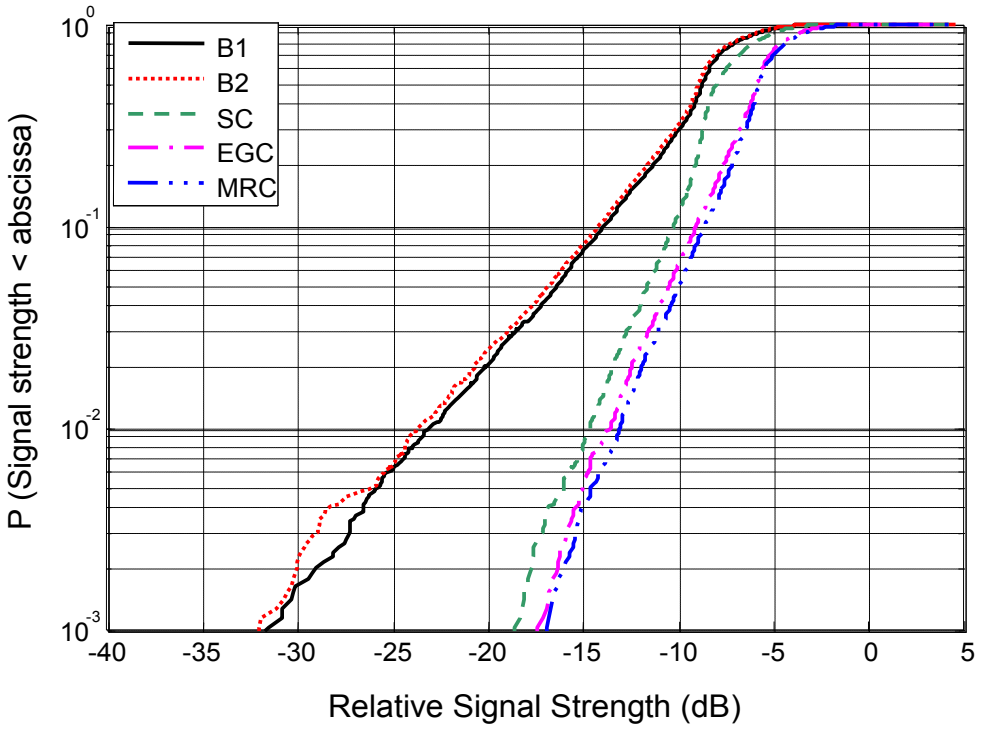

(b) Belt-Head

PTO for full caption

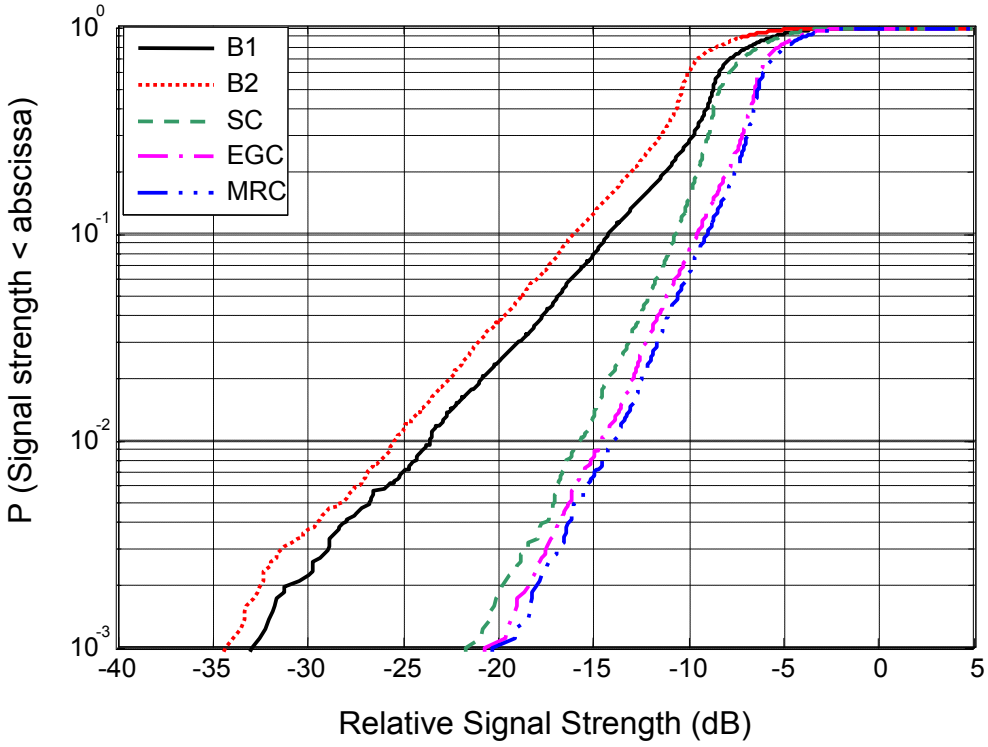

(c) Belt-Wrist

Fig 5.19: CDF plots of the three on-body channels with monopole spacing of λ/2 in the indoor laboratory environment at 10 GHz, signal strength is relative to the maximum value of the reference signal as all the signals were normalized to it

5.5.4 Discussion

It can be seen from the results that apart from the belt-chest channel, significant diversity gains are obtained even at smaller spacings where the correlation is the highest. The belt-chest channel has a direct line-of-sight (LOS) link and hence both the branch signals have high power imbalance, as one antenna is closer, than the other, to the Tx. Low scattering in this case results in high correlation between the branch signals. The DG is thus very low. The power imbalance is high for the belt-back and belt-head channels compared to the other channels, but the low correlation compensates for the high power imbalance and thus significantly high DG values are

achieved. The correlation is low in this case due to relatively high scattering, as the belt-back channel is completely non-LOS (NLOS) and belt-head is partial LOS but has dynamic movement of the Tx and Rx antennas with respect to each other. The high diversity gains and low correlation for the belt-ankle case is due to the high reflections from the floor. The belt-wrist channel is the most dynamic channel, but most of the time, there is a dominant component due to the LOS when the wrist is in front of the torso. By comparing the results for various channels in the anechoic environment in the absence of multipath from the surrounding environment, it can be seen that the dynamic channels, like belt-wrist and to some extent belt-head, give the best results. The static channels, which do not involve relative movement of the antennas, like belt-chest and belt-back, have significant power imbalance, which affects the diversity performance. Belt-ankle channel is an exception in this case as it involves high reflections from the metallic floor in the chamber and cannot be compared to the rest of the results. It can also be noted that the DG drops significantly in the chamber, which validates the fact that diversity is at its best in the presence of rich multipath and works better in a heavy cluttered environment.

The DG values presented here are obtained with the random movements, described in the measurement procedure, and removing the long-term variation caused by shadowing. However, in practical systems, if average received power is very low for postures where losses due to shadowing are high; the diversity gains may not be of much significance.

The comparison of the results at the three frequencies reveals that diversity performance is almost similar at the three frequencies.

5.5.5 Repeatability

It is worth underlining that the repeatability of the measurement procedure has been tested in order to verify the consistency and the reliability of the results presented. Measurements have been repeated identically four times with spacing of λ/2 and λ/4 at 2.45 GHz and λ/2 at 5.8 GHz and 10 GHz. The same postures and movements were replicated for all the channels. The repeatability measurements at 2.45 GHz space diversity monopole antennas were initially conducted by a visiting PhD student, Anda Guraliuc, during her 6 months visit at the University of Birmingham. The same were then repeated at this and the other two frequencies by the author.

Table 5.9 lists the difference recorded in the DG, envelope correlation coefficient, and the mean signal power for the four iterations of each case at 2.45 GHz and Table 5.10 presents the same at the other two frequencies. This is a measure of the error due to the repeatability of the movements done. Although it is impossible to exactly repeat the movements without error, but the results reveal that keeping the same environment and antenna positions on the body, the difference in movements only introduces a slight change in the diversity gain and the correlation. The results suggest that the diversity measurements are repeatable with an error of 2 dB maximum and 1.4 dB on average in the DG, and about 2 dB on average in the mean received power. The correlation is similar in all the iterations. This average error in diversity gain can be considered acceptable for most of the channels having high diversity gains. It follows that the procedure and the channel measurement may be considered reliable.

The measurements were also repeated on another day at 5.8 GHz and 10 GHz frequencies and thus disconnecting and re-mounting the antennas on the body at approximately the same positions. The results presented in Table 5.10 suggest that the error in measurements in terms of difference in diversity gain and correlation is slightly bigger in this case, but still acceptable for most of the channels with high diversity gains. This bigger difference is due to the slight change in the environment and the antenna positions when repeated on another day. Thus, the whole procedure may be considered consistent and repeatable with an error of $\pm$ 1.4 dB in DG on average.

5.5.6 Uplink and Downlink Diversity performance

Uplink and downlink diversity performance has been compared by repeating a number of the measurements reported above with the two-branch diversity antenna at the belt. By swapping the Tx and Rx antennas, the local scattering environment surrounding the diversity antenna changes and this leads to the difference in the results. Table 5.11 shows the results for 2.45 GHz measurements and Table 5.12 presents the results for the other two frequencies. The errors in DG and correlation are within the repeatability error range, and also, cases where it is assumed that the movements were not replicated exactly. However, in general the differences are not large.

TABLE 5.9

DIFFERENCE IN THE DIVERSITY GAIN, CORRELATION COEFFICIENTS, AND MEAN POWER OVER 4 MEASUREMENTS AT 2.45 GHz

Channel	λ/4 Spacing			λ/2 Spacing		
	DG MRC diff (dB)	ρ_e diff	Mean Power diff (dB)	DG MRC diff (dB)	ρ_e diff	Mean Power diff (dB)
Belt-Ankle	1.1	0.1	1.1	1.9	0.1	0.3
Belt-Chest	0.7	0.1	0.6	0.7	0.1	1.2
Belt-Back	2.1	0.1	2.2	0.6	0.1	1.6
Belt-Head	1.7	0.1	1.5	1.8	0.1	1.5
Belt-Wrist	1.9	0.1	0.7	2.1	0.2	0.9

TABLE 5.10

DIFFERENCE IN THE DIVERSITY GAIN, CORRELATION COEFFICIENTS, AND MEAN POWER OVER 4 MEASUREMENTS AT 5.8 GHz AND 10 GHz

	Channel	5.8 GHz			10 GHz		
		DG MRC diff (dB)	ρ_e diff	Mean Power diff (dB)	DG MRC diff (dB)	ρ_e diff	Mean Power diff (dB)
Same day	Belt-Chest	1.0	0.1	2.3	0.8	0.0	0.1
	Belt-Head	0.6	0.0	0.7	0.7	0.1	0.2
	Belt-Wrist	0.6	0.2	2.3	0.5	0.2	0.1
Another day	Belt-Chest	1.6	0.1	2.3	1.3	0.0	0.1
	Belt-Head	1.7	0.1	2.1	1.0	0.1	0.2
	Belt-Wrist	1.3	0.2	3.6	0.5	0.2	0.1

TABLE 5.11

THE UPLINK AND DOWN LINK DIVERSITY GAIN AND CORRELATION, AND THEIR DIFFERENCE FOR BELT-HEAD CHANNEL AT 2.45 GHZ

Spacing (multiple of λ)	Uplink		Downlink		Difference	
	DG MRC (dB)	ρ_e	DG MRC (dB)	ρ_e	DG MRC (dB)	ρ_e
0.08	9.9	0.36	8.9	0.44	1.04	0.08
0.16	8.1	0.46	6.6	0.51	1.50	0.05
0.25	7.7	0.25	7.7	0.23	0.01	0.02
0.33	7.9	0.12	7.8	0.32	0.13	0.20
0.41	8.5	0.23	7.5	0.39	1.04	0.15
0.49	9.3	0.25	6.9	0.31	2.37	0.06
0.65	9.0	0.30	8.2	0.28	0.87	0.03

TABLE 5.12

THE UPLINK AND DOWN LINK DIVERSITY GAIN AND CORRELATION, AND THEIR DIFFERENCE WITH MONOPOLES (λ/2 SPACING) AT 5.8 GHZ AND 10 GHZ

Antenna	Channel	Uplink		Downlink		Difference	
		DG MRC (dB)	ρ_e	DG MRC (dB)	ρ_e	DG MRC (dB)	ρ_e
Monopole at 10 GHz	Chest	5.5	0.13	6.5	-0.02	1.0	0.2
	Head	9.9	0.03	9.9	0.12	0.0	0.1
	Wrist	9.6	-0.10	9.3	0.18	0.3	0.3
Monopole at 5.8 GH	Chest	4.4	0.27	3.5	0.48	0.8	0.2
	Head	9.8	0.16	9.2	0.30	0.6	0.1
	Wrist	8.6	0.13	9.1	0.42	0.5	0.3

5.6 Conclusions

Significant diversity gain values are achieved for most of the on-body channels, which proves the significance of space diversity for body-worn devices. High diversity gains achieved for the on-body channels suggest that multipath due to the environment and body plays a relevant role in the on-body propagation phenomenon. The correlation of the antenna branches is low for most of the channels, which suggests that the diversity can provide very good improvement, if the power imbalance is carefully dealt with. Dynamic channels or channels with NLOS link give higher DG. The exact choice of demeaning window size is not critical, as the DG and correlation is fairly insensitive to the window size within a certain range, which depends on the channel and the movements involved. The diversity gains are higher in the indoor environment compared to the anechoic chamber, which suggests that the scattering due to the body itself is not too much but has a part to play in the diversity improvement. The diversity gain tends to increase with the increase in the antenna spacing. The diversity measurements are repeatable with a small error that is acceptable for most of the cases. The uplink and downlink diversity is reciprocal suggesting that the local off-body scattering environment is dominant. The diversity performance at low and high frequencies is more or less the same although the fading characteristics may change. The path loss at lower frequencies is less compared to that at the higher frequencies and the cost and complexity of hardware at higher frequencies is more. Therefore, low frequency is good choice for cost and path gain, but for future high data rate demand, high frequencies may be better option. Although, the diversity performance is degraded by the presence of a dominant channel in case of belt-chest, it can improve the system performance in terms of the

SNR without using diversity. However, in some cases like heavy cluttered environment, diversity may offer some improvement for belt-chest channel as well. As a system designer, the choice of whether to use diversity or not, for belt-chest channel, depends upon the improvement offered and the cost involved in implementing it.

REFERENCES

[1] P S Hall, Yang Hao, "Antennas and Propagation for Body-Centric Wireless Communications", *Artech House, London, 2006*.

[2] Nechayev Y I, Hall P S, Constantinou C C, Hao Y, Alomainy A, Dubrovka R and Parini C, "Antennas and Propagation for On-Body Communication Systems", *11th International Symposium on Antenna Tech and Applied Electromagnetics – ANTEM, France, 2005*.

[3] M.R Kamarudin, Y.I.Nechayev, P.S.Hall, "Performance of Antennas in the On-body Environment", *IEEE Antennas and Propagation Society International Symposium, 2005, 3-8 July 2005 Page(s):475-478 vol. 3A*.

[4] A.A. Serra, P. Nepa, G. Manara, P.S. Hall, "On the Performance Analysis of Diversity Techniques in Body-Centric Communication Systems," *IET Seminar on Antenna and Propagation for Body-Centric Wireless Communications*, *London, UK, April 24, 2007, pp. 63-66.*

[5] A.A. Serra, P. Nepa, G. Manara, and P.S. Hall, "Diversity Measurements for On-Body Communication Systems," *IEEE Antenna and Wireless Propagation Letters, vol. 6 (1), pp. 361 – 363, 2007.*

[6] I Khan, L Yu, Y I. Nechayev, P S. Hall, "Space and Pattern Diversity for On-body Communication Channels in an Indoor Environment at 2.45 GHz*", 2nd European Conference on Antennas and Propagation (EuCAP), Edinburgh, UK , 11-16 Nov 2007.*

[7] I Khan, M R. Kamarudin, L Yu, Y I. Nechayev, P S. Hall, "Comparison of Space and Pattern Diversity for On-body Channels*", 5th European Workshop on Conformal Antennas, Bristol, UK, 10- 11 September 2007.*

[8] I Khan, Peter S. Hall, "Multiple Antenna Reception at 5.8 and 10 GHz for Body-Centric Wireless Communication Channels", *IEEE Transactions on Antennas and Propagation, Vol. 57, No.1, Jan 2009*.

[9] I Khan, P.S. Hall, A.A Serra, A.R. Guraliuc, P. Nepa, "Diversity Performance Analysis for On-body Communication Channels at 2.45 GHz" *IEEE Transactions on Antennas and Propagation, Vol. 57, No. 4, April 2009.*

[10] R G. Vaughan and J B Andersen, "Antenna Diversity in Mobile Communications*", IEEE transaction on Vehicular Technology, Vol. VT-36. No. 4 Nov 1987*.

[11] N. L. Scott and R. G. Vaughn "The Effect of Demeaning on Signal Envelope Correlation Analysis", *4th Intl. Symposium on Personal, Indoor and Mobile Radio Communications, Yokohama, Japan, Sep. 1993.*

[12] Per-Simon Kildal,, K Rosengren, "Electromagnetic Analysis of Effective and Apparent Diversity Gain of Two Parallel Dipoles*", IEEE Antennas And Wireless Propagation Letters, Vol. 2, 2003.*

[13] J S. Colburn, Y Rahmat-Samii, M A. Jensen, G J. Pottie, "Evaluation of Personal Communications Dual-Antenna Handset Diversity Performance*", IEEE Transactions On Vehicular Technology, Vol. 47, No. 3, August 1998*.

[14] W. C. Y. Lee, "Mobile Communication Engineering", *New York: Wiley, 1982.*

[15] W.C. Jakes, "Microwave Mobile Communication", *New York: Wiley, 1974.*

Chapter 6

Pattern and Polarization Diversity for On-body Channels

6.1 Introduction

Although the monopole antennas are the best in terms of path gain for on-body channels [1], a major problem is the mounting on the body. Its non low-profile shape is inconvenient for many body applications. In addition, due to its omni-directional radiation pattern in the plane parallel to the surface of the body, it can only be used to implement space diversity and is not feasible for achieving pattern or polarization diversity. The study of space diversity for on-body channels has been presented in the previous chapter, but it is worth noting that pattern and polarization diversity can also provide significant benefit to the on-body applications. With dynamic movements of the body, the reflection of the wave from the body parts as well as the surrounding objects may introduce some variation in the angles of arrival at the receiver side. Radiation pattern diversity can thus perform well in this situation. Depolarization of the transmitted wave may also occur due to reflections from the body. Depending upon the amount of depolarization, the use of polarization diversity may be of benefit. The polarization diversity has the benefit of using a single antenna with dual polarization compared to space and pattern diversity, which requires more than one antenna. Polarization diversity may provide good performance and can compensate for the polarization mismatch caused in random movements for the

channels involving dynamic movements and random orientation of the antennas. To investigate the performance of pattern and polarization diversity, some practical antennas were used that are used in current body worn devices. For the on-body channels, pattern and polarization diversity antennas must be designed carefully to prevent one branch antenna signal being dominant compared to the other for various positions and postures of the body, otherwise, the high power imbalance can severely affect the diversity performance. Due to limited changes in the antenna orientations for most of the channels, the power imbalance will be larger if the patterns or polarizations of the diversity antennas are very different. This chapter presents the pattern and polarization diversity analysis and performance for on-body communication channels at 2.45 GHz and 5.8 GHz using different types of antennas in the indoor environment. Diversity gains and correlation coefficients are calculated for some realistic antennas mountable on the body, namely, the printed-inverted F antenna, (printed-IFA) the planar inverted F antenna (PIFA), and a monopole-loop pair for polarization diversity. The description of the antennas used in this study is presented in Section 6.2. Similar measurements, as described for space diversity monopoles, were carried out for five on-body channels at 2.45 GHz and three channels at 5.8 GHz and the data was processed to extract the results in similar way with window sizes given in Table 6.1. The repeatability and uplink-downlink diversity measurements were also carried out. The results are presented in Section 6.3 and the conclusions in Section 6.4. The work presented here has already been published in [2-4].

TABLE 6.1
SIZE OF THE DEMEANING WINDOW FOR VARIOUS CHANNELS WITH PRINTED-IFA, PIFA, AND POLARIZATION DIVERSITY ANTENNA

	Channel	Window size (ms)	
		2.45 GHz	5.8 GHz
Printed -IFA	Belt-Chest	800	636
	Belt-Head	800	636
	Belt-Wrist	740	424
PIFA	Belt-Chest	900	424
	Belt-Head	900	424
	Belt-Wrist	780	424
Polarization diversity antenna	Belt-Chest	1000	-
	Belt-Head	1000	-
	Belt-Wrist	1000	-
	Belt-Ankle	1000	-
	Belt-Back	1000	-

6.2 Antennas used in measurement

6.2.1 Diversity Printed Inverted-F Antenna (Printed IFA)

The first type of antenna used for pattern and polarization diversity analysis was a printed-IFA diversity antenna that is proposed in [5] for 5.2 GHz operation, and used in some current Bluetooth headsets. It was re-designed for 2.45 GHz and 5.8 GHz operations. Three configurations of this antenna were used, which are shown in Fig 6.1. All the antennas were fabricated on a 0.8 mm thick FR4 substrate. Configuration A and B are space and pattern diversity antennas with mirrored patterns. Configuration C is a pattern and polarization diversity antenna with orthogonal patterns. For 5.8 GHz measurements, only configurations A and B were used. The substrate and the ground plane sizes are given for the three configurations and the two frequencies in Table 6.2 along with some other design parameters. In each case, the length of the longer arm of the inverted-F is 22 mm for 2.45 GHz and 10 mm for

5.8 GHz. The length of the shorter arm, and hence the short-circuit element, is 3 mm for both frequencies. The distance between the feeding line and the short-circuit element is 3 mm for 2.45 GHz and 2 mm for 5.8 GHz, whereas, the copper trace width of the antenna element is 1 mm for all cases. The transmitting antenna in each case was the same but a single element printed-IFA. The dimensions and design parameters of the Tx antennas are also given in Table 6.2. (The single element Printed-IFA Tx antenna at 2.45 GHz was designed by an M.Phil student Zen H. Hu for his work. All the other antennas were designed and fabricated for this work by the author).

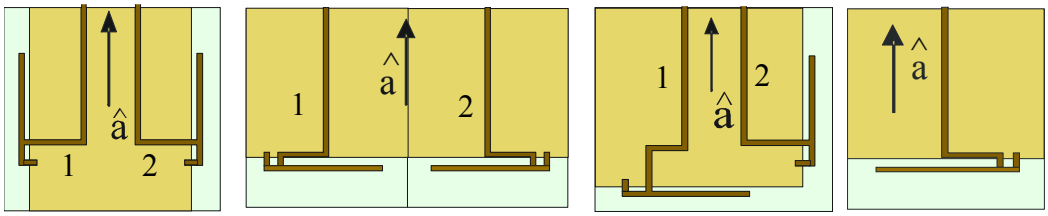

Fig 6.1: The three configurations of the printed-IFA diversity antenna and the single element printed-IFA used as Tx
Dark Brown lines (Black) are the metallic conductors. Metallic ground planes are in light copper color (grey) and the substrate is indicated by light green (light grey)

Very little detuning was observed when the antennas were mounted on the body. Table 6.2 also lists the mutual coupling between the antenna elements and their return losses. Due to the low mutual coupling, they represent a valuable choice for the diversity implementations. These values of the mutual coupling are within the range where reduction in efficiency is acceptable with reasonable correlation between the branches. Numerical simulations have shown that the radiation

efficiency of the diversity antennas was not deeply affected by the mutual coupling between them, when compared with the radiation efficiency of the corresponding single isolated antennas. It reduced by less than 8% for all the configurations of the printed IFA. Figs. 6.2 – 6.5 show the measured radiation patterns, showing directivity plots, of the isolated printed-IFA and each of the two elements of the diversity antennas at 2.45 GHz in xy-plane (assuming the local coordinate system for antennas), which is the plane of interest for the on-body channels. While measuring the radiation pattern of an element of the diversity antenna, the other element was terminated by 50 ohms. Figs. 6.6 – 6.8 show similar patterns for the 5.8 GHz operation. The patterns of the diversity antennas are slightly skewed due to the mutual coupling and asymmetrical due to imperfect matching of the neighboring antenna.

TABLE 6.2

DIMENSIONS AND OTHER PARAMETERS OF THE PRINTED-IFA

Frequency	Configuration	Substrate size (mm)	Ground plane size (mm)	Reflection coefficient (dB)	Mutual coupling (dB)
2.45 GHz	Tx	30 x 30	20 x 30	-14.9	-
	Conf. A	40 x 40	30 x 40	-11.4	-16
	Conf. B	40 x 60	30 x 60	-16.5	-10
	Conf. C	40 x 40	30 x 40	-10.4	-12
5.8 GHz	Tx	15 x 15	15 x 10	-14.3	-
	Conf. A	25 x 16	16 x 16	-15.1	-14.1
	Conf. B	30 x 20	30 x 15	-14.8	-13.3

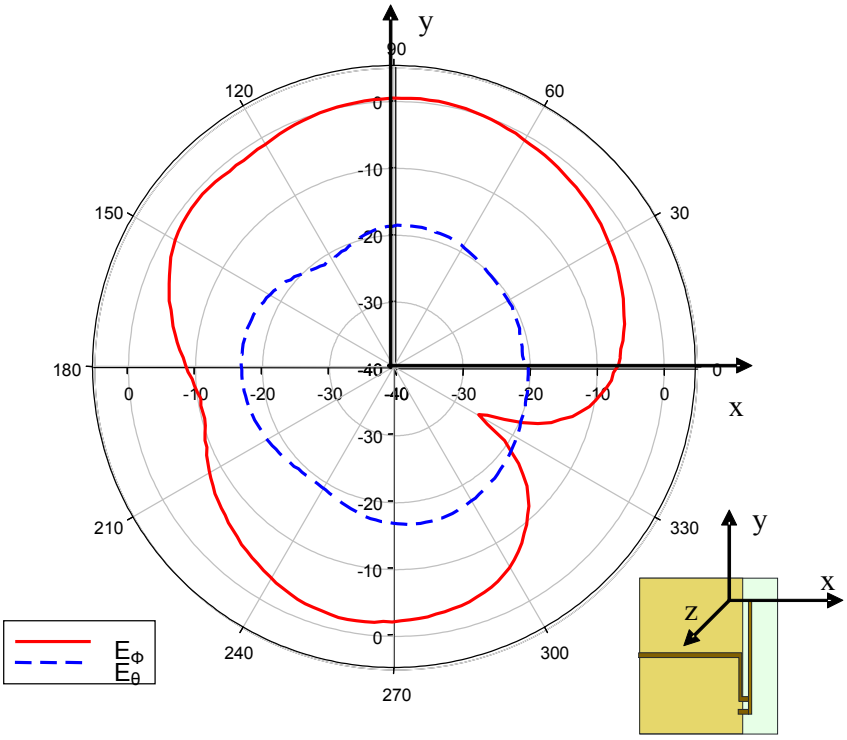

Fig 6.2: Measured radiation patterns of the isolated printed-IFA as a function of φ at 2.45 GHz

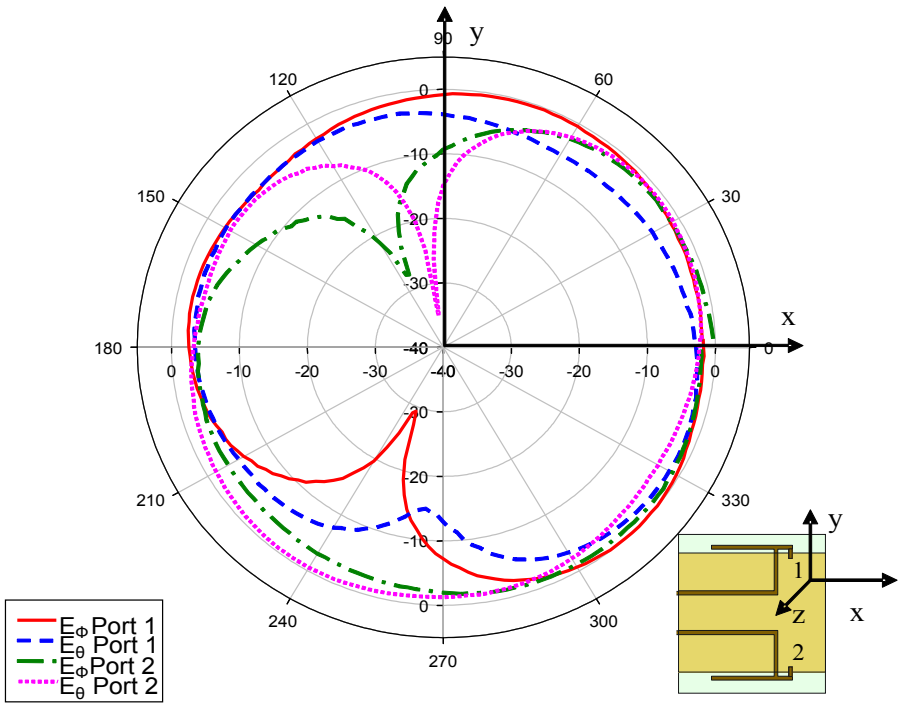

Fig 6.3: Measured radiation patterns of the diversity printed-IFA elements in configuration "A" as a function of φ at 2.45 GHz

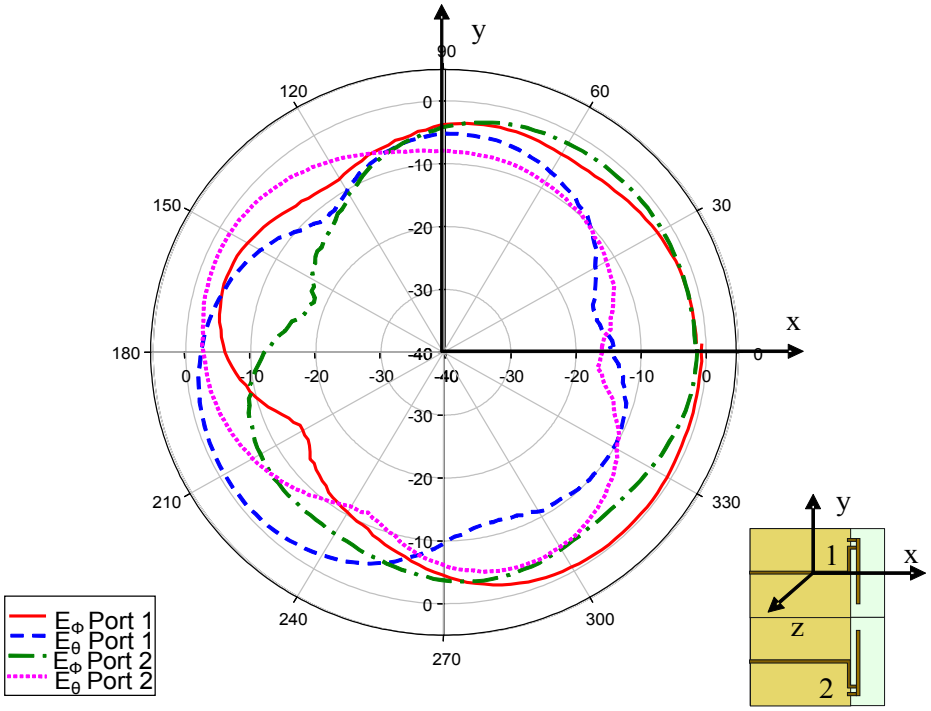

Fig 6.4: Measured radiation patterns of the diversity printed-IFA elements in configuration "B" as a function of φ at 2.45 GHz

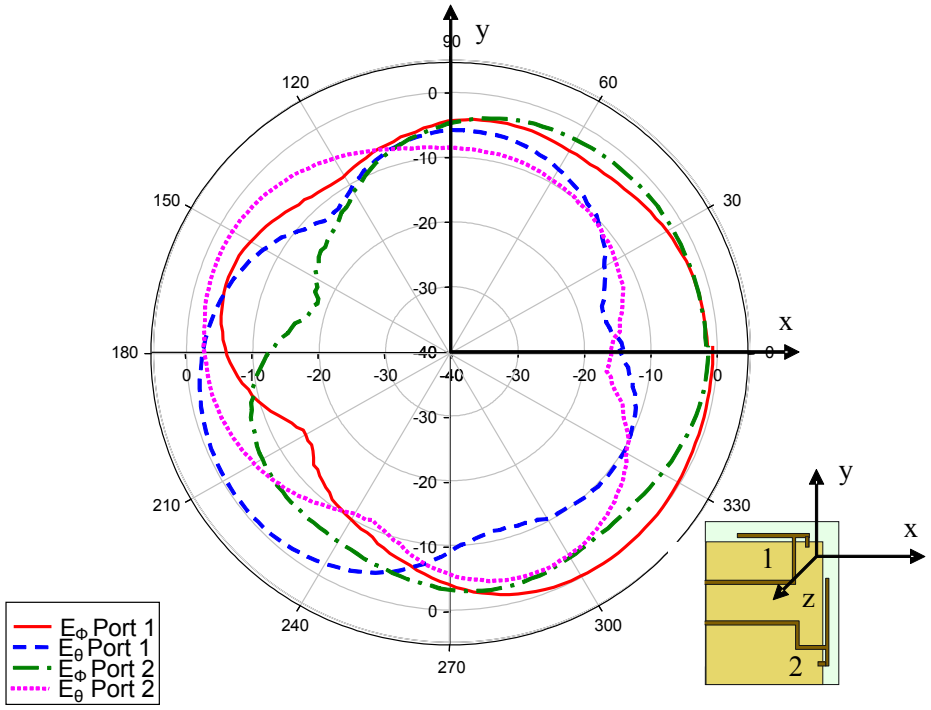

Fig 6.5: Measured radiation patterns of the diversity printed IFA elements in configuration "C" as a function of φ at 2.45 GHz

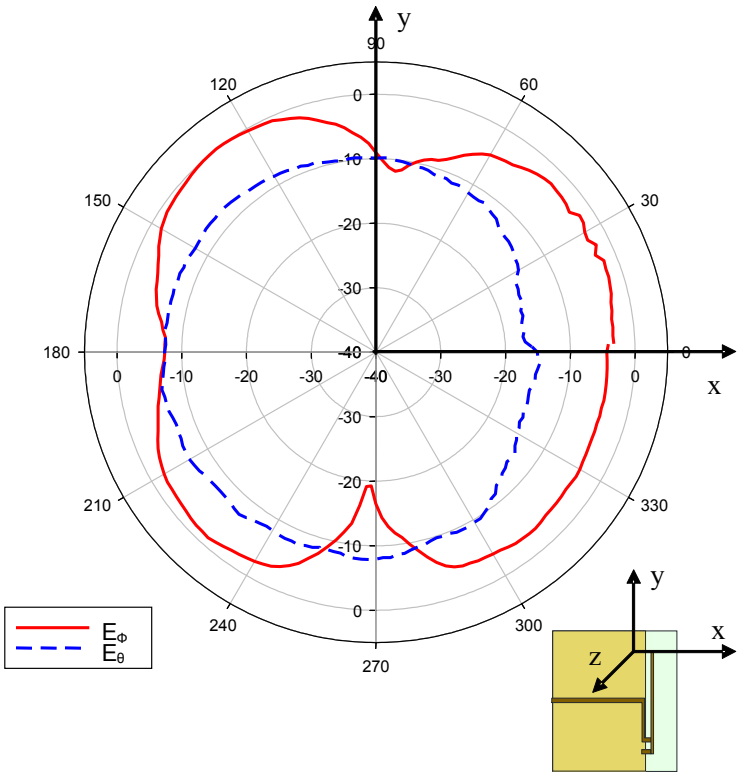

Fig 6.6: Measured radiation patterns of the isolated Printed-IFA as a function of φ at 5.8 GHz

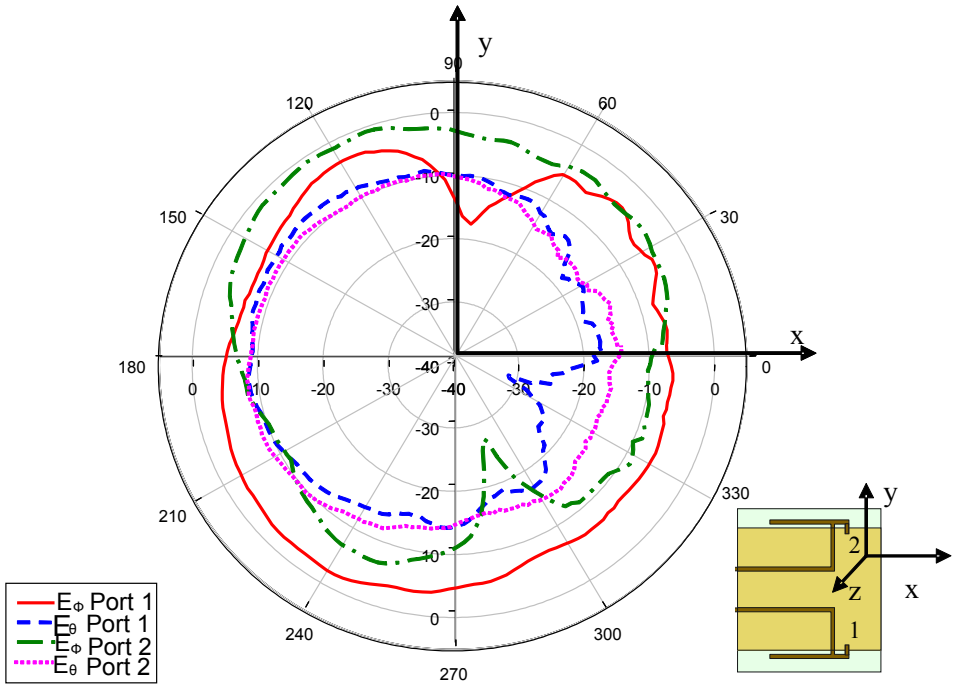

Fig 6.7: Measured radiation patterns of the diversity printed IFA elements in configuration "A" as a function of φ at 5.8 GHz

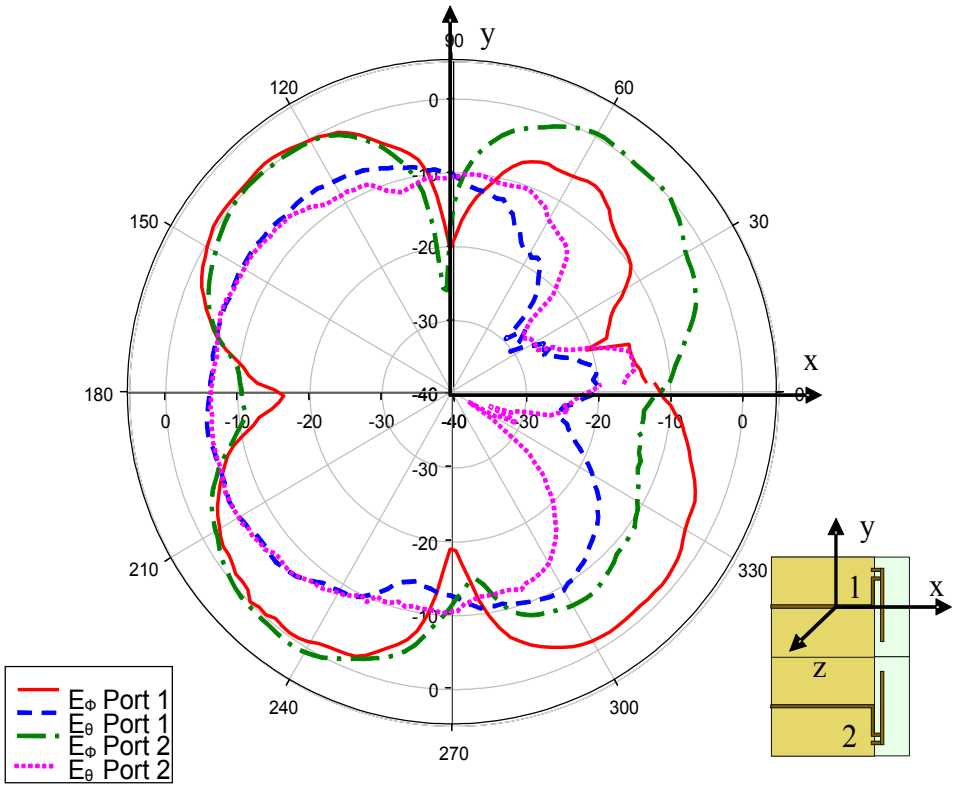

Fig 6.8: Measured radiation patterns the of diversity printed IFA elements in configuration "B" as a function of φ at 5.8 GHz

Assume that $\hat{a}$ is a unit vector pointed towards the direction of the feeding line (as shown in Fig. 6.1) and $\hat{x}$, $\hat{y}$,$\hat{z}$ are the unit vectors corresponding to the x, y, and z axes for the body-coordinate system shown in Fig. 6.9. The three diversity printed-IFA configurations, shown in Fig. 6.1, were oriented in different ways. The orientations for one configuration are shown in Fig 6.10. The other configurations were oriented the same way. For all the five channels $\hat{a} = \hat{z}$ in orientation 1 and $\hat{a} = -\hat{z}$ in orientation 3. In orientation 2, $\hat{a} = \hat{x}$ for belt-head and $\hat{a} = \hat{y}$ for the other four channels, whereas, in orientation 4, $\hat{a} = -\hat{x}$ for belt-head and $\hat{a} = -\hat{y}$ for the others.

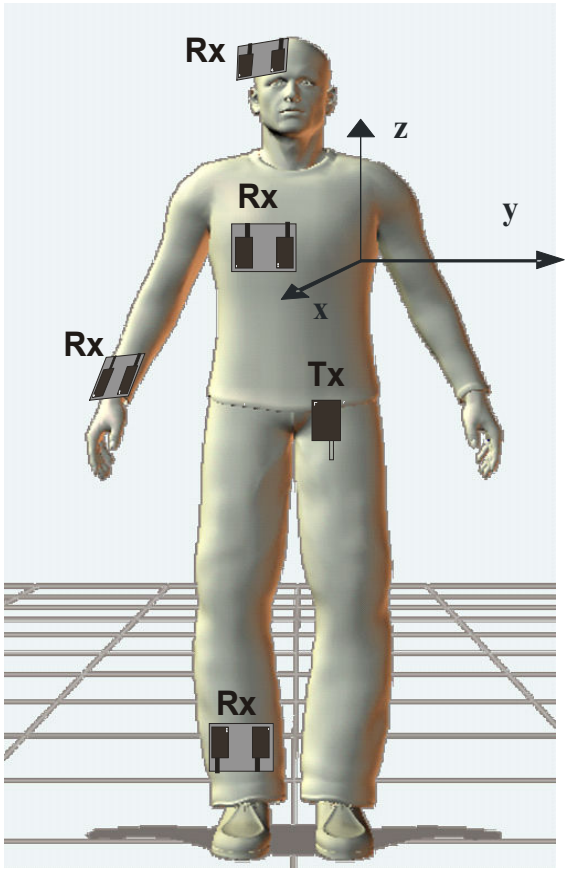

Fig 6.9: Body-fixed reference system.

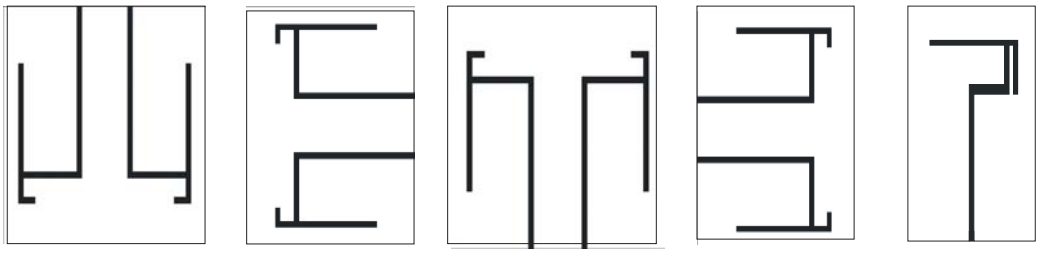

(a) Or1 (b) Or 2 (c) Or 3 (d) Or4 (e) Tx

Fig 6.10: Orientations of printed-IFA on the body for front view of the body: (a) – (d) Rx diversity antenna and (e) Tx on the belt with $\hat{a} = -\hat{y}$ for belt-chest, belt-head, belt-back channels, $\hat{a} = -\hat{z}$ for belt-wrist and $\hat{a} = \hat{y}$ for belt-ankle channel

6.2.2 Diversity Planar-Inverted-F Antenna (PIFA)

The second type of realistic antenna used for pattern diversity in this study is a microstrip-fed PIFA on 0.8 mm FR4 substrate. In the diversity antenna form, it consists of two PIFA elements on a single ground plane, as shown in Fig. 6.11. This is a space and pattern diversity antenna with the same polarization but different patterns. Both radiating plates are identical. The antenna dimensions and some other design parameters are given in Table 6.3 for both the operating frequencies. Very little detuning was observed by placing the antennas close to the body. The radiation efficiency reduced to about 10 % of the isolated antenna due to mutual coupling in this case. The measured radiation patterns of the isolated and diversity PIFA elements are shown in Fig 6.12 and Fig 6.13 for 2.45 GHz operation and in Fig. 6.14 and Fig. 6.15 for the 5.8 GHz operation, respectively, for the xy-plane of the antennas. The same orientations, as described previously for the printed-IFA, were used for all the channels with PIFA.

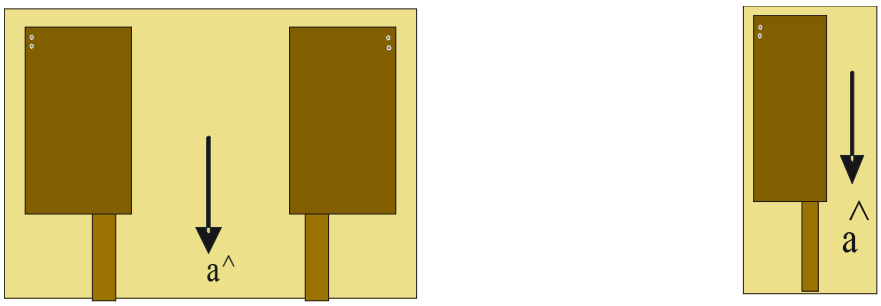

(a) (b)

Fig 6.11: (a) Diversity PIFA with the same orientations as shown in Fig. 6.10 for printed-IFA and (b) PIFA Tx antenna with $\hat{a} = \hat{y}$ for belt-wrist and belt-ankle and $\hat{a} = -\hat{z}$ for belt-chest, belt-back, and belt-head channels

TABLE 6.3
DIMENSIONS AND OTHER DESIGN PARAMETERS OF THE PIFA

	2.45 GHz		5.8 GHz	
	Tx PIFA	Diversity PIFA	Tx PIFA	Diversity PIFA
Substrate/Ground plane size (mm)	20 x 40	50 x 40	20 x 12	20 x 20
Size of radiating plates (mm)	12.5 x 20	12.5 x 20	6 x 9	6 x 9
Height of plate above substrate (mm)	4	4	3	3
Distance between the two nearby edges of the radiating plates (mm)	-	25	-	7
Distance between the short-circuit pin and the feed line (mm)	2	2	3	3
Reflection coefficient (dB)	-12.2	-13.6	-21.1	-16.4
Mutual coupling (dB)	-	-14	-	-17

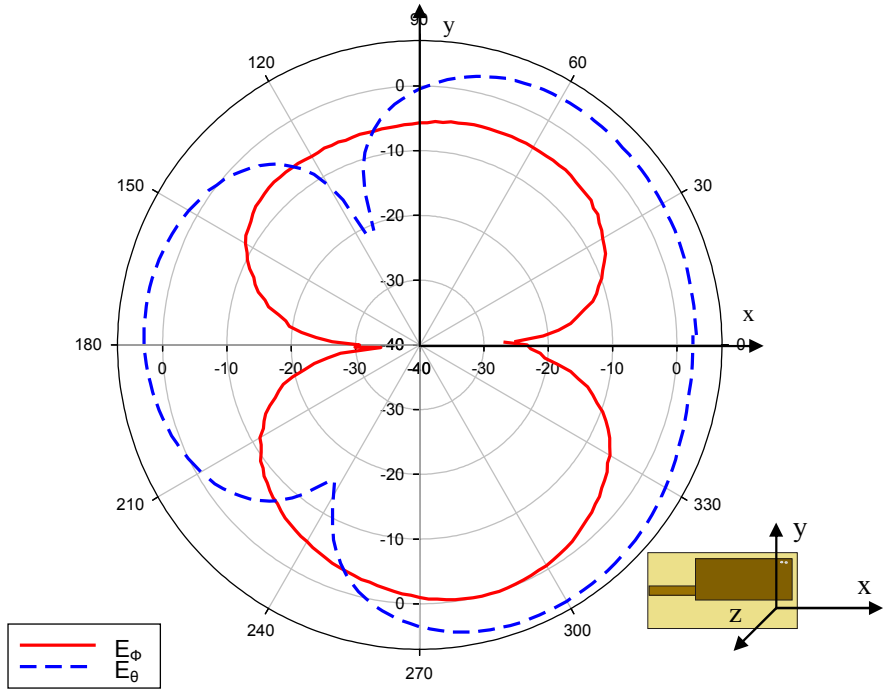

Fig 6.12: Measured radiation patterns of the isolated PIFA in the x-y plane at 2.45 GHz

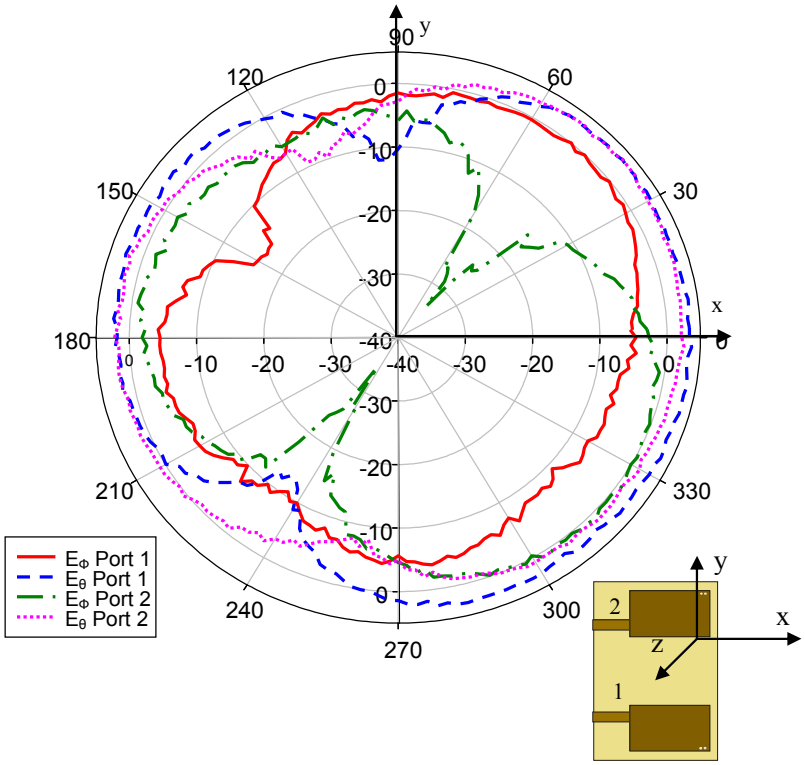

Fig 6.13: Measured radiation patterns of the diversity PIFA elements in the x-y plane at 2.45 GHz

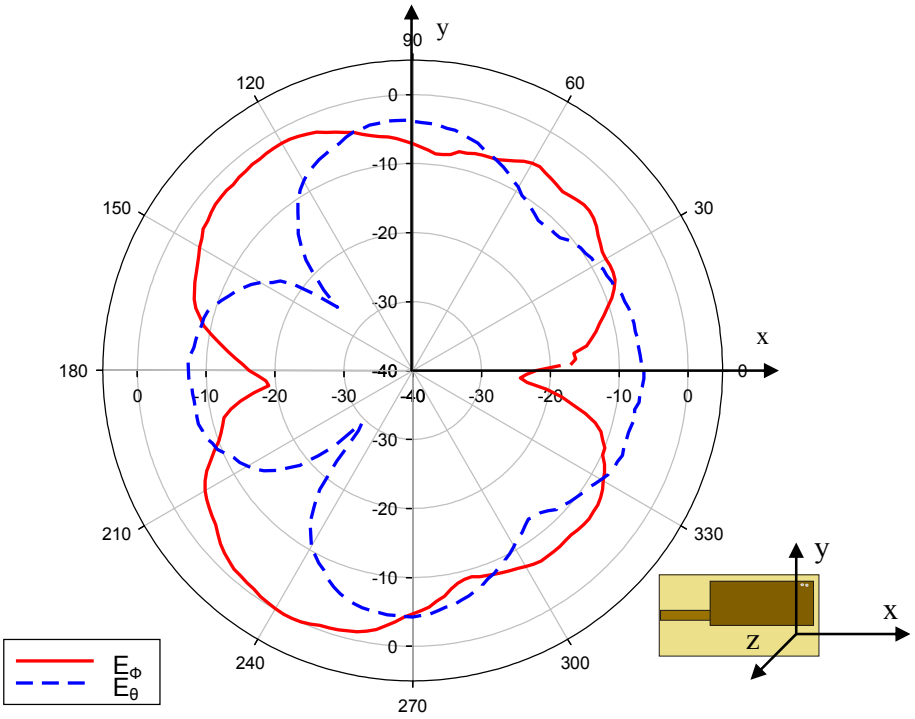

Fig 6.14: Measured radiation pattern of the isolated PIFA in the x-y plane at 5.8 GHz

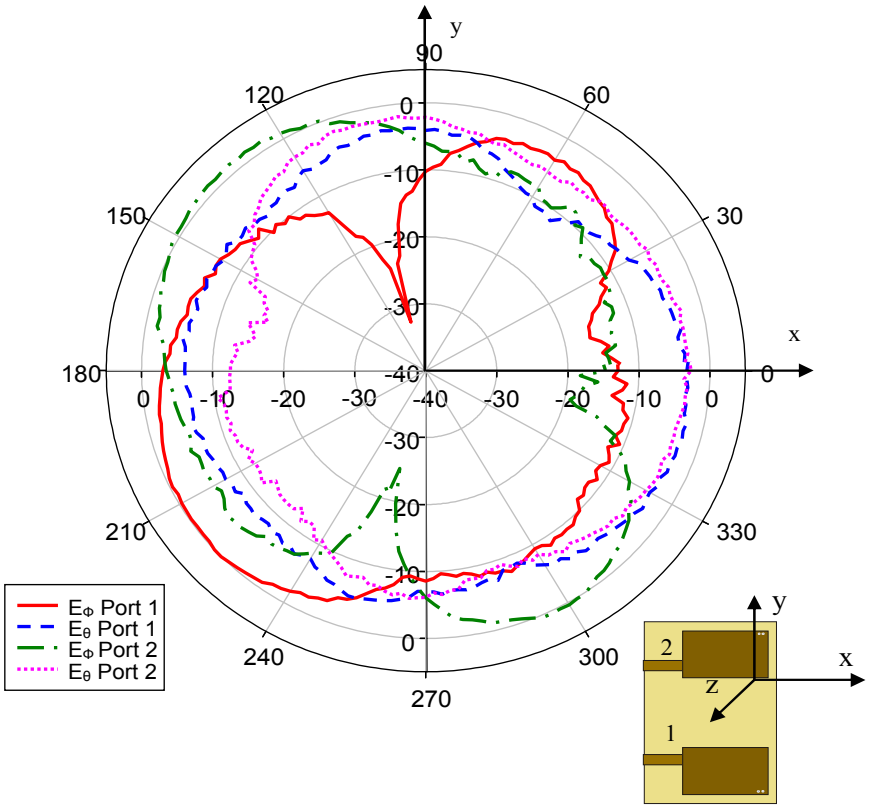

Fig 6.15: Measured radiation patterns of the diversity PIFA elements in the x-y plane at 5.8 GHz

6.2.3 Polarization Diversity Antenna

To carry out a polarization study for on-body channels, a dual-polarization antenna was designed for 2.45 GHz operation by another PhD student, Lida Akhoondzadeh-Asl, for her work. The antenna design details are given in [4]. It is a monopole-loop pair, with the loop antenna and the ground plane for the monopole printed on two different sides of a 0.8 mm thick FR4 substrate, as shown in Fig. 6.16. Radius of the monopole ground plane is 13 mm and inner and outer radii of the loop are 18 mm and 16 mm, respectively. The monopole is made of a copper cylinder with 30 mm length and 2 mm diameter, top-loaded by a copper plate with 5 mm radius. The length and width of coplanar waveguide (CPW) line, which is etched in the

monopole ground plane, are 23 mm and 2 mm, respectively. The measured radiation patterns, giving directivity plots, of the monopole and loop elements are given in Fig. 6.17. This antenna was used to carry out a polarization diversity study as it produces two polarizations, one normal to the surface of the body by the monopole antenna and another tangential to the body surface by the loop element, if the antenna is mounted on the body.

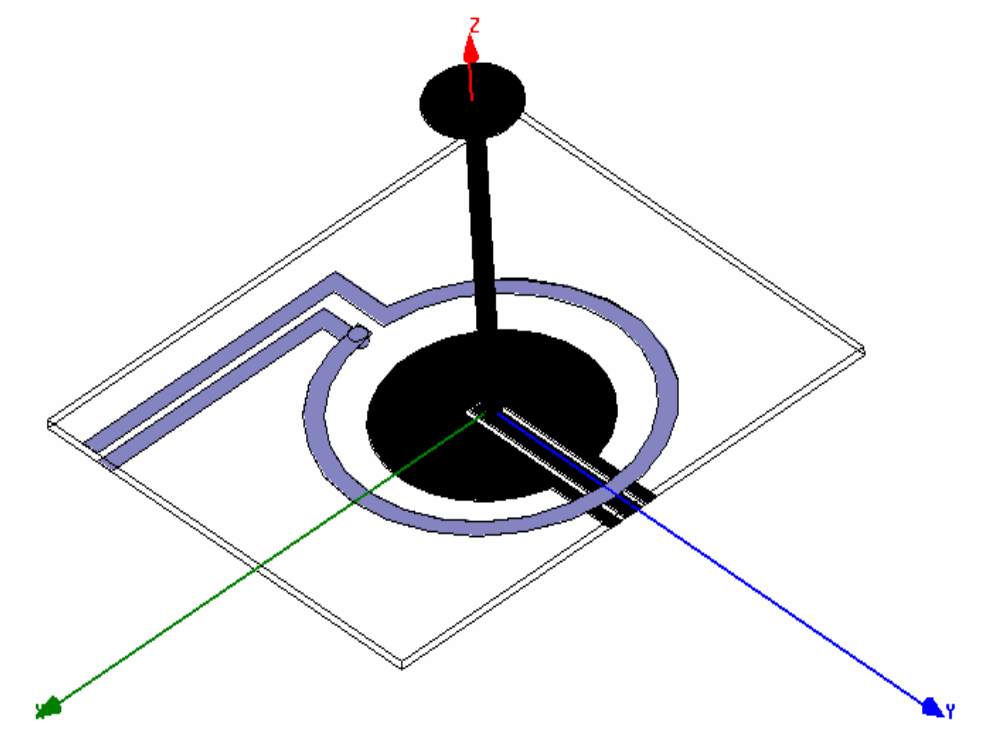

Fig 6.16: Polarization diversity antenna's geometry, which is combination of top loaded monopole and loop antenna

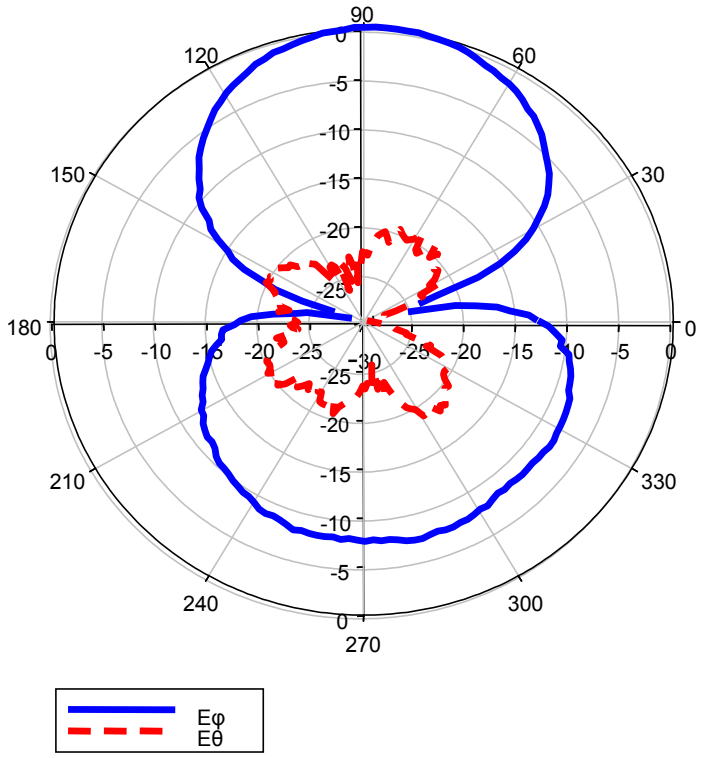

(a)

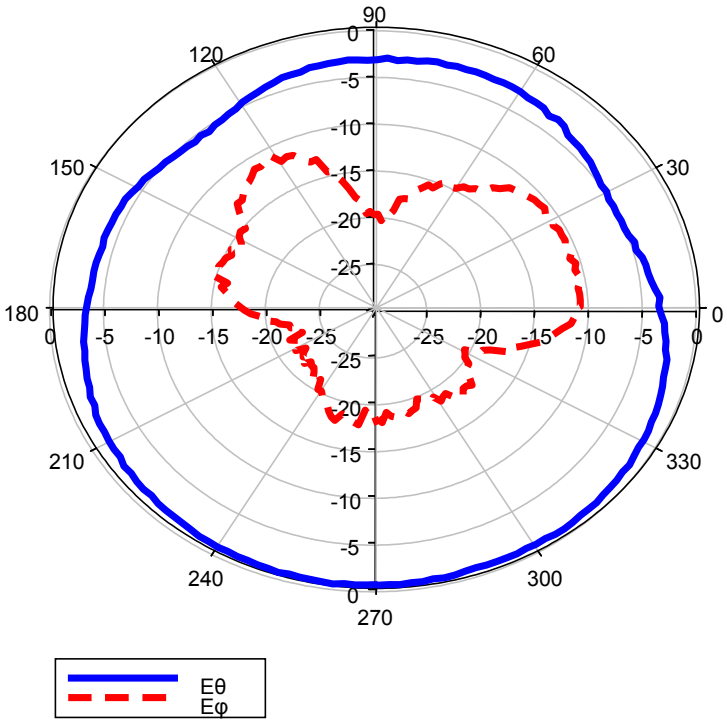

(b)

Fig 6.17: Measured radiation patterns in x-y plane (a) Loop antenna (b) Monopole antenna, with the other element terminated by 50 ohms

6.3 Results

6.3.1 Printed-IFA

Like the space diversity study, the measured data with the printed-IFA was analyzed and similar results, like diversity gains, correlation coefficients, mean power of the branch signals, and the power imbalance between the branches, were obtained. The CDF plots for the five on-body channels at 2.45 GHz and three channels at 5.8 GHz with configuration A of the diversity printed-IFA are given in Figs. 6.18 and 6.19, respectively. The results extracted from the measured data are presented in Tables 6.4 – 6.11 for all the channels at the two frequencies.

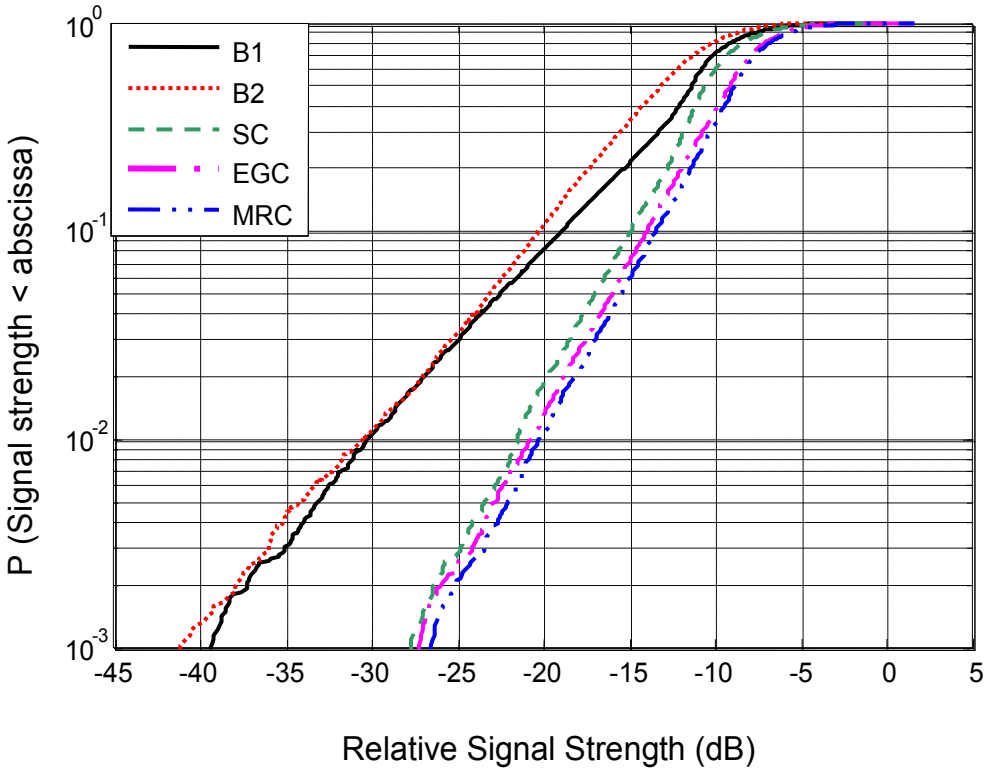

(a) Belt-Ankle

PTO for full caption

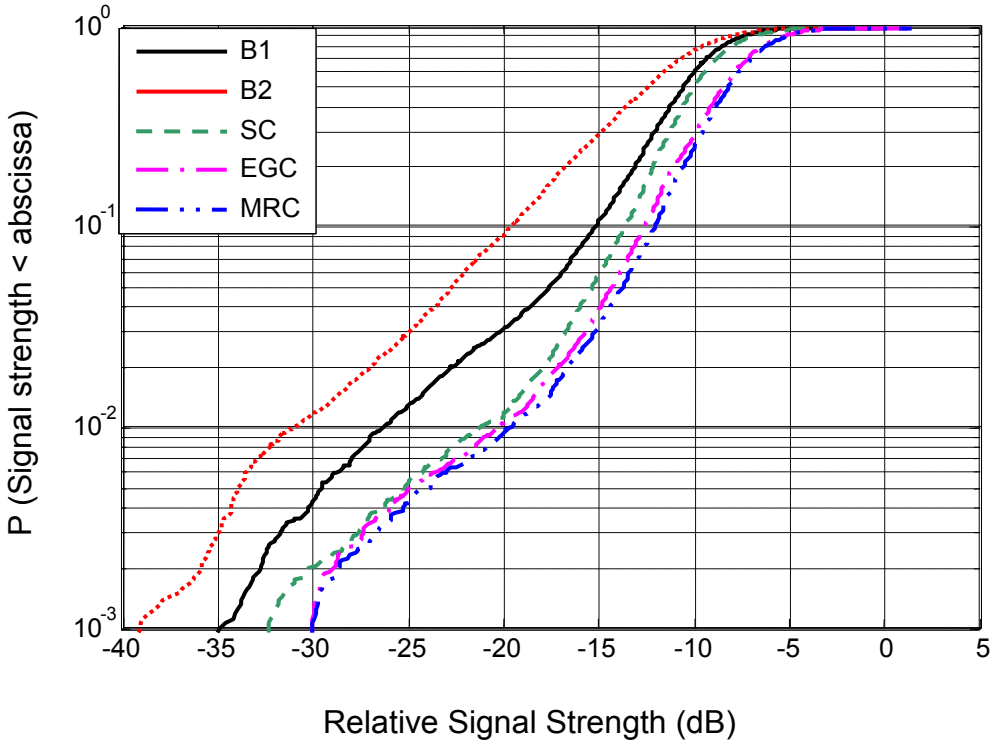

(b) Belt-Chest

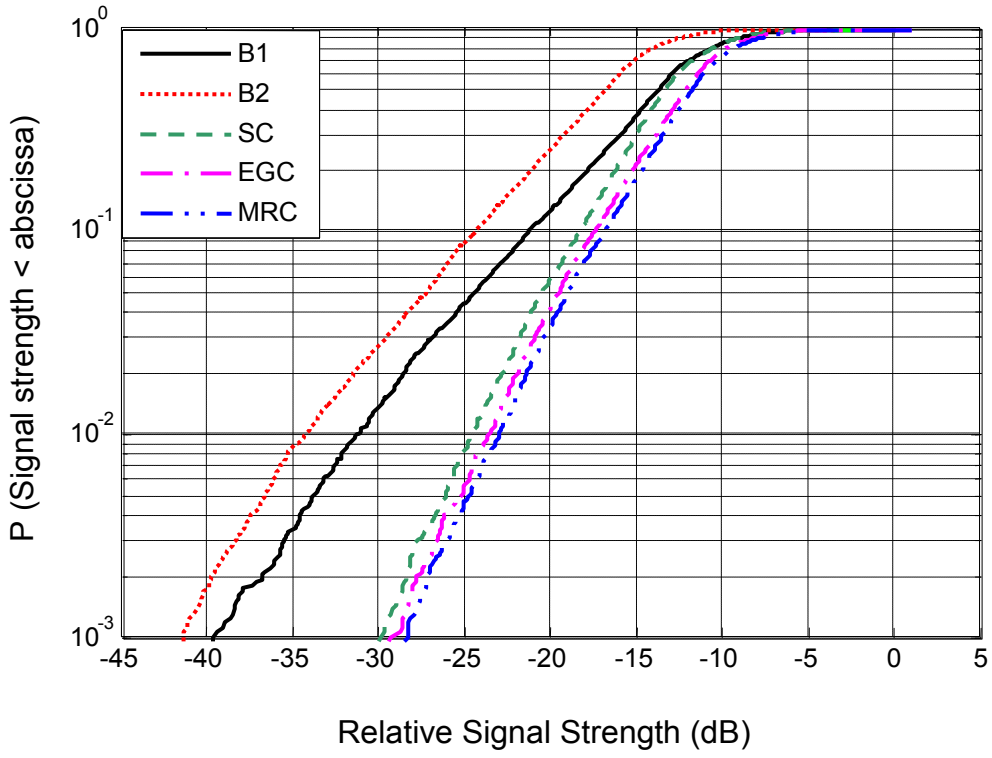

(c) Belt-Back

PTO for full caption

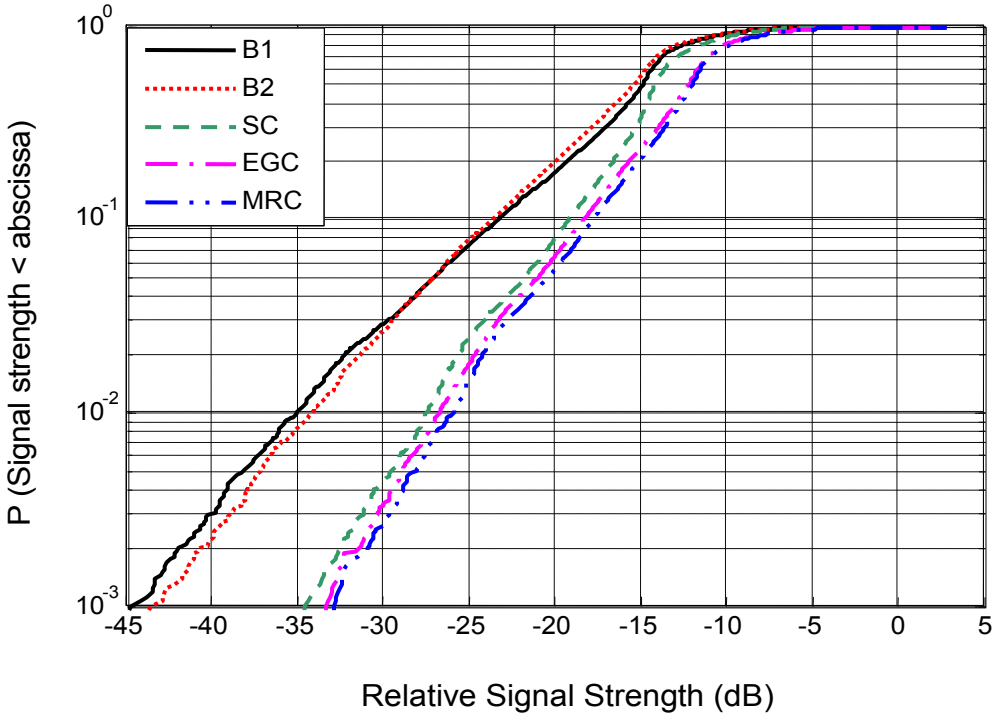

(d) Belt-Head

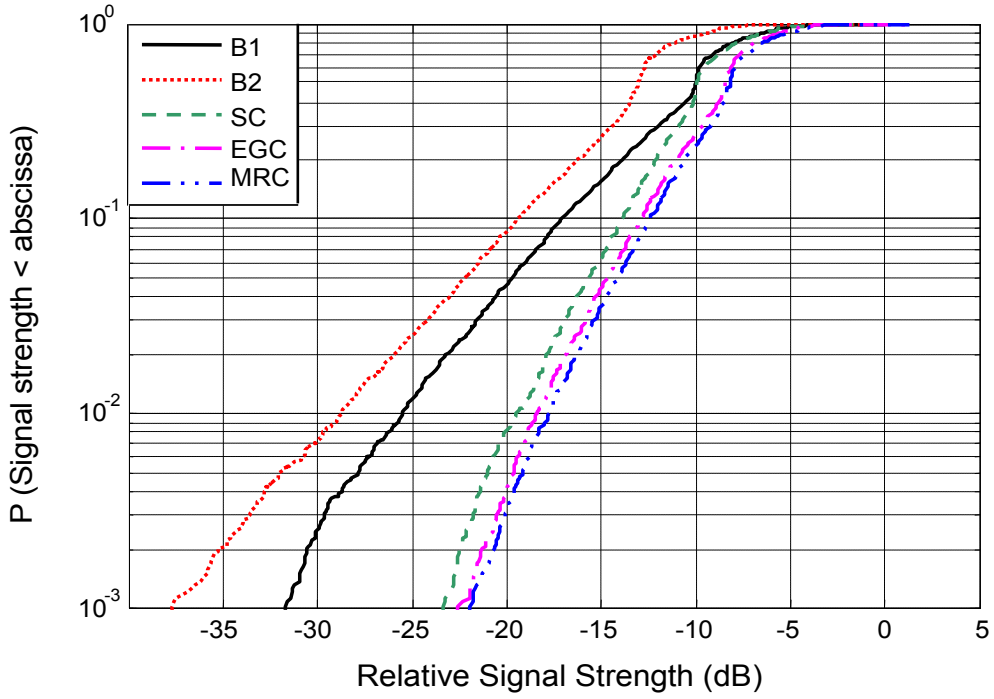

(e) Belt-Wrist

Fig 6.18: CDF plots of branch and combined signals for the five on-body channels with configuration A of printed-IFA in orientation 1 at 2.45 GHz in the laboratory environment, signal strength is relative to the maximum value of the reference signal as all the signals were normalized to it

TABLE 6.4

DIVERSITY PERFORMANCE OF BELT-ANKLE CHANNEL WITH PRINTED-IFA AT 2.45 GHz

	Orientation	DG (dB)			ρ_s	ρ_e	Mean Power (dB)		Power diff (dB)
		SC	EGC	MRC			B1	B2	
Config A	Or1($\hat{a}=\hat{z}$)	8.8	9.6	10.1	-0.19 + 0.12i	0.24	-58.8	-60.3	1.44
	Or2($\hat{a}=\hat{y}$)	4.0	4.8	5.4	-0.57 + 0.27i	0.69	-53.7	-52.5	1.12
	Or3($\hat{a}=-\hat{z}$)	6.0	7.0	7.4	-0.31 + 0.26i	0.47	-59.6	-55.9	3.77
	Or4($\hat{a}=-\hat{y}$)	6.9	8.1	8.6	-0.14 - 0.08i	0.21	-58.5	-60.0	1.57
Config B	Or1($\hat{a}=\hat{z}$)	7.5	8.6	9.1	0.4 - 0.03i	0.34	-56.5	-56.8	0.29
	Or2($\hat{a}=\hat{y}$)	6.2	6.9	7.5	-0.26 + 0.08i	0.31	-53.9	-49.0	4.85
	Or3($\hat{a}=-\hat{z}$)	6.4	7.5	7.9	0.01 - 0.48i	0.32	-60.1	-56.4	3.79
	Or4($\hat{a}=-\hat{y}$)	5.8	6.8	7.2	0.31 - 0.41i	0.44	-50.8	-49.0	1.77
Config C	Or1($\hat{a}=\hat{z}$)	8.0	8.7	9.5	-0.18 + 0.24i	0.43	-53.5	-54.4	0.85
	Or2($\hat{a}=\hat{y}$)	4.2	5.3	5.7	-0.06 + 0.81i	0.67	-41.8	-43.3	1.58
	Or3($\hat{a}=-\hat{z}$)	8.1	9.0	9.7	-0.25 - 0.35i	0.36	-57.0	-56.8	0.18
	Or4($\hat{a}=-\hat{y}$)	5.1	5.6	6.3	-0.54 - 0.33i	0.51	-56.3	-51.5	4.81

TABLE 6.5

DIVERSITY PERFORMANCE OF BELT-CHEST CHANNEL WITH PRINTED-IFA AT 2.45 GHz

	Orientation	DG (dB)			ρ_s	ρ_e	Mean Power (dB)		Power diff (dB)
		SC	EGC	MRC			B1	B2	
Config A	Or1($\hat{a}=\hat{z}$)	5.1	6.1	6.6	-0.31 - 0.03i	0.36	-50.1	-51.4	1.30
	Or2($\hat{a}=\hat{y}$)	6.0	6.8	7.4	0.06 - 0.82i	0.48	-50.1	-48.8	1.27
	Or3($\hat{a}=-\hat{z}$)	1.8	2.6	3.2	-0.73 + 0.49i	0.63	-47.4	-43.0	4.42
	Or4($\hat{a}=-\hat{y}$)	8.2	8.9	9.6	0.4 + 0.33i	0.08	-45.3	-45.9	0.57
Config B	Or1($\hat{a}=\hat{z}$)	4.6	5.7	6.1	0.19 - 0.19i	0.48	-51.3	-46.8	4.50
	Or2($\hat{a}=\hat{y}$)	7.3	8.2	8.8	0.32 - 0.06i	0.32	-46.6	-45.7	0.87
	Or3($\hat{a}=-\hat{z}$)	2.8	3.4	4.2	-0.32 - 0.49i	0.37	-32.5	-26.4	6.11
	Or4($\hat{a}=-\hat{y}$)	7.7	8.6	9.2	0.1 - 0.05i	0.41	-42.1	-45.3	3.18
Config C	Or1($\hat{a}=\hat{z}$)	5.8	6.4	7.1	-0.59 + 0.41i	0.52	-51.6	-49.3	2.31
	Or2($\hat{a}=\hat{y}$)	3.2	4.2	4.9	-0.75 - 0.09i	0.57	-48.3	-45.9	2.29
	Or3($\hat{a}=-\hat{z}$)	2.5	4.2	4.4	-0.08 + 0.88i	0.80	-33.9	-33.4	0.47
	Or4($\hat{a}=-\hat{y}$)	5.5	6.3	6.8	-0.3 - 0.75i	0.50	-44.2	-44.9	0.72

TABLE 6.6

DIVERSITY PERFORMANCE OF BELT-BACK CHANNEL WITH PRINTED-IFA AT 2.45 GHz

	Orientation	DG (dB)			ρ_s	ρ_e	Mean Power (dB)		Power diff (dB)
		SC	EGC	MRC			B1	B2	
Config A	Or1($\hat{a}=\hat{z}$)	7.2	8.0	8.7	-0.46 + 0.21i	0.42	-63.9	-67.4	3.49
	Or2($\hat{a}=\hat{y}$)	5.1	5.8	6.5	-0.49 + 0.49i	0.63	-59.4	-54.5	4.92
	Or3($\hat{a}=-\hat{z}$)	6.5	7.9	8.4	-0.39 + 0.16i	0.49	-64.3	-62.7	1.54
	Or4($\hat{a}=-\hat{y}$)	6.7	7.8	8.2	-0.48 + 0.38i	0.53	-65.4	-63.0	2.47
Config B	Or1($\hat{a}=\hat{z}$)	3.1	4.4	4.8	0.43 - 0.79i	0.89	-43.7	-43.0	0.66
	Or2($\hat{a}=\hat{y}$)	6.1	7.1	7.6	0.3 + 0.1i	0.29	-53.2	-60.2	7.03
	Or3($\hat{a}=-\hat{z}$)	5.4	6.1	6.7	0.17 - 0.05i	0.42	-57.0	-48.7	8.38
	Or4($\hat{a}=-\hat{y}$)	1.9	2.7	3.4	-0.12 + 0.28i	0.50	-45.1	-60.5	15.38
Config C	Or1($\hat{a}=\hat{z}$)	5.4	6.1	6.8	0.37 + 0.75i	0.73	-58.0	-56.9	1.11
	Or2($\hat{a}=\hat{y}$)	6.1	7.1	7.6	0.44 + 0.46i	0.41	-55.4	-55.6	0.17
	Or3($\hat{a}=-\hat{z}$)	4.4	4.7	5.6	0.04 + 0.54i	0.60	-54.9	-50.5	4.42
	Or4($\hat{a}=-\hat{y}$)	7.7	8.9	9.5	-0.3 + 0.45i	0.42	-61.8	-61.3	0.52

TABLE 6.7

DIVERSITY PERFORMANCE OF BELT-HEAD CHANNEL WITH PRINTED-IFA AT 2.45 GHz

	Orientation	DG (dB)			ρ_s	ρ_e	Mean Power (dB)		Power diff (dB)
		SC	EGC	MRC			B1	B2	
Config A	Or1($\hat{a}=\hat{z}$)	6.8	7.4	8.3	-0.39 + 0.02i	0.59	-60.9	-61.2	0.28
	Or2($\hat{a}=\hat{x}$)	7.0	8.0	8.6	-0.37 + 0.48i	0.32	-69.0	-70.0	0.92
	Or3($\hat{a}=-\hat{z}$)	5.6	6.5	7.2	-0.28 + 0.14i	0.36	-70.0	-66.4	3.54
	Or4($\hat{a}=-\hat{x}$)	5.8	6.1	6.8	-0.79 + 0.27i	0.85	-50.4	-51.2	0.80
Config B	Or1($\hat{a}=\hat{z}$)	6.0	7.3	7.9	0.32 - 0.36i	0.41	-59.7	-56.9	2.82
	Or2($\hat{a}=\hat{x}$)	6.7	7.4	7.9	-0.1 - 0.26i	0.45	-33.3	-38.6	5.25
	Or3($\hat{a}=-\hat{z}$)	4.3	5.7	6.0	-0.04 - 0.26i	0.65	-40.0	-38.3	1.70
	Or4($\hat{a}=-\hat{x}$)	6.3	7.2	7.7	0.36 - 0.42i	0.43	-59.3	-56.9	2.36
Config C	Or1($\hat{a}=\hat{z}$)	9.6	10.5	11.1	-0.27 + 0.01i	0.18	-66.8	-66.0	0.76
	Or2($\hat{a}=\hat{x}$)	3.2	3.9	4.5	0.01 + 0.71i	0.62	-37.7	-35.3	2.43
	Or3($\hat{a}=-\hat{z}$)	5.0	5.9	6.5	-0.1 + 0.83i	0.79	-41.2	-39.7	1.54
	Or4($\hat{a}=-\hat{x}$)	8.3	9.0	9.7	-0.38 - 0.13i	0.27	-67.0	-63.5	3.44

TABLE 6.8

DIVERSITY PERFORMANCE OF BELT-WRIST CHANNEL WITH PRINTED-IFA AT 2.45 GHz

	Orientation	DG (dB)			ρ_s	ρ_e	Mean Power (dB)		Power diff (dB)
		SC	EGC	MRC			B1	B2	
Config A	Or1($\hat{a}$=$\hat{z}$)	6.0	7.1	7.8	0.13 + 0.15i	0.16	-62.5	-65.4	2.92
	Or2($\hat{a}$=$\hat{y}$)	6.0	6.8	7.3	-0.35 + 0.15i	0.53	-59.3	-59.4	0.03
	Or3($\hat{a}$= -$\hat{z}$)	8.6	9.6	10.1	0.03 + 0.17i	0.26	-62.7	-62.8	0.09
	Or4($\hat{a}$= -$\hat{y}$)	5.6	6.8	7.2	-0.49 + 0.44i	0.58	-53.8	-52.0	1.78
Config B	Or1($\hat{a}$=$\hat{z}$)	7.1	7.8	8.4	0.52 - 0.52i	0.58	-57.6	-57.7	0.08
	Or2($\hat{a}$=$\hat{y}$)	6.8	7.8	8.3	0.13 - 0.22i	0.33	-32.3	-33.9	1.54
	Or3($\hat{a}$= -$\hat{z}$)	5.0	6.0	6.5	0.42 - 0.39i	0.61	-53.0	-50.7	2.28
	Or4($\hat{a}$= -$\hat{y}$)	2.7	3.8	4.3	-0.06 - 0.07i	0.35	-46.0	-36.6	9.39
Config C	Or1($\hat{a}$=$\hat{z}$)	7.3	8.1	8.7	0.15 + 0.29i	0.30	-60.4	-59.6	0.73
	Or2($\hat{a}$=$\hat{y}$)	5.7	6.4	7.1	-0.09 + 0.74i	0.61	-54.5	-49.2	5.33
	Or3($\hat{a}$= -$\hat{z}$)	8.7	9.4	10.0	-0.22 + 0.06i	0.32	-59.9	-59.8	0.10
	Or4($\hat{a}$= -$\hat{y}$)	4.6	5.4	5.9	-0.2 + 0.78i	0.75	-47.9	-45.3	2.62

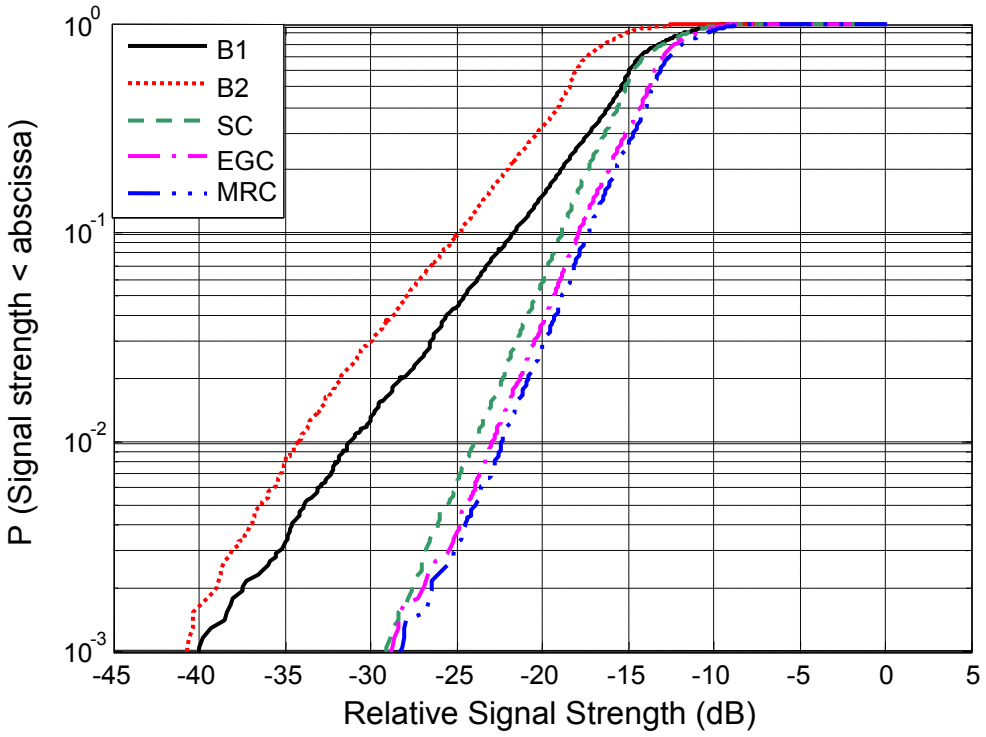

(a) Belt-Head

PTO for full caption

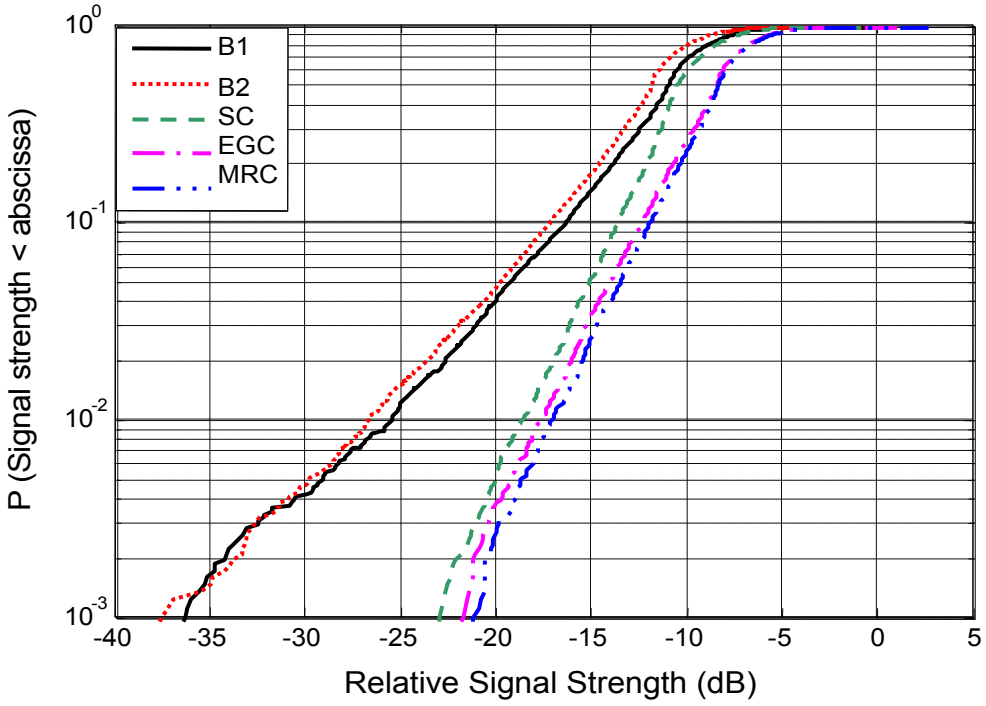

(b) Belt-Chest

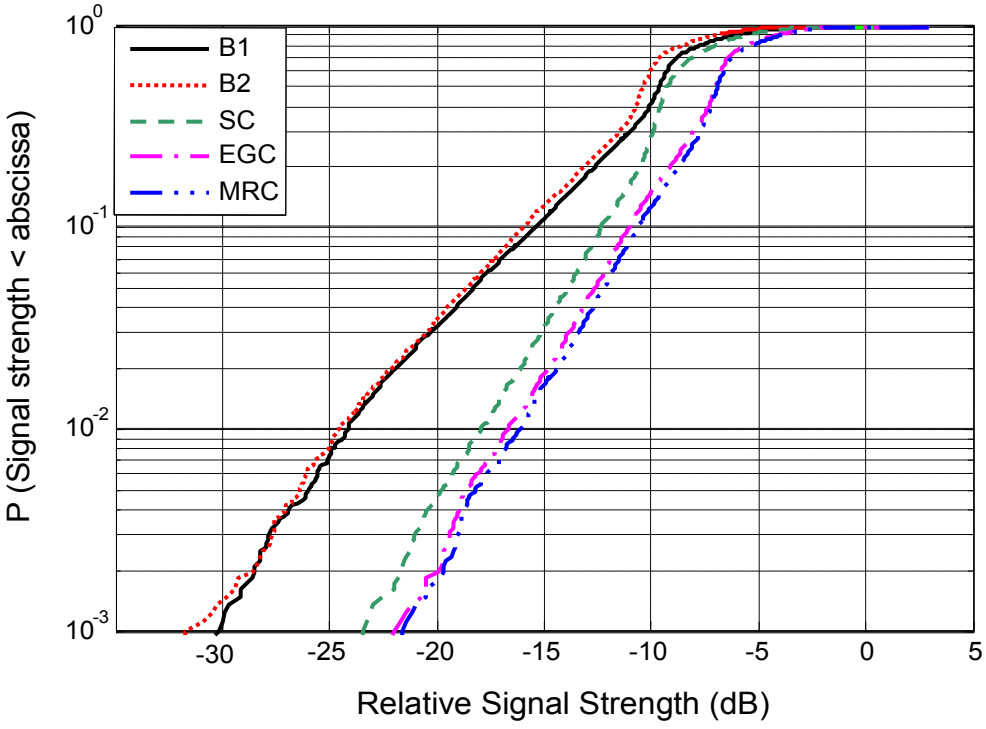

(c) Belt-Wrist

Fig. 6.19: CDF plots of branch and combined signals for the three channels with configuration A of Printed-IFA in orientation 1 at 5.8 GHz in the laboratory environment, signal strength is relative to the maximum value of the reference signal as all the signals were normalized to it

TABLE 6.9

DIVERSITY PERFORMANCE OF BELT-HEAD CHANNEL WITH PRINTED-IFA AT 5.8 GHz

	Orientation	DG (dB)			ρ_s	ρ_e	Mean Power (dB)		Power diff (dB)
		SC	EGC	MRC			B1	B2	
Config A	Or1($\hat{a}=\hat{z}$)	8.5	9.4	10.1	0.11 - 0.06i	0.01	-65.7	-64.0	1.68
	Or2($\hat{a}=\hat{x}$)	6.2	7.3	7.8	0.28 + 0.07i	0.21	-67.5	-69.2	1.72
	Or3($\hat{a}=-\hat{z}$)	6.7	7.8	8.4	0.43 - 0.04i	0.23	-64.1	-66.9	2.75
	Or4($\hat{a}=-\hat{x}$)	7.0	8.3	8.8	-0.11 - 0.17i	0.02	-71.4	-67.1	4.27
Config B	Or1($\hat{a}=\hat{z}$)	7.6	8.8	9.2	-0.45 - 0.12i	0.14	-62.1	-62.0	0.15
	Or2($\hat{a}=\hat{x}$)	9.1	10.0	10.6	0.08 - 0.21i	0.03	-64.3	-64.8	0.52
	Or3($\hat{a}=-\hat{z}$)	7.6	8.6	9.2	-0.23 - 0.13i	0.13	-55.2	-55.1	0.10
	Or4($\hat{a}=-\hat{x}$)	9.2	9.9	10.6	-0.18 + 0.16i	0.07	-65.1	-66.1	0.99

TABLE 6.10

DIVERSITY PERFORMANCE OF BELT-CHEST CHANNEL WITH PRINTED-IFA AT 5.8 GHz

	Orientation	DG (dB)			ρ_s	ρ_e	Mean Power (dB)		Power diff (dB)
		SC	EGC	MRC			B1	B2	
Config A	Or1($\hat{a}=\hat{z}$)	6.4	7.2	7.7	0.55 + 0.38i	0.30	-53.7	-55.8	2.10
	Or2($\hat{a}=\hat{y}$)	9.4	9.9	10.6	-0.11 - 0.13i	0.07	-54.1	-53.3	0.81
	Or3($\hat{a}=-\hat{z}$)	7.2	8.3	8.8	-0.3 - 0.02i	0.13	-57.1	-54.6	2.55
	Or4($\hat{a}=-\hat{y}$)	7.3	8.1	8.7	-0.18 - 0.12i	0.06	-60.9	-56.1	4.71
Config B	Or1($\hat{a}=\hat{z}$)	8.9	9.6	10.2	-0.08 + 0.13i	0.02	-58.4	-58.5	0.16
	Or2($\hat{a}=\hat{y}$)	9.1	9.9	10.5	-0.11 - 0.07i	0.03	-57.2	-57.2	0.00
	Or3($\hat{a}=-\hat{z}$)	7.0	8.5	9.0	-0.17 - 0.26i	0.18	-49.3	-50.1	0.88
	Or4($\hat{a}=-\hat{y}$)	7.2	8.3	8.9	-0.37 + 0.14i	0.16	-53.8	-58.2	4.44

TABLE 6.11

DIVERSITY PERFORMANCE OF BELT-WRIST CHANNEL WITH PRINTED-IFA AT 5.8 GHz

	Orientation	DG (dB)			ρ_s	ρ_e	Mean Power (dB)		Power diff (dB)
		SC	EGC	MRC			B1	B2	
Config A	Or1($\hat{a}=\hat{z}$)	7.2	7.9	8.5	0.2 - 0.01i	0.08	-66.1	-67.7	1.60
	Or2($\hat{a}=\hat{y}$)	7.3	8.5	9.1	0.1 - 0.02i	0.09	-63.3	-63.9	0.57
	Or3($\hat{a}=-\hat{z}$)	6.2	7.0	7.6	0.17 - 0.19i	0.16	-70.0	-65.6	4.35
	Or4($\hat{a}=-\hat{y}$)	7.6	8.1	8.7	0.11 - 0.27i	0.18	-57.4	-57.5	0.13
Config B	Or1($\hat{a}=\hat{z}$)	7.6	8.4	9.1	-0.08 + 0.03i	0.08	-66.0	-68.1	2.14
	Or2($\hat{a}=\hat{y}$)	7.7	8.9	9.4	-0.03 + 0.18i	0.13	-62.1	-63.1	1.04
	Or3($\hat{a}=-\hat{z}$)	6.8	7.9	8.4	-0.12 - 0.26i	0.18	-64.6	-68.9	4.31
	Or4($\hat{a}=-\hat{y}$)	5.9	7.1	7.5	-0.21 + 0.21i	0.15	-59.5	-56.5	3.02

The results confirm the fact that the diversity gain is very low when there is a LOS link between the Tx and Rx. The LOS introduces high correlation and may be responsible for creating a power imbalance for some cases. For all the printed IFA configurations, high DG and low envelope correlation were achieved even for the belt-chest channel, which may be due to weaker direct ray compared to the multipath components, as suggested by the low K-factor values explained later in Chapter 7. For low profile antennas such as printed-IFA, the direct ray is polarized parallel to the surface of the body and propagates along the surface of the body as creeping wave and, therefore, is much more attenuated than a perpendicularly polarized field. Also, the creeping waves attenuate more rapidly over the surface of the body than the free space attenuation. This results in a weaker direct ray and the multipath components being comparable with the direct ray. Thus, as expected, the mean received power was lower compared to the monopole case. From the tables, it can be

seen that the antenna orientation is an important issue for some cases, but mostly, the diversity performance is changed only slightly with changing the orientation. An orientation, which gives high power imbalance and/or high correlation, is undesirable. No significant difference was observed in the performance of the three configurations used. All the configurations perform almost equally for most of the channels apart from few cases where the orientation of a specific configuration introduces high correlation or high power imbalance. Just like the monopole antennas, the mean received signal power is low at the high frequencies due to more attenuation, and the diversity performance at higher frequencies is almost similar to that at the low frequency.

6.3.2 PIFA

Measurements, similar to that of printed-IFA, were performed with PIFA and the same analysis was done on the measured data. The CDF plots of the five channels at 2.45 GHz and three channels at 5.8 GHz with PIFA antennas are shown in Figs. 6.20 and 6.21, respectively. The results are shown in Tables 6.12 and 6.13 for the two frequencies.

Like for the printed-IFA, high DG and low envelope correlation values were achieved with the PIFA for all the channels, except for the belt-chest channel. The high power imbalance and low DG in this case suggest the presence of a stronger direct link compared to printed-IFA. In addition, the mean received power levels are higher than those for the printed IFA, but lower than those for the monopoles. The average DG was higher for PIFA than for printed-IFA. Table 6.12 shows that, for all

PIFA orientations and channels, there is comparatively less difference in DG, correlation, and mean power among various orientations, when compared to the printed-IFA, apart from few cases. This suggests that PIFA may be less sensitive to the orientation of Tx and Rx on the body. In this case as well, the diversity performance at the two frequencies can be considered almost similar.

TABLE 6.12

DIVERSITY PERFORMANCE OF THE FIVE ON-BODY CHANNELS WITH PIFA AT 2.45 GHz

Channel	Orientation	DG (dB)			ρ_s	ρ_e	Mean Power (dB)		Power diff (dB)
		SC	EGC	MRC			B1	B2	
Belt-Ankle	Or1($\hat{a}=\hat{z}$)	7.8	8.7	9.4	0.29 + 0.4i	0.46	-57.5	-53.5	4.02
	Or2($\hat{a}=\hat{y}$)	8.6	9.5	10.1	0.17 - 0.01i	0.14	-52.0	-54.0	2.04
	Or3($\hat{a}=-\hat{z}$)	7.3	8.1	8.9	0.26 - 0.05i	0.24	-57.9	-58.7	0.80
	Or4($\hat{a}=-\hat{y}$)	8.8	9.7	10.4	0.31 + 0.33i	0.27	-57.4	-57.4	0.05
Belt-Chest	Or1($\hat{a}=\hat{z}$)	1.3	2.0	2.8	0.79 + 0.5i	0.56	-39.4	-35.5	3.93
	Or2($\hat{a}=\hat{y}$)	4.6	5.9	6.3	0.34 + 0.72i	0.15	-39.8	-41.3	1.47
	Or3($\hat{a}=-\hat{z}$)	4.1	5.0	5.4	0.6 - 0.47i	0.41	-36.0	-39.2	3.16
	Or4($\hat{a}=-\hat{y}$)	3.5	4.4	5.0	-0.12 - 0.8i	0.39	-39.4	-43.2	3.79
Belt-Back	Or1($\hat{a}=\hat{z}$)	8.6	9.2	9.9	-0.17 - 0.17i	0.13	-55.9	-58.2	2.30
	Or2($\hat{a}=\hat{y}$)	6.5	7.3	7.8	-0.27 + 0.41i	0.13	-45.9	-48.4	2.48
	Or3($\hat{a}=-\hat{z}$)	9.0	9.8	10.7	0.12 + 0.52i	0.30	-56.5	-56.6	0.13
	Or4($\hat{a}=-\hat{y}$)	7.6	8.6	9.1	0.38 + 0.33i	0.29	-58.9	-56.6	2.34
Belt-Head	Or1($\hat{a}=\hat{z}$)	9.3	10.4	10.9	0.01 + 0.23i	0.10	-50.7	-50.3	0.43
	Or2($\hat{a}=\hat{x}$)	9.5	10.5	11.0	-0.07 - 0.04i	0.24	-38.9	-41.3	2.41
	Or3($\hat{a}=-\hat{z}$)	4.5	6.2	6.5	0.49 - 0.24i	0.33	-45.8	-47.6	1.84
	Or4($\hat{a}=-\hat{x}$)	6.9	7.8	8.5	-0.08 - 0.46i	0.24	-53.2	-57.7	4.50
Belt-Wrist	Or1($\hat{a}=\hat{z}$)	7.1	7.5	8.3	-0.17 + 0.39i	0.34	-46.7	-48.1	1.48
	Or2($\hat{a}=\hat{y}$)	6.5	7.6	8.1	0.53 - 0.26i	0.43	-49.6	-50.0	0.44
	Or3($\hat{a}=-\hat{z}$)	6.7	7.7	8.2	-0.16 + 0.02i	0.14	-50.6	-53.4	2.83
	Or4($\hat{a}=-\hat{y}$)	5.0	6.1	6.6	0.41 + 0.27i	0.27	-46.2	-51.3	5.10

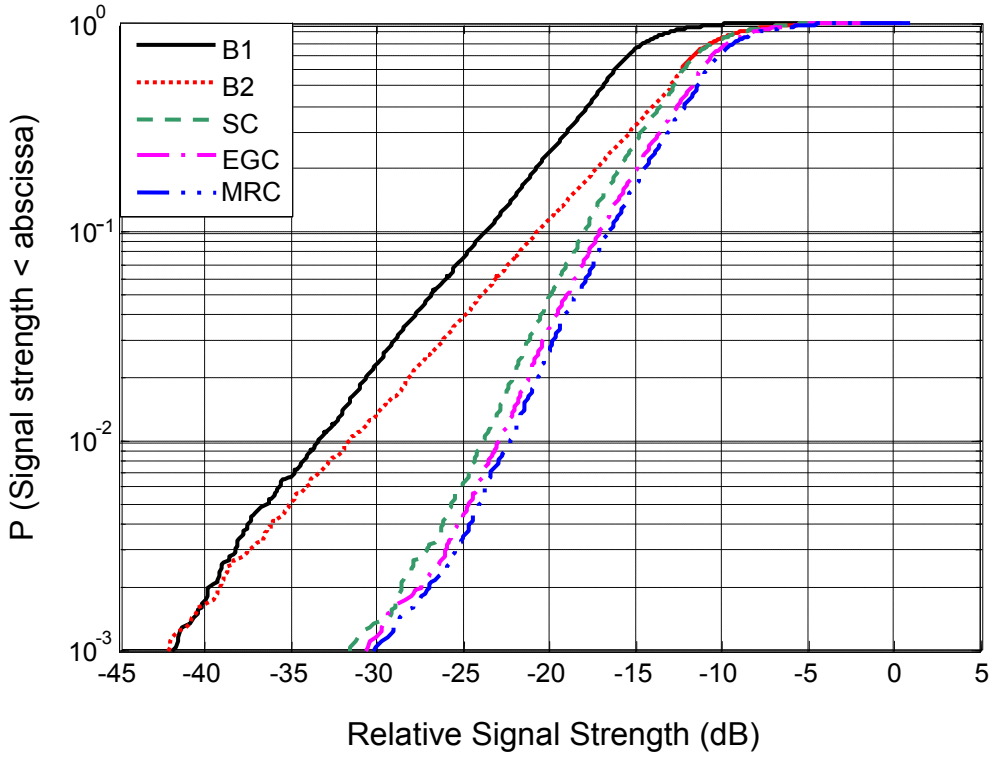

(a) Belt-Ankle

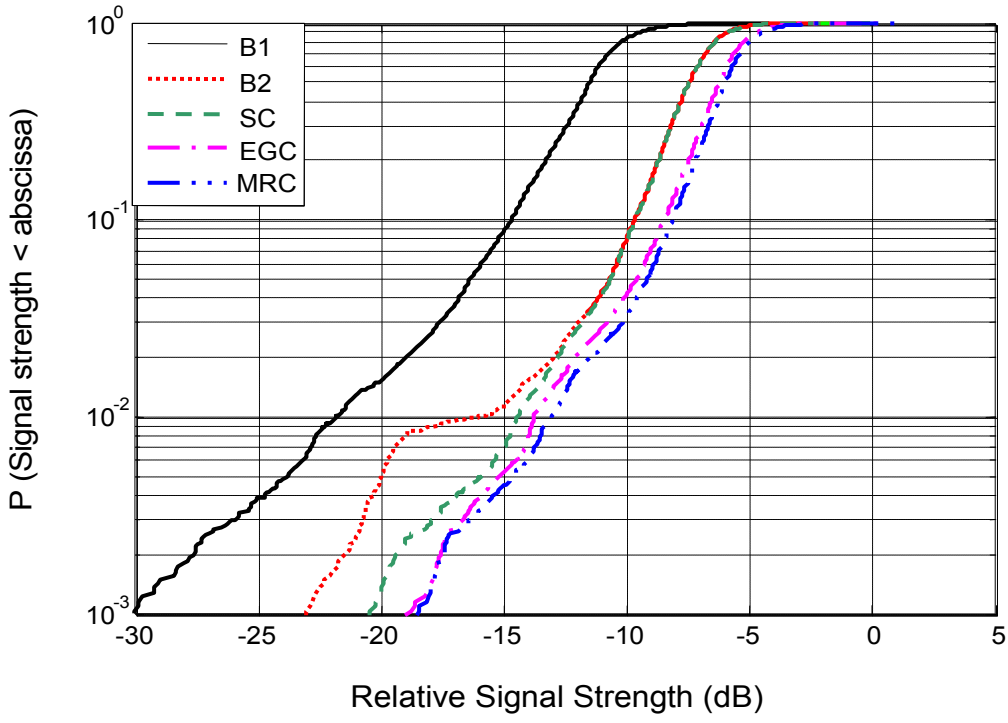

(b) Belt-Chest

PTO for full caption

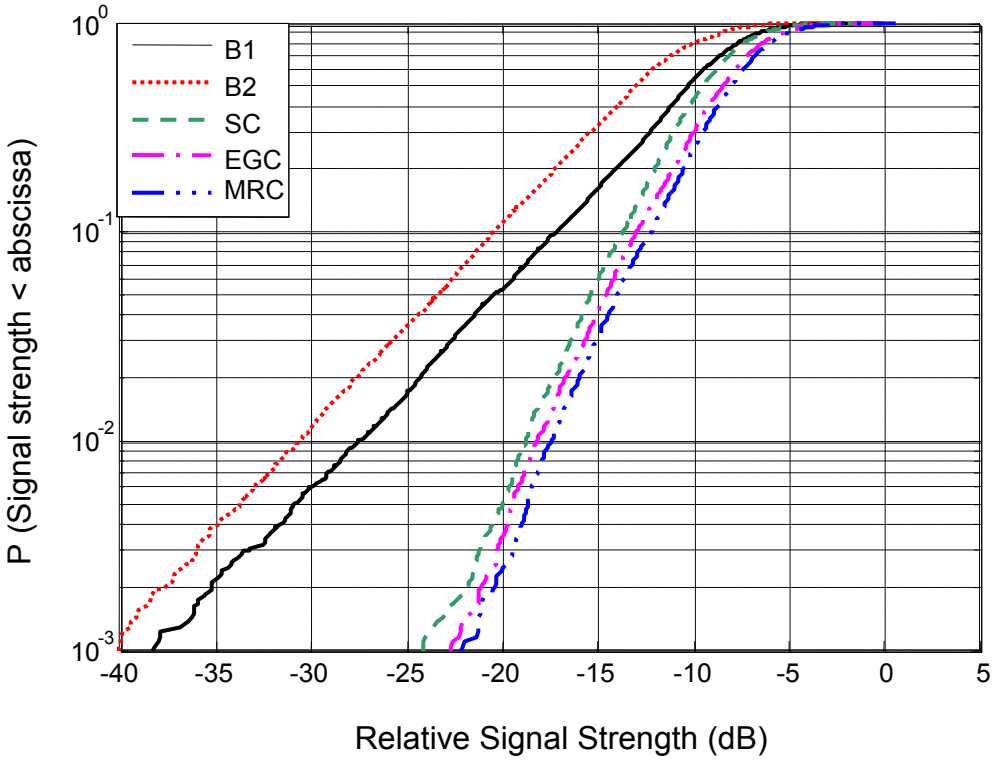

(c) Belt-Back

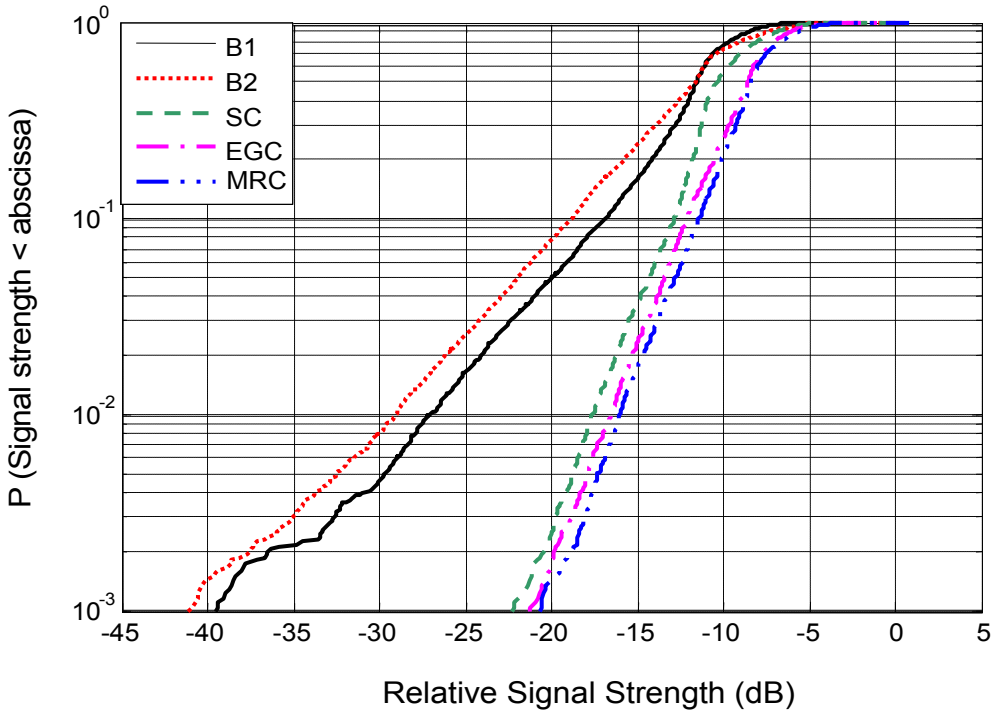

(d) Belt-Head

PTO for full caption

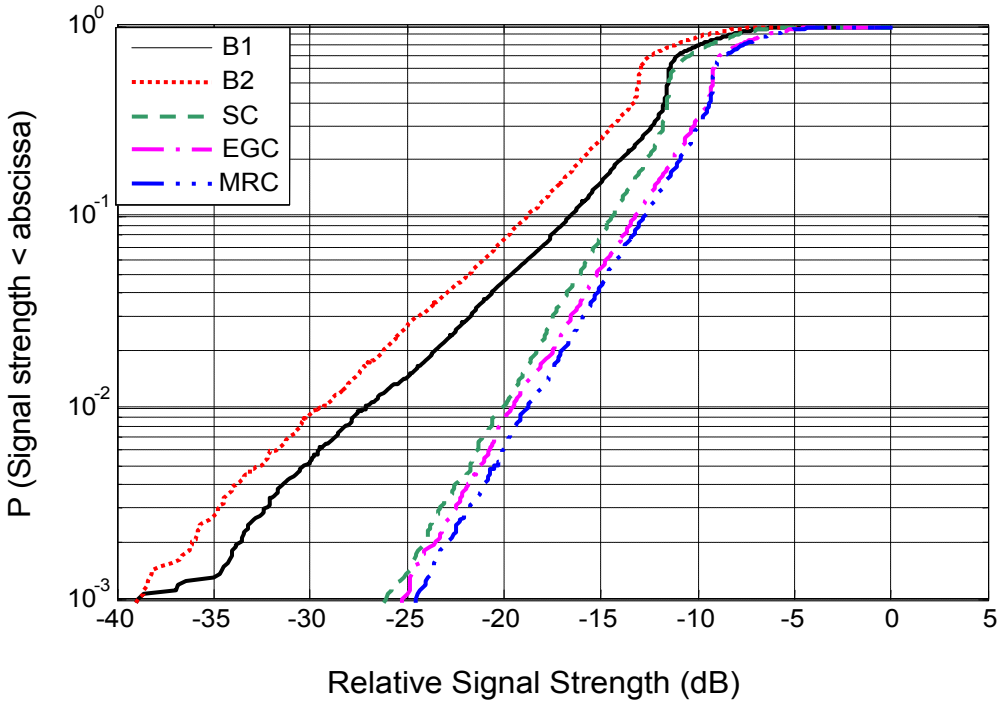

(e) Belt-Wrist

Fig. 6.20: CDF plots of branch and combined signals with PIFA in orientation 1 at 2.45 GHz in the laboratory environment, signal strength is relative to the maximum value of the reference signal as all the signals were normalized to it

TABLE 6.13
DIVERSITY PERFORMANCE OF THE THREE ON-BODY CHANNELS WITH PIFA AT 5.8 GHZ

Channel	Orientation	DG (dB)			ρ_s	ρ_e	Mean Power (dB)		Power diff (dB)
		SC	EGC	MRC			B1	B2	
Belt-Chest	Or1($\hat{a}$=$\hat{z}$)	3.7	5.0	5.3	0.65 + 0.48i	0.31	-51.3	-49.7	1.59
	Or2($\hat{a}$=$\hat{y}$)	4.0	4.9	5.4	-0.82 + 0.06i	0.41	-49.0	-51.5	2.49
	Or3($\hat{a}$= -$\hat{z}$)	3.0	4.2	4.7	0.43 - 0.41i	0.14	-49.2	-53.9	4.74
	Or4($\hat{a}$= -$\hat{y}$)	4.3	5.2	5.7	0.16 - 0.81i	0.31	-48.9	-52.5	3.56
Belt-Head	Or1($\hat{a}$=$\hat{z}$)	7.4	8.0	8.9	0.23 + 0.17i	0.19	-63.9	-61.9	2.02
	Or2($\hat{a}$=$\hat{x}$)	8.8	9.7	10.3	-0.26 + 0.15i	0.13	-63.4	-62.1	1.29
	Or3($\hat{a}$= -$\hat{z}$)	7.1	8.2	8.6	-0.03 - 0.2i	0.20	-62.8	-62.9	0.15
	Or4($\hat{a}$= -$\hat{x}$)	6.0	7.3	7.7	-0.01 - 0.21i	0.18	-61.1	-64.4	3.30
Belt-Wrist	Or1($\hat{a}$=$\hat{z}$)	7.2	8.5	8.9	-0.14 - 0.07i	0.11	-59.6	-63.1	3.45
	Or2($\hat{a}$=$\hat{y}$)	7.7	8.5	9.0	0.17 - 0.13i	0.05	-58.5	-61.4	2.85
	Or3($\hat{a}$= -$\hat{z}$)	6.9	8.0	8.4	-0.12 - 0.16i	0.16	-60.5	-61.5	1.02
	Or4($\hat{a}$= -$\hat{y}$)	6.5	7.2	8.0	0.03 + 0.14i	0.09	-55.4	-58.4	2.96

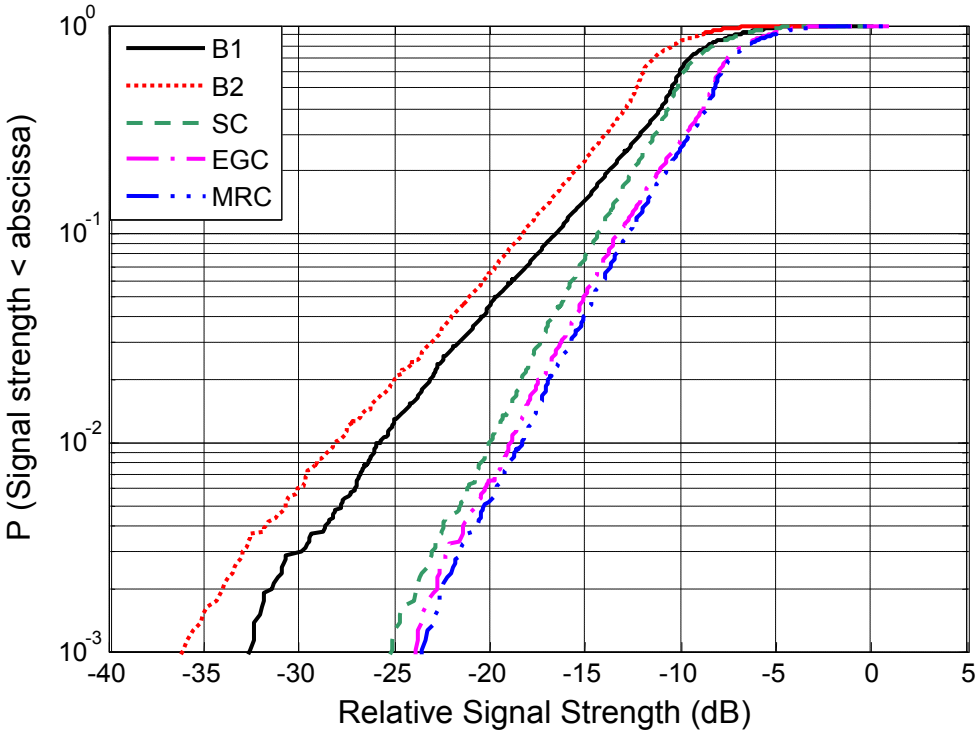

(a) Belt-Head

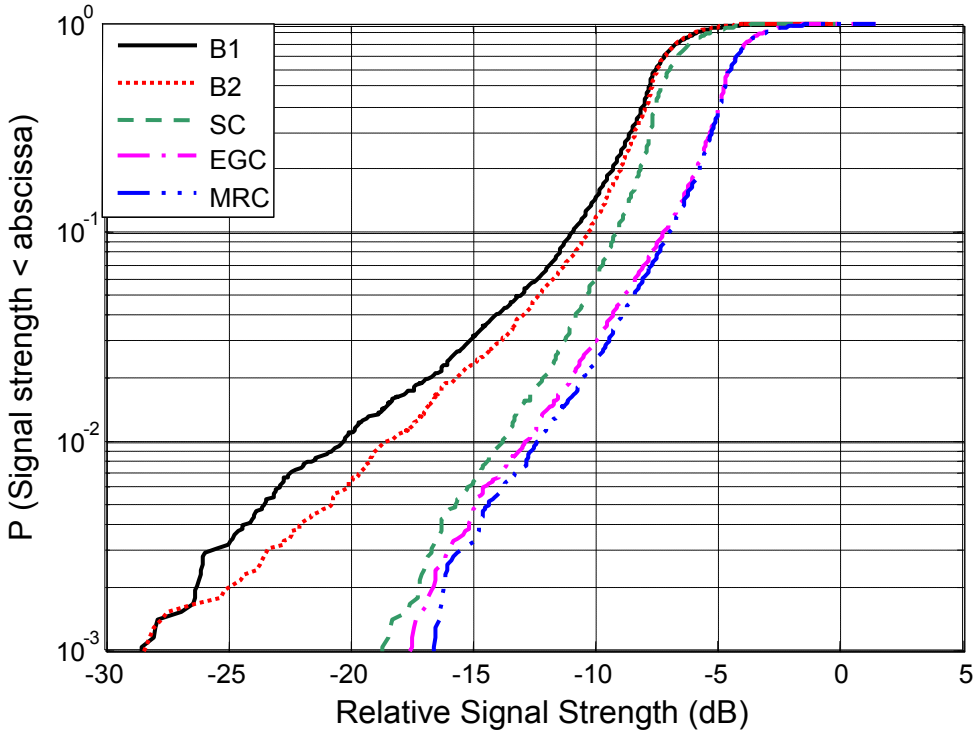

(b) Belt-Chest

PTO for full caption

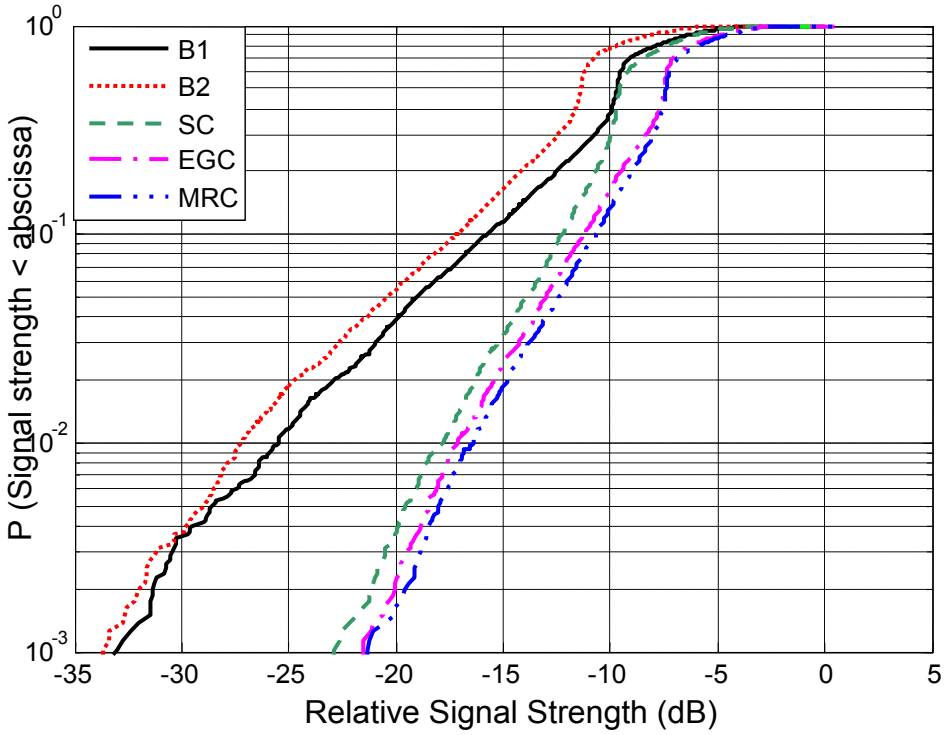

(c) Belt-Wrist

Fig. 6.21: CDF plots of branch and combined signals for the three channels with PIFA in orientation 1 at 5.8 GHz in the laboratory environment, signal strength is relative to the maximum value of the reference signal as all the signals were normalized to it

6.3.3 Polarization Diversity

The five on-body channels, belt-ankle, belt-chest, belt-back, belt-head, and belt-wrist, were measured for the polarization diversity investigation at 2.45 GHz with the same random movements and environment. In this case, the human subject was a female student having weight of 54 kg and height of 160 cm. The polarization diversity antenna described in Section 6.2.3 was used with two different transmitting antennas, one with polarization perpendicular to the surface of the body, i.e. a monopole antenna, and the other with polarization tangential to the surface of the body, i.e. a printed-loop antenna. The CDF plots of the branch and diversity

combined signals for the five on-body channels are given in Fig. 6.22 and Fig. 6.23 for each case and the DG values, along with other results, are depicted in Table 6.14.

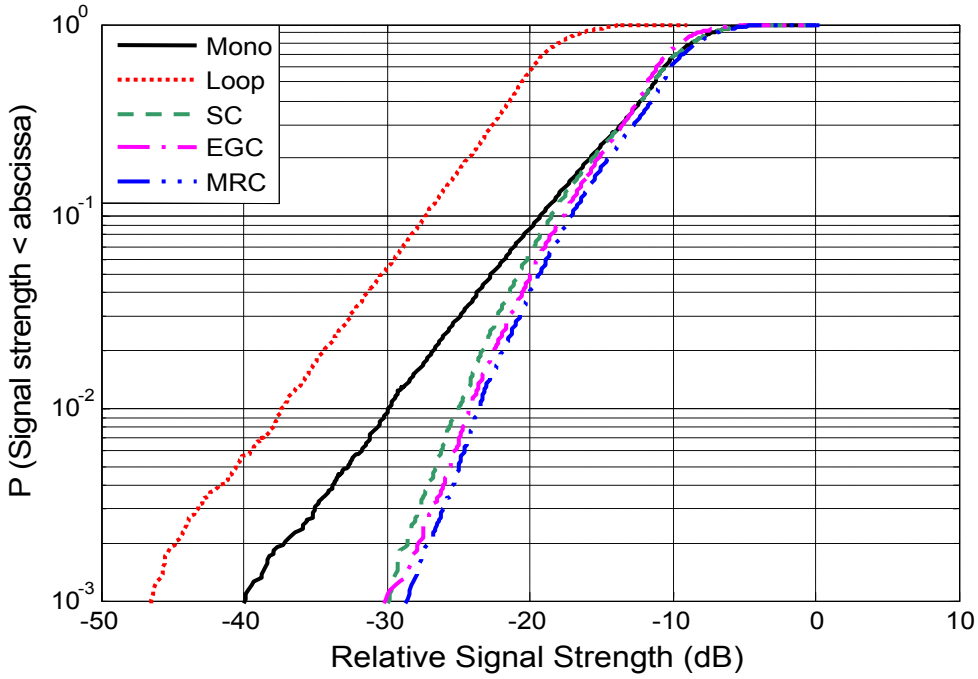

(a) Belt-Ankle

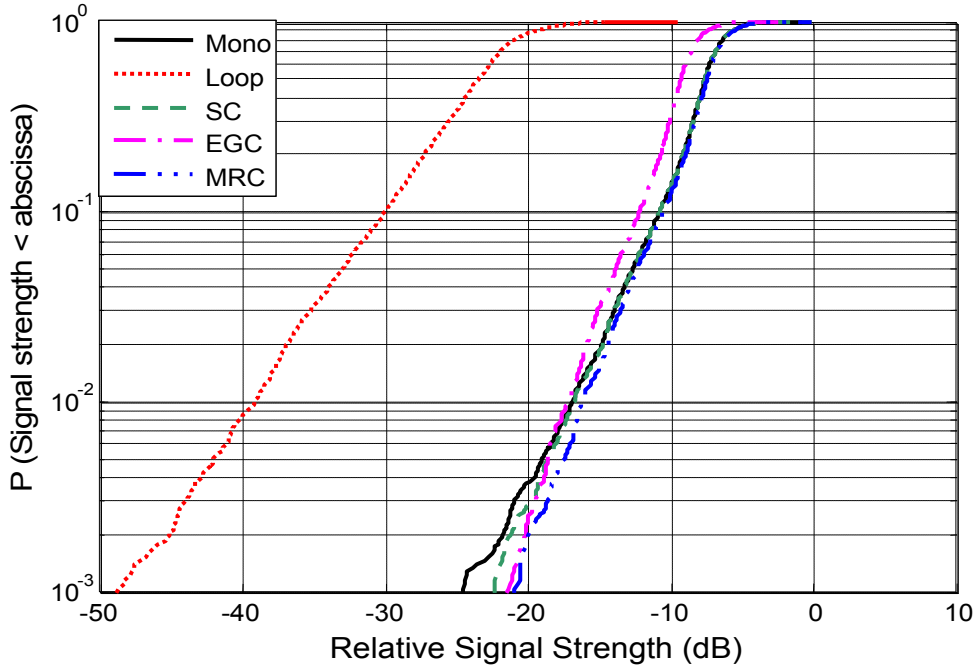

(b) Belt-Chest

PTO for full caption

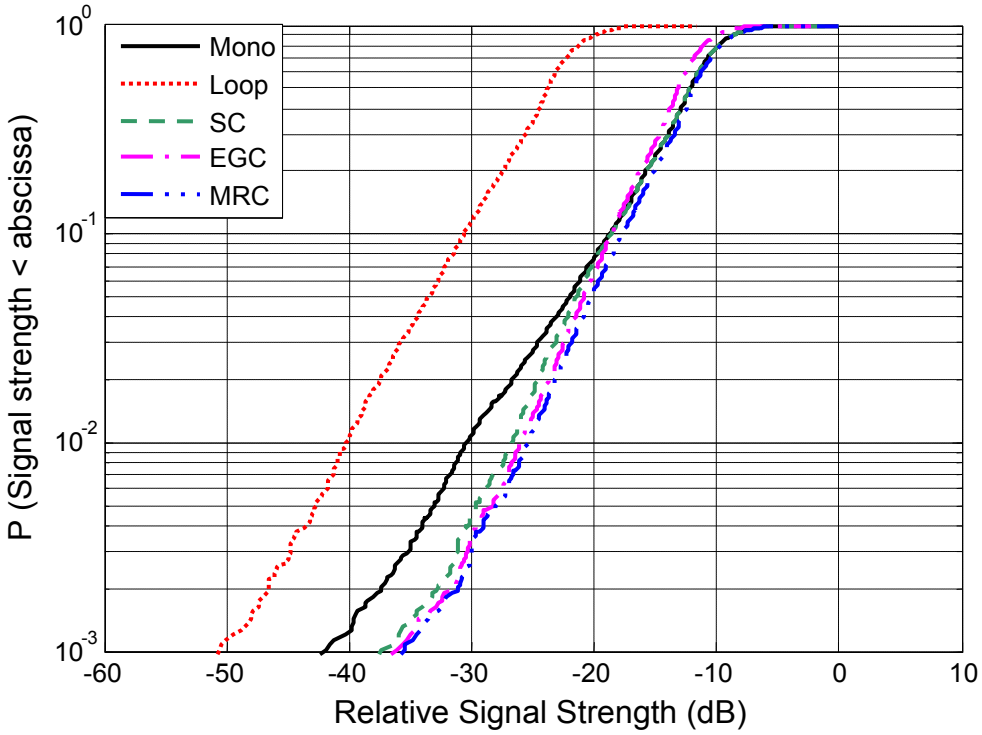

(c) Belt-Back

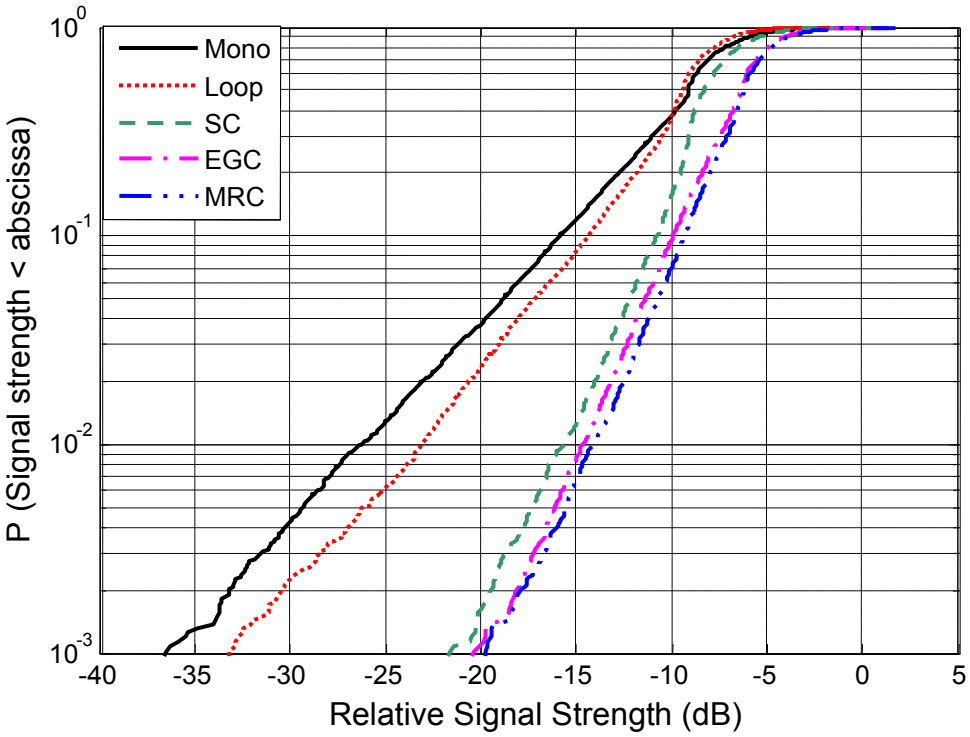

(d) Belt-Head

PTO for full caption

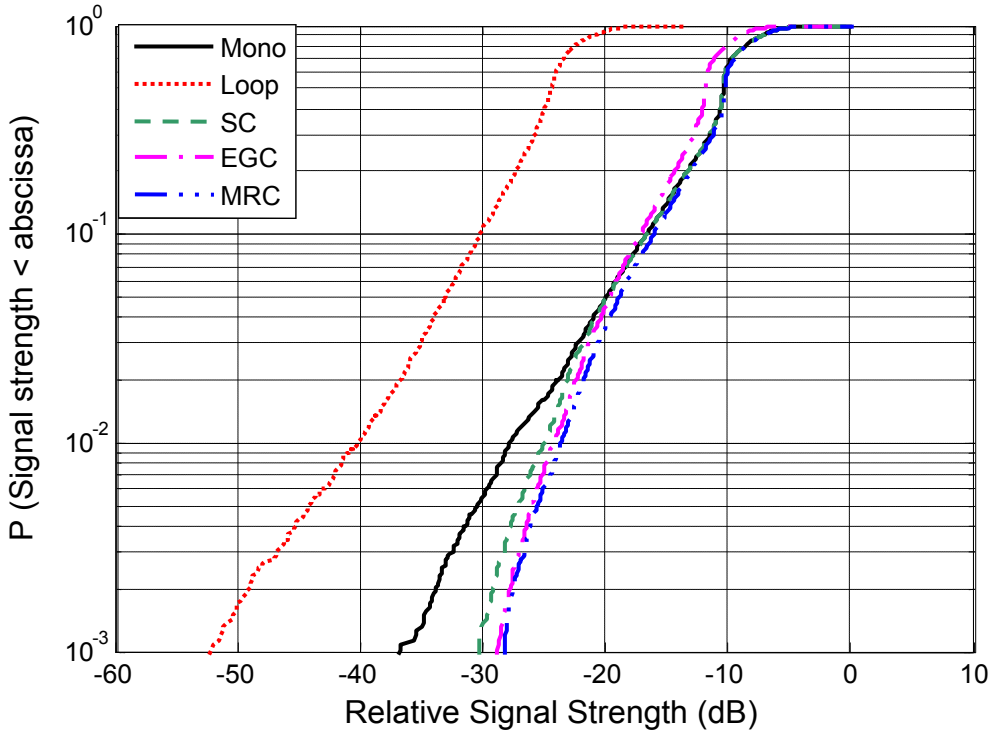

(e) Belt-Wrist

Fig. 6.22: CDF plots of branch and combined signals for the five on-body channels with the polarization diversity antenna and monopole Tx in the laboratory environment at 2.45 GHz, signal strength is relative to the maximum value of the reference signal as all the signals were normalized to it

The transmitted signal from the printed-loop antenna, by the virtue of its polarization, is attenuated much more rapidly on the surface of the body compared to that with monopole transmitter. Hence, the direct ray is much weaker than the one with monopole. This is clear from the comparison of the mean signal values in Table 6.14. One can expect high power imbalance due to this strong direct ray with monopole transmitter, thus reducing the diversity gain. For the belt-chest channel, both the cases give very low DG due to strong correlation and high power imbalance. It has been shown in Chapter 5 that the static channels, which do not involve movement of the antennas in the environment and with respect to each other, show

low diversity gain values. Being a static channel, the belt-back channel also shows low DG values and high power imbalance. The other three channels have reasonable diversity gains. The belt-ankle channel involves high reflections from the floor and thus has significant multipath. The reflections cause significant depolarization as well and hence this channel has high diversity gain values with relatively low power imbalance. The belt-wrist channel involves LOS most of the time and has high power imbalance despite the random orientation of antennas. The random orientation of the diversity branch antennas with respect to a fixed transmitted polarization does not significantly decreases the cross-polarization discrimination (XPD) in this case, due to very high attenuation of the polarization which is parallel to the surface of the body. This is also revealed by the results in Table 6.14, as the monopole antenna branch is always the strongest one, causing a great deal of power imbalance. This is true for all the channels, irrespective of the transmitted polarization being normal or tangential to the body.

The results with two different transmitting antennas, i.e. monopole and printed-loop, are not very different. The diversity gains for all the cases are not as high as reported for the same channels with other antennas, which suggests that polarization diversity is not as effective as space or pattern diversity for the on-body applications. But still, the improvement in some channels is reasonable. If used in combination with some other type of diversity, polarization diversity can provide reasonable diversity performance.

TABLE 6.14

DIVERSITY PERFORMANCE OF THE FIVE ON-BODY CHANNELS WITH POLARIZATION DIVERSITY ANTENNA AT 2.45 GHz

With Monopole transmitting antenna								
Channel	DG (dB)			ρ_s	ρ_e	Mean Power (dB)		Power diff (dB)
	SC	EGC	MRC			Monopole Branch	Loop Branch	
Belt-Ankle	5.2	6.0	6.6	0.14 + 0.13i	0.3	-46.5	-55.6	9.1
Belt-Chest	0.1	0.4	0.7	-0.34 + 0.38i	0.2	-39.6	-54.4	14.8
Belt-Back	2.9	3.8	4.3	0.4 - 0.07i	0.3	-49.4	-60.9	11.5
Belt-Head	4.3	4.8	5.5	-0.22 + 0.04i	0.1	-53.1	-63.8	10.7
Belt-Wrist	2.9	3.6	4.2	-0.29 + 0.07i	0.3	-44.1	-58.1	13.9
With Printed-Loop transmitting antenna								
Channel	DG (dB)			ρ_s	ρ_e	Mean Power (dB)		Power diff (dB)
	SC	EGC	MRC			Monopole Branch	Loop Branch	
Belt-Ankle	6.8	7.3	7.9	0.24 - 0.03i	0.4	-55.1	-59.5	4.4
Belt-Chest	0.1	0.3	1.1	0.71 - 0.08i	0.2	-50.3	-64.3	14.0
Belt-Back	3.4	4.3	4.9	0.28 - 0.05i	0.2	-58.9	-68.8	9.9
Belt-Head	3.1	4.0	4.6	0.17 - 0.27i	0.1	-58.3	-67.8	9.4
Belt-Wrist	3.2	4.2	4.7	0.06 + 0.02i	0.2	-52.8	-64.8	12.0

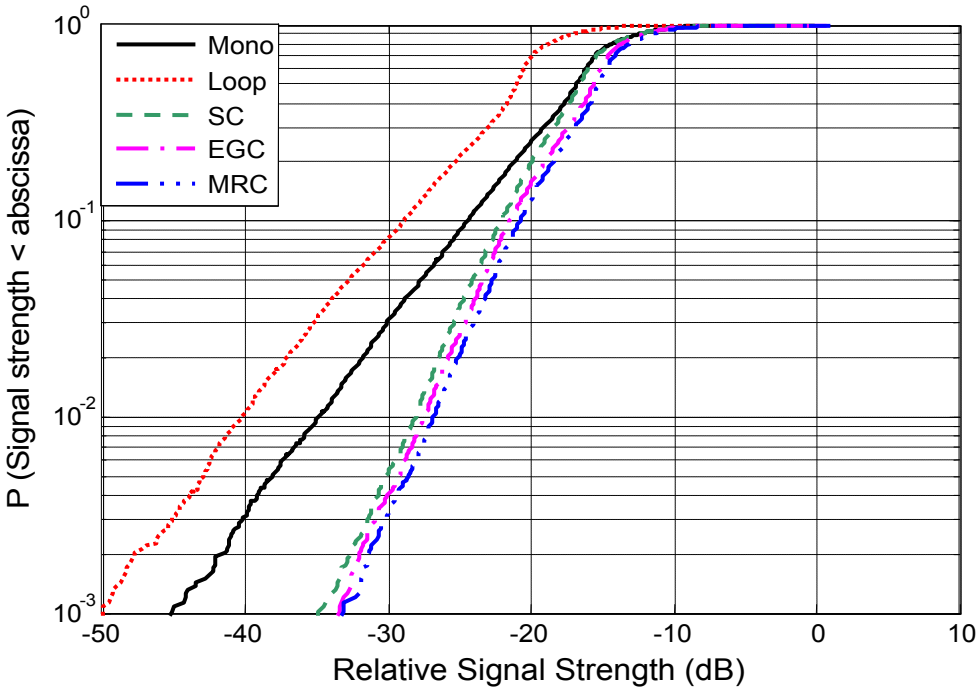

(a) Belt-Ankle

PTO for full caption

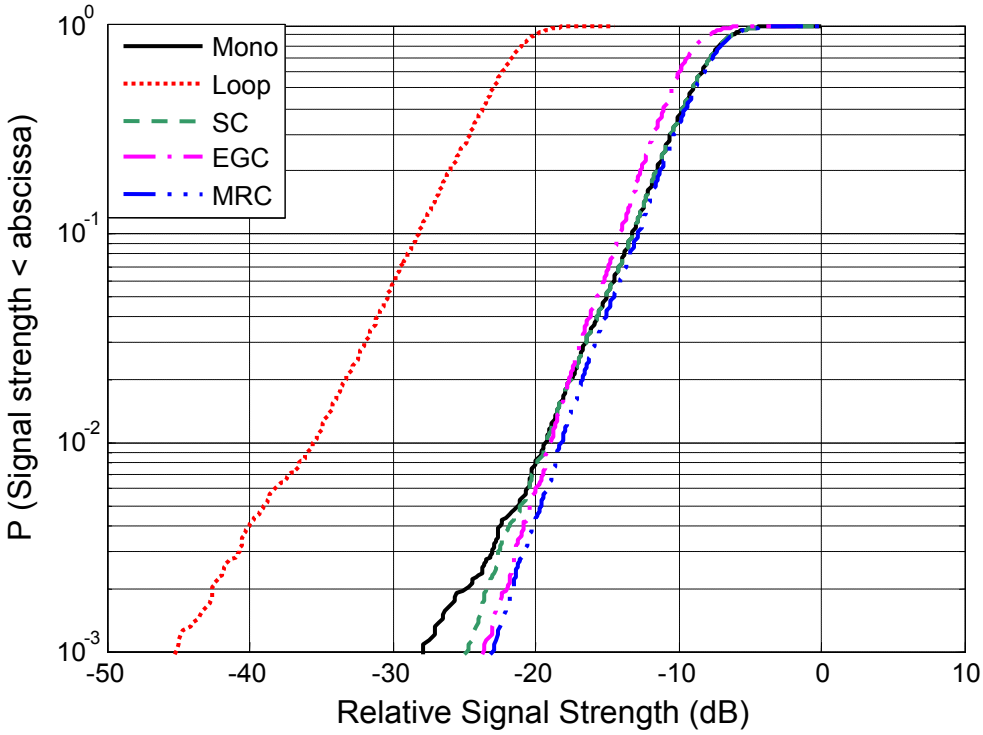

(b) Belt-Chest

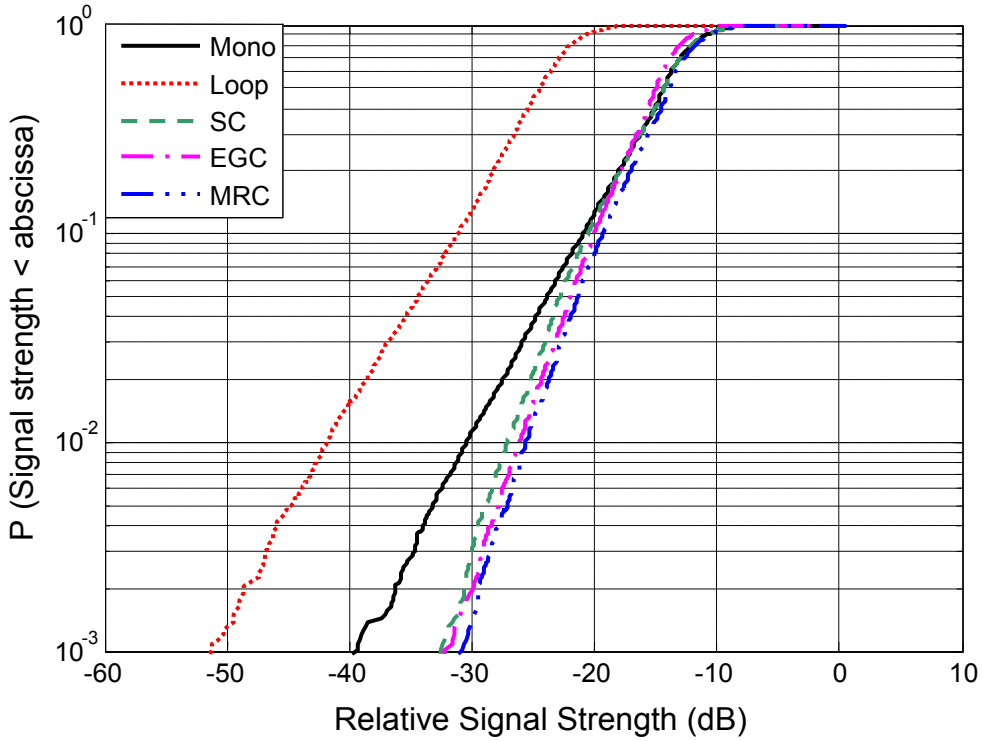

(c) Belt-Back

PTO for full caption

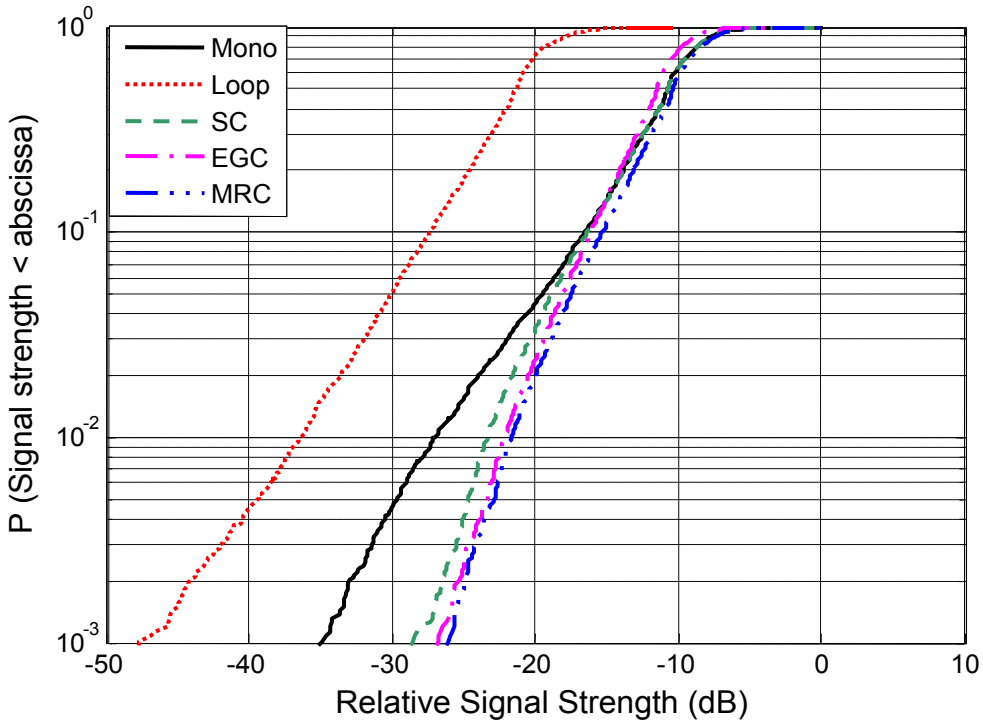

(d) Belt-Head

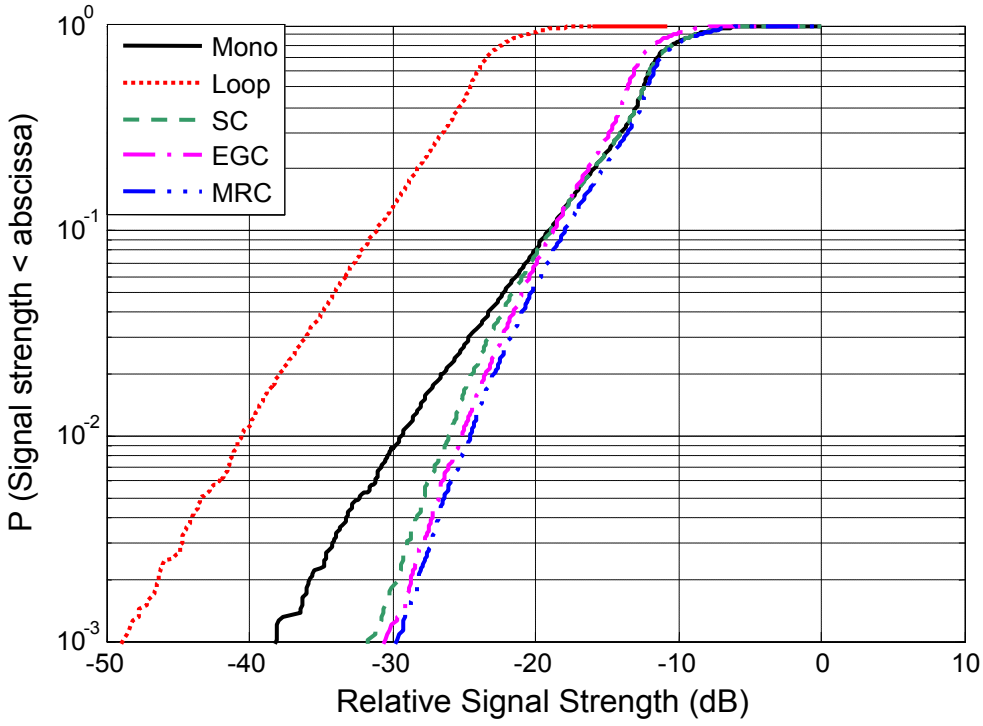

(e) Belt-Wrist

Fig. 6.23: CDF plots of branch and combined signals for the five on-body channels with the polarization diversity antenna and printed-loop Tx in the laboratory environment at 2.45 GHz, signal strength is relative to the maximum value of the reference signal as all the signals were normalized to it

6.3.4 Repeatability and uplink-downlink diversity performance

Like the space diversity monopole antenna measurements described in Chapter 5, the repeatability test and the uplink-downlink diversity measurements were done with printed-IFA and PIFA antennas as well. Measurements were repeated identically four times each for repeatability test and the Tx and the Rx antenna positions were swapped for the uplink-down-link diversity measurements for orientation A of printed-IFA and the PIFA. The same postures and movements were replicated for all the channels. Tables 6.15 and 6.16 list the difference recorded in the DG, envelope correlation coefficient, and mean signal power for the four iterations of each case. The correlation is similar in all the iterations. It further confirms the reliability and repeatability of the procedure and the channel measurements.

The uplink and downlink diversity performance was found similar as well. Tables 6.17 – 6.19 show the uplink and downlink diversity results and their difference. Thus, conclusions similar to Chapter 5 can be drawn that the diversity gain comes mainly from the multipath due to the surrounding environment.

TABLE 6.15

DIFFERENCE IN DIVERSITY GAIN, CORRELATION COEFFICIENTS, AND MEAN POWER OVER 4 MEASUREMENTS USING PRINTED-IFA AND PIFA AT 2.45 GHZ

Channel	Printed-IFA			PIFA		
	DG MRC (dB)	ρ_e	Mean Power (dB)	DG MRC (dB)	ρ_e	Mean Power (dB)
Belt-Ankle	1.5	0.1	1.2	0.9	0.2	1.1
Belt-Chest	2.0	0.1	0.6	0.9	0.0	0.7
Belt-Back	2.0	0.2	4.8	1.4	0.0	1.5
Belt-Head	1.2	0.1	2.7	1.6	0.1	3.6
Belt-Wrist	1.2	0.1	1.1	1.5	0.1	2.2

TABLE 6.16

DIFFERENCE IN DIVERSITY GAIN, CORRELATION COEFFICIENTS, AND MEAN POWER OVER 4 MEASUREMENTS USING PRINTED-IFA AND PIFA AT 5.8 GHz

	Channel	Printed-IFA			PIFA		
		DG diff (dB)	ρ_e diff	Mean power diff (dB)	DG diff (dB)	ρ_e diff	Mean power diff (dB)
Same day	Belt-Chest	1.4	0.1	1.2	1.4	0.2	1.3
	Belt-Head	1.3	0.1	2.4	1.0	0.2	3.7
	Belt-Wrist	0.7	0.2	0.8	0.7	0.1	3.1
Another day	Belt-Chest	1.4	0.1	2.2	2.1	0.3	1.3
	Belt-Head	1.8	0.1	2.4	2.0	0.3	3.7
	Belt-Wrist	1.2	0.2	1.8	1.1	0.1	4.1

TABLE 6.17

THE UPLINK AND DOWN LINK DIVERSITY GAIN, CORRELATION, THEIR DIFFERENCE WITH PIFA AT 2.45 GHz

Channel	Uplink		Downlink		Difference	
	DG MRC (dB)	ρ_e	DG MRC (dB)	ρ_e	DG MRC (dB)	ρ_e
Belt-Ankle	7.8	0.34	10.4	0.27	2.6	0.1
Belt-Chest	3.9	0.51	2.8	0.56	1.1	0.1
Belt-Back	10.2	0.11	9.9	0.13	0.3	0.0
Belt-Head	10.8	0.42	10.9	0.10	0.1	0.3
Belt-Wrist	7.2	0.30	6.6	0.27	0.6	0.0

TABLE 6.18

THE UPLINK AND DOWN LINK DIVERSITY GAIN, CORRELATION, AND THEIR DIFFERENCE WITH PRINTED-IFA AND PIFA AT 5.8 GHz

Antenna	Channel	Uplink		Downlink		Difference	
		DG MRC (dB)	ρ_e	DG MRC (dB)	ρ_e	DG MRC (dB)	ρ_e
Printed-IFA Conf A	Belt-Chest	7.7	0.30	6.7	0.22	1.1	0.1
	Belt-Head	10.1	0.01	8.9	0.18	1.2	0.2
	Belt-Wrist	8.5	0.08	9.5	0.15	1.0	0.1
PIFA	Belt-Chest	5.3	0.31	6.4	0.26	1.1	0.0
	Belt-Head	8.9	0.19	8.9	0.12	0.0	0.1
	Belt-Wrist	8.9	0.10	9.8	0.11	0.9	0.0

TABLE 6.19

THE UPLINK AND DOWN LINK DIVERSITY GAIN, CORRELATION, AND THEIR DIFFERENCE WITH PRINTED-IFA AT 2.45 GHZ

	Channel	Uplink		Downlink		Difference	
		DG MRC (dB)	ρ_e	DG MRC (dB)	ρ_e	DG MRC (dB)	ρ_e
Config A	Belt-Ankle	9.9	0.33	10.1	0.24	0.2	0.1
	Belt-Chest	5.9	0.26	3.2	0.63	2.7	0.4
	Belt-Back	8.7	0.33	8.7	0.42	0.0	0.1
	Belt-Head	6.5	0.55	6.8	0.86	0.4	0.3
	Belt-Wrist	7.5	0.38	7.3	0.53	0.2	0.2
Config B	Belt-Ankle	7.3	0.69	9.5	0.43	2.1	0.3
	Belt-Chest	8.0	0.49	7.1	0.52	0.9	0.0
	Belt-Back	6.3	0.69	5.6	0.60	0.7	0.1
	Belt-Head	5.2	0.71	6.5	0.79	1.3	0.1
	Belt-Wrist	7.6	0.63	10.0	0.32	2.4	0.3
Config C	Belt-Ankle	9.0	0.38	7.9	0.32	1.0	0.1
	Belt-Chest	9.9	0.32	8.8	0.32	1.1	0.0
	Belt-Back	9.4	0.29	7.6	0.29	1.7	0.0
	Belt-Head	7.3	0.43	7.9	0.46	0.7	0.0
	Belt-Wrist	7.3	0.31	8.4	0.58	1.1	0.3

6.4 Conclusions

Significant improvement was observed in terms of diversity gain for almost all the on-body channels at both the frequencies with pattern diversity. The wave on the surface of the body is highly attenuated, particularly in the case of the printed-IFA, and the multipath components are dominant over the direct ray. The results suggest that PIFA is the best choice of antenna, as it gives reasonable path gains and higher DG values. The correlation between the branch signals is low for most of the channels, which suggests that the diversity can provide very good improvement if the power imbalance is carefully dealt with. The printed-IFA is more sensitive to its orientation compared to the other antennas. Polarization diversity is not as useful as

the space and pattern diversity but provides reasonable diversity gains for some channels. A combination of space, pattern, and polarization diversity is more effective than space diversity only or polarization diversity only. The performance of pattern diversity is almost similar to the space diversity monopole antennas for most cases and is rather slightly better. The diversity performance at the two frequencies is comparable and not significantly different. The uplink and downlink diversity is reciprocal, suggesting that the local off-body scattering environment is dominant. The diversity measurements are repeatable with a small error, which is acceptable for most of the cases.

REFERENCES

[1] M.R Kamarudin, Y.I.Nechayev, P.S.Hall, "Performance of Antennas in the On-body Environment", *IEEE Antennas and Propagation Society International Symposium, 2005, 3-8 July 2005 Page(s):475-478 vol. 3A*.

[2] I Khan, Peter S. Hall, "Multiple Antenna Reception at 5.8 and 10 GHz for Body-Centric Wireless Communication Channels", *IEEE Transactions on Antennas and Propagation, Vol. 57, No.1, Jan 2009*.

[3] I Khan, P.S. Hall, A.A Serra, A.R. Guraliuc, P. Nepa, "Diversity Performance Analysis for On-body Communication Channels at 2.45 GHz" *IEEE Transactions on Antennas and Propagation, Vol. 57, No. 4, April 2009.*

[4] Akhoondzadeh-Asl L., Khan I., Nechayev Y I, Hall P. S., "Investigation of Polarization on the Body", *in proceeding of 3rd European Conference on Antennas and Propagation (EuCAP), Berlin, Germany, 23-27March 2009.*

[5] M. Karaboikis, C. Soras, G. Tsachtsiris, V. Makios, "Compact Dual-Printed Inverted-F Antenna Diversity Systems for Portable Wireless Devices", *IEEE Antennas and Wireless Propagation Letters, Vol. 3, 2004.*

Chapter 7

On-Body Diversity Channel Characterization

7.1 Introduction

Mobile radio channels are usually characterized by Rayleigh fading which assumes a random variation in the amplitude of the fading envelope and uniform distribution of the phase of the multipath components with non-line-of-sight environment. Both the diversity branches in a mobile diversity system are assumed to be independent and identically distributed (IID). Rayleigh fading distribution is not valid for the on-body diversity channels, as most of the commonly used on-body channels have a strong line-of-sight link. This type of fading can be characterized by a Rician distribution. Apart from the multipath fading due to the environment, fading is also caused by the movement of the scatterers surrounding the antennas in the form of moving body parts. The diversity branches can be independent but the distributions of the branch channels may not be identical. The scattering due to the motion of the body may change the fading distribution at the two branches [1]. Much attention has been paid to the characterization of antennas for on-body channels, the effect of human body presence on the communication link, antenna position on the body, use of phantoms, the link budget of the on-body channels, and diversity performance [2, 3]. Some work has been done to characterize the on-body and off-body channels with specific antennas and antenna positions, mentioned in Chapter 1 and Chapter 2, but still there

is a need for more general on-body statistical channel model. The absence of any standard statistical model for the on-body channels requires an extensive measurement campaign to determine the channel statistics. Thus, it is important to know the fading distribution and to perform the statistical analysis of the on-body channels. It is also of interest to know the distribution of the diversity combined signals because diversity gain is calculated usually from the distributions of the branch and combined signals. This work focuses on the characterization of the on-body diversity channels and on finding a distribution of short-term and long-term fading. The data collected for diversity performance analysis, as described in Chapters 5 and 6, was used for this work. The results given below have already been presented in [4, 5].

The rest of the chapter is organized as follows. Section 7.2 describes the processing done on the measured data. The branch and combined signal characterization and distribution fitting is presented in Section 7.3. Section 7.4 gives the spectral analysis and Section 7.5 presents the second-order statistics. Conclusions are given in Section 7.6.

7.2 Data processing

The movements performed during the measurements, as described in Chapter 4, were divided into two groups. The first group was a set of postures which cause a dynamic change in the path length and also involves movement of the body and hence the antennas in the environment. This group consists of sweeps 3, 4, 6, 8, 9, and 10 for the belt-head channel and sweeps 1, and 5-10 for the belt-wrist channel (see Chapter

4, Table 4.1). The second group was a set of static postures during which the channel is static in terms of the path length and involves no movement in the environment. This group consists of the rest of the sweeps for each channel.

7.2.1 Separation of short-term and long-term fading

For the separation of long-term and short-term fading envelopes, the measured branch signals and the MRC signal were demeaned by the same procedure as described in Chapter 5, but rather than using eq. (5.2) for normalization, the received signal envelope, *x(t),* was normalized to the local root mean square (RMS) value given below in eq. (7.1) [6]. This method of normalization ensures that the average power of the short-term fading envelope is 1 and thus the number of parameters to characterize a distribution can be reduced in some distributions, like Rician.

$$M(t) = \sqrt{\frac{1}{2w}\int_{t-w}^{t+w} x^2(\tau)\, d\tau} \tag{7.1}$$

The averaging window size $2w$ is critical in separating the short-term and long-term fading [7]. As explained in Chapter 5 as well, the window was selected such that there was sufficient number of short-term fading oscillations (approx. 4 to 6) inside the window and yet small enough compared to the time scale of the long-term variation. The demeaned data for the corresponding individual sweeps in each group of movements were concatenated to constitute the short-term fading data set, *r(t),* for each channel. Similarly, the local RMS values, *M(t),* constituted the long-term fading envelope for the data set in each case.

7.2.2 Sample Autocorrelation and re-sampling

The data was re-sampled to reduce the correlation among the adjacent samples and to get independent data samples for distribution fitting. To find the distribution of the data, there must be sufficiently large number of independent data points. If the adjacent samples are highly correlated, the effective number of independent data points will be less. Fig. 7.1 shows, as an example, the autocorrelation among the data samples for one data set, before and after the re-sampling. The sample autocorrelation reduced to below 0.5 after re-sampling for most of the data sets. The re-sampling for short-term fading data was done by sampling every 4^{th} point for 2.45 GHz data and every 2^{nd} point for 5.8 GHz and 10 GHz data. By doing this, the total no. of points were made approximately the same (2300 approx. for belt-head and 2600 approx. for belt-wrist channel) for all the cases, with a difference of few samples resulting from different window sizes. The long-term fading was extracted by re-sampling with every 10^{th} sample for 5.8 and 10 GHz and every 20^{th} sample for 2.45 GHz.

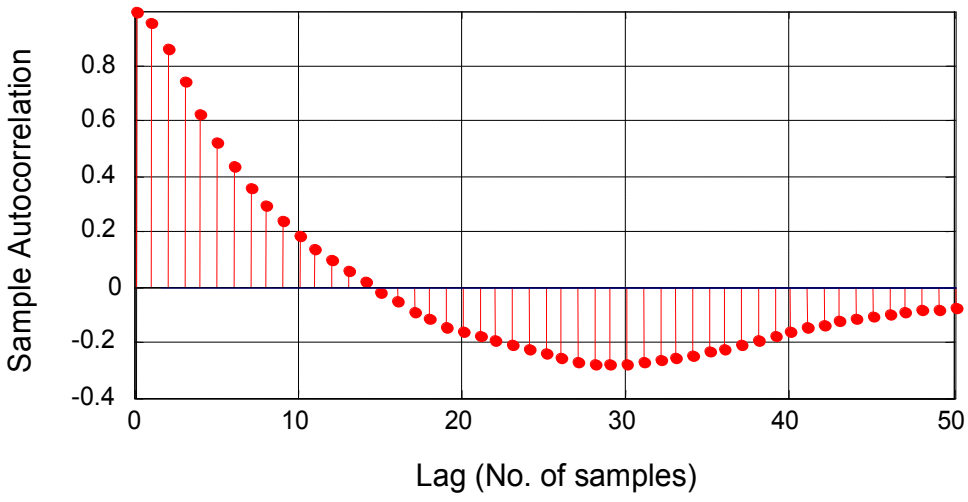

Fig. 7.1 (a)

PTO for full caption

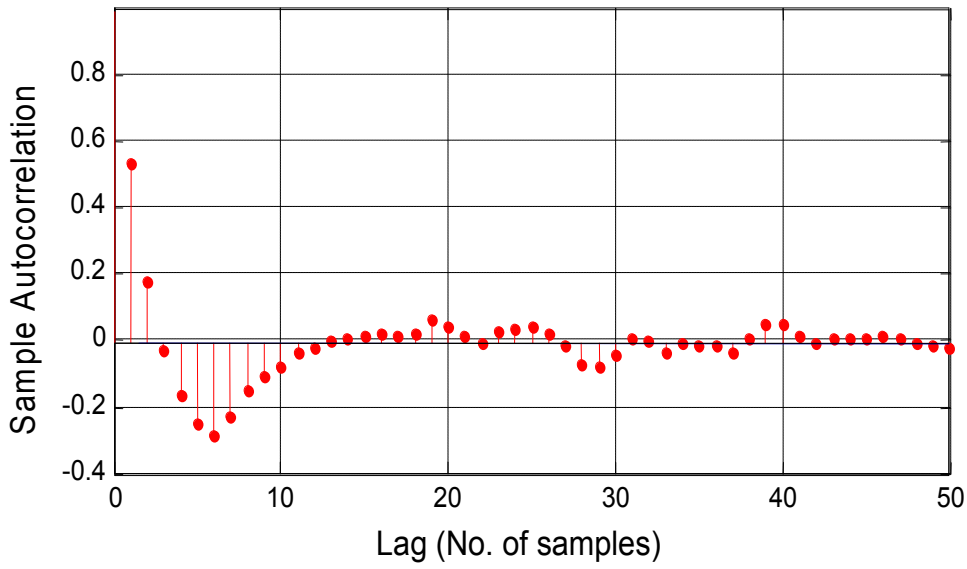

(b)

Fig 7.1: Autocorrelation function of the short-term fading envelope for belt-head channel with PIFA at 2.45 GHz in the laboratory environment (a) before re-sampling and (b) after re-sampling

7.3 Distribution fitting and Statistics

7.3.1 Short-term Fading

Each data set was fitted to seven distributions, namely, Log-Normal, Nakagami, Rician, Rayleigh, Weibull, Gamma, and Normal. The goodness of the fit was verified using Kolmogorov-Smirnov (KS) test [8]. It was observed that the second group of movements, which involves static postures, does not fit any of the distributions and thus only the results for the first group of movements are presented. However, Fig. 7.2 and 7.3 show the histograms of the data for the second group of movements.

Out of the seven distributions tested for the first group of movements, the short-term fading envelope of the branch and combined signal (MRC) for both the on-body channels fitted to four prominent distributions, namely, Rician, Weibull, Normal, and Nakagami, with significance levels above 5%. Among the four distributions, Rician was the best fit for most of the cases with highest p-values, usually above 50%. Normal was the second best but the significance level values were lower for the majority of cases. The p-value of the KS test was used to determine the best fit among the seven distributions. The distribution with the highest p-value was selected to be the best fit. The KS test is based on the maximum deviation between the distribution under test and the theoretical distribution [9, 10]. If the maximum deviation is less than a critical value for a certain p-value, the fit is considered good. It can be seen from the critical value tables of the KS test [11] that the higher the p-value, the lower is the critical value. Thus, if high p-value is assigned to a distribution among a group during the test, it is likely that it will have lowest deviation, as the critical value will be the lowest due to the highest p-value. However, in statistical theory and analysis, some better methods are usually used to determine the best fit. Fig. 7.4 shows the number of times each distribution had significance level above 5% and the number of times each one was best fit (highest p-value) for the 58 cases tested altogether for different orientations and repetitions with each of the three antennas at the three frequencies. It is evident that Rician distribution is the best fit for almost 85% of the cases for the short-term fading envelope. The Rician probability density function (PDF) is given by [12]:

$$p(r,s,\sigma) = I_0\left(\frac{rs}{\sigma^2}\right)\frac{r}{\sigma^2}\exp\left(-\frac{r^2+s^2}{2\sigma^2}\right) \quad (7.2)$$

where r is the random variable representing the short-term fading envelope $r(t)$, $I_0(.)$ is the modified Bessel function of the first kind and 0^{th} order. s and σ are the two parameters characterizing the strongest ray power, s^2, and the average scattered power, $2\sigma^2$, respectively. The Rician K-factor, which represents the ratio of the strongest ray power to the average scattered power, can be calculated as, $K = s^2/2\sigma^2$. The total power, p_o, can be calculated as, $p_o = s^2+2\sigma^2$. Due to the demeaning method used, as described above, p_o = 1 or 0 dB for all the short-term fading envelopes. Thus, the Rician distribution is completely characterized by the K-factor. The average K-factor values for the branch and combined signal (MRC) are shown in Tables 7.1-7.2 for the belt-head and belt-wrist channels, respectively. The averaging was done with dB values of the K-factor over different orientations and repetitions of the measurements for each antenna type and frequency.

The tables also show the maximum absolute deviation (in dB), $|\Delta K|$, with different orientations and repetitions, and the maximum difference (in dB), $|\delta K|$, between average values of the two diversity branches. Only one spacing of the monopole diversity antenna i.e. $\lambda/4$, was used at 2.45 GHz with no repetition and no other orientation, hence, the $|\Delta K|$ values do not exist.

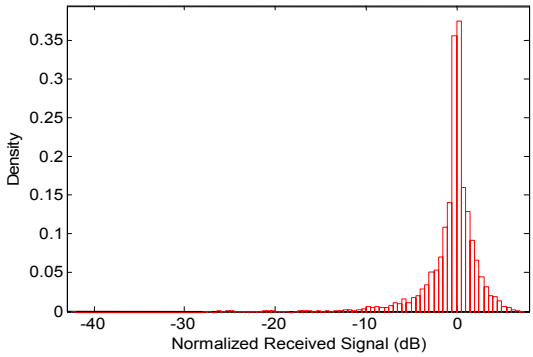

(a) Monopole with λ/2 spacing at 2.45 GHz

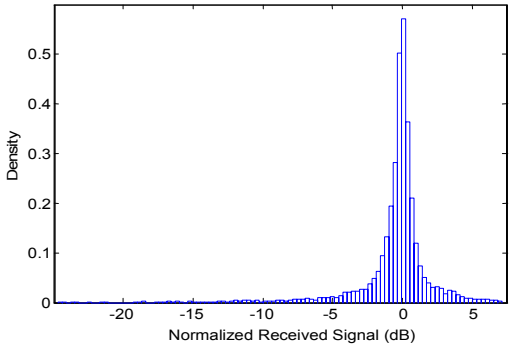

(b) Printed-IFA Conf. A at 2.45 GHz

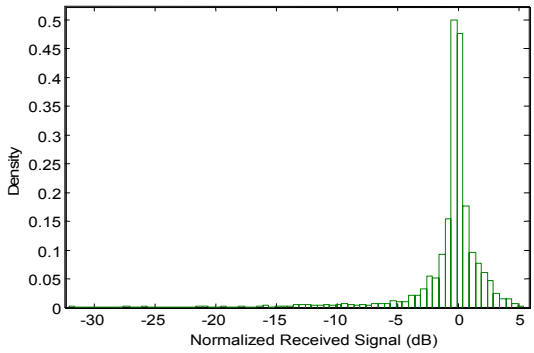

(c) PIFA at 2.45 GHz

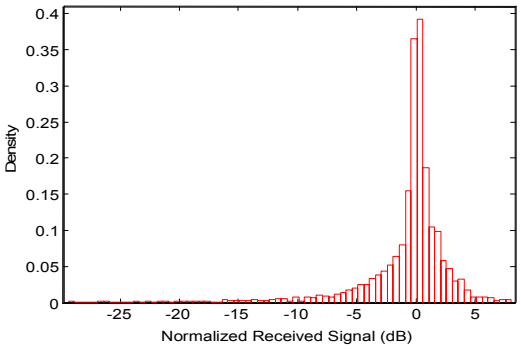

(d) Monopole with λ/2 spacing at 5.8 GHz

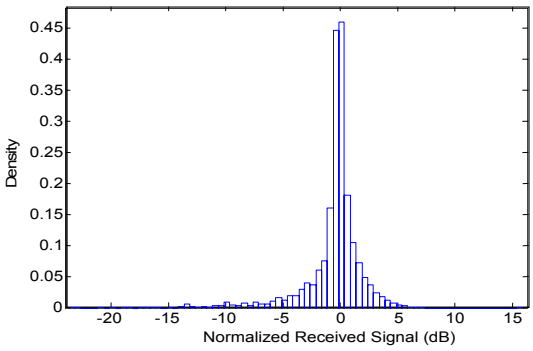

(e) Printed-IFA Conf. A at 5.8 GHz

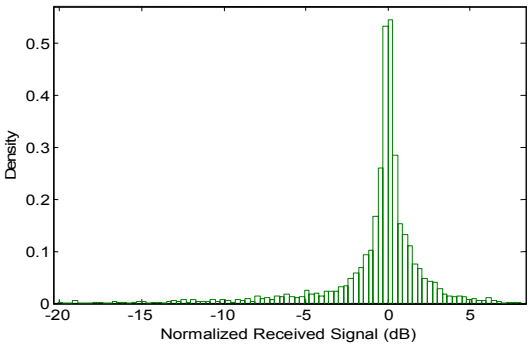

(f) PIFA at 5.8 GHz

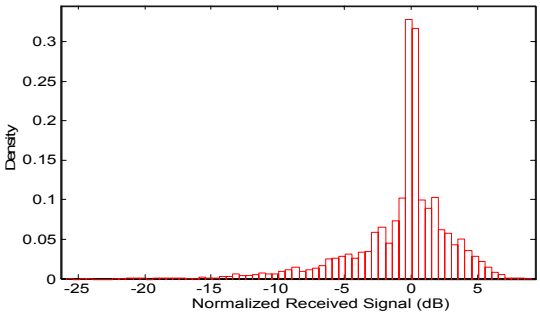

(g) Monopole with λ/2 spacing at 10 GHz

Fig. 7.2: Histograms of the second group of data (Normalized to the mean value) for belt-head channel in the laboratory environment with or.1 of printed-IFA and PIFA

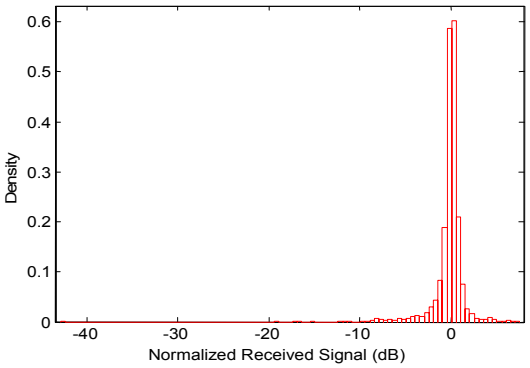

(a) Monopole with λ/2 spacing at 2.45 GHz

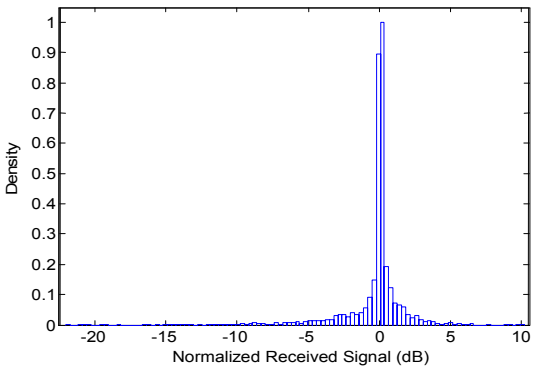

(b) Printed-IFA Conf. A at 2.45 GHz

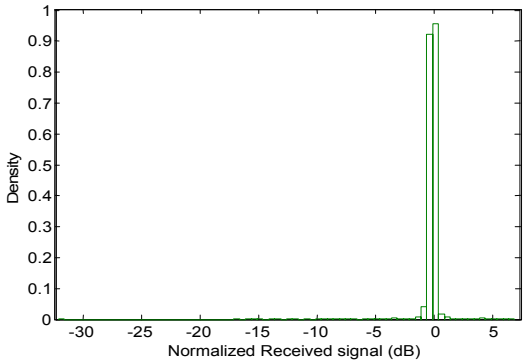

(c) PIFA at 2.45 GHz

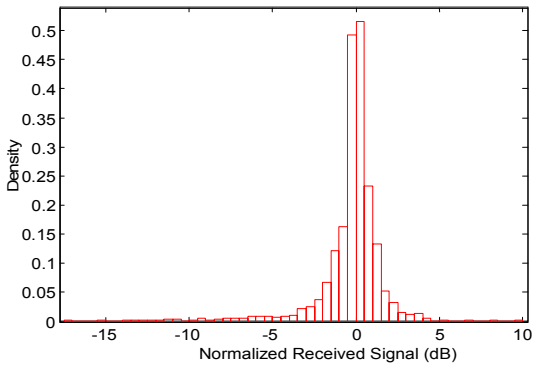

(d) Monopole with λ/2 spacing at 5.8 GHz

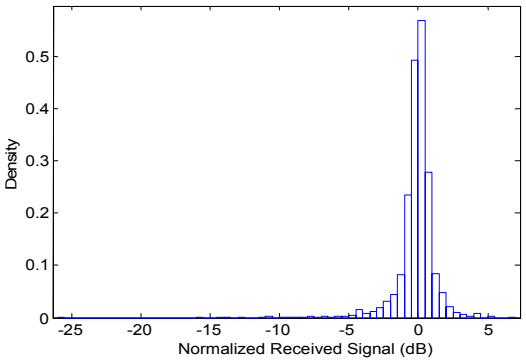

(e) Printed-IFA Conf. A at 5.8 GHz

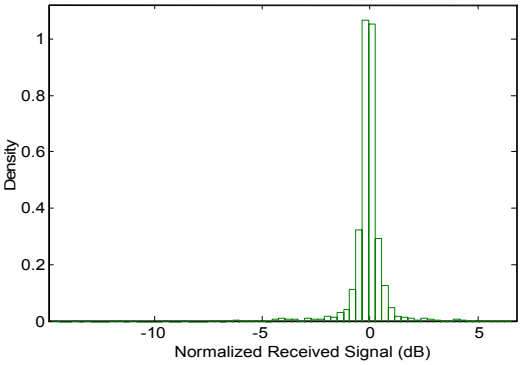

(f) PIFA at 5.8 GHz

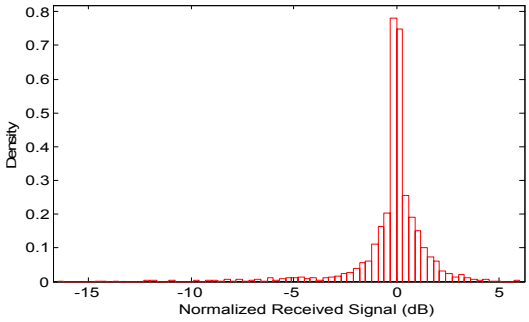

(g) Monopole with λ/2 spacing at 10 GHz

Fig. 7.3: Histograms of the second group of data (Normalized to the mean value) for belt-wrist channel in the laboratory environment with or.1 of printed-IFA and PIFA

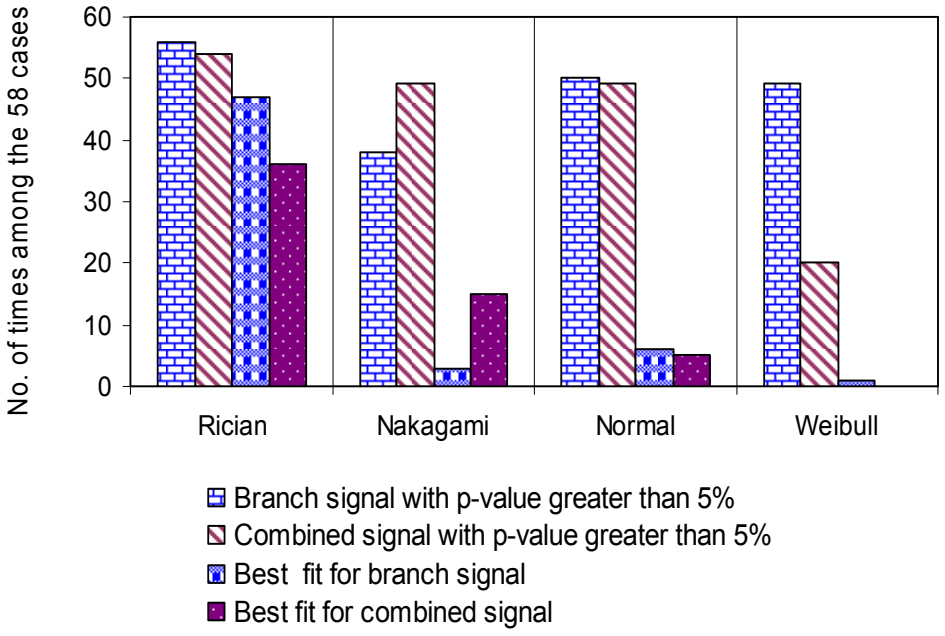

(a)

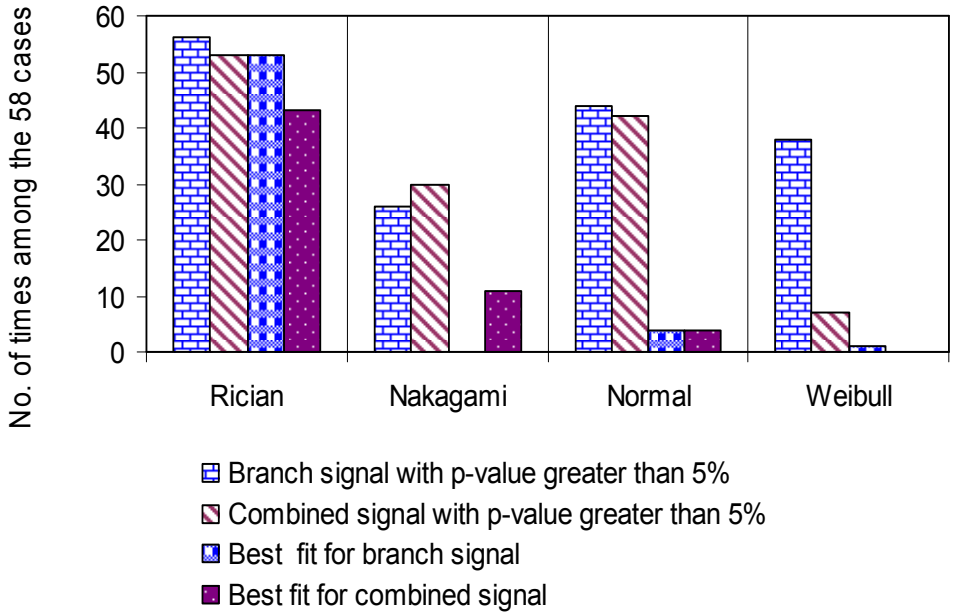

(b)

Fig 7.4: Graphs showing the No. of times short-term fading data sets of branch and combined signals fitted the four dominant distributions with p-values higher than 5% and the best fit (highest p-value) among the 58 cases for (a) belt-head and (b) belt-wrist channel

TABLE 7.1

SHORT-TERM FADING PARAMETERS OF THE RICIAN BRANCH AND COMBINED SIGNALS FOR BELT-HEAD CHANNEL

Frequency (GHz)	Antenna	Average Rician K factor (dB)		Max. deviation with repetition & orientations (dB)		Difference between branches (dB)
		Branch Signal, K_b	Combined Signal, K_C	$\|\Delta K_b\|$	$\|\Delta K_C\|$	$\|\delta K_b\|$
2.45	Monopole	3.3	6.8	-	-	1.9
	PIFA	3.0	6.6	2.7	2.3	0.5
	Printed-IFA	-0.8	3.6	2.0	1.0	0.3
5.8	Monopole	2.4	6.4	0.5	0.4	0.8
	PIFA	2.4	6.1	1.1	1.0	0.3
	Printed-IFA	2.7	7.0	0.7	1.0	0.3
10	Monopole	2.6	6.3	1.5	1.2	0.0

TABLE 7.2

SHORT-TERM FADING PARAMETERS OF THE RICIAN BRANCH AND COMBINED SIGNALS FOR BELT-WRIST CHANNEL

Frequency (GHz)	Antenna	Average Rician K factor (dB)		Max. deviation with repetition & orientations (dB)		Difference between branches (dB)
		Branch Signal, K_b	Combined Signal, K_C	$\|\Delta K_b\|$	$\|\Delta K_C\|$	$\|\delta K_b\|$
2.45	Monopole	2.4	7.3	-	-	2.3
	PIFA	1.6	5.6	1.3	1.0	0.2
	Printed-IFA	-0.2	5.1	2.5	2.6	1.8
5.8	Monopole	1.9	5.4	0.8	0.7	0.7
	PIFA	1.8	6.2	0.8	0.7	0.2
	Printed-IFA	1.7	5.5	1.3	0.6	0.1
10	Monopole	3.2	8.3	0.7	1.1	0.3

7.3.2 Long-term Fading

The same seven distributions were fitted to the long-term fading envelopes of the branch and combined signals. The p-values for all the distributions were low compared to the p-values for the short-term fading. Among all the distributions, only Log-Normal and Gamma were good fits and the rest of the distributions had p-values close to zero. The same significance level of 5% was set for the goodness of fit. Fig. 7.5 shows the number of times Log-Normal and Gamma had p-values of 5% or more out of the 58 cases for each channel, and the number of times each distribution was the best fit. It is clear from the figures that Log-Normal is the best fit for the long-term fading envelope for both the on-body channels. The PDF for the Log-Normal distribution is given by [12]:

$$p(m, \mu, \sigma_s) = \frac{1}{\sqrt{2\pi}\sigma_s m} \exp\left(-\frac{(\ln m - \mu)^2}{2\sigma_s^2}\right) \tag{7.3}$$

where μ and σ_s are the mean and the standard deviation of the natural logarithm of *m,* where *m* is a random variable representing the long-term fading envelope, *M(t)*. The average parameters for the Log-Normal long-term fading are shown in Tables 7.3 and 7.4 for the belt-head, and in Tables 7.5 and 7.6 for belt-wrist channels, along with the maximum absolute deviation from the average value with different orientations and repetitions and their difference between the two diversity branches. Parameters μ and σ_s are presented here in dB to make them consistent with the rest of the results.

TABLE 7.3

LONG-TERM FADING PARAMETERS OF THE LOG-NORMAL BRANCH SIGNALS FOR BELT-HEAD CHANNEL

Frequency (GHz)	Antenna	Log-Normal parameters (dB)		Max. deviation with repetition & orientations (dB)		Difference between branches (dB)	
		μ	σ_s	$\lvert\Delta\mu\rvert$	$\lvert\Delta\sigma_s\rvert$	$\lvert\delta\mu\rvert$	$\lvert\delta\sigma_s\rvert$
2.45	Monopole	-45.8	3.0	-	-	3.3	0.2
	PIFA	-51.9	2.9	5.0	0.7	0.2	0.1
	Printed-IFA	-53.1	5.2	12.9	1.2	0.5	0.2
5.8	Monopole	-60.5	3.2	1.6	0.9	0.8	0.3
	PIFA	-65.3	3.7	1.7	1.1	1.8	0.6
	Printed-IFA	-67.2	4.4	7.2	1.3	1.0	0.4
10	Monopole	-64.0	4.4	2.0	0.9	0.8	0.4

TABLE 7.4

LONG-TERM FADING PARAMETERS OF THE LOG-NORMAL COMBINED SIGNALS FOR BELT-HEAD CHANNEL

Frequency (GHz)	Antenna	Log-Normal parameters (dB)		Max. deviation with repetition & orientations (dB)	
		μ	σ_s	$\lvert\Delta\mu\rvert$	$\lvert\Delta\sigma_s\rvert$
2.45	Monopole	-43.9	2.6	-	-
	PIFA	-48.3	2.5	5.9	0.4
	Printed-IFA	-49.5	4.9	12.2	1.1
5.8	Monopole	-57.7	3.3	1.7	1.0
	PIFA	-62.7	3.8	1.1	1.5
	Printed-IFA	-64.1	3.8	4.3	1.1
10	Monopole	-60.4	4.1	1.5	1.0

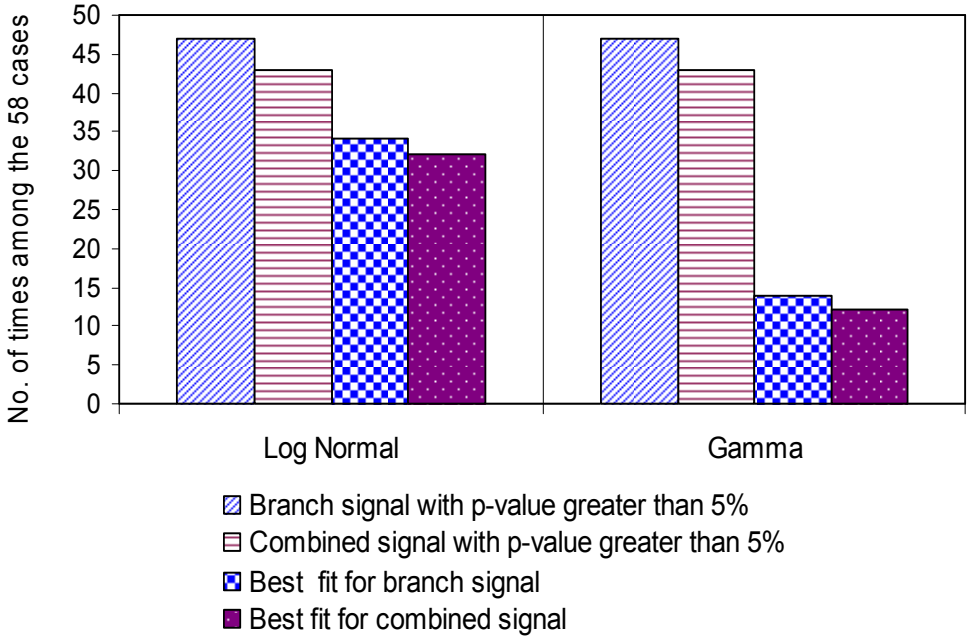

(a)

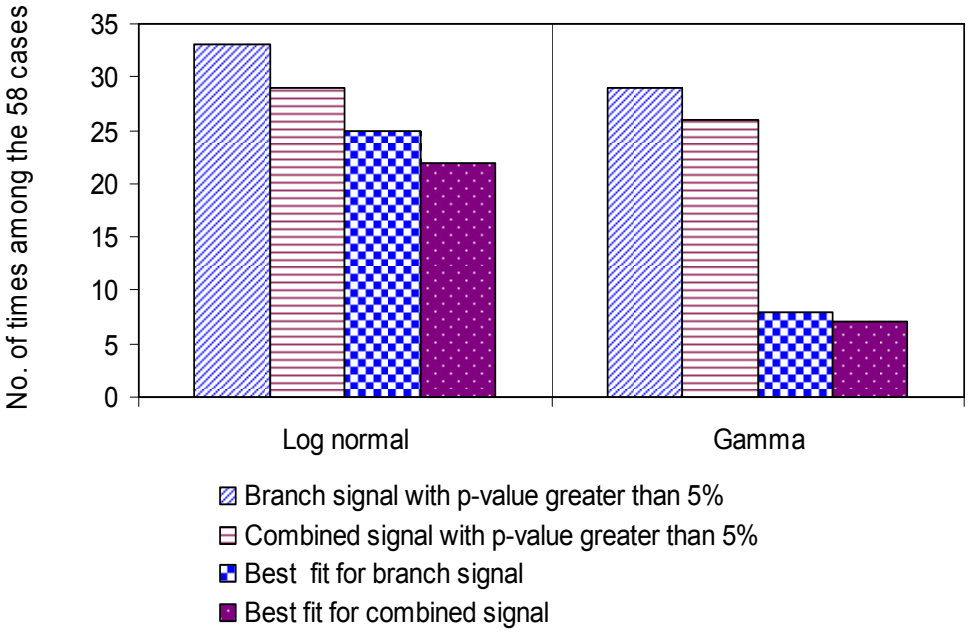

(b)

Fig 7.5: Graphs showing the No. of times the long-term fading data sets of branch and combined signal fitted the two dominant distributions with p-values higher than 5% and the best fit (highest p-value) among the 58 cases for (a) belt-head and (b) belt-wrist channel.

TABLE 7.5

LONG-TERM FADING PARAMETERS OF THE LOG-NORMAL BRANCH SIGNALS FOR BELT-WRIST CHANNEL

Frequency (GHz)	Antenna	Log-Normal parameters (dB)		Max. deviation with repetition & orientations (dB)		Difference between branches (dB)	
		μ	σ_s	$\lvert\Delta\mu\rvert$	$\lvert\Delta\sigma_s\rvert$	$\lvert\delta\mu\rvert$	$\lvert\delta\sigma_s\rvert$
2.45	Monopole	-46.3	3.8	-	-	3.2	0.7
	PIFA	-52.1	3.4	1.2	0.4	1.9	0.0
	Printed-IFA	-61.4	5.2	5.2	1.4	0.6	0.2
5.8	Monopole	-58.5	4.8	1.1	0.8	0.7	0.7
	PIFA	-64.4	4.0	1.2	1.7	1.8	0.4
	Printed-IFA	-68.2	4.8	3.5	1.2	1.4	0.0
10	Monopole	-61.6	4.2	1.4	0.9	0.4	0.3

TABLE 7.6

LONG-TERM FADING PARAMETERS OF THE LOG-NORMAL COMBINED SIGNALS FOR BELT-WRIST CHANNEL

Frequency (GHz)	Antenna	Log-Normal parameters (dB)		Max. deviation with repetition & orientations (dB)	
		μ	σ_s	$\lvert\Delta\mu\rvert$	$\lvert\Delta\sigma_s\rvert$
2.45	Monopole	-41.1	4.0	-	-
	PIFA	-49.6	2.8	2.2	0.6
	Printed-IFA	-57.7	5.1	5.7	1.3
5.8	Monopole	-54.7	4.1	1.0	1.0
	PIFA	-62.0	3.7	0.7	1.1
	Printed-IFA	-65.3	4.3	3.8	1.9
10	Monopole	-58.4	4.0	2.0	1.1

7.3.3 Discussion

It can be noted from Tables 7.1 and 7.2 that the K-factor is not as high as expected in a short range line-of-sight (LOS) communication. This may be due to the fact that the direct ray propagates along the surface of the body as creeping wave and is attenuated much more rapidly compared to the free space propagation. Also, the movement of the body causes significant scattering along with the scattering from the environment. Thus, the scattering ray power is comparable to the direct ray power, resulting in relatively low K-factor. This phenomenon is reflected more clearly in the case of printed-IFA, which has negative K-factor values, i.e., direct ray power is less than the power in the scattering rays. Due to the structure of the printed-IFA, the direct ray is polarized tangentially to the surface of the body and is attenuated much more than the perpendicularly polarized ray of monopole antennas. Thus, monopole antennas have the strongest direct ray followed by PIFA, which also has a strong perpendicularly polarized component. Furthermore, the μ parameter in Tables 7.3-7.6, which represents the mean received power, is the highest for the monopole antenna; followed by the PIFA with the standard deviation, $\sigma_{s,}$ lower than that of the printed-IFA. This signifies better link budget for the monopole antennas and worse for printed-IFA, among the three antenna types tested. Although, the monopole outperforms other antenna types, the structure of the monopole antenna is not suitable for body-worn devices. The PIFA, with moderate performance and low profile structure, seems to be the best choice for BAN applications.

The comparison of the parameters at the three frequencies signifies higher losses at the higher frequencies, as expected. It can be seen from Tables 7.3 and 7.5 that both,

the pathloss and the standard deviation, are higher at high frequencies. No trend was observed for the K-factor with increasing frequency. The maximum deviation in the parameters with various repetitions and orientations is acceptable in most cases, but is slightly higher for the printed-IFA. The reason may be the fact that the direct ray is very weak and the power is mostly in the multipath components, which may vary significantly with the movement of the body and the environment. As the movements cannot be replicated exactly and the antenna position on the body can be slightly offset in various repeated measurements, this can affect the link performance. The maximum deviation in parameters with various orientations of the antennas, in general, is within the repeatability error [2, 3]. Thus, it can be concluded that the orientation of the antenna does not significantly change the statistics apart from the repeatability error. The difference between the two branch signals, which effectively shows the power imbalance, is noticeable for monopole antennas at 2.45 GHz. In this case, the separation between the antennas is larger compared to the separation for other two frequencies for the same *λ/4* spacing, and the body shadowing can produce a difference in the received power at the two branch antennas. This difference signifies the fact that the two branch signals may not be identically distributed. The smaller spacing between the antennas at the higher frequencies results in approximately the same amount of shadowing for both branches and hence lower power imbalance is observed. For the other two antennas, the difference between branches is small.

It can be observed from the Tables 7.1 and 7.2 that the Rician K-factor increases significantly for the combined signals when compared to the K-factors for the

corresponding branch signals, which clearly suggests an improvement of the coherent component over the scattering power with diversity. This improvement is almost similar for all the antennas and at the three frequencies, which shows that use of diversity offers similar improvement at the three frequencies and the three antenna types. This was reported in Chapter 5 and 6 and in [2] and [3] as well. This improvement can also be seen by comparing the μ and σ_s values in Tables 7.3 and 7.4 for branch and combined signals, respectively, for belt-head and, similarly, in Tables 7.5 and 7.6 for belt-wrist channels.

7.4 Spectral Analysis

The transmitter and receiver antennas, mounted on the body, move relative to each other as well as in the environment and hence a Doppler frequency shift is introduced, referred to here as the body Doppler shift. The maximum Doppler shift, f_m, can be calculated by eq. (3.1). The Doppler spectrum of the received branch signal envelope was calculated by taking the Fourier transform of the autocorrelation function of the received signal envelope, *x(t)*[13].

$$P_x(f) = \int_{-\infty}^{\infty} R(\tau) e^{-j2\pi f\tau} d\tau \tag{7.4}$$

where $P_x(f)$ represents the power spectral density, $R(\tau)$ is the autocorrelation function of the signal envelope *x(t)* and is defined as:

$$R(\tau) = E[x(t)x^{*}(t-\tau)] \tag{7.5}$$

E[.] is the expected value operator and * represents the complex conjugate operation. The diversity combined signal was achieved in this case by combining the received branch signals, and the spectrum was calculated the same way. The branch and the corresponding diversity combined signal have identical spectra. A Hamming window was used to reduce the sidelobes. Only the walking movement was selected for this spectral analysis. The average envelope Doppler spectrum at one frequency was obtained by averaging the individual spectra of the three antennas and all their orientations and repetitions at a certain frequency. The averaging was done to eliminate the variations caused by repeatability errors.

Figs. 7.6 and 7.7 show the Doppler spectra for the two channels at the three frequencies. The side lobe level for the Hamming window is -40 dB, so any frequency point with an ordinate value below -40 dB may represent a side lobe, and hence should be ignored. The maximum Doppler shift, f_m, can be approximated from these plots. The frequency where the slope of the curve changes and drops down rapidly is $2f_m$ [14]. The slope of the curves in Figs. 7.6 and 7.7 changes slowly, as opposed to the ideal case, due to the presence of side lobes and the noise in the system. The $2f_m$ point can be identified for the 2.45 GHz case but not for the other two frequencies due to the limitations of the measurement system on the sampling time and the noise level. The maximum Doppler shift at 2.45 GHz, as observed from the plots, was about 4 Hz for belt-head channel, and about 10 Hz for the belt-wrist channel. The belt-wrist channel involves faster movements of the Rx due to wrist

motion and hence has higher Doppler shift. The scenario for the belt-head channel is similar to what is explained in [15] with fixed Tx and Rx antennas and moving scatterers. The belt-wrist scenario is different, as it also involves the motion of Tx and Rx with respect to each other and in the environment. In addition, both these scenarios are different from the mobile moving in the environment with a constant speed of motion.

The several peaks after the first minimum position in Figs. 7.6 and 7.7 can be attributed to various periodic activities during the movements. The first peak after the minimum represents a periodic movement with a time period of about 6s for both the channels. This coincides with the period of walking up and down the room. This peak cannot be observed for the 10 GHz frequency, as the resolution is not high enough due to the limitation of the total sweep time. The speed of motion for the 2.45 GHz and 5.8 GHz measurements was approximately the same and hence the peaks are approximately at the same position. For 10 GHz, the motion was slightly faster and hence the peaks are at slightly higher frequencies. There is a bigger peak at about 0.8 Hz for the belt-wrist channel, which is not present in the belt-head spectrum. This peak corresponds to the periodic movement of Rx antenna on the wrist relative to the Tx with approximately 1.5s period, for 2.45 GHz and 5.8 GHz. This peak is at about 1 Hz for 10 GHz measurements, corresponding to faster oscillation of the arm. The presence of a dominant component introduces two peaks in the spectrum at $f_m(1 \pm cos\alpha_o)$, where α_o is the angle of arrival of the dominant component [16]. There is a dominant component present for both the channels and hence peaks will be introduced in the spectrum, but are undetected due to random speed of motion and

random α_o. The Doppler spectrum with complex signals can be determined by taking the FFT of the autocorrelation of the complex received signal. Figs. 7.8 and 7.9 show the average Doppler spectra calculated for the two channels using complex signals. The spectra are not the typical U-shaped curves but are similar in shape to the spectra presented in [15]. The complex spectrum is asymmetric about the center frequency, as shown in [16] for mobile channels. This asymmetry may be due to the variable speed of motion of the receiver and transmitter relative to each other and also in the environment. Also, the scatterers around the antennas move randomly due to the random movements.

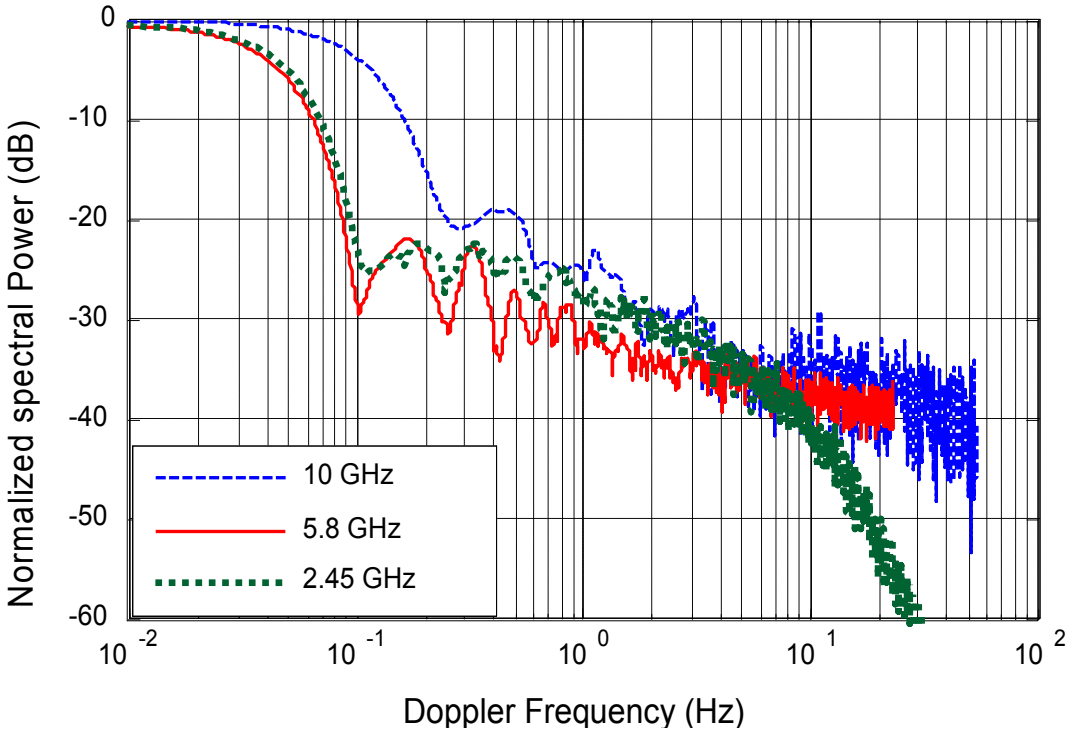

Fig 7.6: Average Doppler spectrum for the belt-head channel and walking movement in the laboratory environment

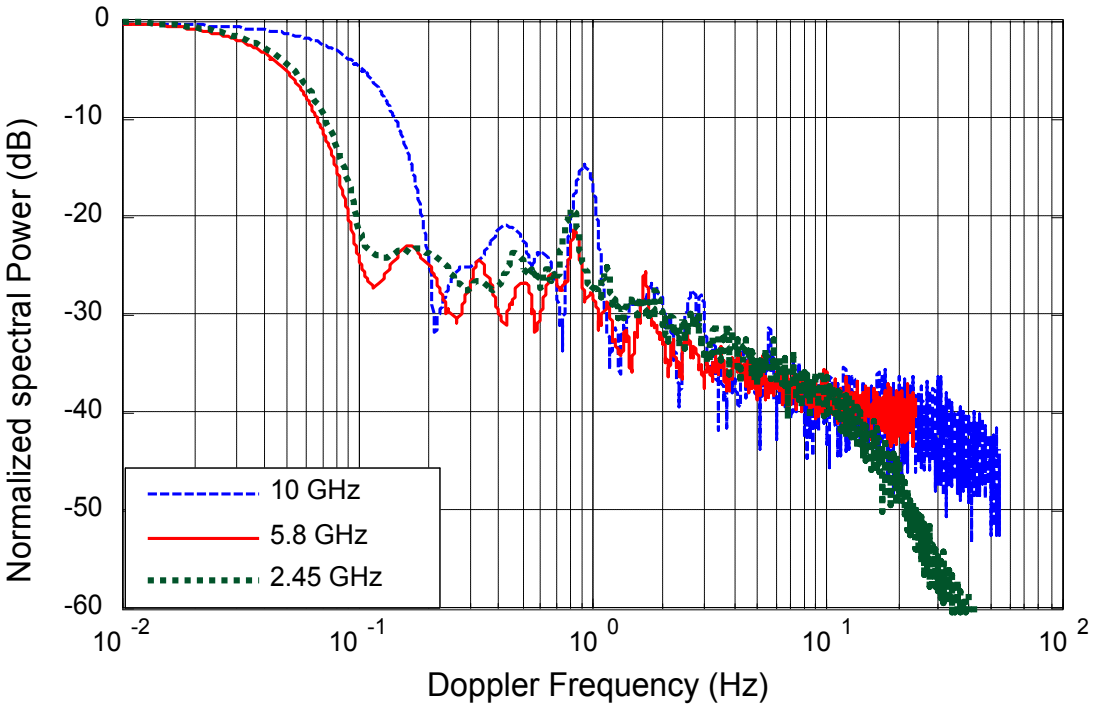

Fig 7.7: Average Doppler spectrum for the belt-wrist channel and walking movement in the laboratory environment

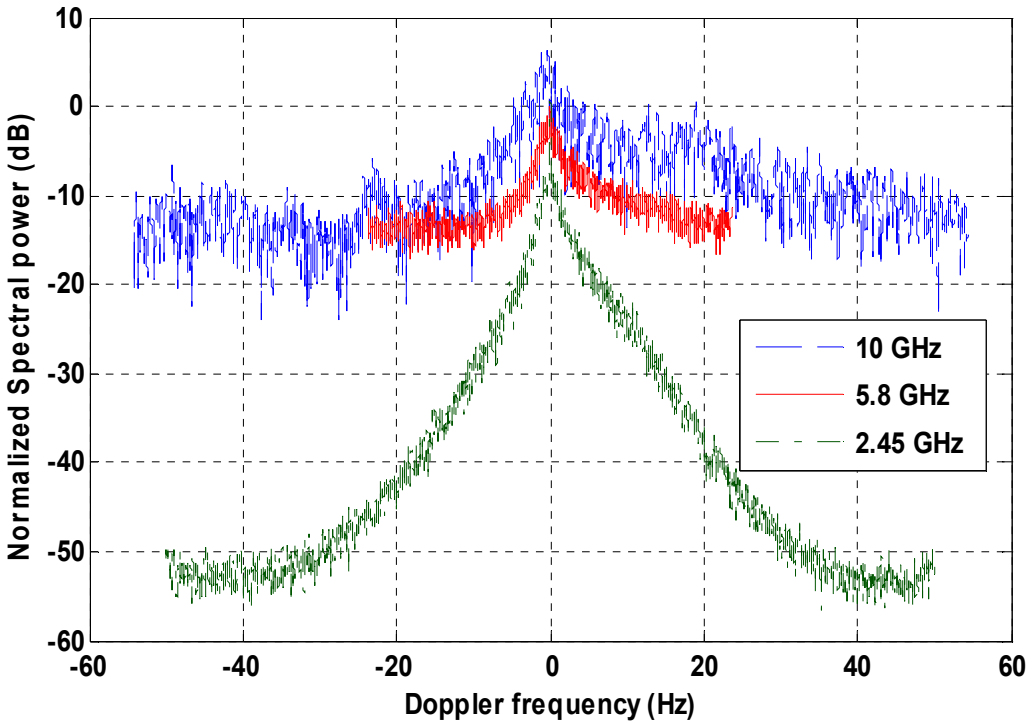

(a)

PTO for full caption

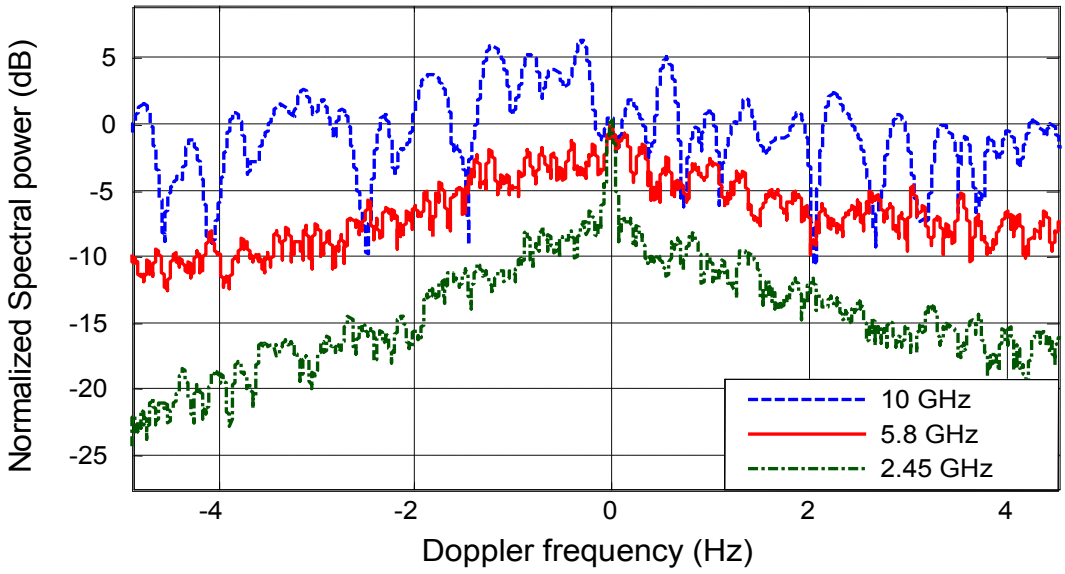

(b)

Fig 7.8: (a) Average Doppler Spectrum for the belt-head channel and walking posture in the laboratory environment using complex signal
(b) A zoomed portion of the spectrum

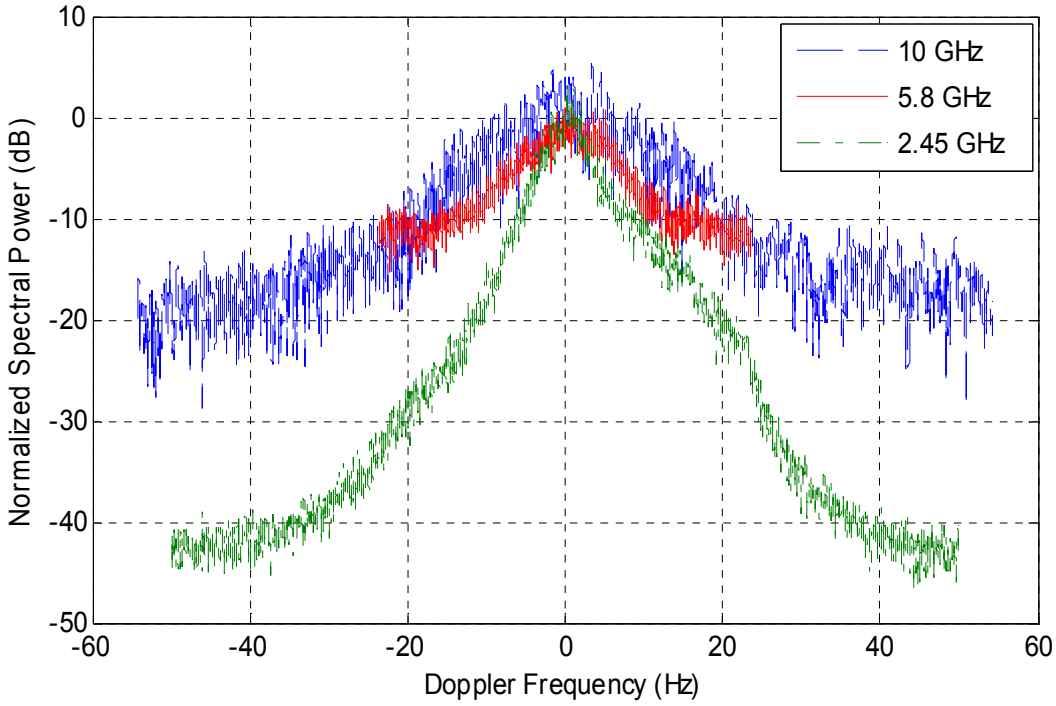

(a)

PTO for full Caption

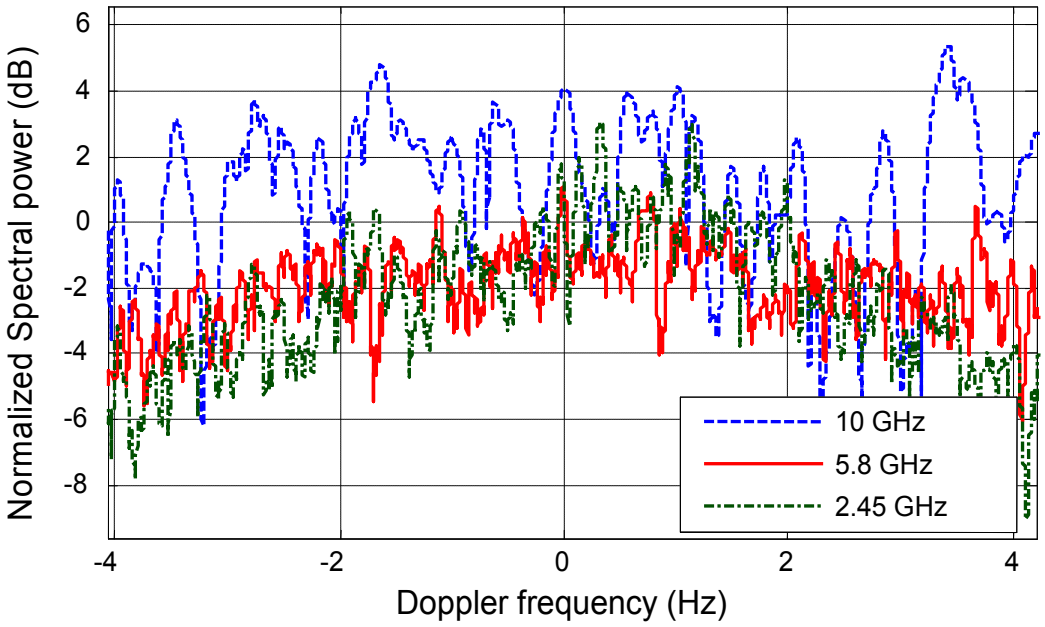

(b)

Fig 7.9: (a) Average Doppler Spectrum for the belt-wrist channel and walking posture in the laboratory environment using complex signal
(b) A zoomed portion of the spectrum

7.5 Second-Order Statistics

The use of diversity removes the deep fades and, as a result, the rate of crossing and the duration of the lower fade levels are reduced for the resultant combined signal. The amount of improvement offered by diversity is quantified by the diversity gain, but can also be estimated from the average fade duration (AFD) and level crossing rate (LCR).

Average parameters such as LCR and AFD are estimated for the belt-head channel at three frequencies. The estimation and comparison of the second order statistics of branch and diversity combined signal has been done extensively for the mobile

indoor scenarios. The AFD, probability of fade (PF), and LCR give a picture of the severity of the fading. The probability of fade, P_r, is the probability that a fading signal envelope remains below a threshold fade level F and can be determined by [12]:

$$P_r(r \leq F) = \frac{N_{r \leq F}}{N_T} \tag{7.6}$$

where $N_{r<F}$ is the number of times the sample magnitude of the short-term fading envelope, r, is below F. N_T is the total number of samples in the data set.

The LCR, N_R, signifies the rapidity of fading, and is the rate at which the short-term fading envelope, r, crosses the threshold fade level, F, in one direction, either positive or negative going [12].

$$N_R \underline{\Delta} \int_0^{\infty} \dot{r} f(F, \dot{r}) d\dot{r} \tag{7.7}$$

where $f(F, \dot{r})$ is the joint PDF of r and $\dot{r}$ at $r = F$, and $\dot{r}$ is the time derivative of $r(t)$. The N_R for this work was estimated by counting the actual number of times the short term fading signal envelope crossed the fade level, F, going in the positive direction, using a program developed in MatLab.

AFD, T_D, is defined as the average time duration for which the fading signal is below the fade level, F, and can be estimated from P_r and N_R as [12]:

$$T_D \triangleq \frac{P_r}{N_r} \tag{7.8}$$

N_R and T_D were estimated for the short-term envelopes of the branch and the MRC signals. These parameters were then averaged for all the orientations and repetitions of the corresponding antenna type at one frequency. Figs. 7.10 - 7.12 show the average LCR, AFD, and PF, respectively, for one of the branch signals with monopole antennas. There was a maximum absolute deviation of around 15% of the average values. The difference between the average parameters of the two branches was around 10% of the average values. The other antennas show the same trend with frequency. It is clear from the figures that the higher frequencies have more severe fading. The LCR for higher frequencies is higher than the LCR for the lower frequencies at the same fade level. But Fig. 7.11 shows that low frequency signals remain for a longer time under that fade. Figs. 7.13 - 7.15 show the comparison of average parameters for the three antennas at 5.8 GHz. The same trend was observed for the other frequencies. The printed-IFA is more prone to fading due to the fact that the strong ray is weaker than the scattering rays. The monopole and PIFA are somewhat similar to each other. LCR is different at the fade levels close to the medians but the difference is low at the lower and higher fade levels. AFD for the three antennas is almost the same.

Figs. 7.16 - 7.18 show the comparison of the parameters for branch and combined (MRC) signals. For comparison, the branch and combined signals, in each case, were both normalized to the median of the branch signals rather than their respective

medians. It can be observed from Fig. 7.16 that the LCR for the lower levels is reduced significantly by using MRC. Thus, the resulting combined signal has lower LCR for the lower fades and higher LCR for the higher fades. There is also an improvement in the power level with the diversity combining. The LCR profile for the MRC is narrower than the branch signal profile, which signifies that the resultant signal remains closer to its median value and the variation due to fading is reduced. Fig. 7.17 shows that diversity combining reduces the AFD, as the combined signal remains under the fade for less time compared to the branch signals, and the probability of the fade is also reduced. It can be observed that the improvement offered by diversity is almost similar at all the frequencies.

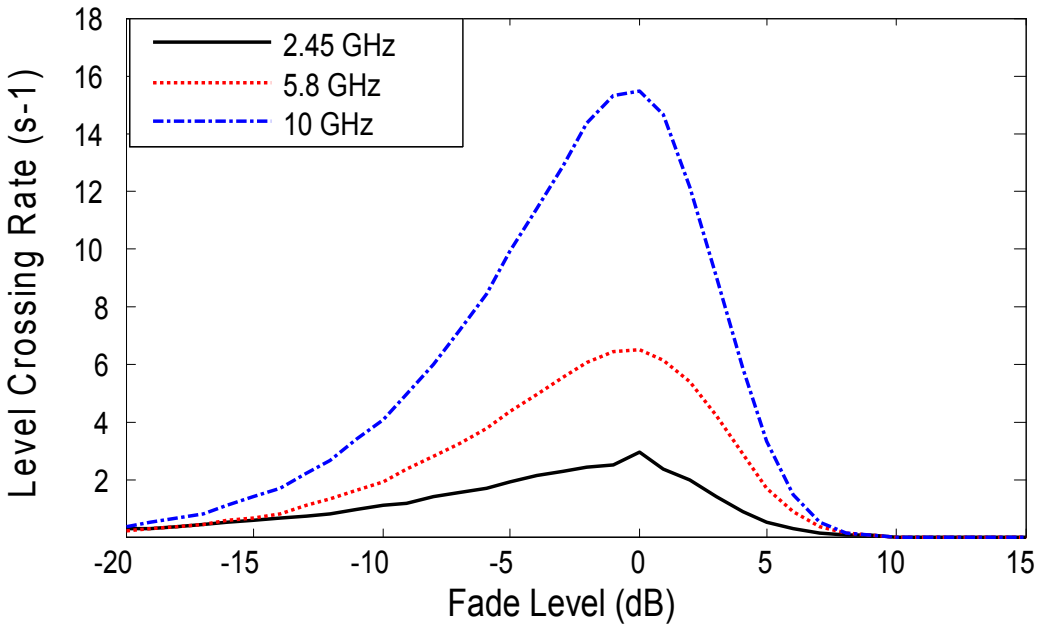

Fig. 7.10: LCR for the branch signals averaged over all orientations and repetitions with monopole antennas in the laboratory environment

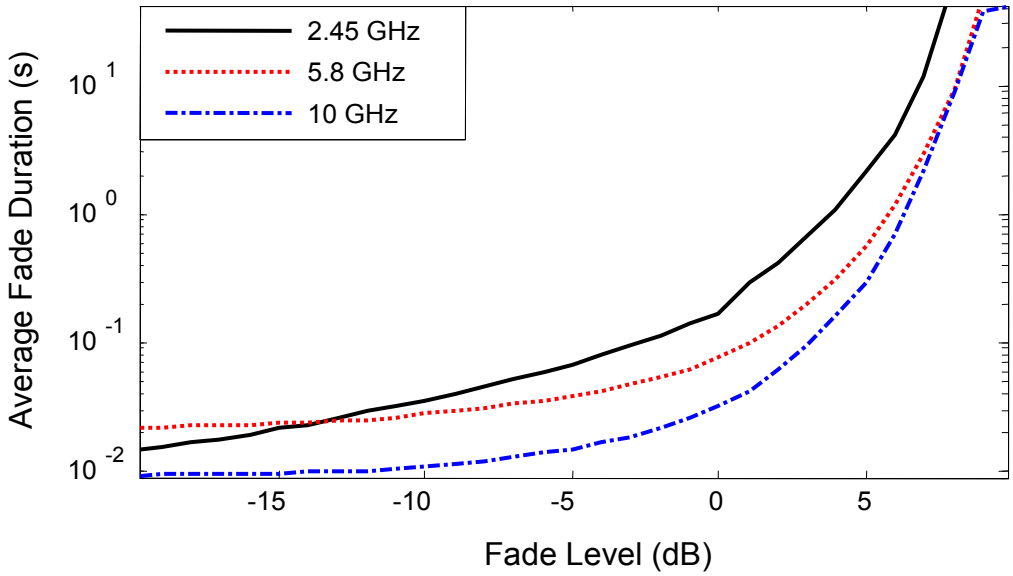

Fig. 7.11: AFD for the branch signals averaged over all orientations and repetitions with monopole antennas in the laboratory environment

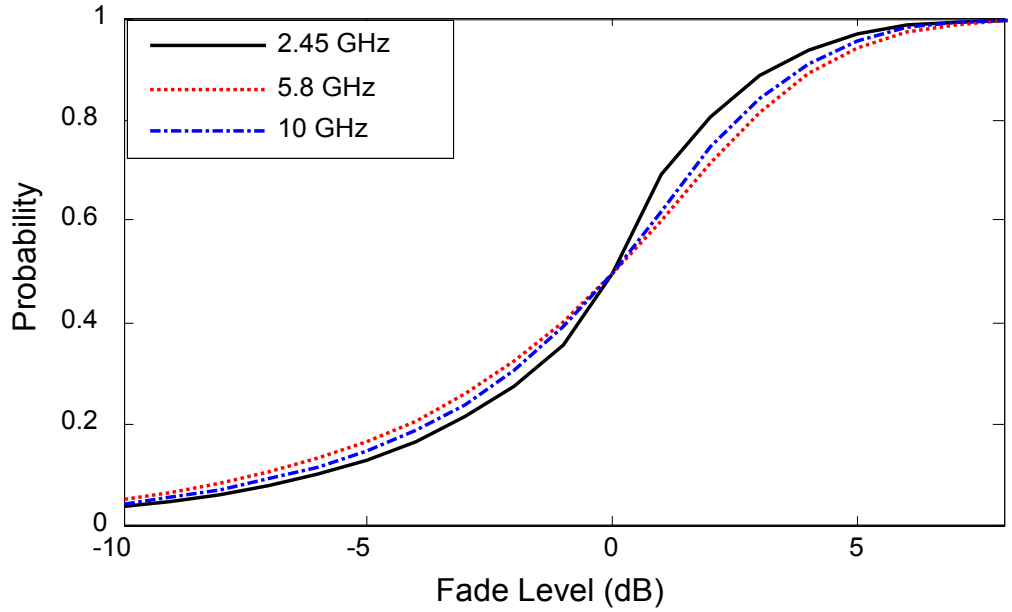

Fig.7.12: Probability of fade for the branch signals averaged over all orientations and repetitions with monopole antennas in the laboratory

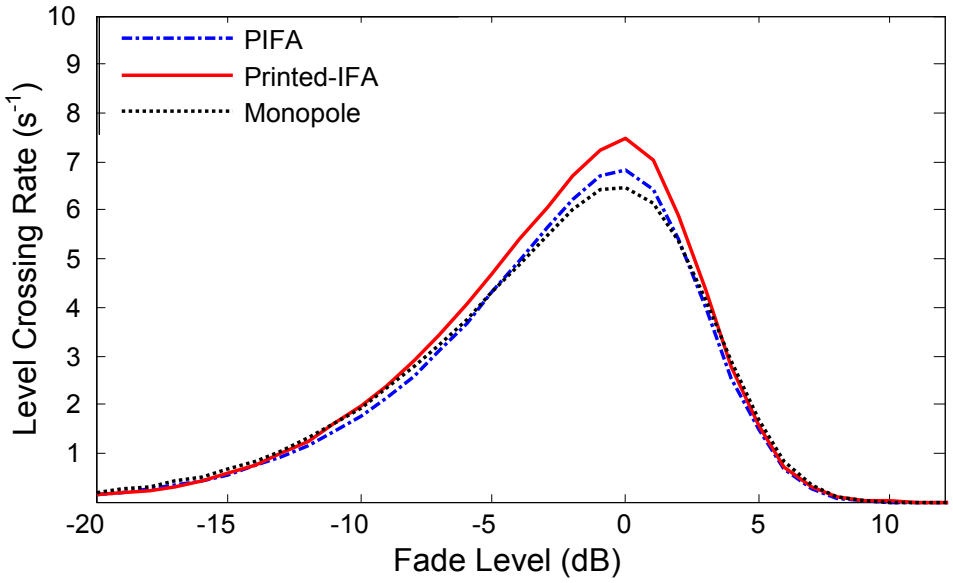

Fig. 7.13: Comparison of LCR with the three antennas at 5.8 GHz in the laboratory environment

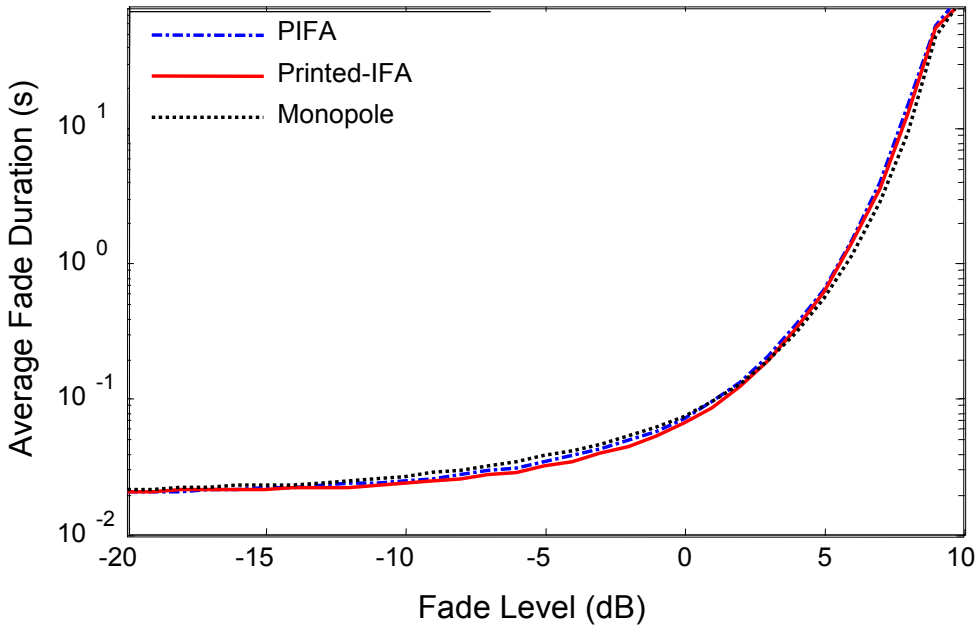

Fig.7.14: Comparison of AFD with the three antennas at 5.8 GHz in the laboratory environment

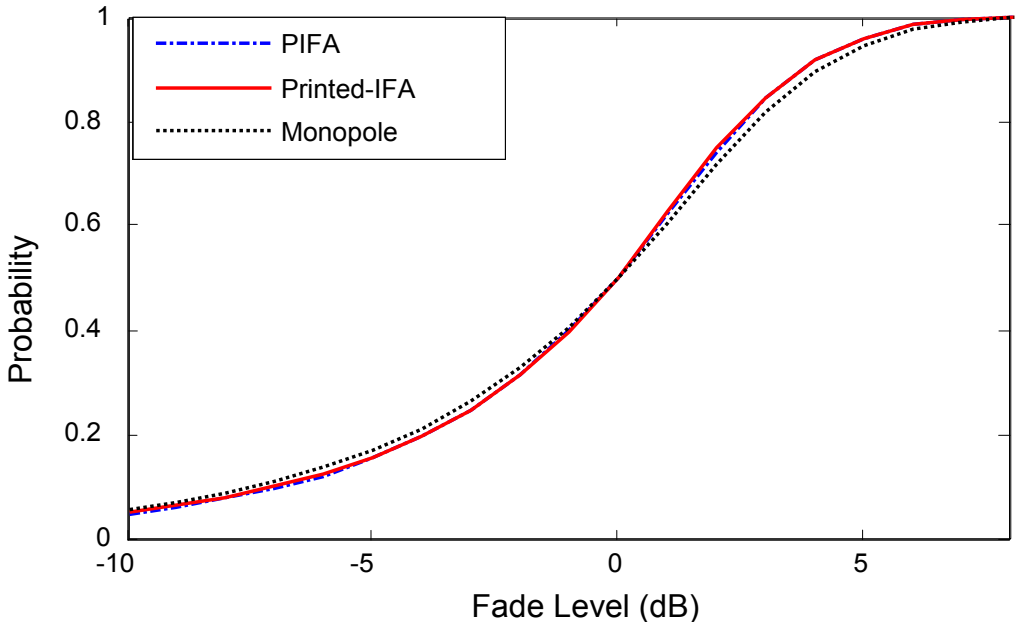

Fig. 7.15: Comparison of PF with the three antennas at 5.8 GHz in the laboratory environment

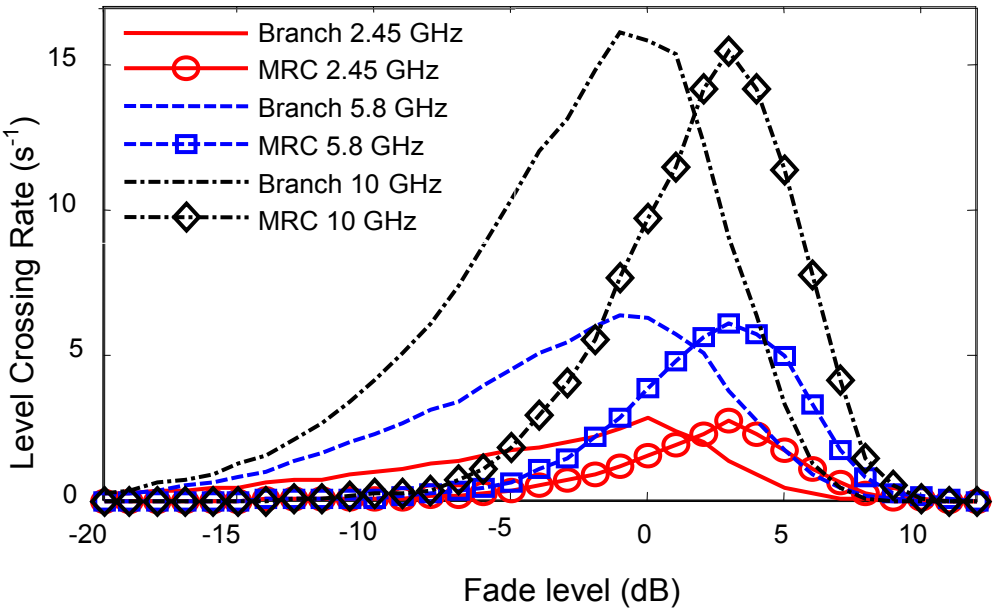

Fig. 7.16: LCR for branch and combined signals with monopole antennas at the three frequencies in the laboratory environment

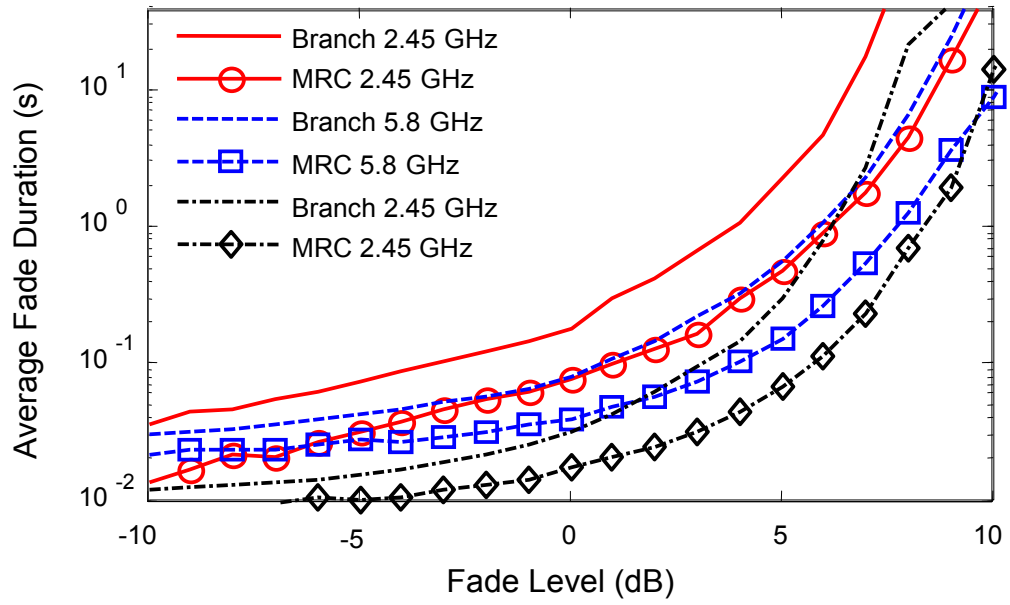

Fig. 7.17: AFD for branch and combined signals with monopole antennas at the three frequencies in the laboratory environment

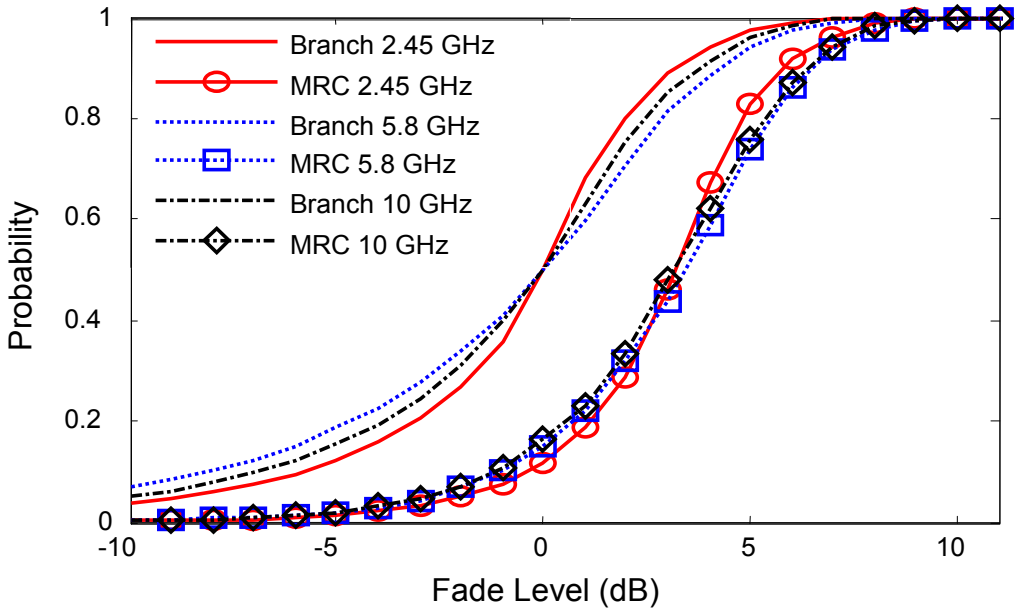

Fig. 7.18: PF for the branch and combined signals with monopole antennas at the three frequencies in the laboratory environment

7.6 Conclusions

Statistical and spectral analyses of two on-body diversity channels are presented at three frequencies using three different types of antennas. The short-term and long-term fading envelopes of the diversity branch and combined signals were fitted to seven distributions and the best fit was evaluated for each case using KS test. The short-term fading branch and combined signals best fit the Rician distribution. Long-term fading best fits the Log-Normal distribution. The average best-fit parameters were presented for each case along with the maximum deviation from the average values with different orientations and repetitions for each antenna at each frequency. The maximum difference of the parameters between the two branch signals was also presented, which suggested that the two branch signals might not be identically distributed. The monopole antenna gives better performance for the on-body channels followed by the PIFA, as the mean path gain for the monopole antennas is the highest among the three types. For printed-IFA, the direct ray is polarized parallel to the surface of the body and, therefore, is attenuated much more than a perpendicularly polarized ray. The Rician K-factors for printed-IFA were very small, which suggest that for this antenna, the local off-body scattering is dominant over the direct ray. The K-factor values for the branch and combined signals were compared, which clearly indicated that there is an improvement due to diversity reception. The average Doppler spectra are presented for both channels and the maximum body Doppler shift is estimated. Average LCR and AFD are presented for belt-head on-body channel for branch and diversity combined signals at three frequencies using three different types of antennas. Higher LCR at higher frequencies suggests that the fading is more severe and the comparison of branch and combined signals clearly

suggests an improvement offered by the use of diversity. The three antennas have almost the same fading statistics, with printed-IFA being a bit more prone to fading than monopole and PIFA due to weak direct link and dominant multipath components. Diversity performance is similar at the three frequencies.

REFERENCES

[1] Y. I. Nechayev and P. S. Hall, "Multipath Fading of On-body Propagation Channels," in *IEEE International AP-S Symposium - USNC/URSI National Radio Science Meeting, San Diego, CA, 2008.*

[2] I Khan, P. S. Hall, "Multiple Antenna Reception at 5.8 and 10 GHz for Body-Centric Wireless Communication Channels", *IEEE Transactions on Antennas and Propagation; Vol. 57, No. 1, January, 2009.*

[3] I Khan, P.S. Hall, A.A Serra, A.R. Guraliuc, P. Nepa, "Diversity Performance Analysis for On-body Communication Channels at 2.45 GHz" *IEEE Transactions on Antennas and Propagation, Vol. 57, No. 4, April, 2009.*

[4] I. Khan, Y. I. Nechayev, P.S. Hall, "On-body Diversity Channel Characterization", *IEEE Transactions on Antennas and Propagation, 2009 in press.*

[5] I. Khan, Y. I. Nechayev, P.S. Hall, "Second-order Statistics of Measured On-body Diversity Channels", *Microwave and Optical Technology letters, Vol. 51, No. 10, October, 2009.*

[6] Steele R. editor, "Mobile Radio Communications", *London, New York: Pentech Press, 1994*.

[7] N. L. Scott and R. G. Vaughn "The Effect of Demeaning on Signal Envelope Correlation Analysis" *4th Intl. Symposium on Personal, Indoor and Mobile Radio Communications, Yokohama, Japan, Sep. 1993.*

[8] R B D'Agostino, M A Stephens, editors, "Goodness-of-Fit Techniques", *Marcel Dekker, Inc., New York, 1986.*

[9] A Diamantopoulos, Bodo B. Schlegelmilch, "Taking the fear out of data analysis: a step-by-step approach", *Thomson Learning, London, 1997*.

[10] http://www.mathwave.com/articles/goodness_of_fit.html#ks

[11] http://www.eridlc.com/onlinetextbook/index.cfm?fuseaction=textbook.appendix&FileName=Table7

[12] R Prasad, "Universal Wireless Personal Communications", *pp. 55, Artech House, London, 1998.*

[13] Leon W. Couch II, "Digital and Analog Communications Systems", *sixth ed., Prentice Hall, New Jersey. pp. 406–409.*

[14] William C.Y. Lee, "Mobile Communications Engineering", *McGraw-Hill New York, 1982, Ch. 6, pp. 202.*

[15] A Domazetovic, L J. Greenstein, N B. Mandayam, I Seskar "Estimating the Doppler Spectrum of a Short-Range Fixed Wireless Channel", IEEE Comms Letters, Vol. 7, No. 5, May 2003.

[16] J D Parsons, J G Gardiner, "Mobile Communication Systems*", Blackie USA, Halsted Press, pp.35 and 54.*

Chapter 8

BAN – BAN Interference Rejection

8.1 Introduction

Receiver diversity is a very effective technique to combat fading, as demonstrated in the previous chapters. In a scenario where, apart from the desired transmitted signal, the receiving device receives significant level of unwanted signal from other surrounding transmitters transmitting in the same frequency band, receiver diversity can be exploited to enhance the desired signal and reject the unwanted interfering signal in variety of ways. If an appropriate combining technique is used at the receiver side equipped with multiple antennas, a sufficient level of interference rejection can be achieved. With the ever increasing use of body-worn devices in the personal area networks (PAN) and body-area networks (BAN), on-body channels are prone to interference from neighboring BANs. Rejection of the interference from a nearby BAN becomes more significant when the BANs are operating very close to each other and the level of the desired and interference signals are almost the same. In diversity combining, the branch signals are combined to increase the signal to noise ratio (SNR) of the signal at the output of the combiner. Interference rejection combining (IRC), on the other hand, is a combining technique in which the branch signals are combined in such a way that the interference signal is suppressed at the receiver and the output signal-to-interference-plus-noise ratio (SINR) is increased.

Interference rejection can be employed by using adaptive arrays at the receiver side [1, 2, 3]. An IRC technique, known as optimum combining, is described in [1]. Optimum combining needs to calculate complex optimum weight vector for the receiving antenna array signals. The weight vectors are optimized using various algorithms. For rejection of the interference, smart antenna arrays generate nulls in the direction of the interferer [1, 4]. To steer the null and/or maximum beam direction, the direction of arrival of the interference and desired signal is required. Receivers with interference rejection capabilities can become very complex and a lot of signal processing is required to be done if smart antenna techniques are applied. This complexity can add up to the cost and size of the receivers. It is desirable that devices mounted on the body are smaller and less expensive. Thus, low complexity IRC algorithms are needed for BAN applications.

Most of the work on diversity and multiple antennas emphasizes on the improvement in the desired signal strength and increase the diversity gain. No significant work has been done yet on the BAN-BAN interference rejection to the best of the author's knowledge. This chapter presents some experimental results and significance of the interference rejection for the on-body wireless communication channels. The optimum combining technique [1, 5, 6] along with the implementation of Weiner-Hopf optimum solution [1-3] are applied to the interference limited BAN systems, and their ability to suppress the interference coming from a neighboring BAN, and thus improve the output SINR, is discussed. Due to the high correlation and power imbalance between the received signals at the two diversity branch antennas for some of the on-body channels, the conventional IRC algorithms may not provide

significant amount of interference rejection. The Weiner-Hopf solution relies on the covariance between the branch signals to calculate the weight vector [2, 3]. The high covariance of the branch signals for some of the on-body channels thus degrades the performance of such algorithms.

In this work, a simple interference rejection technique is proposed, referred to as Interference Cancellation with Interrupted Transmission (ICIT). This technique, which relies on switching the desired signal off at regular intervals, is applicable to the on-body channels and may not be feasible for the mobile communication channels, where one base station transmits to many receivers. The performance of the conventional optimum combining techniques is compared with that of the proposed method. The interference rejection gain (IRG), defined here as the improvement in the output SINR, over the highest SINR among the branches, at 1% probability, is used as the metric for comparison. Extensive measurement campaign was carried out by mounting the desired signal transmitting antennas and the receiving arrays on a human body and the interference signal transmitting antenna on another person's body. Three on-body channels, which show importance in the current applications, were investigated namely the belt-chest, belt-head, and belt-wrist channels. The work has also been presented in [7].

The rest of the chapter is organized as follows. The system model along with a brief overview of IRC techniques is described in Section 8.2. The description of the antennas and the measurement setup are presented in Section 8.3. The results and analysis are given in Section 8.4. Section 8.5 summarizes the results.

8.2 System Model and IRC Techniques

Consider an *m*-branch diversity combiner, as shown in Fig. 8.1, with receiving antennas and the desired transmitting antenna mounted on a human body to form an on-body channel. It is also assumed that the receiving antennas also receive an interference signal coming from another BAN in the close proximity. The received signal, $x_i(t)$ at the i^{th} antenna of the diversity combiner is thus:

$$x_i(t) = d_i(t) + i_i(t) + n_i(t) \tag{8.1}$$

where $d_i(t)$ is the received desired signal, $i_i(t)$ is the received interference signal, and $n_i(t)$ is the additive white Gaussian noise, at the i^{th} branch antenna. If the signal transmitted from the desired transmitting antenna is $r(t)$, then

$$d_i(t) = h_i r_i(t) \tag{8.2}$$

where h_i is the channel transfer function of the i^{th} branch. The received branch signals are combined in an optimum way to suppress the interference signal and improve the output SINR. The aim of optimum combining scheme is to calculate the optimum weight, w_i, for each branch [1]. For a two branch diversity receiver, the received signal vector, X, and the weight vector, W, can be defined as:

$$X = \begin{bmatrix} x_1(t) & x_2(t) \end{bmatrix}^T \tag{8.3}$$

$$W = [w_1 \quad w_2]^T \tag{8.4}$$

where $[\ldots]^T$ represents the transpose of the vector. The array output, *y(t)*, is then

$$y(t) = W^T X \tag{8.5}$$

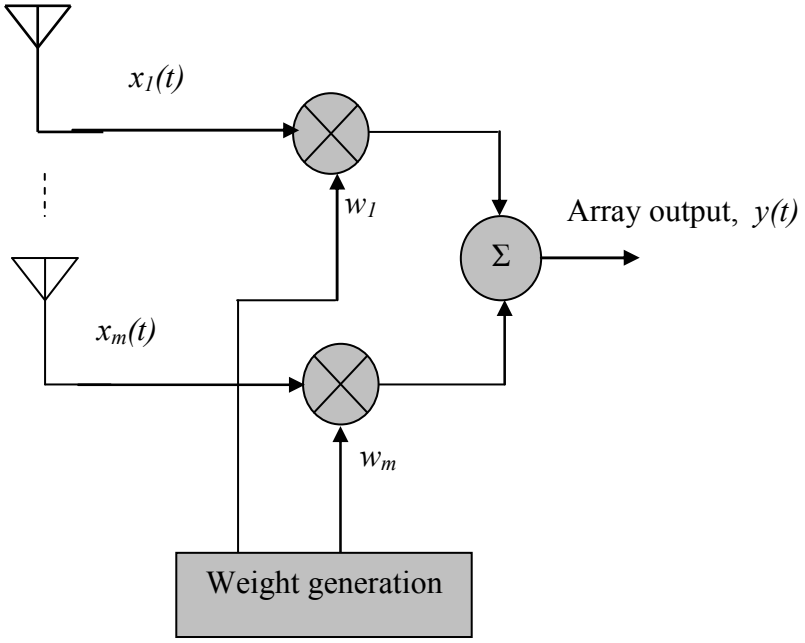

Fig 8.1: Simplified Diversity combiner

Similarly, the desired signal vector, *D*, interference signal vector, *I*, and RMS noise signal vector, N_{rms}, are given as:

$$D = [d_1(t) \quad d_2(t)]^T \tag{8.6}$$

$$I = \left[i_1(t) \quad i_2(t) \right]^T \tag{8.7}$$

$$N_{rms} = \left[\sqrt{<|n_1(t)|^2>} \quad \sqrt{<|n_2(t)|^2>} \right]^T \tag{8.8}$$

where <…> represents the mean value. Various IRC schemes have been proposed in the literature. A brief description of the optimum combining and the Weiner-Hopf (WH) solution is given below. The details of the proposed interference cancellation with interrupted transmission scheme are also given.

8.2.1 Optimum Combining (OC)

In the model presented above, the weight vector, *W*, for the optimum combining is generated as [1, 6]:

$$W = R^{-1} H \tag{8.9}$$

where *H* is the desired channel transfer gain vector and *R* is the covariance matrix of interference plus noise ($U = I+N$) called the error covariance matrix [1, 6], i.e.,

$$R = E(UU^{'}) \tag{8.10}$$

where $(\ldots)^{'}$ represents the complex conjugate transpose and *E(.)* is the expected value operator. *U* can be estimated by using a known transmitted training sequence and the channel response knowledge [5-6].

8.2.2 Weiner-Hopf (WH) Solution

The weight matrix, *W*, can be calculated using the Weiner-Hopf solution as [2, 3]:

$$W = \Phi^{-1} Z \tag{8.11}$$

where Φ is the covariance matrix of the received signals, $x_1(t)$ and $x_2(t)$, and is defined as [2, 3]:

$$\Phi = E(XX') \tag{8.12}$$

Z is the correlation matrix of the received signal, $x_i(t)$, and the reference signal $z(t)$. The reference signal can be achieved by various methods given in Chapter 7 of [2]. It must be correlated to the desired signal and uncorrelated to the interference signal. For processing the measured data in this work, the sum of the desired signals at the two receiving antennas is taken as the reference signal, i.e.

$$z(t) = d_1(t) + d_2(t) \tag{8.13}$$

and

$$Z = E(X^* z(t)) \tag{8.14}$$

where * represents the complex conjugate operation.

In both of the algorithms defined above, an optimum weight vector is calculated for a given channel and the value of optimum weight is updated if the channel changes significantly. Thus, the covariance and correlation matrices are computed over a large portion of the channel data for which the channel is stationary. The larger the portion of channel data, the greater will be the computation time taken to calculate the covariance matrix and its inverse. This conventional solution may not give the optimum solution for the on-body channels due to the fast variation and non-stationary nature of the channels. For this reason, both the algorithms are applied at each instant of the measured data, i.e., an optimum weight vector is calculated for each sample of the data for the on-body channels under investigation. To calculate the covariance and correlation matrices in this situation, a local sliding window, constituting the previous samples, was selected. The previous local samples were selected because in real systems, the future values cannot be used. A training sequence is needed for the estimation of the channel during the first local window, whereas, the rest of the values can be estimated from the received data.

8.2.3 Interference Cancellation with Interrupted Transmission (ICIT) scheme

A simpler approach to interference rejection, which is applicable to BAN, is proposed for the two-branch diversity receiver system. It works on the principle that at a certain instance, if the amplitude and phase of the interference signal is known, the two received branch signals can be combined with such a weight vector, which can make the interference signal at one branch equal and out of phase to the interference signal at the other branch. A mechanism is thus required to measure the

phase and amplitude of the interference signals at the two receiving antennas, to reasonable accuracy, at a certain time instant. To do this, the desired signal transmitter is turned off temporarily at regular intervals, using a pre-defined algorithm. Thus, at a particular instance, *k*, when the desired signal transmitter is turned off, only the interference signal is received. The phase and amplitude of the interference signal is measured and stored. The estimated value of the interference signal is then used as an estimate to calculate the weight vector, *W*, for the forthcoming time interval until the desired signal is interrupted and turned off again. Such a signal, however, is subject to fast fading and thus should be averaged over time to achieve an accurate estimate. This leads to a larger amount of desired signal interruption, which results in throughput degradation. The larger the averaging window, the more is the throughput degradation and vice versa. Considering the model presented above, if at any time instant, *k*, the average estimated interference signal at the i^{th} branch is:

$$\bar{i}_i(k) = \left|\bar{i}_i(k)\right| < (\overline{\psi}_i(k)) \tag{8.15}$$

then the weight vector, *W*, at that instant, *k*, is calculated as:

$$W = \begin{bmatrix} 1 & \dfrac{\left|\overline{i_1}(k)\right|}{\left|\overline{i_2}(k)\right|} < (\Delta\psi) \end{bmatrix} \tag{8.16}$$

where

$$\Delta\psi = \overline{\psi}_1(k) - \overline{\psi}_2(k) + 180^{o} \tag{8.17}$$

A quick look at eq. (8.16) reveals that the weight of the first branch is 1, i.e., the signal goes unchanged. The second branch has the weight associated with it, which makes the interference at this branch equal in magnitude and 180^{o} out of phase to the interference signal at branch 1. The same value of *W* is then used for the rest of the interval until the next interruption. This way, the received signal at one antenna is scaled such that the interference signals at both the branches have equal amplitudes but are 180 degrees out of phase. The performance of the scheme depends upon the accuracy of the estimate and hence on the interruption period (time interval after which the desired transmitted signal is to be switched off). If the interruption period is too long, the estimate of the interference may be outdated and the performance will be degraded. As an upper limit, with estimation of interference signal at every instant, complete cancellation of interference can be achieved and the output SINR becomes equal to the output signal to noise ratio (SNR).

The scheme can also be represented by the simplified block diagram of the combiner shown in Fig. 8.2. At the particular time instant, *k,* when the desired signal transmitter is turned off, the processor records the phase and amplitude of the interference signals at the two branches. It then calculates the phase difference and the amplitude scaling factor, which are used to control the phase shift circuit and the variable gain amplifier (VGA) at the second branch to produce the weight vector, *W*, given in eq. (8.16).

The desired and interference signals were measured and the weight vector, *W*, was calculated for each IRC algorithm. Keeping in view eq. (8.5), the input and the output SINR for each case were calculated as [8]:

$$SINR_{in(i)}(t) = \frac{|d_i(t)|^2}{|i_i(t)|^2 + \left\langle |n_i|^2 \right\rangle} \tag{8.18}$$

$$SINR_{out}(t) = \frac{|W^T D|^2}{|W^T I|^2 + |W^T N_{rms}|^2} \tag{8.19}$$

The Cumulative Distribution Function (CDF) of the output and the branch SINR were plotted and the SINR improvement with IRC, i.e. IRG, was calculated for each case at 1% probability.

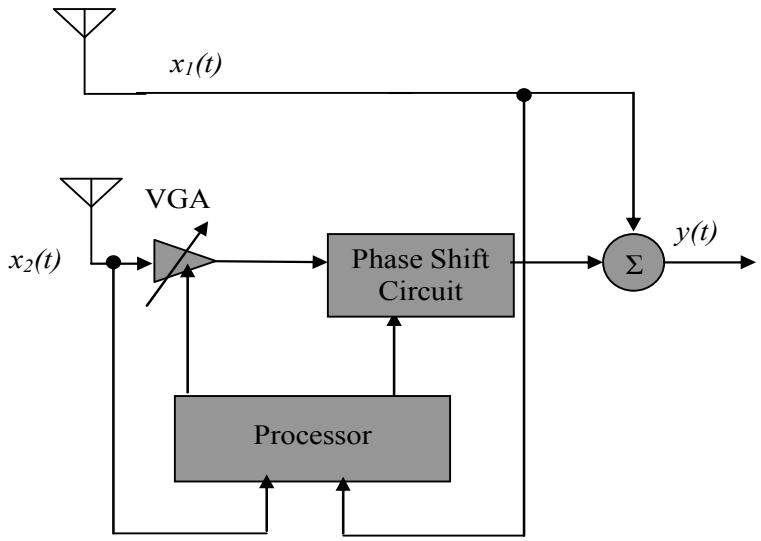

Fig 8.2: Simplified block diagram of combiner implementing the ICIT scheme

8.3 Measurement Procedure

Measurements were performed at 2.45 GHz. The receiving antenna was an array of two microstip-fed planar inverted-F antennas (PIFA) on 0.8 mm thick FR4 substrate, as shown in Fig. 8.3. The ground plane size was the same as the substrate size, which was 45 mm x 40 mm. The thickness of the radiating plate of PIFA was 1mm and the distance between the short-circuit pin and the feeding pin was 3mm. Other dimensions of the antenna are shown in Fig. 8.3. The mutual coupling between the two elements of the PIFA array was -12.5 dB. Due to the mutual coupling, the radiation efficiency of the antennas was slightly degraded. Very little detuning was observed when the antennas were mounted on the body. The return loss for all antenna ports at the desired frequency was still above 10 dB. The measured radiation patterns, showing the directivity plots, of each of the two PIFA elements, when the other element is terminated by 50 ohms, are shown in Fig. 8.4 for the xy-plane, which is the plane of interest for the on-body channels. The transmitting antenna was the single element PIFA described in Chapter 6.

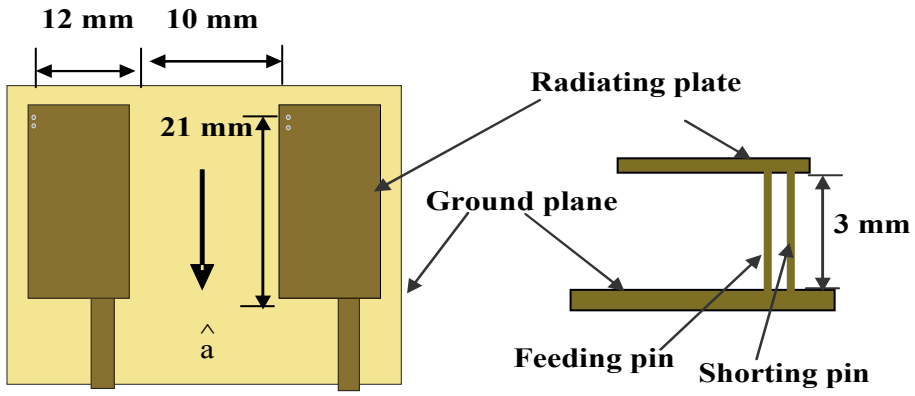

Fig 8.3: Top and side view of the PIFA array

The desired signal transmitting antenna was mounted at the belt position and the antenna transmitting the interference signal was mounted at the same position on another person's waist, as shown in Fig. 8.5. All the antennas were oriented such that vector $\hat{a}$, shown in Fig. 8.3, was pointing downwards for the transmitting antennas and upwards for the receiving array for all the three channels measured, assuming the subject standing straight. The measurement procedure is given in detail in Section 4.4.3 of Chapter 4. During the measurement, the two subjects were walking around each other in the room in a random manner. The distance between them was randomly changed during the walking within a range of about 0.1 m to 4 m.

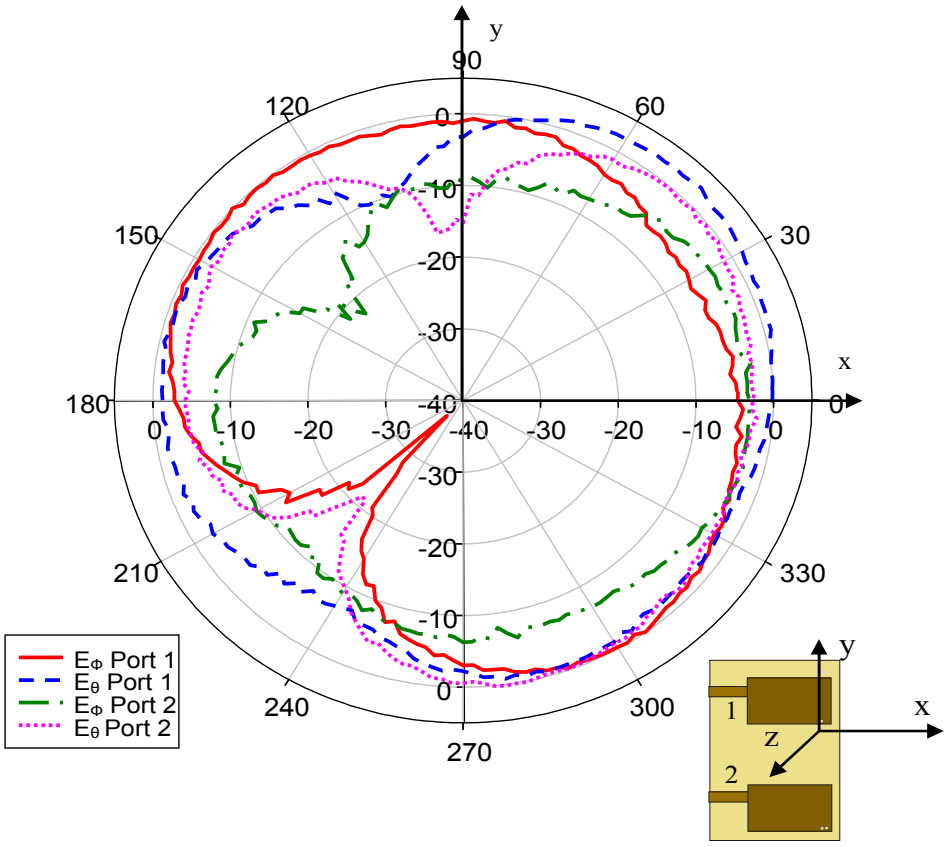

Fig 8.4: Measured radiation patterns as a function of φ of each PIFA element with the second element terminated by 50 ohms

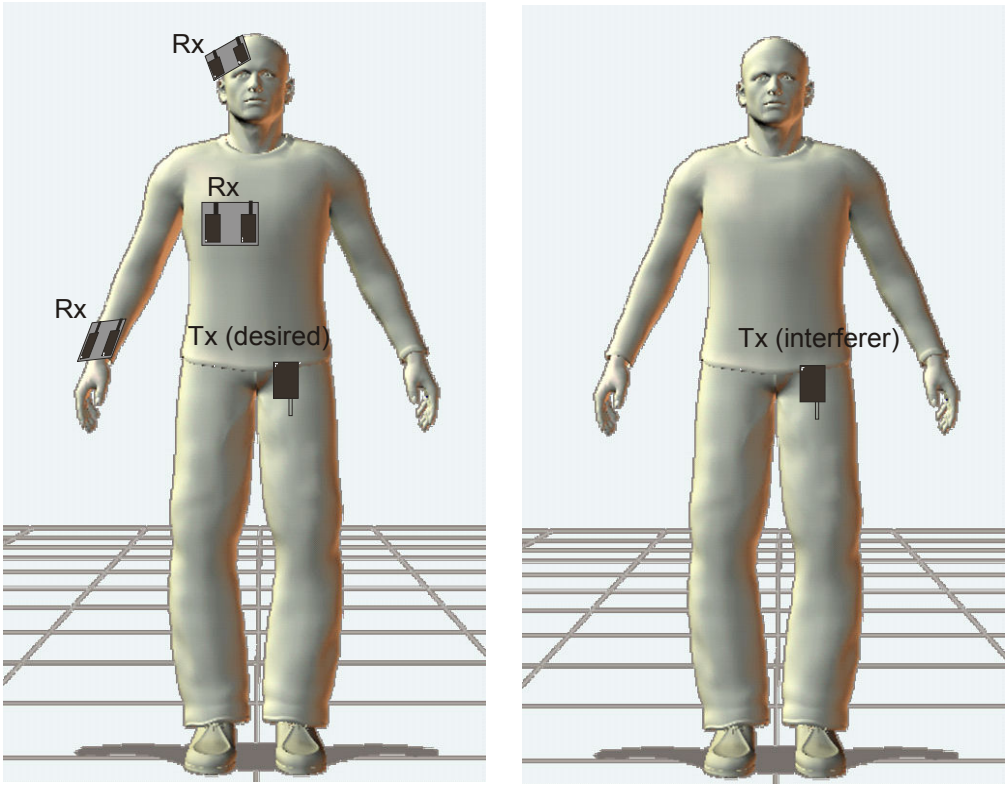

Fig 8.5: Placement of the antennas on the body. The Rx antenna array was placed at the three positions separately for the three on-body channels. Tx antenna remained at the waist position.

8.4 Results

As explained in Section 8.2, the weight vector was calculated at each instant and a local sliding window was selected to calculate the covariance and correlation matrices in case of optimum combining and Weiner-Hopf solution. Various window sizes were tried for both the algorithms and the window size giving the best IRG was used. These were 600 ms for belt-wrist and belt-head channels and 225 ms for the belt-chest channel. In the ICIT scheme, various averaging window sizes were used for the estimation of the interference signal, and the performance of the algorithm is compared. In addition, the interval period was varied to see its effect on the SINR

improvement. The IRG as a function of interval period is plotted for belt-head channel in Fig. 8.6 for various averaging window sizes. For a single instant (no averaging), the desired signal transmitter is kept shutdown for 40 μs (switching time of the switch used in the measurement). The other two channels showed similar trend. It can be noted from the figure that increasing the averaging window size does not provide any significant improvement in the IRG over the single instant estimate of the interference signal. On the other hand, averaging degrades the throughput of the system, as the desired signal is turned off for a larger amount of time. An estimate of the throughput degradation can be achieved by the ratio of the averaging window size (time for which the desired signal is kept off) to the total interval period (time until the next interruption). This degradation of the data rate with different averaging window sizes is shown in Fig. 8.7 as a function of interval period. Due to the fact that time averaging of the estimated interference signal does not provide significant improvement in the IRG but degrades the throughput of the system, an averaging window size of one instant is used for the rest of the results, as this gives negligible data rate reduction.

The IRG vs. interval period is shown in Fig. 8.8 without averaging, i.e., interference signal estimated at a single instant for the three on-body channels. It was noticed that for the belt-chest channel, the interruption interval period can be as high as about 60 ms to achieve some reasonable IRG values (around 2 dB or more). For belt-wrist and belt-head channels, the period can be increased to about 250 ms and 600 ms, respectively. Increasing the period size from the values specified for each channel, the IRG value decreases significantly and no effective improvement is observed in

the output SINR. The IRG reaches a certain minimum level (on average) upon increasing the interval length. If the IRG is sacrificed for less interruption of the desired signal, this minimum level can be used. Nevertheless, for belt-chest channel, IRG goes to negative values close to about 80 ms interval period, which signifies that the performance is worse than the system without interference rejection. The shorter duration for the belt-chest channel reveals that the interference estimate is outdated very quickly. This is because the interference signal transmitter is shadowed much strongly and more frequently due to the body shadow area by the virtue of the receiver position compared to the other channels. For consistency, an interval period of 60 ms was used for the ICIT scheme. The CDFs of the branch and output SINR were plotted for each of the three IRC algorithms and the three on-body channels, as shown in Figs. 8.9-8.11. The interference rejection gain was calculated from the CDFs at 1% probability for each case and the results are presented in Table 8.1.

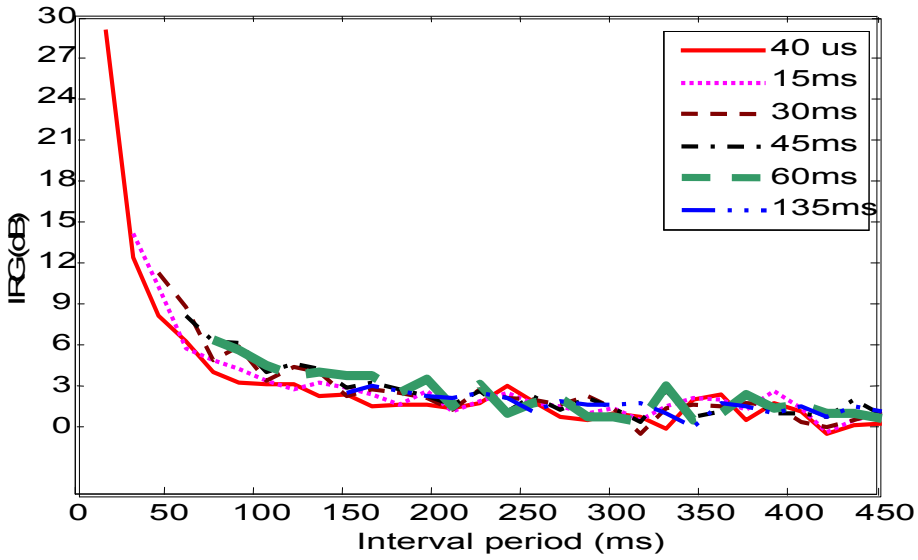

Fig. 8.6: IRG vs. interval period with various averaging window sizes for belt-head channel in the laboratory environment

TABLE 8.1

RESULTS FOR THE THREE CHANNELS

		Belt-Head	Belt-Chest	Belt-Wrist
IRG (dB)	ICIT with 60 ms interval length	6.4	1.2	4.7
	Weiner-Hopf solution	2.2	-3	2.2
	Optimum Combining	4.5	0.2	3.0
Mean power desired signal, $<\|s_1\|^2>$ (dB)		-53.7	-37.4	-48.1
Mean power desired signal, $<\|s_2\|^2>$ (dB)		-56.6	-41.3	-51.4
Mean power interference signal, $<\|i_1\|^2>$ (dB)		-54.3	-52.8	-51.9
Mean power interference signal, $<\|i_2\|^2>$ (dB)		-55.9	-53.4	-48.5
SIR_{avg} (dB)		8.13	21.8	10.9

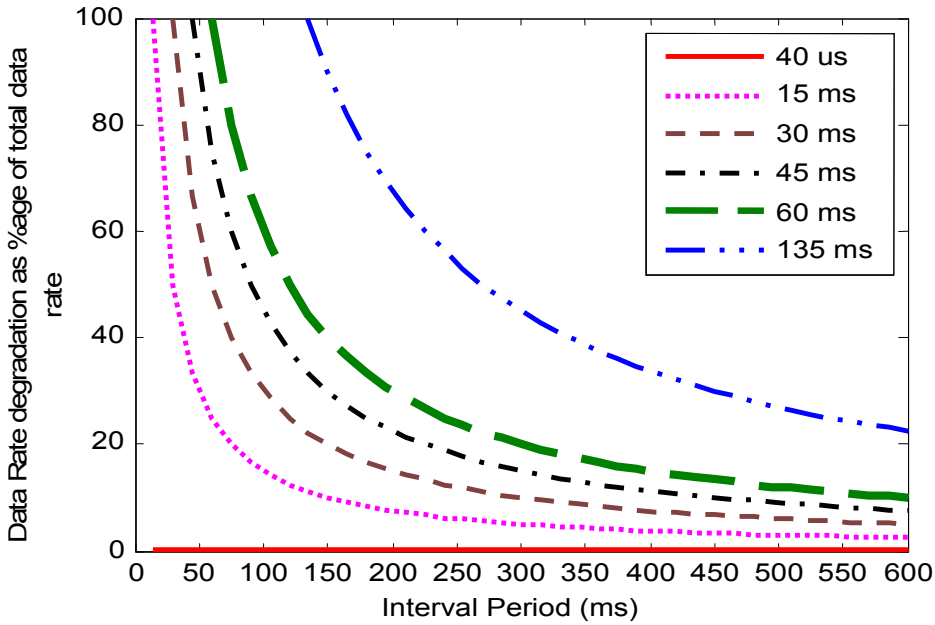

Fig 8.7: Data rate degradation as percentage of total rate vs. interval period for various averaging window sizes

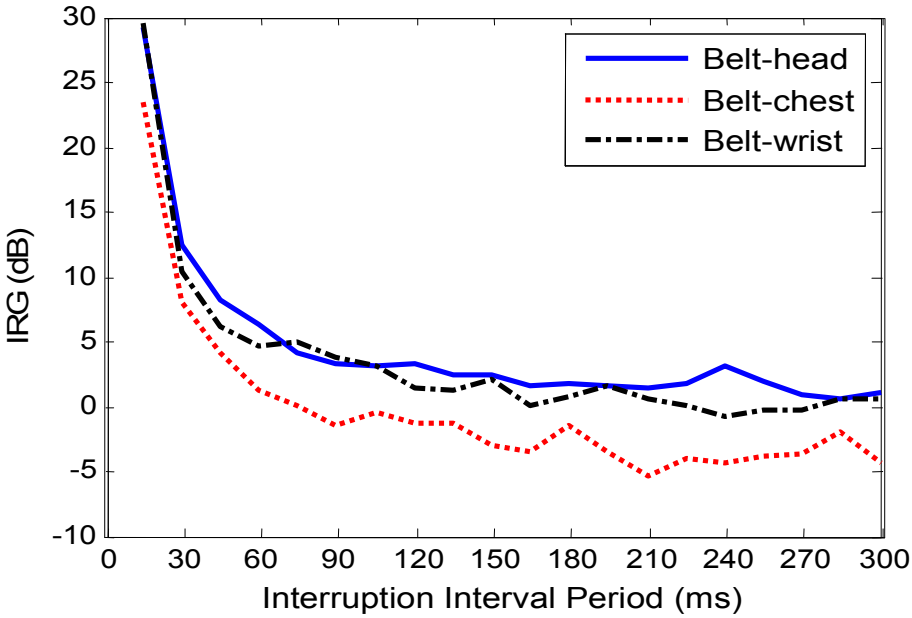

Fig. 8.8: IRG vs. interval period for ICIT with interference estimate at a single instant

It can be seen from Table 8.1 and Figs. 8.9-8.11 that WH solution does not give better interference rejection when compared to the other two schemes. The poor performance of the WH solution may be due to the fact that it relies on low correlation between the two received branch signals. The two received branch signals are correlated in the on-body communication scenario, as shown in Chapter 5 and 6 and also in [9, 10]. The belt-chest channel has the highest correlation between the two branch signals due to the line of sight (LOS) link [9, 10]. The presence of LOS is associated with a low degree of scattering and thus leading to high correlation. For the belt-chest channel, the covariance of the received signals, i.e. Φ, is high compared to the covariance of the other two channels and the weight vector will have low values, resulting in low IRG values for this channel. The other two channels show somewhat better performance compared to the belt-chest channel. The

covariance matrices (Φ) of the branch signals and the error covariance matrices (R), calculated for the whole data set in each case, are shown below for the three channels. The same is true for the optimum combining, which depends upon the covariance of the noise plus interference signals (R) at the two branches. As *R* is slightly lower than Φ, the optimum combining gives better performance than the WH solution.

Belt-Head

$$R = 10^{-4} \times \begin{bmatrix} 0.037 & 0.002 + 0.003\,i \\ 0.002 - 0.003\,i & 0.025 \end{bmatrix}$$

$$\Phi = 10^{-4} \times \begin{bmatrix} 0.078 & -0.003 + 0.003\,i \\ -0.003 - 0.003\,i & 0.048 \end{bmatrix}$$

Belt-Wrist

$$R = 10^{-4} \times \begin{bmatrix} 0.06 & 0.02 - 0.03\,i \\ 0.02 + 0.03\,i & 0.14 \end{bmatrix}$$

$$\Phi = 10^{-4} \times \begin{bmatrix} 0.21 & -0.005 - 0.004\,i \\ -0.005 + 0.004\,i & 0.22 \end{bmatrix}$$

Belt-Chest

$$R = 10^{-4} \times \begin{bmatrix} 0.05 & 0.006 + 0.007\,i \\ 0.006 - 0.007\,i & 0.045 \end{bmatrix}$$

$$\Phi = 10^{-4} \times \begin{bmatrix} 1.8 & -0.4 - 0.4\,i \\ -0.4 + 0.4\,i & 0.8 \end{bmatrix}$$

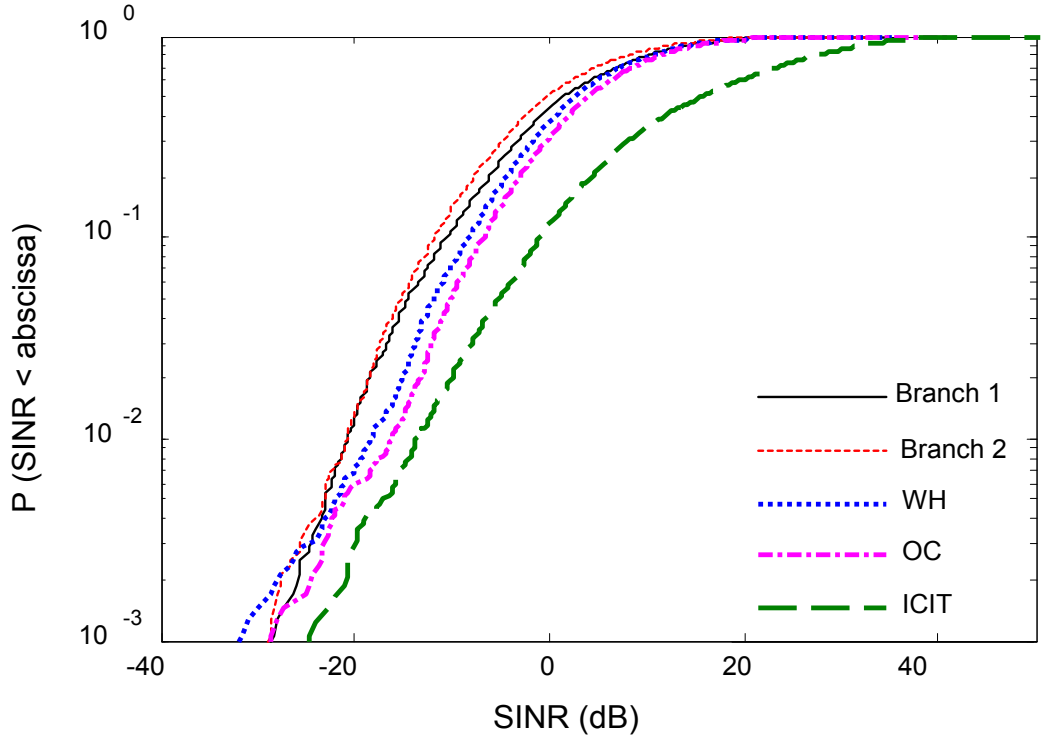

Fig. 8.9: SINR CDF plots of belt-head channel in the laboratory environment

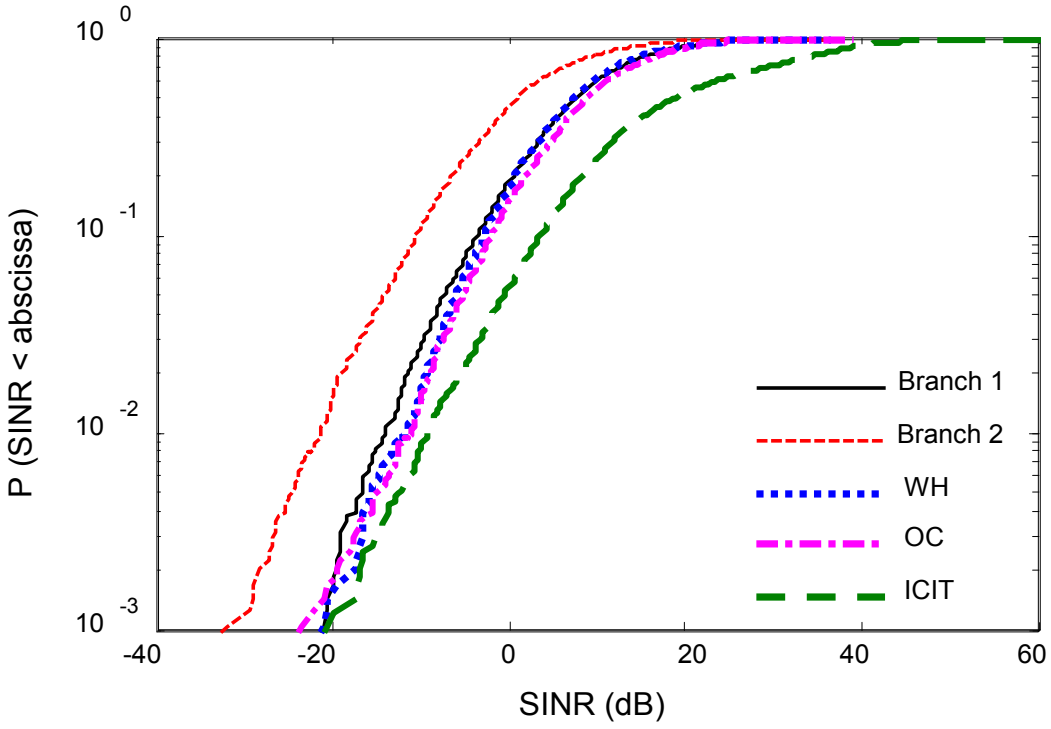

Fig. 8.10: SINR CDF plots of belt-wrist channel in the laboratory environment

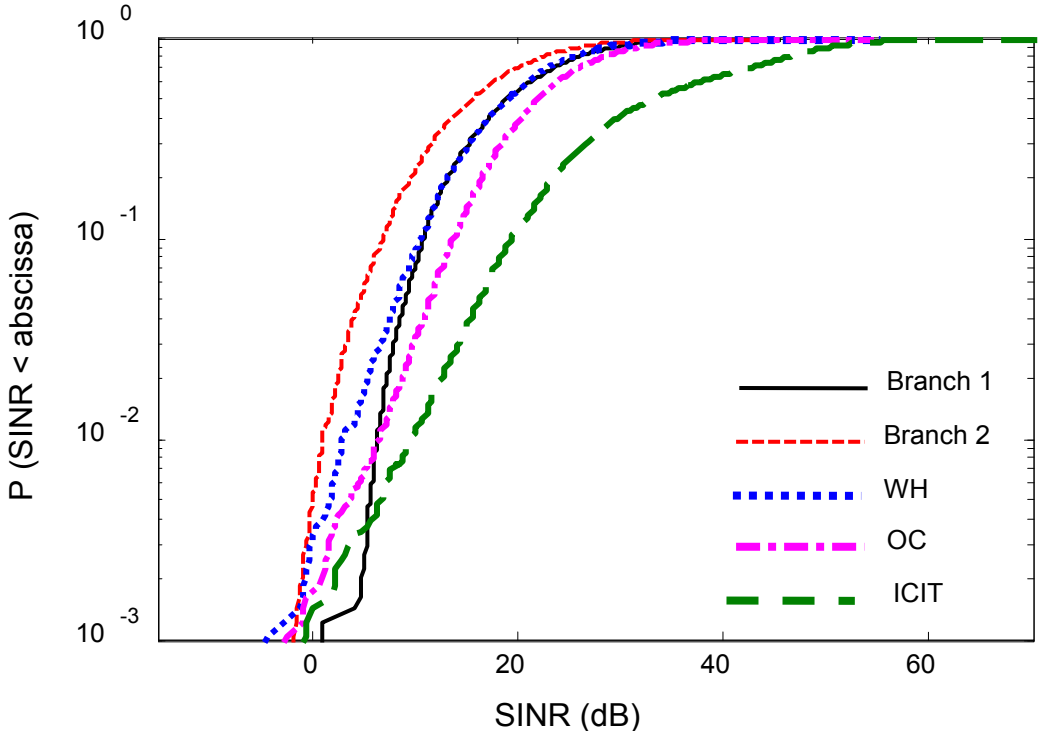

Fig. 8.11: SINR CDF plots of belt-chest channel in the laboratory environment

The comparison of the ICIT scheme with the two conventional algorithms reveal that ICIT can perform better interference rejection if a proper interval of estimation is selected. In contrast to the other two schemes, there is a handle on the performance of ICIT combiner, which is the interruption interval period. If a high level of interference rejection is desirable, the interval can be made shorter and hence, the rejection gain can be increased significantly. The drawback of ICIT is the frequent interruption of the desired signal, which can degrade the overall throughput of the system. In fact, in packet radio systems, the gap between two transmitted packets can be used to estimate the interference and the throughput degradation can be avoided. However, the disadvantage will be increased power consumption at the receiver end, as the sleep time for the receiver will be decreased and utilized in estimating the interference signal. On the other hand, ICIT provides a simple and robust solution for

interference rejection compared to the complex and expensive smart antenna techniques.

The mean desired and interference signal powers were also calculated and presented in Table 8.1. The table also contains the average "desired signal to interference ratio" (SIR_{avg}), which was calculated as given below in eq. (8.20).

$$SIR_{avg} = 10 \times \log_{10}\left(\left\langle \frac{|s_1(t)|^2 + |s_2(t)|^2}{|i_1(t)|^2 + |i_2(t)|^2} \right\rangle\right) \tag{8.20}$$

The level of interference was varied to see its effect on the performance of the IRC algorithms. In other words, the average SIR value (SIR_{avg}) was decreased gradually from a higher value to a lower value and the IRG was plotted as a function of SIR_{avg} in Fig. 8.12 for belt-head channel, as an example. The same behavior was observed for the other two channels. It is clear from the figure that IRG shows a downward trend with increasing values of average SIR (low interference signal level compared to the desired signal level) and is fairly constant with SIR_{avg} close to 0 dB. This means that the IRC algorithms work well to suppress the interference signals, which are comparable with the desired signal level. For interference levels, which are much lower than the desired signal levels, none of the algorithms gives reasonable rejection gains. It is important to note that the WH algorithm gives negative IRG values at SIR_{avg} values higher than 5 dB. For the belt-chest channel, the situation is worse with negative IRG values even for low SIR_{avg} values. This suggests that WH solution is not recommended for the on-body applications.

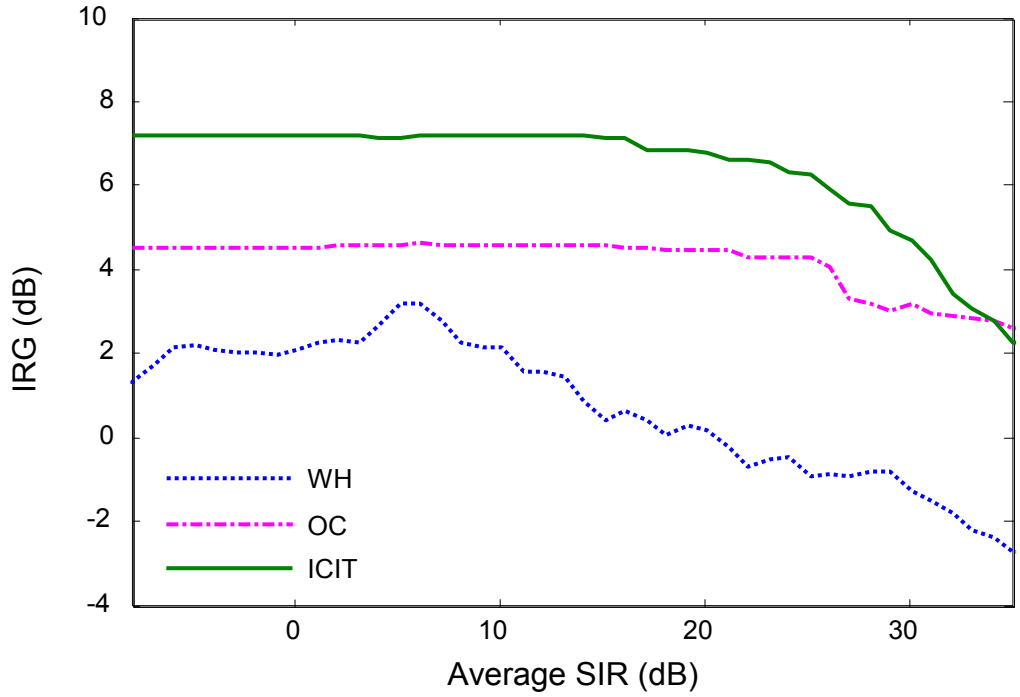

Fig. 8.12: IRG vs. Average SIR for belt-head channel with interval length for ICIT = 60 ms in the laboratory environment

Out of the three on-body channels, the belt-chest channel shows worst performance for all the three algorithms. This is due to two reasons. Firstly, due to the relatively high covariance between the branches and secondly, due to a relatively high average SIR value for the measured case, as shown in Table 8.1. Due to the short range and line-of-sight communication between the desired signal transmitter and the receiver, the level of interference is much lower than the desired signal level for most of the time. Hence, interference rejection may not be required for this channel. The other two channels showed reasonable improvement with the WH solution and the optimum combining schemes. The belt-head channel, which is the most important on-body channel for the handset-headset communication, shows much better improvement.

8.5 Conclusions

In a situation, where two BANs are operating in close proximity of each other, BAN-BAN interference can significantly disturb the performance of the systems, and interference rejection becomes an important aspect of the receiver design. Interference rejection schemes can be deployed using two-branch diversity at the receivers. The WH solution and optimum combining IRC schemes do not provide significant interference rejection for the on-body communication case, but these algorithms are still useful in keeping the interference level low and not allowing it to reach or exceed the desired signal level. The new proposed IRC algorithm, i.e. ICIT, provides a flexible way to handle the BAN-BAN interference. The performance of the ICIT scheme is greatly depended upon the interval of interruption. The belt-chest channel gives the lowest values of interference rejection gain due to the presence of strong LOS links and very high SIR values. The belt-head and belt-wrist channels show considerable improvement in output SINR with the three IRC techniques. The interference rejection gain depends upon the average SIR value at the receiving antennas. IRC works better when the SIR values are close to 0 dB, and the IRG values are almost constant for a certain range of SIR. The interference rejection gain value decreases rapidly with increasing SIR outside that range.

REFERENCES

[1] J H Winters, "Optimum Combining in Digital Mobile Radio with Co-Channel Interference", *IEEE Journal on selected areas in communications, Vol. SAC-2, No. 4, July, 1984.*

[2] R.T. Compton, “Adaptive Antennas, Concepts and Performance”, *Prentice-Hall Inc., New Jersey, 1988*.

[3] X N Tran, T Taniguchi and Y Karasawa, “Subband Adaptive Array for Multirate Multicode DS-CDMA”, *2003 IEEE Tropical Conference on Wireless comm. Tech., Honolulu, HI, October 15-17, 2003.*

[4] M L McCloud, L Scharf, M K Varanasi, “Beamforming, Diversity, and Interference Rejection for Multiuser Communication Over Fading Channels with a Receiver Antenna Array”, *IEEE Transactions on Communications, Vol. 51, No. 1, Jan 2003.*

[5] E Tiirola, J Ylitalo, “Performance of Smart Antenna Receivers in WCDMA Uplink with Spatially Coloured Interference”, *IST Mobile Communications Summit 2001, Barcelona, Spain, 9-12 Sep. 2001.*

[6] D Bladsjo, A Furuskar, S Javerbring, E Larsson, “Interference Cancellation using Antenna Diversity for EDGE-Enhanced Data Rates in GSM and TDMA/136”, *in Proc. of the 50th IEEE Vehicular Tech Conf., Fall 1999.*

[7] I Khan, Y.I. Nechayev, K. Ghanem, P.S. Hall, “BAN-BAN Interference Rejection with Multiple Antennas at the Receiver”, *submitted to IEEE Transactions on Antennas and Propagation in March 2009.*

[8] C Braun, M Nilsson, R D Murch, “Measurement of the Interference Rejection Capability of Smart Antennas on Mobile Telephones”, *IEEE Vehicular Technology Conference, 1999.*

[9] I Khan, Peter S. Hall, “Multiple Antenna Reception at 5.8 and 10 GHz for Body-Centric Wireless Communication Channels”, *IEEE Transactions on Antennas and Propagation, Vol. 57, /o.1, Jan 2009.*

[10] I Khan, P.S. Hall, A.A Serra, A.R. Guraliuc, P. Nepa, “Diversity Performance Analysis for On-body Communication Channels at 2.45 GHz”, *IEEE Transactions on Antennas and Propagation, Vol 57, /o. 4, April, 2009.*

Chapter 9

MIMO for On-body Channels

9.1 Introduction

The use of multiple antennas at the transmitter and receiver is a well known technique to increase the capacity of wireless communication systems without increasing the bandwidth. The multiple-input multiple-output (MIMO) systems have been studied extensively for the mobile and personal communication links [1, 2, 3]. The benefits of MIMO are limited by the correlation and power imbalance among the spatial sub-channels, mutual coupling between the spatially separated antennas, and the presence of a strong direct link between the transmitter (Tx) and receiver (Rx) in the line-of-sight (LOS) transmission [2, 4]. Most of the work done so far in the field of body-centric communications has concerned the on-body channel and antenna characterization. The high data rate and reliable transmission between the body-worn wireless devices and sensors, such as in military applications, sports and entertainment, and patient monitoring systems, demand the use of multiple antennas for the on-body and off-body channels to increase the channel capacity. Multiple antenna study for on-body channels has been presented so far by using multiple antennas only at the receiver side. The use of MIMO for off-body link (body to far away device) has been extensively studied but so far no significance work has been done to signify the use of MIMO for the body-worn devices. It may be due to the common perception that the on-body channels exhibit a strong LOS link and hence

MIMO may not be useful to increase the throughput. Some preliminary MIMO measurements for on-body channels have been reported in [2] as a small section in the context of personal area networks, but some detailed analysis is still needed.

It has been shown in [5] that the fading envelope for the on-body channels is Rician distributed. The capacity increase in Rician fading channels depends upon the degree of de-correlation offered by the scattering environment, i.e. the multipath richness, and also on the SNR. The body movement may change the fading distribution of the spatially separated subchannels when multiple antennas are used. For a fixed transmitted power, the presence of LOS means a high signal-to-noise ratio (SNR) at the receivers, which may increase the channel capacity compared to a non-line of sight (NLOS) link with the same configuration. On the other hand, LOS links have a low degree of scattering, which introduces a high correlation among the spatial subchannels. Thus, for a specific value of SNR, i.e. variable transmitted power, LOS can decrease the channel capacity compared to NLOS link at the same level of SNR. Hence, there is a tradeoff between the effect of increased SNR or increased correlation on the channel capacity. It has been shown in [6] that at high SNR values, the reduction in capacity due to increase in correlation is overcome by the high SNR.

This chapter presents the use of multiple antennas at both the Tx and Rx for the on-body channels by mounting 2 transmitting and 2 receiving antennas at various positions on the body, thus forming various 2 x 2 on-body channels. The experimental characterization of 2x2 MIMO channel at frequency of 2.45 GHz, for the on-body scenario with random movements in an indoor environment, is

presented. The spatial channel correlation matrices are analyzed and the effect of correlation on the capacity is discussed. The channel capacity for 2 x 2 MIMO channel is calculated and its Cumulative Distribution Function (CDF) is plotted. The channel capacities for 2 x 2 MIMO, 1 x 2 multiple-input single-output (MISO), 2 x 1 single-input multiple-output (SIMO), and 1 x 1 single-input single-output (SISO) links have been compared. The relationship between the average capacity and SNR is also shown. The variation of capacity with and without the effect of pathloss is compared with the average pathloss variation. The change of average capacity with varying K-factor is also presented. The results presented here have also been published in [7].

9.2 MIMO Channel Model

For a narrowband, single-user MIMO channel with m transmit and n receive antennas, the input-output relationship between the Tx and Rx is expressed as [1]:

$$Y = HX + N \tag{9.1}$$

where X is the [m x 1] transmitted vector, Y is the [n x 1] received vector, N is receive additive white Gaussian noise (AWGN) vector, and H is the n x m channel matrix. For a 2x2 MIMO channel, H can be written as [1]:

$$H = \begin{bmatrix} h_{11} & h_{12} \\ h_{21} & h_{22} \end{bmatrix} \tag{9.2}$$

where h_{ij} is the complex random variable representing the channel fading coefficients or the complex subchannel gains from transmitting antenna *j* to receiving antenna *i,* as shown in Fig. 9.1. The *H* matrix was constructed by measuring the actual complex subchannel transfer gains h_{ij}. The Tx and Rx antenna arrays mounted on the human body, as shown in Fig. 9.1, are surrounded by local scatterers in the form of moving body and also distant scatterers in the environment. The *H* matrix, representing the measured channel, includes the effect of mutual coupling between the antenna elements and the correlation among the subchannels, as the subchannel gains were measured at the actual antenna ports with antenna elements placed next to each other. If the channel is completely unknown at the transmitter, i.e., channel state information (CSI) is not available at the transmitter, the channel capacity can be expressed by eq. (3.18) and recalled below as eq. (9.3), assuming transmitted power to be uniformly distributed among the *m* transmitting antennas [1,8]:

$$C = \log_2\left(\det\left[I_n + \frac{\xi}{m} H_n H_n'\right]\right) \quad \text{bps/Hz} \tag{9.3}$$

where I_n is *n* x *n* identity matrix and ξ is the average signal-to-noise ratio per receive antenna. Here, H_n is the normalized channel matrix and *(.)'* represents the complex conjugate transpose. Eq. (9.3) is used for the case when $n<m$. For $n \geq m$, the term $H_n H_n'$ is replaced by $H_n' H_n$ and identity matrix I_n is replaced by I_m [9, 10]. The normalization assures that the average receive power per element of the channel matrix is 1, and is usually done by two methods. In the first method, the *H* matrix is normalized such that at each instance or each realization [11, 12]:

$$\left\| H_n \right\|_F^2 = nm \tag{9.4}$$

where $\|.\|_F$ represents the Frobenius Norm. However, this normalization removes any power variation along the measurement path and thus the changes in the pathloss with time are not included. This normalization is used for scenario, where the transmitted power compensates for the total received power variation to keep the average SNR per receiver antenna fixed for each realization of the channel, irrespective of path loss. This method is useful to investigate the multipath richness of the environment [11, 12]. The second method of normalization assumes a fixed transmitted power and hence the average SNR at the receiver for each realization of the channel changes with variation in pathloss [12]. This normalization is done such that the average Frobenius Norm (averaged over all instances) of H_n is [1, 8, 11]:

$$\left\langle \left\| H_n \right\|_F^2 \right\rangle = nm \tag{9.5}$$

where <.> represents the averaging over all the instances. Thus, all the instances of the H matrix are normalized to a single constant and path loss changes remain intact. The capacity calculated by eq. (9.3) is a random quantity and can be represented by plotting its CDF. The outage capacity can be calculated from these CDF curves at a certain probability. In an ideal channel model, the subchannels of the MIMO channel are assumed to be independent and identically distributed (iid) with Rayleigh distribution of the envelopes and hence perfectly uncorrelated. However, in practical systems, and especially in LOS scenario, the subchannels are correlated.

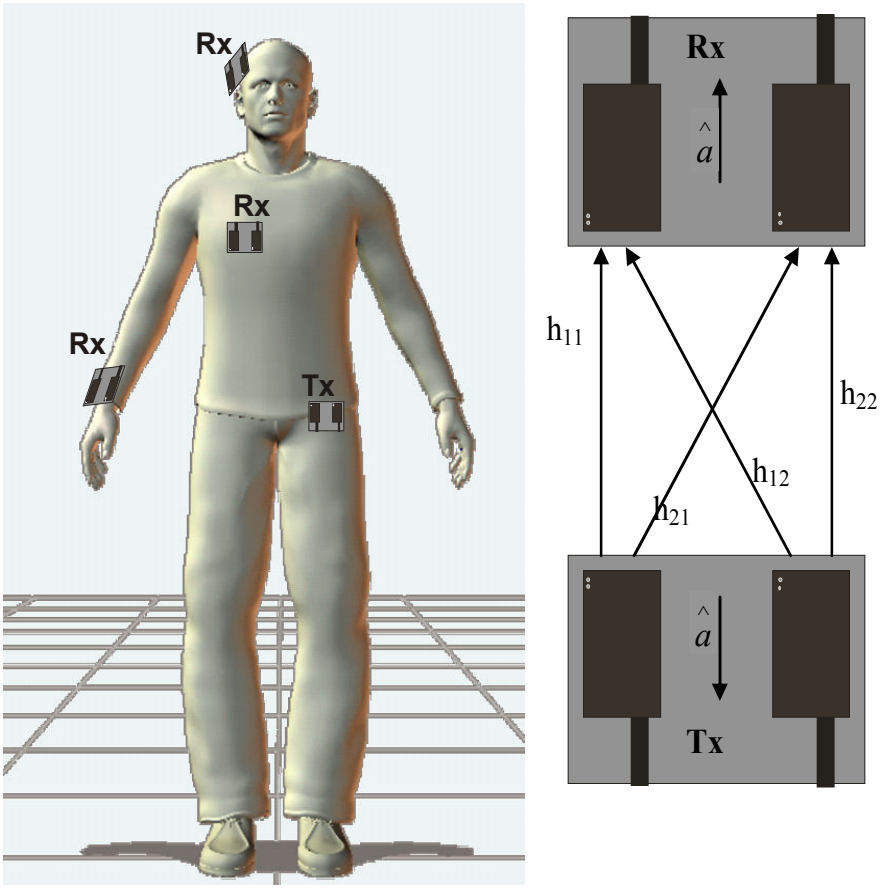

Fig 9.1: Placement of the antennas on the body, and the MIMO channel. The Rx antenna array was placed at the three positions separately for the three on-body channels. Tx antenna remained at the waist position.

The complex signal correlation coefficients (ρ_s) and the power correlation coefficients (ρ_p) among the subchannels were calculated using eqs. (3.10) and (3.11), respectively. The complex correlation coefficients are useful in system modeling and characterizing the channel, while the power correlation coefficients give good insight into the correlated power and are useful for measured MIMO channel analysis. The spatial correlation matrix, consisting of the correlation coefficients among the subchannels of the MIMO system, gives a comprehensive view of the degree of

correlation among the subchannel. The spatial correlation matrix, ρ, for the 2x2 MIMO channel can be constructed using ρ_p or ρ_s [13] as:

$$\rho = \begin{bmatrix} 1 & \rho_{11}^{12} & \rho_{11}^{21} & \rho_{11}^{22} \\ \rho_{12}^{11} & 1 & \rho_{12}^{21} & \rho_{12}^{22} \\ \rho_{21}^{11} & \rho_{21}^{12} & 1 & \rho_{21}^{22} \\ \rho_{22}^{11} & \rho_{22}^{12} & \rho_{22}^{21} & 1 \end{bmatrix} \tag{9.6}$$

where ρ_{ab}^{cd} is the correlation coefficient between subchannel h_{ab} and h_{cd}. The symmetry $\rho_{ab}^{cd} = \rho_{cd}^{ab\,*}$ reduces the total number of significant coefficients to 6.

9.3 Measurement Procedure

To characterize 2 x 2 narrowband MIMO channels for the on-body wireless links, measurements were performed at frequency of 2.45 GHz ISM band using an array of two microstip-fed planar inverted-F antennas (PIFA) on 0.8 mm thick FR4 substrate, described in Chapter 8, at both transmitter and receiver locations. Three on-body channels, i.e., belt-head, belt-wrist, and belt-chest, were selected for the measurement, as depicted in Fig. 9.1. The transmitter and receiver arrays were oriented such that vector $\hat{a}$ in Fig. 9.1 was pointing downwards for transmitting array and upwards for receiving array for all the three channels measured, assuming the subject standing straight. The measurement setup, description of the environment and on-body channels, and the movements done are given in Chapter 4. To recall from Chapter 4, a total of 4800 instances of the 2 x 2 MIMO channel matrix with

four subchannels were constructed. Apart from the 2x2 MIMO measurements, some 2x1, 1x2, and 1x1 measurements, with *n* x *m* representing *n* Rx and *m* Tx antennas, were also carried out separately and the channel capacity results are compared.

9.4 Results

9.4.1 Spatial correlation matrices

The presence of a strong ray introduces strong correlation among the subchannels [3-4]. The belt-chest channel is a good example of this, for which the direct ray is much stronger than the multipath components and hence the subchannels are highly correlated. A high correlation among the MIMO subchannels reduces the throughput gain and thus less improvement in the channel capacity is observed [4, 13]. The complex signal and power envelope correlation coefficients among the subchannels of the 2x2 on-body MIMO channels were calculated and the spatial correlation matrices, as described in eq. (9.6), were constructed for each on-body channel. The spatial correlation matrices are given below for each channel in Table 9.1.

Referring to eq. (9.6), the correlation between the two transmitting signals is ρ_{11}^{12} at receiving antenna 1, and is ρ_{21}^{22} at receiving antenna 2. It is clear from the matrices given above that the correlation between the two transmitting signals is high for all the cases. This may be due to the absence of local scatterers in the near vicinity of the transmitting antennas, as the transmitting array was mounted on the waist position and there was less movement of the hands and other body parts near it to cause any significant local scattering.

TABLE 9.1

SPATIAL CORRELATION MATRICES (a) WITH COMPLEX SIGNAL CORRELATION COEFFICIENTS (b) WITH POWER CORRELATION COEFFICIENTS

(a) Complex signal correlation coefficients	
Channel	Spatial correlation matrix
Belt-Head	$\begin{bmatrix} 1 & 0.67 + 0.39i & 0.31 - 0.27i & 0.27 - 0.02i \\ 0.67 - 0.39i & 1 & 0.13 - 0.36i & 0.17 - 0.24i \\ 0.31 + 0.27i & 0.13 + 0.36i & 1 & 0.56 + 0.33i \\ 0.27 + 0.02i & 0.17 + 0.24i & 0.56 - 0.33i & 1 \end{bmatrix}$
Belt-Chest	$\begin{bmatrix} 1 & 0.92 + 0.22i & 0.14 - 0.63i & 0.23 - 0.54i \\ 0.92 - 0.22i & 1 & 0.00 - 0.60i & 0.12 - 0.61i \\ 0.14 + 0.63i & 0.00 + 0.60i & 1 & 0.88 + 0.19i \\ 0.23 + 0.54i & 0.12 + 0.61i & 0.88 - 0.19i & 1 \end{bmatrix}$
Belt-Wrist	$\begin{bmatrix} 1 & 0.78 - 0.01i & -0.26 + 0.08i & -0.24 + 0.10i \\ 0.78 + 0.01i & 1 & -0.13 + 0.01i & -0.23 + 0.11i \\ -0.26 - 0.08i & -0.13 - 0.01i & 1 & 0.81 + 0.22i \\ -0.24 - 0.10i & -0.23 - 0.11i & 0.81 - 0.22i & 1 \end{bmatrix}$
(b) Power correlation coefficients	
Channel	Spatial correlation matrix
Belt-Head	$\begin{bmatrix} 1 & 0.71 & 0.44 & 0.32 \\ 0.71 & 1 & 0.27 & 0.21 \\ 0.44 & 0.27 & 1 & 0.70 \\ 0.32 & 0.21 & 0.70 & 1 \end{bmatrix}$
Belt-Chest	$\begin{bmatrix} 1 & 0.69 & 0.82 & 0.56 \\ 0.69 & 1 & 0.44 & 0.69 \\ 0.82 & 0.44 & 1 & 0.59 \\ 0.56 & 0.69 & 0.59 & 1 \end{bmatrix}$
Belt-Wrist	$\begin{bmatrix} 1 & 0.73 & 0.06 & 0.02 \\ 0.73 & 1 & 0.05 & 0.04 \\ 0.06 & 0.05 & 1 & 0.96 \\ 0.02 & 0.04 & 0.96 & 1 \end{bmatrix}$

Similarly, the correlation between the received signals at the two receiving antennas is ρ_{11}^{21}, assuming the signal transmitted from transmitting antenna 1, and is ρ_{22}^{12} with signal transmitted from transmitting antenna 2. These values are low for all the cases except the belt-chest channel, which is more static channel compared to the other two. Also, the LOS component is much stronger and is occasionally shadowed by the movement of hands. The positioning of the receiving antennas at the body for other two channels is such that the antennas are surrounded by large number of local scatterers in the form of moving body parts. These channels also involve rapid movement of the receiving antennas in the environment as well as with respect to the Tx, thus high degree of scattering results in lower correlation. This low correlation shows that the body movement and the relative movement of Tx and Rx antennas de-correlate the subchannels significantly. The same sort of result is reported in [14, 15], where the correlation between the received diversity branch signals is quite low, resulting in high diversity gains.

The coefficients ρ_{22}^{11} and ρ_{21}^{12} are the correlation coefficients between the subchannels that do not share any antenna. It is clear from the matrices that the correlation among these subchannels is very low apart from belt-chest channel, in which it is moderate. In general, correlation among the subchannels for the three on-body channels is not significantly high, apart from the belt-chest channel.

9.4.2 Channel Capacity

MIMO channel capacities were calculated using eq. (9.3) for the three on-body channels. The second technique, using eq. (9.5), was used to normalize the *H* matrix for each channel, as the transmitted power for these channels was fixed and movement of the body introduced body shadowing which had to be kept intact while calculating the capacity. The CDF plots of the channel capacity at various values of average receive SNR, ξ, are shown in Fig. 9.2, 9.3, and 9.4 for the belt-wrist, belt-head, and belt-chest channels, respectively, by thin lines. The figures also show the CDFs of channel capacity for other configurations, i.e., MISO, SIMO, and SISO, at ξ = 25 dB, which are represented by thick lines. It can be observed that the 2x2 MIMO outage capacities, at the same probability level, are almost similar for the three channels at the lower SNR values. At the higher SNR values, there is slight difference, but this difference is not significant for belt-head and belt-wrist channels, whereas, the capacity for belt-chest channel is comparatively lower. This is due to the higher correlation among the subchannels of the belt-chest link. At low SNR level, the direct ray is not strong enough to produce significant difference in the correlation, and even becomes weaker while propagating along the surface of the body in the form of creeping waves [16 (pp. 47)], thus the three channels behave almost similar because the multipath signals are dominant. In the high SNR regime, the direct ray is much stronger and the channels with more dominant direct ray, like belt-chest, as depicted by the high K-factor values shown in Chapter 7, are significantly affected by the correlation among the subchannels. It can also be noted that the slope of the curves for the belt-chest channels are steeper than that of the other two channels, showing less spread in the capacity. This can be explained by

less variation of the pathloss for the belt-chest channel, as the antennas are fixed with respect to each other and the path length changes only in few postures.

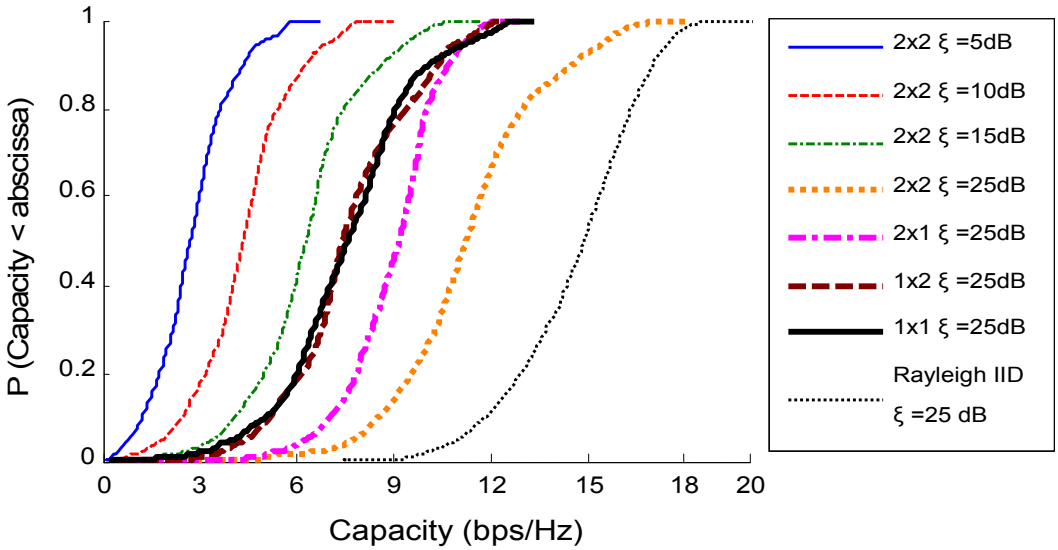

Fig. 9.2: Capacity CDF plots of the belt-wrist channel in the laboratory environment

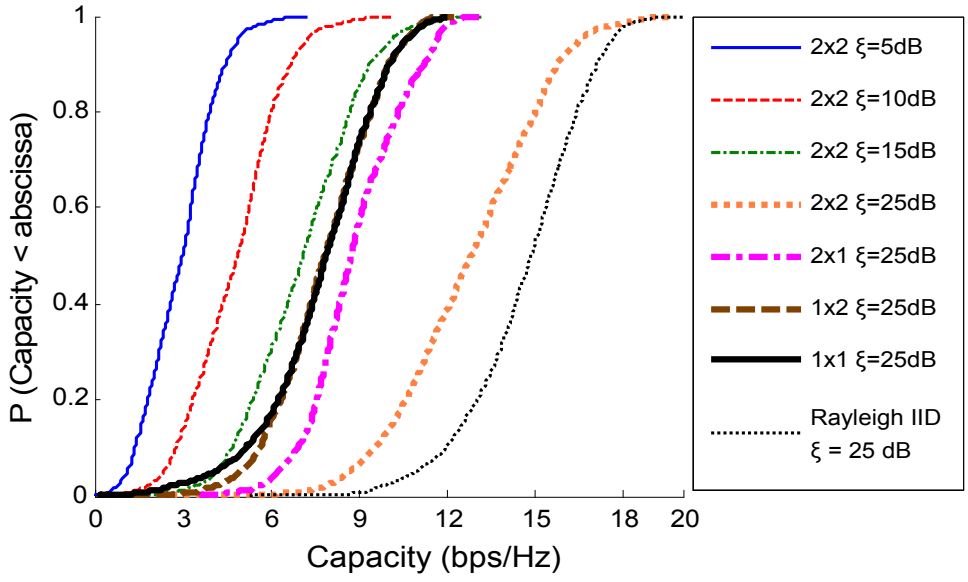

Fig. 9.3: Capacity CDF plots of the belt-head channel in the laboratory environment

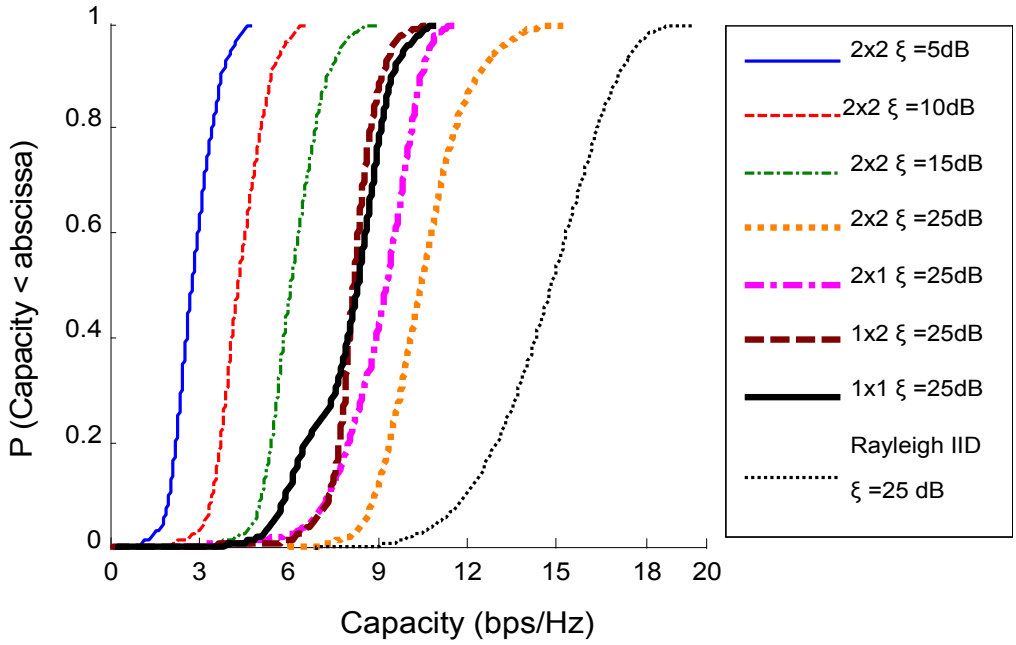

Fig. 9.4: Capacity CDF plots of the belt-chest channel in the laboratory environment

Despite the strong correlation among the sub-channels and the presence of a strong direct link due to LOS for the belt-chest channel, the improvement in capacity offered by MIMO over the same channel with SISO, MISO, and SIMO links, is noticeable. The capacity improvement may be due to a number of factors. The most dominant is the multipath richness of the environment. Although there is strong LOS, the direct ray due to the creeping wave is attenuated while propagating on the surface of the body. This fact and the presence of rich scattering environment mean that the Rician K-factor is not as high as expected [14, 15]. The other reason may be due to the fact that the communication is short range, and the assumption of planar wave-front may not be valid. This means that the spherical wave-front is being exploited to achieve high capacities, as explained in [2]. Thirdly, it has been shown in [6] that at higher SNR values, there is less decrease in capacity due to high correlation.

By comparing the capacity of the 2x2 MIMO channel with corresponding SISO channel capacity, the throughput gain can be calculated. This gain reflects the amount of improvement offered by MIMO over SISO. For an ideal, *n x n* MIMO channel, this gain is approximately *n,* i.e., SISO capacity is increased by *n* times for a fixed SNR level [1]. It is clear from the figures that the throughput gain for all the on-body channels is less than 2 due to some degree of correlation between the subchannels, with lowest values for the belt-chest channel. The MISO system offers effectively no improvement in the capacity over the SISO system. This may be justified by the very high correlation between the transmitting signals, as discussed above. In addition, it has been shown in [17] that MISO systems are not as good as SIMO and MIMO systems in throughput gain. SIMO offers an improvement due to low correlation between the signals at the two receiving antennas.

Besides the outage capacity, the average capacity for all the random movements was calculated by averaging *C* obtained from eq. (9.3) for each on-body channel. The variation of average capacity with SNR (in dB) is shown in Fig. 9.5 for the three channels. It is clear from the figure that for all the three channels, the average capacity increase with each 3 dB increase in SNR is less than 2 bps/Hz, compared to [1], where it has been shown that in the high SNR regime, the increase in capacity with every 3 dB increase in SNR for independent *n* x *m* MIMO system is *min*(*n,m)* bps/Hz. In general, the values are not too far away from 2 bps/Hz for belt-head and belt-wrist channels, where the correlation is comparatively low.

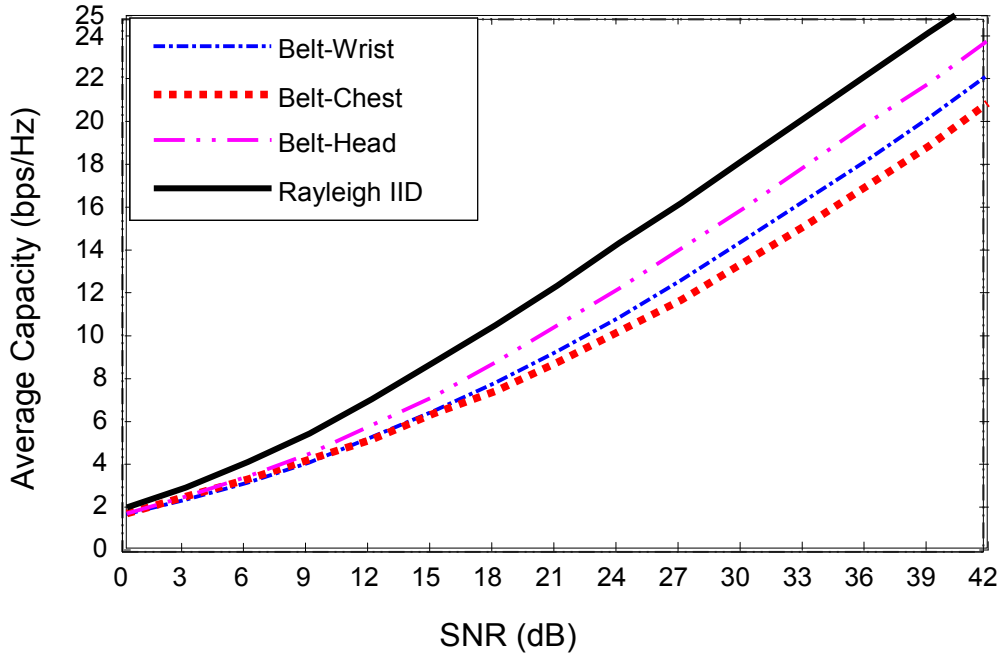

Fig. 9.5: Average capacity vs. SNR in the laboratory environment

9.4.3 Comparison of channel capacity with different normalization methods

It is also important to find out the capacity without the pathloss effect, which is only due to the multipath richness. To see the difference between the two normalization techniques (with and without the path loss), some results are presented with the first type of normalization, i.e., normalizing *H* matrix using eq. (9.4). An SNR level of 15 dB was selected for this purpose. The CDF of the capacities without pathloss at SNR level of 15 dB are shown in Fig. 9.6. Comparison with figures 9.2, 9.3, and 9.4 shows that the capacities with and without the pathloss are almost similar at high outage. At low outage, the capacity without pathloss effect is slightly higher than the capacity calculated with pathloss included. It was also noted that the average capacity is slightly higher with this second normalization, but the difference was very

small. As the difference in capacity is not high, it can be concluded that the multipath richness of the environment is a significant factor in the capacity improvement.

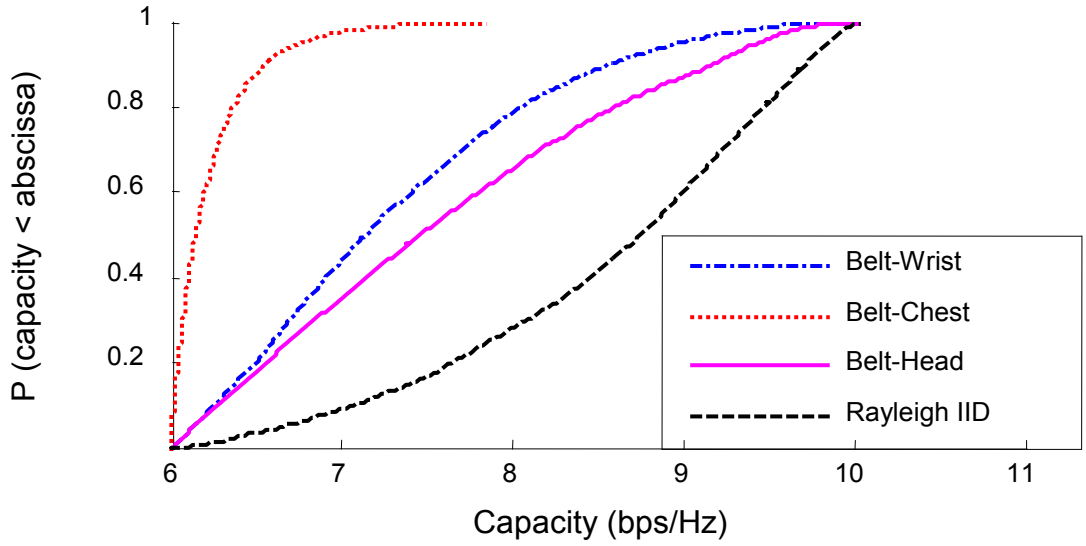

Fig. 9.6: Capacity CDF plots, with Path loss normalized, at ξ = 15dB for the three channels in the laboratory environment

Fig. 9.7 shows the capacity with the two types of normalization, i.e., with and without the pathloss effect, and its comparison with the average pathloss for equivalent SISO link (P_L), for a small portion of the data for one of the on-body channels as an example. The other two channels showed the same behavior. P_L was calculated as defined in [3-4]:

$$P_L = \left| 10 \log_{10} \left(\frac{1}{nm} \sum_{i=1}^{n} \sum_{j=1}^{m} |h_{ij}|^2 \right) \right| \tag{9.7}$$

The capacity with pathloss included (Fig. 9.7b) has a downward trend with increase in the average pathloss (Fig. 9.7a), which shows that the capacity relies heavily on the SNR at the receiving antennas in this case, provided that the multipath environment is not changing significantly [3]. At any particular instant, an increase in pathloss means lower received power or decrease in the receiver SNR, and hence the capacity decreases at that instance or realization. The capacity with pathloss normalized (Fig. 9.7c) shows the opposite trend. It increases with increase in pathloss or decrease in SNR at any particular realization, and vice versa, with less spread and faster variation. The SNR would decrease with obstruction of the direct ray or shadowing due to the moving body parts, which would increase the scattering and hence the multipath richness, resulting in an increase in the capacity at that instant. Similar comparison of capacity variations with the two normalizations are shown for a mobile indoor scenario in [11].

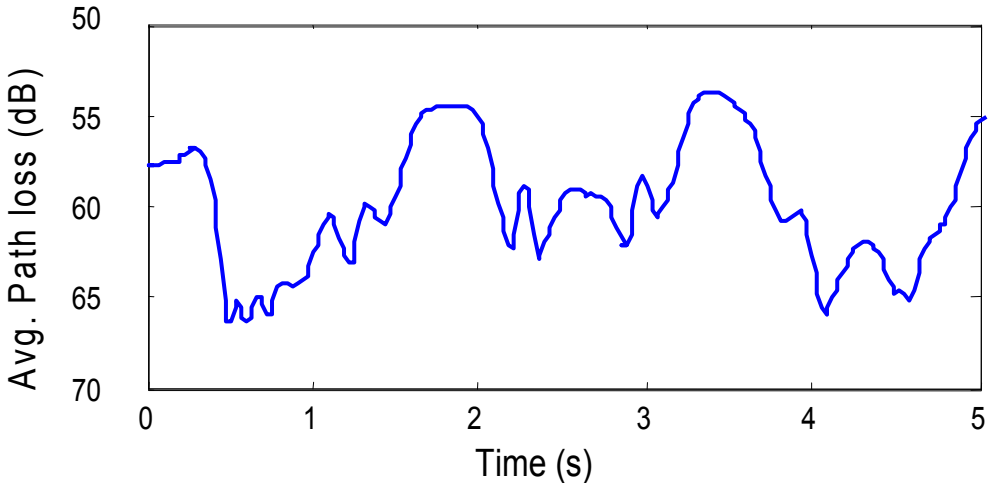

(a) Average Path Loss (P_L)

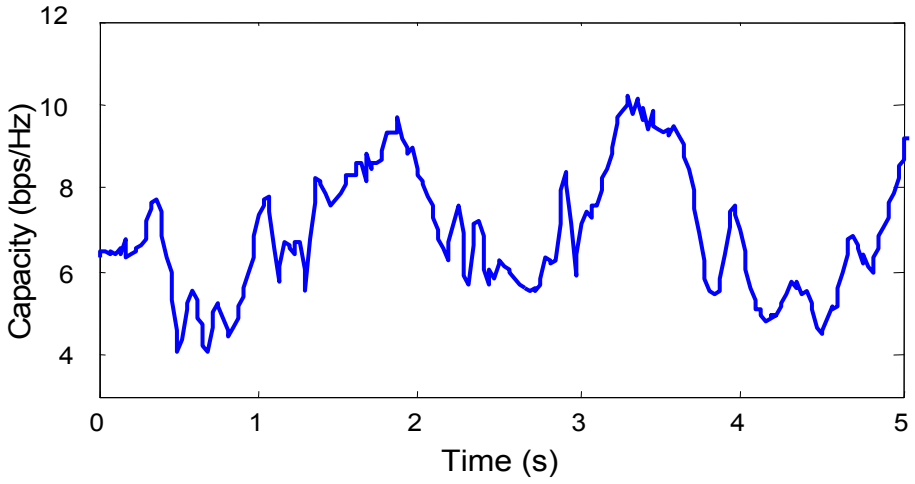

(b) Capacity with the P_L

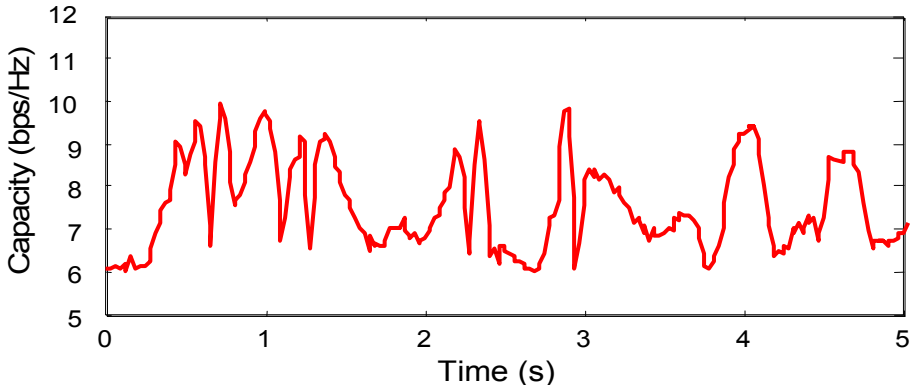

(c) Capacity with P_L normalized

Fig. 9.7: Variation of capacity with the two normalizations of the channel matrix and the average path loss (P_L) for the belt-head channel at ξ = 15 dB in the laboratory environment

9.4.4 Effect of Rician K-factor on channel capacity

Lastly, the effect of Rician K-factor on the average capacity was studied by plotting the average capacity against the Rician K-factor for several portions of the measured channel data. The K-factor was calculated from the measured data using the moment method presented in [18]. The K-factor was calculated for each subchannel and then averaged for the four subchannels to obtain an average K-factor for the 2x2 MIMO

channel. As explained above, the measurement involved various movements, which contained postures with perfect LOS, obstructed LOS, and varying path lengths. Thus, the K-factor for the different portions of the data set was varying.

The estimated K-factor and the corresponding calculated average capacity are plotted in Figs. 9.8-9.10 as a scatter plot for the three channels. It has been reported in [3, 19] that the capacity has a downward trend with increasing K-factor. At a fixed SNR level, higher K-factor means more spatial correlation and hence a decrease in capacity. The correlation coefficients between the K-factor value and the corresponding capacity were -0.022, -0.18, -0.009, for belt-chest, belt-head, and belt-wrist channels, respectively. The negative correlation coefficient suggests that the capacity has an opposite trend to that of the K-factor. However, the correlation is very low, which may suggest less dependence of the average capacity on the K-factor.

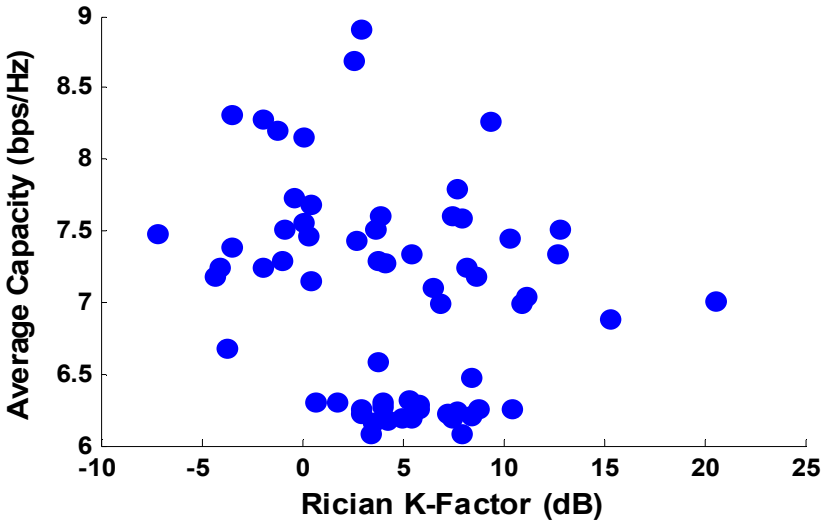

Fig. 9.8: Variation of capacity with Rician K-factor for the belt-chest channel at ξ = 15 dB in the laboratory environment

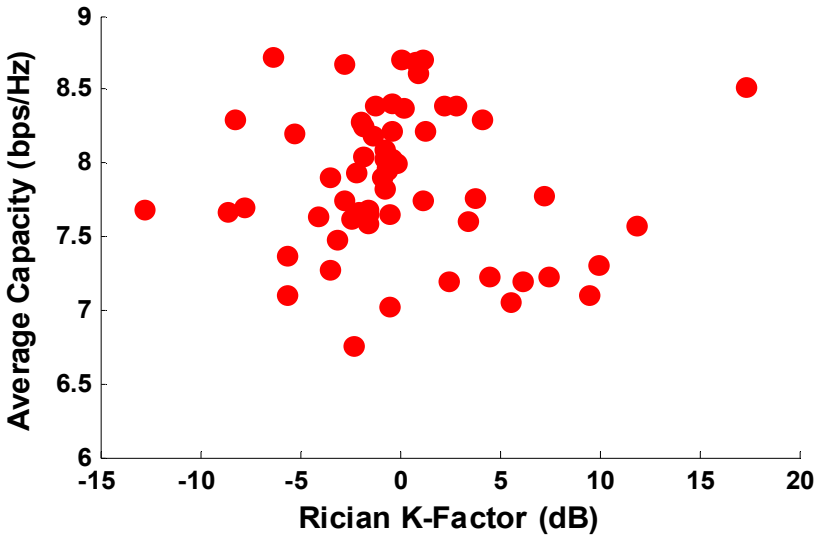

Fig. 9.9: Variation of capacity with Rician K-factor for the belt-head channel at ξ = 15 dB in the laboratory environment

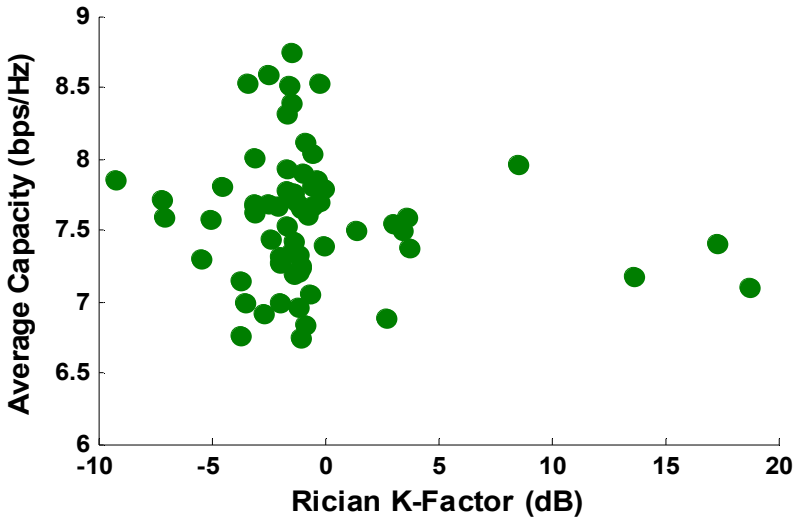

Fig. 9.10: Variation of capacity with Rician K-factor for the belt-wrist channel at ξ = 15 dB in the laboratory environment

9.5 Conclusions

The significance of using narrowband MIMO for body-centric wireless communication channels has been shown through measurements, in an indoor environment, for a 2x2 MIMO link on three on-body channels with practical PIFA antennas mountable on the body at frequency of 2.45 GHz. The MIMO channels were characterized by the correlation among the subchannels and the spatial correlation matrices were derived for the three channels. The analysis of the spatial correlation matrices shows that the movement of the body and the antenna in the environment produces sufficient de-correlation among the subchannels despite the presence of LOS link. The transmitting signals are highly correlated due to less local scatterers around the transmitting antennas, whereas, the received signals at the two receiving antennas have very low correlation, as the fading for the two signals is more or less independent due to the presence of scatterers in the close proximity of the receiving antennas. The channel capacity improvement with MIMO over the SISO is considerably high and capacity gains close to a maximum gain of 2 were observed for some channels. The belt-chest channel does not provide high capacity gains due to high correlation among the subchannels. As the creeping wave propagating along the surface of the body is attenuated rapidly, the multipath components play a significant role in the capacity increase. The MISO system does not provide any improvement in channel capacity due to high correlation among the transmitted signals by the virtue of the location of transmitting array. A SIMO system provides some improvement in channel capacity but less than MIMO.

REFERENCES

[1] E Biglier, R Calderbank, A Constantnides, A Goldsmith, A Paulraj, H. V Poor, " MIMO Wireless Communications", *Cambridge Uni. Press, New York, 2007.*

[2] D Neirynck, C. Williams, A Nix, M. Beach, "Exploiting Multiple-Input Multiple-Output in the Personal Sphere", *IET Microwaves, Antennas and Propagations, Vol. 1, No. 6, Dec. 2007.*

[3] H Ozcelik, M. Herdin, R. Prestros, E Bonek, "How MIMO Capacity is Linked with Single Element Fading Statistics*", International Conference on Electromagnetics in Advanced Applications, Torino, Italy, 8-12 Sep. 2003, pp. 775-778.*

[4] L Garcia, N Jalden, B Lindmark, P Zetterberg, L Haro, "Measurements of MIMO Indoor Channels at 1800 MHz with Multiple Indoor and Outdoor Base Stations", *EURASIP Journal on Wireless comms and Networking, Vol. 2007, Article ID 28073*.

[5] I. Khan, YI. Nechayev, P S. Hall, "On-Body Diversity Channel Characterization", *IEEE Transaction on Antennas and Propagations, 2009, in press.*

[6] K Sakaguchi, HY Chua, K Araki, "MIMO Channel Capacity in an Indoor Line-of-Sight Environment*", IEICE Transactions on Comm. Vol. E88-B, No. 7, July 2005.*

[7] I. Khan, P S. Hall, "Experimental Evaluation of MIMO Capacity and Correlation for Narrowband Body-centric Wireless Channels", *IEEE Transaction on Antennas and Propagations, 2009, in press.*

[8] GJ Foschini, MJ Gans, "On Limits of Wireless Communications in Fading Environment When Using Multiple Antennas", *Wireless Personal Communications 6: pp 311-335, March 1998.*

[9] I Hen, "MIMO Architecture for Wireless Communication", *Intel Technology Journal, Vol. 10, Issue 2, May 2006.*

[10] B Vucetic, J Yuan, "Space Time Coding", *pp. 7-9, John Wiley & Sons, 2003.*

[11] T Svantesson, J Wallace, "On Signal Strength and Multipath Richness in Multi-Input Multi-Output Systems", *IEEE International Conference on Communications, Vol. 4 , pp. 2683-2687, May 2003*.

[12] H Carrasco, R Feick, HD Hristov, "Experimental Evaluation of Indoor MIMO Channel Capacity for Compact Arrays of Planar Inverted-F Antennas", *Microwave and Opt. Tech letters, Vol. 49, No. 7, July 2007.*

[13] R Jaramillo E, O Fernandez, RP Torres, "Empirical Analysis of 2x2 MIMO Channel in Outdoor-Indoor Scenarios for BFWA Applications", *IEEE Antennas and Propagation Magazine, Vol. 48, No. 6, Dec. 2006.*

[14] I Khan, Peter S. Hall, "Multiple Antenna Reception at 5.8 and 10 GHz for Body-Centric Wireless Communication Channels", *IEEE Transactions on Antennas and Propagation, Vol. 57, No.1, Jan 2009*.

[15] I Khan, P.S. Hall, A.A Serra, A.R. Guraliuc, P. Nepa, "Diversity Performance Analysis for On-body Communication Channels at 2.45 GHz" *IEEE Transactions on Antennas and Propagation, Vol. 57, No. 4, April 2009.*

[16] P S Hall, Yang Hao, "Antennas and Propagation for Body-Centric Wireless Communications", *Artech House, London, 2006.*

[17] J.Gong, J.F.Hayes and M.R.Soleymani, "Comparison of Capacities of the Transmit Antenna Diversity With The Receive Antenna Diversity In The MIMO Scheme*", IEEE CCECE, May 4–7, 2003, vol. 1, pp. 179–182.*

[18] LJ Greenstein, DG Michelson, V Erceg, "Moment-Method Estimation of Rician K-Factor", *IEEE comms letters, Vol. 3, No. 6, June, 1999*.

[19] Z Tang, A S Mohan, "Experimental Investigation of Indoor MIMO Ricean Channel Capacity", *IEEE Antennas and Wireless Prop letters, Vol. 4, 2005.*

Chapter 10

Conclusions and Future Work

10.1 Final Conclusions

The use of multiple antennas at the receiving end, i.e. receive diversity, has been found to be very effective in combating the fading caused by the environment and the body movement. Significant diversity gain values are achieved, using 2-branch diversity, for most of the on-body channels, especially for dynamic channels. The correlation between the branch signals is low for dynamic channels and the channels with NLOS link in the indoor scattering environment. Low correlation value suggests that diversity can be very effective if power imbalance is carefully dealt with. For static channels, like belt-chest, the diversity is not useful and very low diversity gains were observed. The reason is the high correlation due to the presence of LOS and low scattering. Power imbalance between the two branch signals is also high for belt-chest channel in most cases.

The diversity gains are higher in the indoor environment compared to the anechoic chamber, which suggests that the scattering due to the body itself is not too much, but has a part to play in the diversity improvement. Due to the presence of metallic floor in the anechoic chamber used for measurements, there was scattering and the presence of multipath components, as a result, lead to slightly higher diversity gain values and do not reflect the diversity performance in the absence of scatterers. The

diversity performance at low and high frequencies is more or less the same, although the fading characteristics may change. The path loss at lower frequencies is less compared to that at the higher frequencies and also the cost and complexity of hardware at higher frequencies is more. So low frequency is a good choice for cost and path gain but for future high data rate demand, high frequencies may be better option.

Pattern diversity, using printed-IFA and PIFA, performs almost similar to the space diversity rather a bit better in some cases. Communication takes place on the surface of the body as creeping wave and attenuation is more than that of the free space attenuation. The wave on the surface of the body is highly attenuated, particularly in the case of the printed-IFA due to the polarization of transmitted wave being parallel to the surface of the body, and the multipath component is dominant over the direct ray. The results suggest that the PIFA is the best choice of antenna, as it gives reasonable path gains and higher DG values and has a shape that is convenient for body-worn devices. The printed-IFA is more sensitive to its orientation compared to the other antennas.

Polarization diversity is not as useful as the space and pattern diversity but provides reasonable diversity gains for some channels. A combination of space, pattern and polarization diversity is more effective than space diversity only or polarization diversity only.

The diversity performance presented is limited to narrowband systems or channels with very small delay spread. Also, it is limited to the antennas, the environment used in the measurements, and the use of a single human body for the measurements. Different environment and different antennas may lead to slightly different results. The presented DG values are achieved by removing the shadowing effect and hence considering a constant average signal level for whole of the data set covering the entire measurement duration. If the average signal level is low due to shadowing, the DG values may not appear to be significant as 7 to 8 dB of improvement in a very weak signal may not contribute to offer significant improvement. However, it may be very effective if the average signal level is considerably high.

The uplink and downlink diversity is reciprocal, suggesting that the local off-body scattering environment is dominant. The diversity measurements are repeatable with a small error, which is acceptable for most of the cases. The exact choice of demeaning window size is not critical as the DG and correlation is fairly insensitive to the window size within a certain range, which depends on the channel and the movements involved.

The short-term fading envelopes of the branch and combined signals best fit the Rician distribution with moderate K-factor values. Long-term fading envelope best fits the Log-Normal distribution. The maximum difference of the best fit parameters between the two branch signals suggests that the two branch signals may not be identically distributed. The Rician K-factors for printed-IFA are very small, which suggest that for this antenna the local off-body scattering is dominant over the direct

ray. The comparison of K-factor values for the branch and combined signals clearly indicates that there is an improvement due to diversity reception. Higher LCR at higher frequencies suggests that the fading is more severe, and the comparison of branch and combined signals' LCR clearly suggests an improvement offered by the use of diversity. The three antennas have almost the same fading statistics with printed-IFA being a bit more prone to fading than monopole and PIFA, due to weak direct link and dominant multipath components. Again, the channel characterization presented here is valid for narrowband systems and with the antennas used. The Doppler spectrum is an average Doppler spectrum, averaged over different orientations of the antenna and various repetitions. Thus, it does not provide the worst case scenario.

BAN-BAN interference, which can significantly disturb the performance of the body-centric wireless systems, can be controlled by using diversity reception. The Weiner-Hopf solution and optimum combining IRC schemes do not provide significant interference rejection gain values for the on-body communication case but these algorithms are still useful in keeping the interference level low and not allowing it to reach or exceed the desired signal level. The new proposed IRC algorithm, i.e. ICIT, provides a flexible way to handle the BAN-BAN interference. The belt-chest channel gives the lowest values of interference rejection gain due to the presence of strong LOS links and very high SIR values. The belt-head and belt-wrist channels show considerable improvement in output SINR with the three IRC techniques. The interference rejection gain depends upon the average SIR value at the receiving antennas. IRC works better when the SIR values are close to 0 dB, and

the IRG values are almost constant for a certain range of SIR. The interference rejection gain value decreases rapidly with increasing SIR outside that range.

Narrowband MIMO on-body channels were characterized by the correlation among the subchannels, and the spatial correlation matrices were derived for the three channels. The analysis of the spatial correlation matrices shows that the movement of the body and the antenna in the environment produces sufficient de-correlation among the subchannels despite the presence of LOS link. The channel capacity improvement with MIMO over the SISO is considerably high and capacity gains close to a maximum gain of 2 were observed for some channels. The belt-chest channel does not provide high capacity gains due to high correlation among the subchannels.

10.2 Future Work

The work presented in this thesis concerned the diversity reception and MIMO capacity analysis using real measurement data in indoor environment for narrowband systems. There is still a lot of scope in terms of multiple antennas use for on-body applications. Some of the issues that still need attention are described below:

- The use of diversity antennas at the transmitter side, or transmit diversity, can be carried out and compared to the receive diversity performance. The conventional Alamouti codes can be used and there is a scope in defining some new algorithms for the transmit diversity.

- The use of jointly optimized transmit-receive diversity can be investigated with MIMO. In other words, the diversity gains achievable with MIMO can be quantified.

- This work was done for the narrowband systems. The use of diversity for wideband and ultra wideband (UWB) can be studied. An important issue is the proper measurement mechanism for UWB diversity with random movements. Work can be done to device a proper and accurate measurement procedure for UWB diversity measurements.

- There is still a need to design compact and low-profile multiple antenna structures for the on-body diversity and MIMO applications. The issue of SAR needs to be addressed.

- The on-body channel characterization needs more attention and there is a need for a standard statistical model for the on-body propagation channels. Diversity and MIMO channel models are also needed and there is a big scope in the MIMO channel modeling for on-body channels.

- The diversity gain can be improved more by mounting the diversity branch antennas on different locations on the body. This way diversity can be used to compensate for the shadowing loss, which needs to be quantified.

- The use of water-filling technique is quite useful for MIMO systems with non-uniform power distribution among the transmitting antennas. Through water-filling, the power can be distributed to utilize the subchannels with less impairment and avoid the channels with high impairments. This area needs to

be investigated for on-body channels and suitable water-filling schemes needs to be proposed.

- The use of higher-order diversity and higher-order MIMO system performance can be quantified as a next piece of work.

Appendix A

Circuit Diagram and Programming code for Controlling the RF Switch

The RF switch used in the measurements was a Single-Pole 4-Throw (SP4T) SW4AD-A14 absorptive switch operating in 2-12 GHz frequency range with SMA connectors and TTL logic control driver. The insertion loss was approximately 1.5 dB. The maximum switching time of the switch was 100 ns. The minimum isolation of the switch was 55 dB [1] and the measured isolation at the desired frequency was above 70 dB. The voltage and current specifications and the TTL control logic are given below.

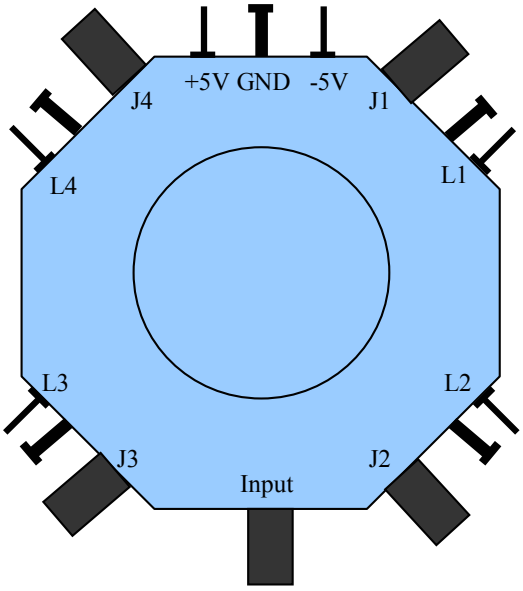

Fig. A1: A sketch of the SP4T RF switch

Voltage / Current Specification [1]:

+ 5V DC @ +80 mA typical

-5 V DC @ -40 mA typical

TTL Logic [1]:

Control Inputs				Output Port			
L1	L2	L3	L4	J1	J2	J3	J4
0	1	1	1	C	I	I	I
1	0	1	1	I	C	I	I
1	1	0	1	I	I	C	
1	1	1	0	I	I	I	C

C = Connected

I = Isolated

Logic “0” = -0.3V to +0.8V

Logic “1” = +2.0V to +5.0V

Schematic of the circuit to control the switch

The RF switch was operated and controlled by PIC 16F648A microcontroller. Only two ports of the switch were used as the measurements were only limited to 2 branches. As explained in Chapter 4, the measurements with the switch were done on a switch-and-sample approach. The VNA was set to external-trigger-on-point mode and the trigger signal was provided by the microcontroller. The microcontroller first sends a control signal to switch for switching to one position and then sends the

trigger signal. A schematic diagram of the circuit is shown below. The portion of the circuit that drives the microcontroller was designed by a PhD student, K M Ramlee [2]. The microcontroller code written by him was modified to achieve the desired results.

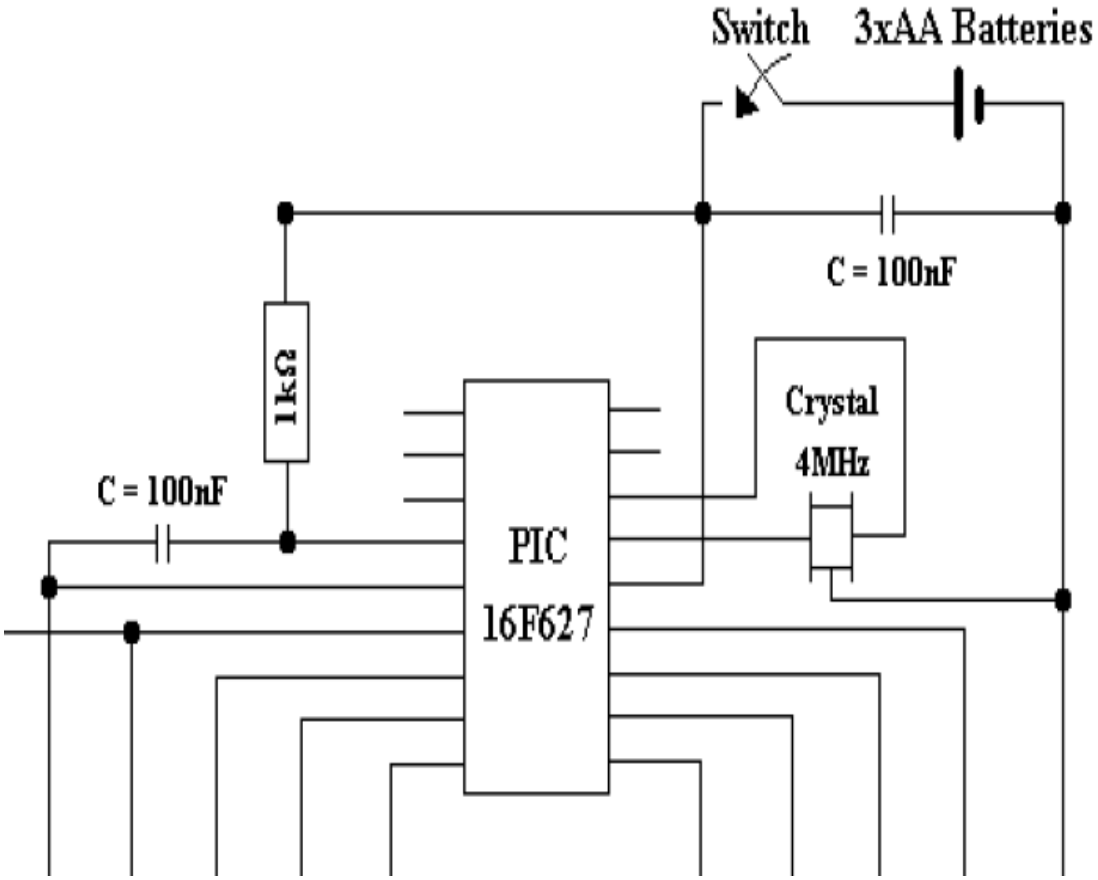

Fig. A2: Circuit to drive the PIC microcontroller [2]

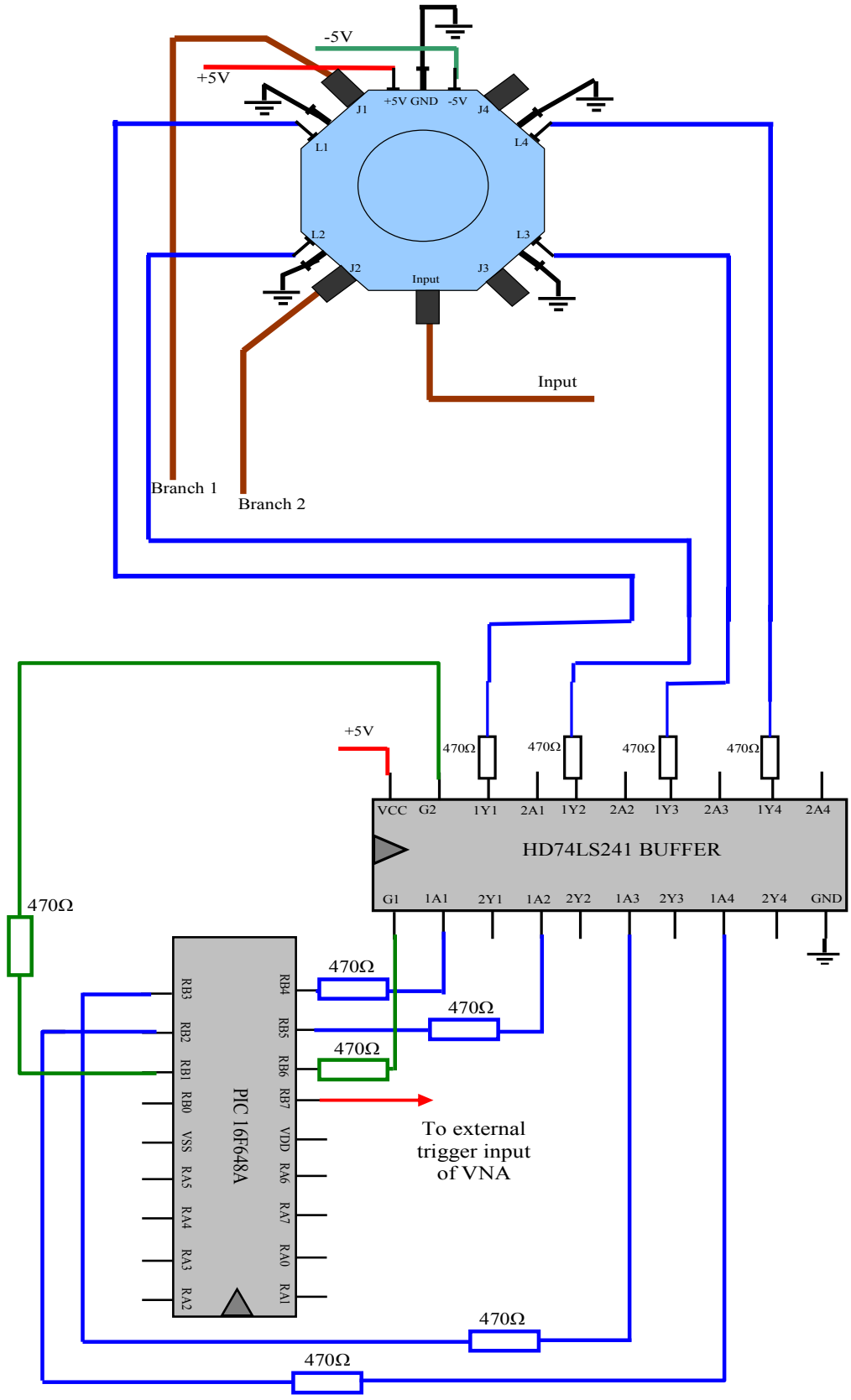

Fig. A3: Schematic of the switch control circuit

Assembly language code for the PIC microcontroller

```
; DEVICE                16F648A
; RESONATOR             XT (4MHz)
; WATCHDOG              DISABLED
; CODE PROTECT          OFF
; FUNCTION              Control an RF switch and VNA triggering with PIC
        LIST F=INHX8M,p=16F648A, R=HEX
        __config  3F61
; ----- General equates ----------------------------------------
w       equ     0
f       equ     1
; ----- I/O equates       ----------------------------------------
porta   equ     0x05        ;assign PORTA register to the label 'porta'
portb   equ     0x06        ;assign PORTB register to the label 'portb'
status  equ     0x03        ; status register address
c       equ     0           ; carry bit within status
z       equ     2           ; zero bit
rp0     equ     5           ; register bank 0 bit
rp1     equ     6           ; register bank 1 bit
; ----- register equates ----------------------------------------
pc      equ     0x02        ; Program counter
mcount          equ             0x20                ; counter for delay
ncount          equ             0x21                ; counter for delay
```

```
count           equ             0x22                    ; counter
time_adjust     equ             0x23                    ;
; -----------------------------------------------------------------
                        org             0x00
                        goto            start
; ---------------------- subroutine 'delay_long' ------------------------
delay_long              movlw           d'50'   ; change this hex number to adjust speed
                        movwf           mcount
get_n_long              movlw           d'72'   ; change this hex number to adjust speed
                        movwf           ncount                  ;
dec_n_long              decfsz          ncount,f                ;
                        goto            dec_n_long              ;
                        decfsz          mcount,f                ;
                        goto            get_n_long              ;
                        return
; ---------------------- main programme ---------------------------
start                   movlw  0x00             ;configure portb as output
                        bsf       status,rp0            ;
                        movwf  portb                    ;
                        bcf       status,rp0            ;
                        clrf      portb                 ;clear the portb register
reset_count             movlw  0x00                     ;
                        movwf  count            ;initialize count for output
cycle                   call      sequence      ;
```

```
                movwf  portb          ;output the control word
                incf   count,f        ;increment count
                movf   count,w        ;copy count to w
                btfsc  count,3        ;test if count =8 i.e. seq. done
                goto   reset_count    ;reset 'count' if seq. complete
                goto   cycle
sequence        addwf  pc,f
                retlw  b'11111000'    ;switch to pos 1
                call   delay_long     ;delay for 17.03 ms for 21.2 ms
                                      ;sampling time
                retlw  b'11111001'    ;Trigger for pos1
                retlw  b'11110100'    ;switch to pos2
                retlw  b'11110101'    ;Trigger for pos2
                end
```

Data Sheets of PIC 16F48A and the buffer HD74LS241

For the data sheet of PIC 16F648A microcontroller see [3].

The data sheet of the buffer is given below: source [4].

HD74LS241 ●Octal Buffers/Line Drivers/Line Receivers (non inverted three-state outputs)

■BLOCK DIAGRAM (½)

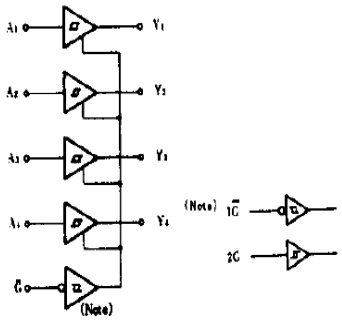

■FUNCTION TABLE

Inputs			Output
$1\overline{G}$	2G	A	Y
H	L	×	Z
L	H	H	H
L	H	L	L

Note) H; high level,
L; low level,
X; irrelevant
Z; off (high-impedance) state of a 3-state output

■PIN ARRANGEMENT

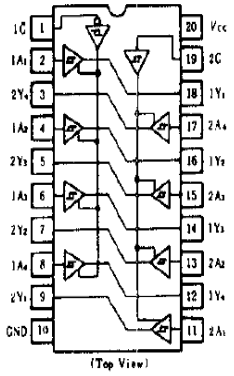

■ELECTRICAL CHARACTERISTICS ($Ta=-20\sim+75°C$)

Item		Symbol	Test Conditions		min	typ*	max	Unit
Input voltage		V_{IH}			2.0	–	–	V
		V_{IL}			–	–	0.8	V
Hysteresis		$V_{T^+}-V_{T^-}$	$V_{CC}=4.75V$		0.2	0.4	–	V
Output voltage		V_{OH}	$V_{CC}=4.75V$, $V_{IH}=2V$, $V_{IL}=0.8V$, $I_{OH}=-3mA$		2.4	–	–	V
			$V_{CC}=4.75V$, $V_{IH}=2V$, $V_{IL}=0.5V$, $I_{OH}=-15mA$		2.0	–	–	
		V_{OL}	$V_{CC}=4.75V$, $V_{IH}=2V$, $V_{IL}=0.8V$	$I_{OL}=12mA$	–	–	0.4	V
				$I_{OL}=24mA$	–	–	0.5	
Output current		I_{OZH}	$V_{CC}=5.25V$, $V_{IH}=2V$, $V_{IL}=0.8V$	$V_O=2.7V$	–	–	20	μA
		I_{OZL}		$V_O=0.4V$	–	–	−20	
Input current		I_{IH}	$V_{CC}=5.25V$, $V_I=2.7V$		–	–	20	μA
		I_{IL}	$V_{CC}=5.25V$, $V_I=0.4V$		–	–	−0.2	mA
		I_I	$V_{CC}=5.25V$, $V_I=7V$		–	–	0.1	mA
Short-circuit output current		I_{OS}	$V_{CC}=5.25V$		−40	–	−225	mA
Supply current**	Outputs high	I_{CC}	$V_{CC}=5.25V$		–	13	23	mA
	Outputs low				–	27	46	
	All outputs disabled				–	32	54	
Input clamp voltage		V_{IK}	$V_{CC}=4.75V$, $I_{IN}=-18mA$		–	–	−1.5	V

* $V_{CC}=5V$, $Ta=25°C$
** I_{CC} is measured with all outputs open.

■SWITCHING CHARACTERISTICS ($V_{CC}=5V$, $Ta=25°C$)

Item	Symbol	Test Conditions	min	typ	max	Unit
Propagation delay time	t_{PLH}	$C_L=45pF$, $R_L=667\Omega$	–	12	18	ns
	t_{PHL}		–	12	18	
Output enable time	t_{ZL}		–	20	30	ns
	t_{ZH}		–	15	23	ns
Output disable time	t_{LZ}	$C_L=5pF$, $R_L=667\Omega$	–	15	25	ns
	t_{HZ}		–	10	18	ns

Note) Refer to Test Circuit and Waveform of the Common Item

Fig. A4: Data Sheet of Buffer HD74LS241 [4]

REFERENCES

[1] http://www.pulsarmicrowave.com

[2] Kamarudin M Ramlee, "Design and Performance of Antennas for On-Body Communication Channels and Antenna Diversity", *PhD thesis, University of Birmingham, September 2007.*

[3] http://www.microchip.com/wwwproducts/Devices.aspx?dDocName=en010212

[4] http://www.datasheetcatalog.org/datasheet/HitachiSemiconductor/mXrzvur.pdf

Appendix B

Derivation of Equations for EGC (eq. 3.8) and MRC (eq. 3.9)

Suppose r_i be the signal envelope received at the i^{th} branch of an M-branch diversity combiner. Then, the local average power per branch denoted by p_i is:

$$p_i = \frac{r_i^2}{2} \tag{B.1}$$

and the average noise power per branch $\overline{n_i^2}$ =N is the same for all branches. Then, the local average SNR per branch, γ_i is:

$$\gamma_i = \frac{r_i^2}{2N} \tag{B.2}$$

If y is the diversity combined signal at the output of the combiner, then assuming that the co-phasing has been done:

$$y = \sum_{i=1}^{M} a_i r_i \tag{B.3}$$

where a_i is the weight of the *ith* branch. Let the total noise power at the output of the combiner is N_T , where

$$N_T = \sum_{i=1}^{M} a^2 N \tag{B.4}$$

Then, the total output SNR at the combiner out is:

$$\gamma = \frac{y^2}{2N_T} \tag{B.5}$$

Equal Gain Combining (EGC)

The weight is 1 for all the branches, i.e.

$$a_i = 1 \tag{B.6}$$

Thus, from eqns. (B.3), (B.4), and (B.5), the output SNR for EGC is:

$$\gamma_{EGC} = \frac{(\sum_{i=1}^{M} r_i)^2}{2N\sum_{i=1}^{M} 1} = \frac{(\sum_{i=1}^{M} r_i)^2}{2NM} \tag{B.7}$$

$$\Rightarrow \qquad \gamma_{EGC} = \frac{(r_1 + r_2 + ...r_M)^2}{2NM} \tag{B.8}$$

Thus, the power in the combined signal is:

$$p_{EGC} = \frac{(r_1 + r_2 + ... r_M)^2}{2M} \tag{B.9}$$

which implies that the EGC signal envelope will be:

$$y_{EGC} = \frac{r_1 + r_2 + ... r_M}{\sqrt{M}} \tag{B.10}$$

Maximal Ratio Combining (MRC)

The weight for MRC is proportional to the corresponding branch signal envelope to the noise power ratio, i.e.:

$$a_i = \frac{r_i}{N} \tag{B.11}$$

Thus, from eqns. (B.3), (B.4), and (B.5) the output SNR for MRC is:

$$\gamma_{MRC} = \frac{(\sum_{i=1}^{M} \frac{r_i}{N} r_i)^2}{2(\sum_{i=1}^{M} \frac{r_i^2}{N^2} N)} = \frac{(\sum_{i=1}^{M} \frac{r_i^2}{N})^2}{2(\sum_{i=1}^{M} \frac{r_i^2}{N})} = \frac{(\sum_{i=1}^{M} \frac{r_i^2}{N})}{2} = \frac{\sum_{i=1}^{M} r_i^2}{2N} \quad \text{(B.12)}$$

$$\Rightarrow \qquad \gamma_{MRC} = \frac{r_1^2 + r_2^2 + \ldots\ldots\ldots r_M^2}{2N} \quad \text{(B.13)}$$

Thus, the MRC signal envelope is:

$$y_{MRC} = \sqrt{r_1^2 + r_2^2 + \ldots\ldots\ldots \quad .r_M^2} \quad \text{(B.14)}$$